DOCTOR OF PHILOSOPHY

Investigating DNA Methylation Changes in a Preclinical Murine Model of Cutaneous Squamous Cell Carcinoma

Roth, Kevin

Award date:
2019

University of Dundee

Investigating DNA Methylation Changes in a Preclinical Murine Model of Cutaneous Squamous Cell Carcinoma

Kevin Roth

PhD Thesis
University of Dundee
School of Medicine
September 2019

To my family and friends who were always there for me.

Especially my amazing wife Catharina,

I will forever be grateful to have you by my side.

Table of Contents

List of Tables

List of Figures

Acknowledgments

At first, I would like to thank **Dr. Richard Weller** and **Dr. Laureano de la Vega** for agreeing to be my examiners. I am looking forward to a relaxed and engaging viva. I'd also like to thank Mr. George Lucas, sorry I mean **Dr. Colin Henderson** for being my convener.

My gratitude goes to **Professor Albena Dinkova-Kostova**, who was an excellent supervisor. When I met her during an internship in 2014, I immediately knew that I wanted to come back to her lab and do my PhD with her. Whenever I thought that the latest results would contradict everything I have done in the past year, she had the amazing ability to see the positive in it and I left her office, not with a sense of frustration, but the feeling that everything will be fine. She always had an open ear for me, and her door was always open to approach her and address my questions and needs. I was free to do my PhD as I wanted it to, and although this made things more difficult for me and I probably would have been able to be more efficient with more guidance, it made me grow as a person and as a scientist.

A big thank you has to go to **Professor John Hayes** for his supervision. Although he was not that involved, his "grey eminence" (no insult intended) made me think about myself as a scientist and what I want to achieve. He also was fun to have around and occasionally have a bit of silly talk or get inspired to listen to some classic rock.

The bioinformatics part of my PhD was quite challenging. Although I like the field, I would have been lost without the help of **Professor Tim de Meyer** and **Louis Coussement** from the Cancer Research Institute Ghent. Thank you for all the help making sense out of the data throughout my time in Ghent and later in Dundee. If I will visit Belgium again, I promise to come for a visit!

I was very fortunate to have completed my Masters degree with **Dr. Clarissa Gerhäuser** at the DKFZ in Heidelberg and never to have lost the connection with her lab. Spending some time in my hometown Heidelberg to perform additional methylation analysis was crucial. Thanks to **Ms. Clarissa Feuerstein** for her help finding the correct tracks in the UCSC genome browser, **Dr. Cornelia Jäkel** for her

help designing the MassARRAY experiments and especially **Mr. Oliver Mücke** for his assistance performing the MassARRAY and analysing everything.

Thanks to my TMC, **Professor Sara Brown**, **Dr. Gillian Smith** and **Professor Gareth Inman**, who supported me during my PhD, gave me valuable feedback, occasionally told me off, reminded me to focus and supported me through some emotional distress.

I would also like to thank **Professor Charlotte Proby** (University of Dundee), **Professor Irene Leigh** (University of Dundee) and **Professor Catherine Harwood** (Barts & the London School of Medicine and Dentistry, Queen Mary University of London) for making the cSCC cell lines and cSCC samples available to me.

I would extend my deepest gratitude to **Ms. Maureen Higgins** and **Dr. Elena Knatko** for their work with the solar simulated cSCC model prior to my arrival. Their work was the foundation of my thesis. Without their commitment I would have had no samples to work with. Additionally, I would like to thank the other members of the ADK and JDH labs, former and present. **Dr. Dina Dikovskaya** for her help improving my western skills, suggesting valuable experiments and the occasional conversation in German, **Dr. Ying Zhang** for her help in the lab and being a great landlord, **Dr. Ritu Sharma** for always knowing where to find the antibodies I needed, introducing me to Rishi's and her Samosas, sharing the secrets of the Indian cuisine with me as well as all the great banter about either Apple vs. Windows or star signs, as well as **Dot** and **Diane**.

I would also like to thank all the people working on skin cancer in Dundee. Especially **Dr. Victoria Sherwood, Dr. Lauren Strathearn, Dr. Lindsay Spender** and **Dr. Jasbani Dayal.**

I would also like to thank **Dr. Aparajitha Vaidyanathan** and **Mr. Hugh Nicholson** from the lab of Dr. Gillian Smith for kindly sharing their ovarian cancer DNA samples with me.

My time in Dundee was defined by all the wonderful people I met. There were so many, that I am sure I will forget someone, so sorry in advance. Thanks to all the other PhD students and post docs in our division, there were so many great moments in and outside the lab with you that I cannot name all. Thank you **Aparajitha, Lauren,**

Giulia, Lisa, Richard, Marilia, Anna, Mariam, Linda, Magda, Lauren, Natasha, Hugh, Morven, **Kimi, Kris, Oleg** and so many more for making my time in Dundee enjoyable and the stressful times bearable.

I would like to thank a few special people in more detail:

Thank you **Sha**, for all you support during my first internship in Dundee, for letting me stay in your home when I did not have place of my own yet, for pointing out all the mistakes I made to help me improve my English, for guiding me in the lab and helping me with anything from Uni regulations to bank accounts. Thank you for the great time in Singapore at your wedding, I will cherish this memory forever. But most of all, thank you for your continuing friendship. Thank you **Laura**, for having crazy curly hair (not anymore sadly), for helping me to finally get a decent FILIP1L blot, for the help in the lab and the great evenings in Duke's and Rishi's. Thank you **Holly**, for all the fun on level 6, for teaching me about Scottish curse words and slang, for driving me to the other side of Dundee so I could pick up my parcels, for pizza and movies at your place and for saying "cimanin" for me to make me laugh. Thank you **Claudia**, for showing me that I don't struggle alone, for your recipe suggestions (although I passed on the vegan sausages), for getting angry about the same things with me and for flying all the way to Germany for the wedding. And last but not least thank you **Daniella**, for matching my craziness (even surpassing it sometimes) and sharing the experience of working on WNT in skin with me, it was great to see that it wasn't always my fault, it was WNT's fault (at least most of the time). Thank you for supporting me with your knowledge, passion and resilience, for cheering me up when I was grumpy and laughing with me through lab days full of failed experiments and data that makes no sense. I think without you joining the lab, I probably would have quit. I will always think back and laugh at the thought of the crazy Portuguese girl that I grew to cherish as my good friend.

A huge thanks goes to the spiciest PiCLS symposium committee ever. It was quite a ride and we may have had our differences (maybe mostly me) but we managed to organize an awesome day. Thank you**, Giulia, Aparajitha, Lauren, Elda, Lucas** and our mascot **Balaji**. I will always remember the year of work and fun!

Thank you MeDeN committee! I really enjoyed our lunch meetings and all the great events we organized. From the pub golf (boy that escalated quickly!) to the Easter egg

hunt and Christmas parties. Thank you, **Richard, Hugh, Lisa, Claudia** and **Daniella** for the great memories!

In order to thank my family and closest friends, I will switch to German now:

Vielen Dank an **Oliver** und **Ralf**. Ihr beide seid meine besten Freunde und ohne die TS oder Skype Gespräche mit euch wäre es in Schottland ab und an sehr frustrierend gewesen. Zusammen zocken oder über Skype einen Film schauen und dabei Gin oder Whisky (oder beides) trinken gab mir das Gefühl für einen Abend wieder zu Hause zu sein. Eure Besuche waren beide Highlights (auch wenn Edradour samstags nicht geöffnet ist) und über den JGA brauche ich gar nicht zu reden. Aber wir sollten definitiv das „Dessertsteak“ weiterführen!

Vielen Dank an meinen **Opa Dieter**. Ich habe viel von dir gelernt. Obwohl wir aus sehr verschiedenen Generationen kommen, habe ich das Gefühl, dass du mich immer verstanden hast und immer meinen Weg unterstützt hast. Ich vermisse die Abende, an denen ich abends noch bei euch im Wohnzimmer saß und wir über Gott (weniger) und die Welt (wesentlich mehr) diskutiert haben oder „Wer wird Millionär“ geschaut haben (und laut Oma schon lange Millionäre sein könnten).

Danke an meine Schwester **Franziska**. Auch wenn wir nicht immer so viel Kontakt haben wie wir beide gerne hätten, so bist du doch ein sehr wichtiger Mensch für mich. Auf jeden Fall hast du als Kind meine Frustrationstoleranz sehr geschult (was mir im Labor wahrscheinlich geholfen hat!). Danke für deine mentale Unterstützung, die Hilfe mit all den Geschenken, die du ausgesucht hast und auf die ich nur maximal meinen Namen geschrieben habe und für deine Hilfe bei der Hochzeit, vor allem die weltklasse Torte!

Besonders danken möchte ich meinen Eltern **Susanne** und **Gerhard**. Ihr bin euch unendlich dankbar für eure bedingungslose Unterstützung. Ohne euch würde ich heute nicht hier stehen und das sind keine leeren Worte. Danke dass ihr immer meinen Weg unterstützt habt und mich immer, wenn es notwendig war in die richtige Richtung geschubst habt. Ich bin kein Freund großer Worte und oft fällt es mir schwer zu sagen was ich fühle (so auch jetzt). Aber ihr beide seid große Vorbilder für mich geworden. Das war nicht immer so, aber je älter ich werde desto mehr verstehe ich euch und schätze wert wie ihr mich erzogen habt. Sicherlich war nicht immer alles leicht, aber

wie ihr mich unterstützt wird mir immer als Blaupause für mein eigenes Leben dienen. Danke für alles!

Und zuletzt möchte ich noch meiner Partnerin **Catharina** danken. Ohne dich hätte ich es niemals geschafft. Du hast mir während unserer Zeit in Schottland und während des Schreibens so unglaublich viel Kraft gegeben, vor allem dann, wenn ich keine mehr hatte. Deine Liebe und Unterstützung haben mich durch die teilweise schweren Tage gebracht. Deine Stärke und dein Durchhaltevermögen sind eine große Inspiration für mich. Danke dass du mich immer unterstützt hast, auch wenn ich dich mit meiner Laune und meiner fehlenden Motivation zur Weißglut gebracht habe. Danke dass du mir in den Allerwertesten getreten hast als ich es brauchte und danach gnädig mit mir warst, wenn ich meine Versprechen nicht einhalten konnte. Danke dass du mir meinen Freiraum gegeben hast und mir gleichzeitig klar gemacht hast, dass ich jetzt mal loselegen muss. Du bist das Beste was mir je passieren konnte und ich verspreche dir, dass ich dich auch mit allem was ich habe unterstützen werde, wenn du deine Thesis schreibst. Ich liebe dich!

Declaration

I declare that this thesis is an original report of the results obtained from my research that was carried out in the Division of Cancer Research, School of Medicine at the University of Dundee from October 2015 to August 2018 using funding from the British Skin Foundation. I declare that this report has been written by me and all references cited have been consulted by me. This report has not been submitted for any previous degree. Any work other than my own is clearly stated in the text and acknowledgments.

Signed: [redacted] Date: 02/12/2019

Kevin Roth

I confirm that Kevin Roth is the author of this thesis and he has fulfilled the conditions of the relevant Ordinance and Regulations of the University of Dundee, therefore qualifying him to submit this thesis in application for the Degree of Doctor of Philosophy.

Signed: _____ Date: _____

Professor Albena Dinkova-Kostova

Abbreviations

5mC	5-methyl-Cytosine
5hmC	5-hydroxymethyl-Cytosine
5fC	5-formyl-Cytosine
5caC	5-carboxyl-Cytosine
5hmU	5-hydroxymethyl-Uracile
A	Adenosine
AI	Apoptotic Index
AID	Activation Induced Deaminase
AIDS	Acquired Immune Deficiency Syndrome
AJCC	American Joint Committee of Cancer
AK	Actinic Keratosis
AKT	Protein Kinase B
APOBEC	Apolipoprotein B mRNA Editing Enzyme Complex
ApoLP-III	Apolipophorin-III
ATF3	AMP-dependent Transcription Factor
ATM	Ataxia Telangiectasia Mutated
ATR	Ataxia Telangiectasia and Rad3-related
BCA	Bicinchoninic Acid
BCC	Basal Cell Carcinoma
BER	Base Excision Repair
BLAST	Basic Local Alignment Search Tool
BRCA1	Breast Cancer type 1 Susceptibility Protein
BS	Bisulphite
BSA	Bovine Serum Albumin
btDNA	bisulfite-treated DNA
C	Cytosine
CAGE	Cap Analysis of Gene Expression
CCND1	Cyclin D1
CDKN2A	Cyclin-dependent Kinase Inhibitor 2A
cDNA	complementary DNA
CDS	Coding Sequence
CFA	Complete Freund's Adjuvant

circRNA	circular RNA
CLL	Chronic Lymphatic Leukaemia
CM	Conditioned Medium
CortBP2	Cortactin-Binding Protein 2
CpG	CG Dinucleotide
CpG islands	CGI
CRISPR	Clustered Regularly Interspaced Short Palindromic Repeats
CT	Cycle Threshold
ctDNA	circulating cell-free DNA
CTL	Control
Da	Dalton
DAC	5’-aza-2’-deoxycytidine
DAPK	Death-Associated Protein Kinase
DHC-N1	Dynein Heavy Chain N-terminal Region 1
DMBA	7,12-dimethylbenz[a]anthracene
DMEM	Dulbecco’s Modified Eagle Medium
DMR	Differentially Methylated Region
DMSO	Dimethyl Sulfoxide
DNA	Deoxyribonucleic Acid
DNMT	DNA Methyltransferase
DOC-1	Down-regulated in Ovarian Cancer 1
DOX	Doxycyclin
DS	Dorsal Skin
DTT	Dithiothreitol
EDTA	Ethylenediaminetetraacetic Acid
EGCG	Epigallocatechin Gallate
EGF	Epidermal Growth Factor
EGFR	Epidermal Growth Factor Receptor
EGTA	ethylene glycol-bis(β-aminoethyl ether)-N,N,N′,N′-tetraacetic acid
ELISA	Enzyme-Linked Immunosorbent Assay
EMAP-II	Endothelial Monocyte Activating Polypeptide-II
EMT	Epithelial-Mesenchymal Transition

EV	Empty Vector
EZH2	Enhancer of Zeste Homolog 2
FAM	Fluorescein Amidites
FBS	Fetal Bovine Serum
FDR	False Discovery Rate
FFPE	Formalin-Fixed Paraffin-Embedded
FILIP1L	Filamin A-interacting protein 1-like
FZD	Frizzled
G	Guanine
GAPDH	Glyceraldehyde 3-Phosphate Dehydrogenase
GLOBOCAN	Global Cancer Observatory
GSC	Glioblastoma Stem Cell
GSK3β	Glycogen Synthase Kinase 3β
H3K27me3	Histone 3 Lysin 27 tri-methylation
H3K4me3	Histone 3 Lysin 4 tri-methylation
HCl	Hydrochloric Acid
hcSCC	human cSCC
HDAC	Histone Deacetylases
HEPES	4-(2-hydroxyethyl)-1-piperazineethanesulfonic acid)
Herpes-BLLF1	Herpes Virus major outer Envelope Glycoprotein
HH	Hedgehog
HIF-1α	Hypoxia-Inducible Factor 1
HIV	Human Immunodeficiency Virus
HMEC	Human Mammary Epithelial Cells
HMT	Histone Methyltransferases
HOSE	Human Ovarian Surface Epithelial
HPEI	Heparin-Polyethyleneimine
HPV	Human Papilloma Virus
Hras	Harvey-Ras
HSF1	Heat Shock Factor 1
HSP72	Heat Shock Protein 72
HUVEC	Human Umbilical Vein Endothelial Cell
IFN-α	Interferon-α

iHS	independent Healthy Skin
INDEL	Insertion and Deletion
IOSE	Immortalized Ovarian Surface Epithelial
IPA	Ingenuity Pathway Analysis
IVT	*in vitro* transcription
KMT2D	Histone-lysine N-methyltransferase 2D
LB	Luria-Bertani (medium)
LEF	Lymphoid Enhancer Factor
LRP	low-density Lipoprotein Receptor-related Protein
MAPK	Mitogen-Activated Protein Kinase
Mb	Megabase
MBD	Methyl-CpG Binding Domain
MC1R	Melanocortin Receptor 1
mcSCC	mouse cSCC
MeCP	Methyl-CpG-Binding Domain Containing Protein
MeDIP	Methylated DNA Immunoprecipitation
MIRA	Methylated-CpG Island Recovery Assay
miRNA	micro RNA
MMP	Matrix Metalloprotease
MOPS	3-(N-morpholino)propanesulfonic acid
MSH	Melanocyte Stimulating Hormone
MSP	Methylation Specific PCR
MVD	Micro Vessel Density
NA	not available
NCBI	National Center for Biotechnology Information
NER	Nucleotide Excision Repair
NF1	Neurofibromin 1
NGS	Next Generation Sequencing
NHEK	Normal Human Epithelial Keratinocytes
NHK	Normal Human Keratinocytes
NICD	NOTCH Intracellular Domain
NLS	Nuclear Localization Sequence
NMSC	Non-Melanoma Skin Cancer

NRAS	Neuroblastoma RAS Viral Oncogene Homolog
Nrf2	NF-E2 p45-related factor 2
NSC	Neuronal Stem Cell
oxRRBS	oxidative Reduced Representation Bisulfite Sequencing
PBS	Phosphate Buffered Saline
PCA	Principal Component Analysis
PCR	Polymerase Chain Reaction
POU2F1	POU domain, class 2, transcription factor 1
PRC2	Polycomb Remodelling Complex 2
PTCH1	Protein Patched Homolog 1
qPCR	quantitative PCR
RAP	RNA-based Arbitrary primed PCR
RASSF1A	Ras association Domain-Containing Protein 1
Rb	Retinoblastoma
RISC	RNA-Induced Silencing Complex
RNA	Ribonucleic Acid
RNS	Reactive Nitrogen Species
ROS	Reactive Oxygen Species
RRBS	Reduced Representation Bisulfite Sequencing
RT	Room Temperature
RT-qPCR	Reverse Transcription quantitative PCR
SAEC	Small Airway Epithelial Cell
SAP	Shrimp Alkaline Phosphatase
SbcC	Nuclease SbcCD Subunit C
SDS	Sodium Dodecyl Sulfate
SFM	Serum Free Medium
siRNA	small interfering RNA
SLUG	Snail Family Transcriptional Repressor 2
SMO	Smoothened
SMUG1	Single-strand selective Monofunctional Uracil DNA Glycosylase 1
SNAIL	Snail Family Transcriptional Repressor 1
SNP	Single Nucleotide Polymorphism

SOTR	Solid Organ Transplant Recipient
ssUVR	solar-simulated UV Radiation
T	Thymine
TAE	Tris, Acidic Acid, EDTA
TAMRA	5-Carboxytetramethylrhodamine
TBS	Tris Buffered Saline
TCF	T-Cell Factor
TCGA	The Cancer Genome Atlas
TDG	Thymine DNA Glycosylase
TEMED	Tetramethylethylenediamine
TERT	Telomerase Reverse Transcriptase
TET	Ten-Eleven-Translocase
TF	Transcription Factor
TGF-β	Transforming Growth Factor beta
TNM	Tumor, Nodes, Metastasis
TP53	Tumor Protein 53
TPA	12-O-tetradecanoylphorbal-13-acetate
Trp53	Transformation-Related Protein 53
TSA	Trichostatin A
TSS	Transcription Start Site
TUNEL	Terminal Deoxynucleotidyl Transferase dUTP Nick End Labelling
UBA	Ubiquitin Associated Domain
UCSC	University of California (genome browser)
UK	United Kingdom
US	United States (of America)
UT	Untreated
UTR	Untranslated Region
UV	Ultra Violet
UVA	Ultra Violet Radiation A
UVB	Ultra Violet Radiation B
UVC	Ultra Violet Radiation C
UVR	Ultra Violet Radiation

VEGF-A	Vascular Endothelial Growth Factor A
VS	Ventral Skin
WGBS	Whole Genome Bisulfite Sequencing
WNT	Wingless/Integrated
WT	Wild Type
β-ME	2-Mercaptoethanol

Abstract

Non-melanoma skin cancers (NMSC) are the most common human malignancy. They can be divided into basal cell carcinomas (BCC) and cutaneous squamous cell carcinomas (cSCC), with the latter being responsible for the majority of NMSC deaths. Incidence rates for NMSC are rising due to increased exposure to UV radiation, caused by active sun-seeking behaviour and increased cumulative sun-exposure in aging population. In addition to the general populations, there are high risk groups, such as organ transplant recipients, who are in urgent need for strategies to treat aggressive cSCC.

Most animal models only partly reflect the complex genetic landscape of cSCC or leave out important parts of the carcinogenic process. We have developed a preclinical mouse model for cSCC by irradiating SKH-1 mice with low chronic doses of solar simulated UVR. The resulting tumors are remarkably similar to human cSCC in terms of histopathology and genetics. In this study, we provide a comprehensive analysis of global DNA methylation of this murine model and compare it to the methylome of human cSCC. We found that methylation changes in the murine cSCC tumors occur predominantly at regions of potential regulatory function, such as enhancers, promoters and intergenic regions of tumor suppressor genes that may be involved in regulation of gene expression or alternative splicing. Deactivation of tumor suppressor genes is an important feature for cancer, especially cSCC and our data suggest, that silencing of tumor suppressor genes by DNA methylation could be important in cSCC. Furthermore, we discovered differential methylation in the tumor suppressor gene Filamin A interacting protein 1 like (Filip1l). Down-regulation of the FILIP1L gene has been linked to ovarian, prostate and pancreatic cancer aggressiveness and metastatic potential and is an independent prognostic marker in ovarian cancer patients. The levels of Filip1l protein were significantly down-regulated in murine cSCC as well as in 9 out of 15 tested human cSCC cell lines. Although the exact function of the FILIP1L protein is incompletely understood, the strongest evidence points to its regulation of β-catenin stability and therefore WNT signalling activity. We found evidence that FILIP1L may regulate WNT signalling in skin, although FILIP1L did not regulate proliferation of the human cSCC cell lines that we tested.

When we compared the methylome of human cSCC patients to the methylome of mouse cSCC, the general features of the DNA methylation were similar. For example, average methylation levels increased in a subset of human cSCC cases and the mouse tumors, an effect that has been previously reported for UV irradiated skin (both human and mouse). We identified 214 genes that have at least one differentially methylated CpG in our dataset. Using R and the Ensemble gene annotation, we identified 153 of these genes that had a human orthologue. Of these 153 genes, 150 (93%) were also differentially methylated in human cSCC.

The remarkable similarities in histopathology, genetics and DNA methylation between human cSCC and the solar simulated UV induced mouse cSCC model suggest that this model could be advantageous over existing models and may provide new possibilities to investigate cSCC and develop new treatment strategies, especially for high risk groups. Furthermore, extending previous observations that most mutations in this tumor type occur not within oncogenes, but within tumor suppressor genes, our findings highlight the importance of inactivation of tumor suppressors (by both genetic and epigenetic mechanisms) for the development of cSCC.

1 Introduction

The primary energy source on earth is the sun. Despite some forms of life at deep sea vents that receive their energy by chemosynthesis from inorganic sources, all life on earth, directly or indirectly, depends on energy produced by plants or other photosynthetic organisms. Furthermore, most processes on our planet, e.g. wind, weather or oceanic streams, also are fuelled by the sun's energy.

Despite our dependence on solar energy and the beneficial effects of ultraviolet radiation (UVR) for e.g. vitamin D production and the mobilisation of nitric oxide from nitrate stores in skin, with consequent reduction in blood pressure [1,2], the sun's UVR also possesses a major health risk. UVR that reaches the earth comprises of 95% UVA (315-400 nm) and 5% UVB (290-315 nm), while UVC wavelengths (100-280 nm) are completely blocked by the ozone layer. Due to depletion of the stratospheric ozone, changes in our lifestyle that lead to increased exposure to UVR and longer life expectancy, skin cancer cases are increasing [3]. Since the early 90s, the incidence of melanoma has increased by 134% [4] and non-melanoma skin cancer cases have increased by 163% [5] in the UK. Although adequate protection against UVR, e.g. sunscreen or responsible habits when it comes to time spent in the sun, is undoubtedly the best protection against skin cancers, studies have shown that even in high-risk groups, awareness for these preventive measures is limited and programs to raise awareness do not have sufficient success [6].

Therefore, developing new strategies to prevent and treat skin cancers are urgently needed. To achieve this, it is necessary to fully understand all aspects of skin cancer biology and develop adequate animal models or other means to study this heterogeneous disease. The work described in this thesis, aims to analyse the global DNA methylation landscape of cutaneous squamous cell carcinoma (cSCC) in preclinical mouse model for cSCC, which was previously developed in our lab.

1.1 Structure of the human skin

With 1.5 to 2 m^2 in adults, the skin is one of the largest human organs and covers the whole body [7,8]. Its primary function is to protect the underlying structures from injury, dehydration, chemicals and invasion by harmful organisms. The skin also has an important role as a sensory organ, as it is covered with sensory nerve ends and is the part of our body that is in contact with our surrounding. Furthermore, the skin is responsible for thermoregulation by both, protecting the body from heat and heat loss, as well as regulating the body temperature by producing sweat.

The skin also serves as protection against ultraviolet radiation. Structural aberrations that are sometimes precursors for cancer, can therefore often be found at areas of high sun exposure. These areas include the face, hands, neck, forearms, forehead and the scalp [9,10].

The skin structure can be broken down into the epidermis, the most superficial layer, the dermis, and subcutaneous tissue.

The subcutaneous tissue, or hypodermis, is the deepest layer of the skin, dividing the dermis and the underlaying muscle tissue. It mostly consists of adipocytes, that not only serve as an energy reservoir, but also as a protective layer against heat loss and mechanical injury [11].

The dermis gives the skin its elastic and tough features. The main cells are fibroblasts, which extracellular matrices contain collagen fibres that bind water. Other structures in the dermis include blood vessels, sensory nerve endings, hairs and arrector pili muscles and sweat glands.

The most outer layer of the skin is the epidermis (**Figure 1**). It mainly consists of keratinocytes and melanocytes. It can be subdivided into for layers: the basal layer, the spinal layer, the stratum granulosum and the stratum corneum. The epidermis does not harbour any blood vessels. Instead, its layers are constantly supplied with oxygen and nutrients by intestinal fluid from the dermis, that drains away as lymph. The basal germinative layer consists of undifferentiated basal keratinocytes and constantly spawns epithelial cells that gradually undergo differentiation as they move up as epidermal layers or strata. When basal keratinocytes differentiate, they move upwards to the spinal layer. Here, they change shape and begin producing their defining proteins, the keratins. When keratinocytes move further up to the stratum granulosum,

they become granulated as they produce keratohyalin granules. These keratohyalin granules are filled with proteins that are rich in histidine and cysteine and bind keratin filaments together [12,13]. Reaching their final differentiation stage in the stratum corneum, keratinocytes become flat and thin. At this point, they are dead, have lost their nuclei and are called squames. Their cytoplasm has been replaced with keratin. These cells are constantly rubbed off by wear and tear. Within a month, humans completely renew their epidermis [9,14].

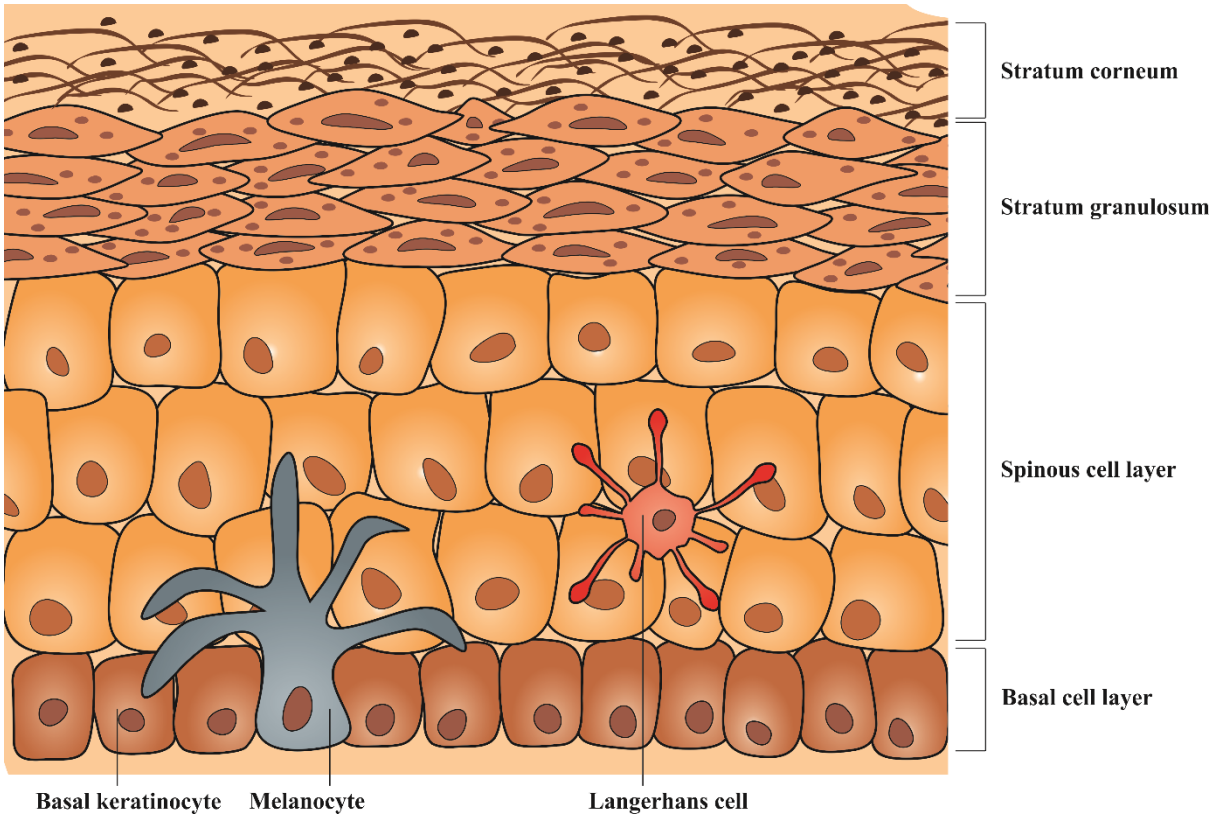

Figure 1: Structure of the epidermis. The basal layer is formed of the **basal keratinocytes**, which have stem cell like properties and give rise to all keratinocytes. When basal keratinocytes divide, the daughter cells move upwards in the **spinous cell layer** and begin to differentiate. As they move upwards, their maturation continues, and they adapt a flattened shape and form keratohyalin granules in the **stratum granulosum**. Keratinocytes end their maturation process in the **stratum corneum**. Here, cells are dead, have lost their nuclei and their cytoplasm is substituted with keratin fibres. Constant wear and tear sheds of the stratum corneum and new keratinocytes move upwards to replace it. The basal cell layer also contains **melanocytes.** These cells produce the pigment **melanin**, which protects the skin from UV radiation and gives hair its colour. **Langerhans cells** are dendritic cells in the spinous cell layer that phagocytose pathogens that invade the skin. They then travel to nearby lymph nodes to stimulate an immune response by presenting pathogenic antigens [12]. Figure self-generated.

1.1.1 Keratinocytes

As all keratinocytes are derived from the basal layer of the epidermis, the proliferative potential of these basal cells must be maintained throughout life. Furthermore, keratinocytes must express a distinct set of keratins during their differentiation process to ensure normal skin formation. In basal keratinocytes, expression of Keratin 5 and 14 (K5, K14) as well as their proliferative potential is maintained by *Tp63* gene expression. This member of the p53 family inhibits expression of cyclin-dependant kinase inhibitor 1 (p21) and therefore allows proliferation [15]. When keratinocytes move up to the spinous cell layer, the activation of Notch signalling represses p63 activity and keratinocyte differentiation and cell cycle arrest are initiated [16–18]. Additionally, Notch regulates expression of specific keratins (e.g. K14) as well as loricrin and filaggrin.

The progressing differentiation stages of keratinocytes define the layers of the epidermis. Basal keratinocytes express K5 and K14, while keratinocytes in the spinal layer express K1 and K10. When they further differentiate, keratohyalin granules are formed and cells adopt a flattened shape, a characteristic feature of the corneocytes. These cells are filled with keratins and eventually lose their nucleus to form the stratum coronium. Aberrant regulation of this process can lead to abnormal growth of the epidermis and skin diseases such as cancer [19,20].

1.2 Cancers of the human skin

Cancers of the human skin can be divided into two general types: melanoma and non-melanoma skin cancer (NMSC, also called keratinocyte cancers). Skin cancers are the most common malignancy in Caucasians and their incidence is steadily rising. Over the past 50 years, melanoma cases in adults have risen by 0.6% annually, while the average rise of NMSC cases is 3-8% per year since the 1960s [21].

The GLOBOCAN Global Cancer Statistics 2018 reported 1,042,056 new cases of NMSC worldwide (5.8% of all cancers) and 287,723 new cases of melanoma (1.6% of all cancers). While NMSC related deaths contributed to 0.7% of all cancer related deaths (65,155 deaths), the much rarer melanoma lead to almost the same number of deaths (60,712 deaths, 0.6% of all cancer related deaths). It is worth noting, that skin cancers, both melanoma and NMSC are over-represented in Oceania, where melanoma contributes to 6.9% of the new cancer cases (compared with 1.6% worldwide) and NMSC accounts for 28.1% of new cancer cases (compared with 5.8% worldwide). But NMSC are also very common in North America (20.3% of new cancer cases) and Europe (7.5% of new cancer cases) [22,23]. However, these statistics may be biased, as some cancer registries, the basis for the GLOBOCAN statistics, do not adequately register NMSC [21,24,25].

1.2.1 Skin cancer risk factors

The risk for certain types of cancer is influenced by lifestyle factors. In 1761 the English physician John Hill discovered a correlation between excessive tobacco snuff and nasal cancer (despite this, tobacco companies denied a connection between tobacco consumption and cancer for another 200 years). A few years later, the London surgeon Percivall Pott noticed that there was a substantial number of skin cancers of the scrotum in men, who in their youth had been working as chimney sweeps. The evidence that certain cancers were more prevalent in certain groups of workers became more apparent and gave rise to occupational medicine. Examples include lung cancer in miners (later found to be caused by radiation from ores), breast cancer in nuns or increased rates of cancer in physicians and others, exposed to X-rays. The most compelling studies came in 1949 and 1950, when two groups of epidemiologists reported that lung cancer incidence was more than 20 times higher in heavy cigarette smokers [26].

Solar radiation, especially UVR, is the most ubiquitous carcinogen in the world. For skin cancers, UVR is the main risk factor. UVR directly damages DNA, when energetic UVB (280-315 nm) give rise to pyrimidine dimers and other photoproducts, which cannot be appropriately repaired, leading to mutations [27]. Furthermore, UVR causes the formation of reactive oxygen species (ROS) as well as reactive nitrogen species (RNS) thus causing oxidative DNA damage, e.g. 8-hydroxy-2'deoxyguanosine [28]. Additionally, UVR leads to immunosuppression, a known risk factor for NMSC [21]. The skin has a build-in defence against UVR. The melanocytes produce a dark pigment, melanin, which is synthesised from the amino acid tyrosine. Melanin absorbs UVR and protects against its harmful effects [14].

Risk factors for cutaneous squamous cell carcinoma will be discussed in more detail in **Section 1.2.3.2**.

1.2.2 Melanoma

While the majority of skin cancers are NMSCs, melanomas have a much higher mortality rate. In 2018, worldwide there were 5 times more NMSC than melanoma cases, while the deaths related to both skin cancer types were almost the same [22]. Melanoma's cells of origin are melanocytes, cells that can be found in the basal epidermis, hair follicles, in the choroidal layer of the eye and at mucosal surfaces. They express melanocortin receptor 1 (MC1R) and produce and release melanin after stimulation by melanocyte stimulating hormone (MSH). MSH is produced by keratinocytes in response to UVR and subsequent DNA damage [29,30].

As for all types of skin cancer, UVR is the primary carcinogen contributing to melanoma development. In Caucasians, melanoma arising at chronically sun-exposed areas (e.g. the head and neck), are often diagnosed in middle age and older patients (>55 years of age). The main genetic drivers in melanoma are B-Raf proto-oncogene (*BRAF*), neurofibromin (*NF1*) and *NRAS* mutations, but melanomas also bear a high mutation burden. Melanoma in younger patients (<55 years of age), often arise at intermediately sun-exposed areas (e.g. the trunk and proximal extremities) and usually bear the $BRAF^{V600E}$ mutation and a lower overall mutation load [31–33].

Interestingly, 80% of benign melanoma precursors, have a *BRAF* mutation, that only results in limited melanocyte proliferation, pointing towards the need for additional

driver mutations (usually *CDKN2A* or *TERT*). Melanoma development clearly does not follow a singular evolutionary pattern [34–40].

Melanomas are one of the most aggressive types of skin cancer. In contrast to most NMSCs, melanoma often possess a high metastatic potential. This is due to gene mutations, that favour the invasion of adjacent tissues and a tumor microenvironment, which facilitates such infiltration. A key player in melanoma invasion are matrix metalloproteases (MMPs), particularly MMP-9 and MMP-2. These MMPs cleave proteins of the extracellular matrix and therefore allow tumor cells to enter the bloodstream [41–43].

The majority of melanoma (up to 90%) harbour mutations that lead to aberrant mitogen-activated protein kinase (MAPK) activation and subsequent cell cycle deregulation and limited apoptotic potential. This common feature has led to new treatment options: tyrosine kinase inhibitors and immune checkpoint inhibitors. In fact, melanoma survival has increased by 22% in England and Wales over the past 40 years (from 75% to 97%) [44].

Biomarkers for melanoma therapy response or detection of tumor-derived circulating cell-free DNA (ctDNA) specific to melanoma (liquid biopsy) are being developed, but the best "treatment" for melanoma certainly is prevention. Cancer Research UK states, that 86% of melanoma in the UK are caused by overexposure to UVR and therefore are preventable [45].

1.2.3 Non-melanoma skin cancers

Non-melanoma skin cancers (NMSC), also known as keratinocyte skin cancers, represent the most common type of skin cancer in humans. As their name suggests, the progenitor cells for keratinocyte skin cancer are keratinocytes. NMSCs are the most common human malignancy, with the highest incidence in Australia, where there are more than 1000 cases per 100,000 person-years [3]. Depletion of stratospheric ozone, increased exposure to solar radiation and longer life expectancy has led to an increase in NMSC incidence. Cancer Research UK states, that NMSC incidence has increased by 147% since the early 1990s and by 59% in the past decade alone. Although NMSCs have a relatively low mortality rate, accounting for less than 1% of cancer-related deaths, in 2016 there were around 950 NMSC-related deaths in the UK and NMSC is among the 20 most common causes of death from cancer [46].

In general, NMSC are treatable and mostly, lesions can be easily removed by various techniques (curettage, electrodisection, cryotherapy, Mohs surgery of standard surgical excision) with cure rates as high as 96%. However, most of these therapies are associated with high morbidity and reduced quality of life. Treatments for NMSC are discussed in **Section 1.2.3.5**.

The vast majority (99%) of NMSC can be further divided into two subgroups: basal cell carcinoma (BCC) and cutaneous squamous cell carcinoma (cSCC), with a ratio of 80:20 between BCC and cSCC.

1.2.3.1 Basal Cell Carcinoma

While Basal Cell Carcinoma (BCC) typically is slow growing and has a low rate of metastasis and seldom causes death but can be destructive and disfiguring locally. BCC is most common in Caucasians and elderly people [47–49], but incidences are on the rise, especially among younger females (likely due to increased tanning behaviours, both naturally and in tanning salons) [50,51].

The main pathological event in BCC genetics is upregulation of hedgehog (HH) signaling, a pathway involved in development, stem cell maintenance as well as tissue repair and regeneration. Inactivation or loss of Protein patched homolog 1 (PTCH1) function is a feature of over 90% of BCCs as well as activating Smoothened (SMO) mutations. Other relevant mutations in BCC include *TP53*, Ras family members, *NOTCH 1* and *2* as well as mutations in the telomerase reverse transcriptase (*TERT*) promoter (summarized in [49]).

As this thesis is focussing on the other form of NMSC, cutaneous squamous cell carcinoma, BCC will not be discussed further.

1.2.3.2 Cutaneous Squamous Cell Carcinoma

The precursor lesion of cutaneous Squamous Cell Carcinoma (cSCC) is actinic keratosis (AK). AKs appear as single or multiple lesions on sun exposed skin, especially the forehead, hairless scalp areas, the nose and ears, cheeks, bottom lip as well as forearms and the back of the hand. Men are more likely to get AK than women, and incidences are higher in elderly people [52]. People that are highly exposed to sunlight, are more likely to develop AK (e.g. people working outdoors). Chronically immunosuppressed individuals are also at high risk. AKs greatly vary in size (between 1 mm and 2.5 cm) and can either be the same colour as the skin (in these cases they

are easier felt than seen), reddish or brownish and can have white keratosis or yellow encrustation. Histologically characteristic for AK are atypical (sometimes mitotic) keratinocytes with enlarged, hyperchromatic or pleomorphic nuclei. In contrast to cSCC, AK is clearly demarcated from normal epidermis [53,54].

Cutaneous SCC is a malignant epithelial tumor with keratinocytic diffentiation. Premalignant forms often only present as hyperkaratinic plaques but if they proliferate unchecked, the plaques become thicker, erode and can ulcerate. Ulcerating cSCC also tend to have bacterial superinfections. Especially for elderly people, returning bleeding or secretion rather than the, often slowly growing, tumors are the reason to consult a dermatologist. Although cSCC is mostly known as a disease of elderly people, genetic prepositions or extensive exposure to UVR can lead to the development of these tumors in younger individuals (for risk factors see **Section 1.2.3.2.1**). For people that are highly sensitive to UVR (e.g. Xeroderma pigmentosum or albinism), cSCC even may develop in childhood [53,54].

Cutaneous SCC accounts for roughly 20% of all NMSC cases. In contrast to BCC, cSCC carry a substantial risk for metastasis with an annual incidence of 4% and accounts for the majority of metastasis related deaths [21].

While cure rates for localized cSCC are as high as 96% when appropriately treated (mostly by excision of the affected area), locoregional and metastatic cSCC have a dismal prognosis at more advanced stages, with 5-year survival rates below 30%. Metastasis of cSCC occurs in 85% of cases in regional lymph nodes and 15% of cases in more distant locations (e.g. lungs, liver, brain, skin or bone). The ten-year survival chances for patients with lymph node metastases are 20% and only 10% for patients with distant metastasis [21].

1.2.3.2.1 Risk factors for cutaneous squamous cell carcinoma

The main risk factor for cSCC is exposure to UVR. This leads to a very high mutation burden with as much as 1 mutation per 30 kb of coding sequence, making cSCC the most mutated cancer type [55]. The vast majority of these mutations are “UV-signature mutations”, i.e., G to A or C to T transitions, which makes G- and C-rich genes more likely to become mutated [56]. Known driver mutations in cSCC are *TP53* (90% of cSCC, early event), *NOTCH* (75%), *CDKN2A* (50% with additional epigenetic inactivation) and *TGF-β*. Interestingly, *Ras* mutations are relatively

uncommon [57,58]. This is particularly notable when considering that the most commonly used chemically- and genetically-induced mouse models for cSCC are often Ras driven [59,60].

Although UVR is the main carcinogen leading to development of NMSC, other risk factors include exposure to arsenic, tar or certain polycyclic aromatic substances. Cutaneous SCCs may also develop in areas of radiodermatitis and on keratoses caused by X-rays or arsenic [54].

Furthermore, infection with human papilloma viruses (HPV) is associated with cSCC [54] and HPV DNA can be detected in 30%-60% of cSCC of immunocompetent patients. Interestingly, the prevalence of HPV infections is even higher in AK (up to 93%) and can reach 100% in immunosuppressed individuals, which indicates the crucial role of the immune system in preventing cSCC [61–65]. It has been proposed, that vaccination against HPV types associated with cSCC may be an efficient prevention strategy, as it has been demonstrated for HPV types causing cervical cancer [66–68].

Especially for high risk groups, cSCC represents a significant problem. Individuals, who are genetically predisposed, immunosuppressed patients and/or those receiving thiopurine therapies or people living in high-risk areas (e.g. Oceania) are all more likely to develop cSCC. Solid organ transplant recipients (SOTRs) for example, have a greatly increased risk (60 to 200-fold compared to the general population) to develop cSCC [69]. This risk increases with the duration of immunosuppression and decreases if immunosuppression is terminated. Conventional means of treating cSCC are also only partially successful as lesions are multiple, span large areas and frequently relapse [70,71]. In a single patient, more than 100 lesions may develop in one year and are likely to metastasize [3,72,73].

In the US, the incidence ratios of cSCC are estimated at 1,355 per 100,000 person-years in SOTRs, while this number is only 38 per 100,000 person-years in the general population. The National Cancer Institute states that the incidence rate for cSCC in SOTRs is nearly 5 times that of all other cancers combined and that additional risk factors include age at transplantation, duration of immunosuppressive therapy, skin type, gender and the transplanted organ [74]. Other diseases, which are treated with immunosuppressive drugs, such as inflammatory bowel disease, autoimmune diseases

or rheumatic arthritis, carry an increased risk for development of cSCC [75–77]. Diseases associated with acquired immunodeficiency, like HIV/AIDS or leukaemia, also show higher incidence rates of cSCC. For HIV infected individuals, adequate therapy with antiretroviral medication may reduce cSCC risk [78], but in chronic lymphatic leukaemia (CLL), cSCC prognosis is worse with increased rates of metastasis and recurrence [79,80].

How exactly the innate and acquired immunodeficiency causes such a massive increase in cSCC risk is not entirely clear. It is likely, that in immunosuppressed individuals, tumor surveillance is impaired and these individuals are more susceptible to HPV infection. Furthermore, certain immunosuppressive drugs themselves can have carcinogenic effects and are likely to add to the already elevated risk [3]. Thiopurines, especially azathioprine, cause enhanced UVA sensitivity and UVA-induced DNA damage as well as an increase in mutations caused by UVB due to reduced UVB-induced DNA damage repair [81,82]. Interestingly, there is a specific azathioprine-associated mutation signature in cSCC [83]. Another immunosuppressant, cyclosporin, reduces UVR-induced DNA damage repair and apoptosis, as well as ATF3 induction and suppression of senescence via p53 [84,85]. Other drugs used in transplantation or treatment of immune diseases may also contribute to cSCC risk, but due to limited data available, the evidence is not conclusive [86–88].

In addition to mutations, epigenetic alterations are considered one of the hallmarks of cancer, including skin cancer [89–94]. These will be discussed in **Section 1.3.4**.

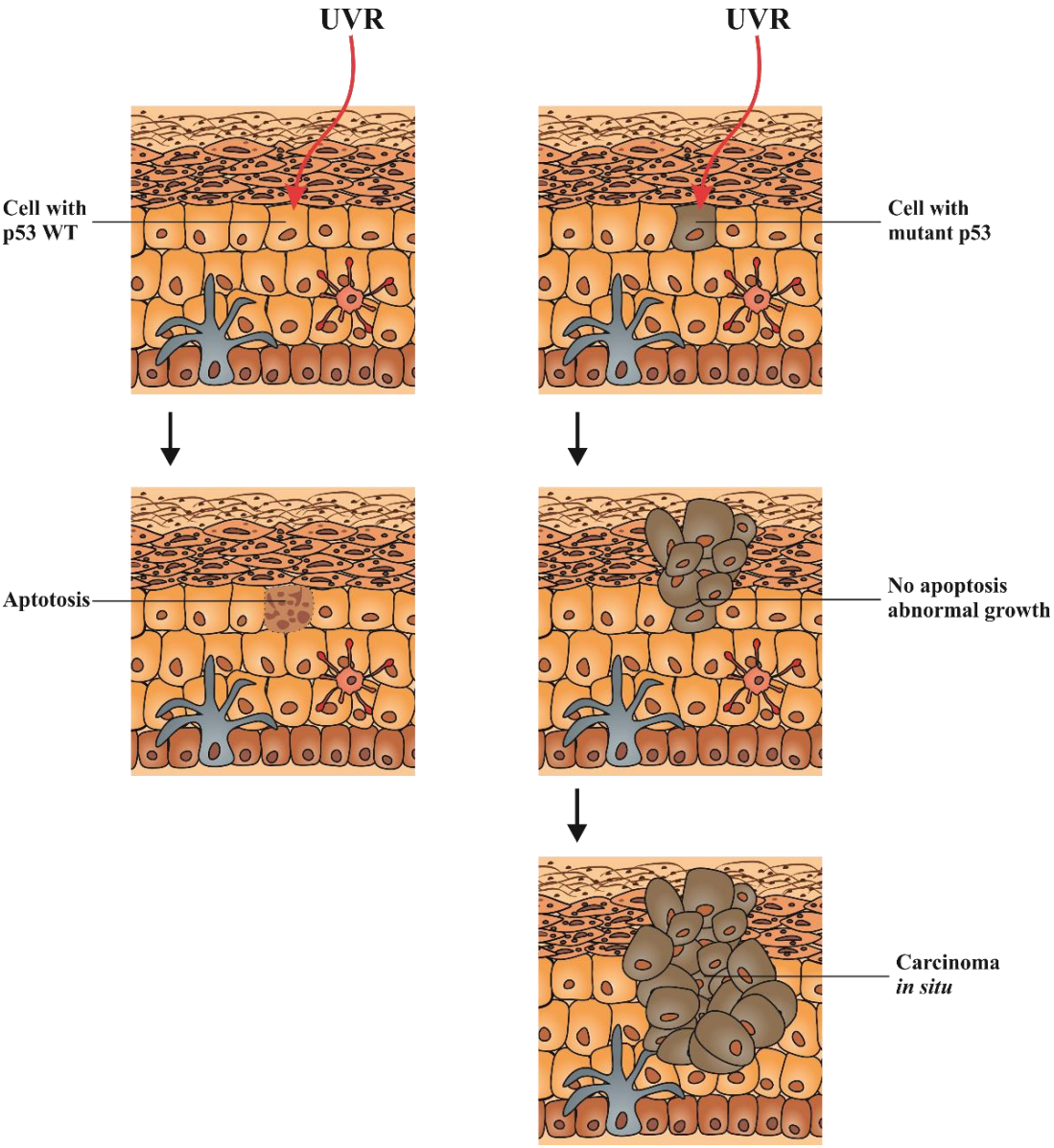

Figure 2: The effect of UV radiation (UVR) on the human skin. UVR can damage the DNA of skin cells. In cells with p53 wild type (WT), DNA damage is repaired, or cells undergo apoptosis if the damage is too severe to be repaired. Cells with p53 mutations do not undergo apoptosis and allow damaged cells to grow abnormally leading to the development of cancer. Figure adapted from Alam and Ratner 2001 [21].

1.2.3.3 Cutaneous squamous cell carcinoma genetics

As mentioned previously, cSCC is the most mutated human cancer. The sheer amount of mutations makes is challenging to identify driver mutations of cSCC. Chromosomal aberrations and copy number alterations show cSCC's genomic instability and create a complex molecular landscape. Furthermore, a mutation burden similar to the one seen in many cancers and genes that are considered driver mutations in cSCC are also present in keratinocyte clones in skin that appears to be completely normal [56].

The vast majority of mutations in cSCC are "UV-signature mutations", i.e., G to A or C to T transitions, which makes G and C rich genes more likely to undergo mutations [56,57,59]. The tumor suppressor gene *TP53*, encoding the protein p53, is frequently mutated in human cSCC. *TP53* mutations are considered and early event in cSCC development and interestingly, these mutations do also exist in normal-appearing skin [95,96]. Furthermore, *TP53* mutations are more frequent in metastatic cSCC (85%) compared to non-metastatic cSCC (54%) [97]. Up to 70% of *TP53* mutations in cSCC can be attributed to UVR. Normally, UV induced DNA damage is repaired or, if the damage is too severe, cells enter apoptosis through p53 induced pathways. Cells with *TP53* mutations not only have a proliferative advantage [98], they furthermore cannot enter these apoptotic pathways and may give rise to cSCC [99] (see **Figure 2**).

The *KMT2D* encodes for the Lysine Methyltransferase 2D and is one of the most frequently mutated genes in cancer, especially epithelial cancers [100] including cSCC where *KMT2D* is mutated in 69.2% of cases [101]. KMT2D has been shown to with p63 and loss of KMT2D is associated with reduced p63 target gene expression, likely due to a global loss of enhancer histone marks [100].

In skin, NOTCH receptors are important for stemness and promote epidermal differentiation, thereby inhibiting skin tumorigenesis. NOTCH1 and NOTCH2 are mutated in 75% of human cSCCs [57,58,96]. In the canonical NOTCH signalling pathway, NOTCH ligand binds to the NOTCH receptor on the cell surface. Binding leads to cleavage of the NOTCH intracellular domain (NICD) from the receptor by ADAM protease. The NICD then translocate to the nucleus and activates transcription. Inhibition of NOTCH signalling promotes keratinocyte-dependant cSCC formation and NOTCH signalling is down-regulated in cSCC [102,103].

The *CDKN2A* locus encodes for the $p16^{INK4a}$ and $p14^{ARF}$ tumor suppressor genes. UVR can lead to mutations in sporadic cSCC and BCC, as well as cSCCs that develop in patients with xeroderma pigmentosa (these patient have severe defects in nucleotide excision repair (NER) proteins and are extremely sensitive to UVR) [104–107]. Additionally, *CDKN2A* genes are frequently silenced by promoter hypermethylation in cSCC [108]. Transforming growth factor beta (TGF-β) possesses a tumor suppressor role in skin and can also be mutated in cSCC [109,110]. Ras mutations are relatively uncommon in cSCC [57,58]. This is particularly interesting when considering that chemically and genetically induced models for cSCC are often Ras driven [59,60] (models for cSCC will be further discussed in **Section 1.2.3.6**).

Table 1: Mutation rates of genes in aggressive cSCC according to Pickering *et al.* 2014 [101]**.** Mutations in *TP53* are present in the majority of cSCCs. *KMT2D, NOTCH 1* and *2* and *CDKN2A* are also frequently mutated. Activating *RAS* mutations are relatively uncommon.

	Pickering *et al*. 2014 [n=39]	
	n	**%**
TP53	37	94.90%
KMT2D	27	69.20%
NOTCH1	23	59.00%
NOTCH2	20	51.30%
CDKN2A	17	43.60%
HRAS	8	20.50%
NRAS	2	5.10%

Depending on the type and frequency of genomic aberrations, cancer genomes can be classified into different mutation signatures. These signatures can help to identify cancers into different subtypes (see https://cancer.sanger.ac.uk/cosmic/signatures) [111,112]. Interestingly, a novel mutation signature has been identified in human cSCC from patients, that received the immunosuppressive drug azathioprine [83]. This again highlights the profound effect of azathioprine on cSCC development and the need to further investigate the disease in the high-risk group of immunosuppressed individuals.

1.2.3.4 Cutaneous squamous cell carcinoma pathology

Commonly, cSCCs begin as asymptomatic small plaques or nodules. They can enlarge over time and become keratoachantoma-like, ulcerate, become necrotic or botryomycotic (a chronic granulomatous bacterial infection) [113,114]. cSCCs can be subdivided into the following subtypes:

Verrucous cSCC [113,114]:

- Well-defined, exophytic, cauliflower like growth
- Locally invasive
- Low metastatic potential

Spindle cSCC [113–115]:

- Relatively rare but highly aggressive
- Arising from sun-exposed sites
- Not always keratinocyte differentiation
- Positive staining for cytokeratins and epithelial membrane antigen

Desmoplastic cSCC [113,114,116]:

- High infiltrative growth
- Often perineural or perivascular
- High amounts of stroma and narrow cord cells
- High risk for perineural invasion, metastasis and recurrence

Acantholytic cSCC [114,117]:

- Intramural pseudo gland structures
- Greater metastatic risk compared to common cSCC

Adenosquamous cSCC [114,117]:

- Expression of Keratin 7
- Mucosecretory tubular structures

According to the TNM (Tumor, Nodes, Metastasis) system of the American Joint Committee of Cancer (AJCC), cSCC can be classified into four clinical stages (see **Table 2** and **Table 3**) [114].

Table 2: TNM classification of cSCC according to AJCC.

	TUMOR
TX	Primary tumour cannot be assessed
TIS	Carcinoma in situ
T1	Tumour <2 cm at largest horizontal width +0–1 high-risk feature
T2	Tumour ≥2 cm but ≤ 4 cm at largest horizontal width +2–5 high-risk features or tumour >2 cm at largest horizontal width
T3	Tumour ≥4 cm or minor bone erosion or perineural invasion or deep invasion
T4A	Tumour with gross cortical bone/marrow invasion
T4B	Tumour skull base invasion and/or skull base foramen involvement
	Lymph nodes metastasis
NX	Regional lymph nodes cannot be assessed
N0	No regional lymph node metastases
N1	Metastasis in a single ipsilateral lymph node, ⩽3 cm in greatest dimension and ENE (-)
N2A	Metastasis ipsilateral lymph node larger than 3 cm but no larger than 6 cm in greatest dimension and ENE (-)
N2B	Metastases in multiple ipsilateral lymph node, none larger than 6 cm in greatest dimension and ENE (-)
N2C	Metastasis in bilateral or contralateral lymph nodes, none larger than 6 cm in greatest dimension and ENE (-)
N3A	Metastasis in a lymph node larger than 6 cm in greatest dimension and ENE (-)
N3B	Metastasis in any node(s) and ENE (+)
	Distant metastasis
M0	No distant metastases
M1	Distant metastases

Table 3: Clinical stages of cSCC according to AJCC.

CLINICAL STAGES			
STAGE 0	Tis	N0	M0
STAGE I	T1	N0	M0
STAGE II	T2	N0	M0
STAGE III	T3	N0	M0
	T1	N1	M0
	T2	N1	M0
	T3	N1	M0
STAGE IV	T1	N2	M0
	T2	N2	M0
	T3	N2	M0
	Every T	N3	M0
	T4	Every N	M0
	Every T	Every N	M1

1.2.3.5 Cutaneous squamous cell carcinoma treatment

Treatment of locally confined cSCCs normally involves surgical excision of the affected area. The vast majority (approximately 96%) of cSCCs are curable by this method. However, the remaining 4% can metastasize and have 3-year survival rate of 56% and a 5-year survival rate of just 25-35% [118].

Normally, complete excision is performed, and methods have been developed (such as Mohs microscopical surgery) to allow histopathological control of the tumor type and complete excision. Excision margins should be adapted to the tumor size and aggressiveness [119]. Surgery can also be combined with plastic reconstruction [120]. Surgery has a lower chance of cSCC recurrence than other techniques, including curettage, cryotherapy, radiotherapy or photodynamic therapy [120]. Radiotherapy can be used as a complementation therapy to surgery, especially when complete excision of the affected area is unsuccessful or not possible [121]. However, especially in immunosuppressed patients, radiotherapy can lead to the formation of new tumors and should therefore only be applied in immunosuppressed patients with short life expectancy [114]. Furthermore, a higher rate of metastasis has been observed for verrucous cSCCs treated by radiotherapy [114]. If cSCC has spread to lymph nodes, dissection of the affected and possibly additional nearby nodes is the treatment of choice [122].

Advanced cSCCs can be treated with chemotherapy. Especially platinum-based drugs, 5-floururacil, gemcitabine and methotrexate show good initial responses in approximately 80% of cases. However, very few tumors respond to these drugs for longer periods of time, so that chemotherapy is mostly palliative [122–125].

Cetuximab, a monoclonal antibody against epidermal growth factor receptor (EGFR) in recent years has been used for treatment of advanced cSCCs. Although efficacy is good, severe side-effects limit cetuximab's potential [126,127]. EGFR inhibitors have response rates that vary from 31 to 69% and are an additional option for advanced cSCC treatment [3,128].

A combination therapy with 13-cis-retinoic acid, Interferon-α (IFN-α) and cisplatin shows a response rate of 34% for patients with advanced cSCC, with 17% of patients showing complete and 17% showing partial remission [129]. Furthermore, 90% of advanced local, but, inoperable, cSCCs and 23% of patients with distant metastasis respond positively to the combination of 13-cis-retinoic acid and IFN-α [130].

1.2.3.6 Modelling Cutaneous squamous cell carcinoma

cSCC is a common malignancy, and therefore it is crucial to have adequate models to investigate this type of cancer. Patient samples are readily available, but intervention studies in humans are not feasible, as cSCCs can take decades to develop. Animal models are essential to test candidate agents for prevention in a manageable timespan. Because of the high mutation burden, modelling cSCC is challenging.

A commonly used skin carcinogenesis model is Harvey-Ras ($Hras^{Q61L}$) driven formation of papilloma. This is induced by topical administration of the carcinogen 7,12-dimethylbenz[a]anthracene (DMBA), followed by chronic application of the tumor promoter 12-*O*-tetradecanoylphorbal-13-acetate (TPA). The resulting mouse tumors (90%) have driver mutations in *Hras*, *Kras* or *Rras2*, with the characteristic DMBA/TPA mutation signature (A>T and G>T transversions) [131,132]. Other mutations in those tumors have a different mutation signature, suggesting that these mutations occur at later time points during tumor development [131]. The DMBA/TPA model is an excellent model for Ras driven tumors, but in contrast to human cSCC, skin tumors produced by the DMBA/TPA model, do not carry the broad spectrum of mutated genes or the extraordinarily high number of mutations, with an

average of 5.2 mutations per Mb [132] compared to 30 to 50 mutations per Mb [58] for the human tumours and therefore do not adequately reflect the human disease.

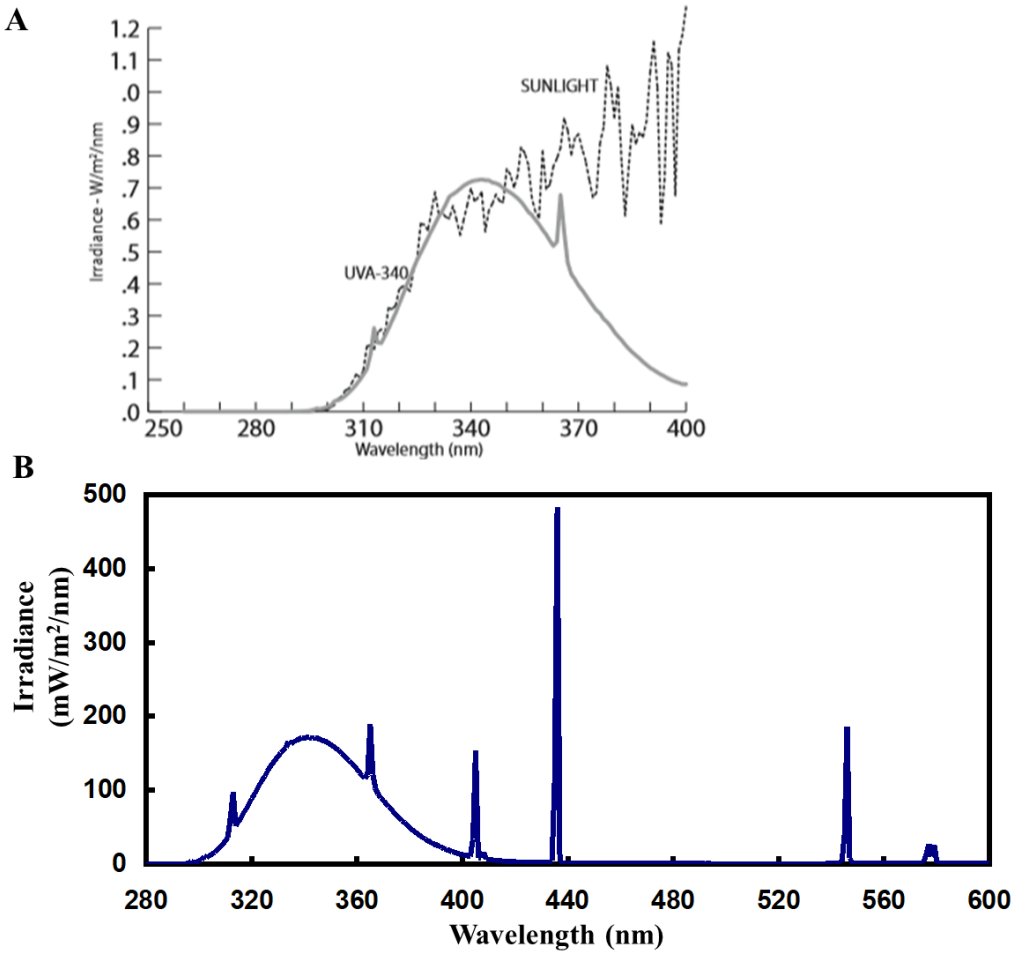

Figure 3: Emission spectrum of UVA-340 lamps. A: Emission spectrum of UVA-340 lamps compared to sunlight according to the lamp manufacturer (Q-Labs). **B:** Emission spectrum of UVA-340 lamps as measured in our lab [60]. **UVA-340 lamps are the best available simulation of sunlight in the critical UV region.**

Another way to reliably produce skin tumors in mice is exposure to UVB radiation. UVB however, only comprises 5% of the solar UVR that reaches the surface of the earth. Undoubtedly, UVB is more carcinogenic, but 95% of the solar UVR is UVA and is not accounted for in this model. Especially for high risk populations, the UVA component is highly relevant. This includes patients that receive life-long immunosuppressive or anti-inflammatory therapy (e.g. SOTRs or patients with inflammatory bowel disease). Thiopurine (administered as immunosuppressive drugs) metabolites are incorporated in the DNA of proliferating skin cells and sensitize these cells particularly to UVA radiation damage [71,82,133,134]. These high-risk groups

are in dire need for strategies to prevent cSCC, as their risk to develop cSCC is approximately 100-fold higher compared to the general population. Models that solely use UVB may not fully display the molecular mechanisms that lead to tumor formation in these individuals.

We previously developed a preclinical mouse model to overcome the limitation of the existing models for cSCC. The principal aim was to mimic human cSCC carcinogenesis and development. The hope was, that by subjecting mice to a very similar carcinogen (a combination of UVA and UVB) the resulting murine tumors would resemble the human disease.

We therefore chose immunocompetent SKH-1 hairless mice and chronically and intermittently (2 times a week for 15 weeks) subjected them to suberythermal doses of solar-simulated UVR (ssUVR), consisting of both, UVA and UVB wavelengths with a similar spectrum compared to solar UVR (see **Figure 3**) [60]. UV irradiation is then discontinued, and mice are monitored. Essentially all mice develop skin tumors in the subsequent 15 to 20 weeks. Histological examination of the murine tumors revealed a spectrum of mouse cSCCs (mcSCCs) that is very similar to the spectrum of human cSCCs (hcSCCs), ranging from AK with no invasion, to AK with early dermal invasion and both, moderately to well differentiated cSCCs [60,135]. Tumors were also microdisected and isolated DNA was used for whole exome sequencing. With a median single nucleotide polymorphism (SNP) rate of 155 mutations per Mb, mutation burden was higher than in hcSCC. The majority (>78%) of mutations were C.G>T.A transitions, consistent with a UVR signature. Also consistent with hcSCCs, the most frequently mutated genes were *Trp53* (83% of mcSCCs) as well as *Notch* (~55%) receptor family genes. Furthermore, the mutations in key driver genes were in similar positions in ssUV cSCC compared to human cSCC [59]. The similarities between mcSCC arising in our model and hcSCC in histology and genetics suggest, that this model is superior to the DMBA/TPA model, that produces papilloma, and may have advantages over models that only use UVB as the carcinogen.

In this thesis, we aimed to further validate our ssUVR induced mouse model by investigating changes in global DNA methylation and comparing it to DNA methylation in human cSCC.

1.3 Epigenetic regulation of gene expression and genome stability in normal and cancer cells

In addition to mutations leading to constitutively active oncogenes or inactive tumor suppressor genes, epigenetic alterations have been demonstrated to play a crucial role in cancer development and progression. Epigenetic regulations are defined as heritable, but potentially reversible alterations that, in contrast to mutations, do not result in changes in the DNA sequence. Epigenetic mechanisms include:

- DNA methylation, that can inactivate promoters, enhancers or other regulatory elements
- histone tail modifications, packing the chromatin more or less tightly, therefore influencing DNA accessibility for transcription factors and the translational machinery
- expression of micro RNAs (miRNAs) that control gene expression by RNA interference as well as long non-coding RNAs (lncRNAs) that can bind mRNAs and even carry out enzymatic functions

The epigenetic regulation of gene expression is briefly summarized in **Figure 4**. DNA methylation, especially at promoter regions is recognised by methyl-CpG-binding domain containing proteins (MeCP). This class of proteins, depending on the cellular context and structure of the CpG island, can recruit DNA methyltransferases (DNMTs) and histone modifiers like histone deacetylases (HDAC) and histone methyltransferases (HMT). This in turn can further modify the epigenetic landscape of the region. Normally, CpG-dense promoter regions are unmethylated, while intragenic and repetitive elements are silenced by high methylation. Unmethylated promoters can bind transcription factors (TF) and activate transcription via RNA polymerase and co-activators. If these regions are methylated, TF binding is inhibited, and transcription of the gene is prohibited. Genes that are silenced by DNA methylation can be re-activated by ten-eleven-translocases (TET) that remove methyl-groups from DNA. DNA methylation and TET proteins will be discussed in greater detail in **Sections 1.3.1** and **1.3.2**. Gene expression is highly regulated by dynamic positioning of active (histone acetylation, H3K4me3) and repressive (H3K27me3) histone marks at promoter regions and regulatory elements. HDACs deacetylate, while HATs acetylate histone tails. Histone methyltransferases (HMTs) and their counterpart enhancer of zeste homolog 2 (EZH2) add or remove methylation

marks from histone tails. In cancer, EZH2 is often overexpressed and silences expression by H3K27 tri-methylation. Furthermore, micro RNAs (miRNA) genes underlay the same regulatory processes as other genes. miRNAs can inhibit gene expression by destroying mRNA transcripts via the RNA-induced silencing complex (RISC). miRNAs are further regulated by expression of the proteins that are responsible for their maturation and function. These components often are also regulated by epigenetic mechanisms (summarized in [89,90,136]).

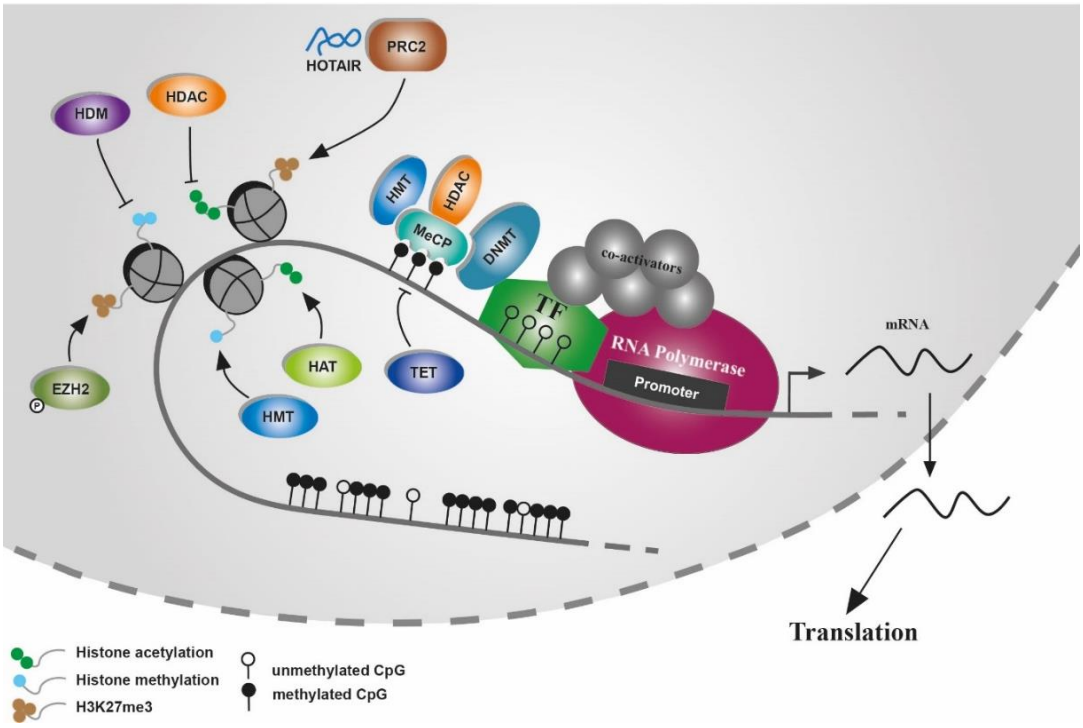

Figure 4: Epigenetic regulation of gene expression. Further explanations are given in the text. **Abbreviations: TF (**Transcription factor), **HDAC** (histone deacetylase), **HAT** (histone acetyl transferase), HMT (Histone methyl transferase), **HDM** (Histone demethylase), **DNMT** (DNA methyl transferase), **TET (ten-eleven-translocase), MeCP** (methyl-CpG-binding domain containing protein), **PRC2** (polycomb remodelling complex 2), **EZH2** (enhancer of zeste homolog 2), Figure modified from Pudenz *et al*. 2014 [89].

1.3.1 DNA methylation

DNA methylation was first discovered and therefore is the best studied of the three type of epigenetic modifications. DNA methylation occurs at the 5C position of cytosine (5-methyl-cytosine, 5mC) in the context of CG dinucleotides (CpG) but can also be observed outside of CpGs in a CHH or CHG context (where H is either an A, C or T) in embryonic stem cells and plants. The key writers of DNA methylation are DNA methyltransferases (DNMTs) 1, 3a and 3b as well as ten-eleven translocases

(TETs) 1, 2 and 3 (**Figure 5**). While DMNT1 is responsible for maintaining the existing DNA methylation pattern after DNA replication, DNMT3a and 3b are involved in the *de novo* methylation of previously unmethylated regions. TET proteins convert 5mC to 5-hydroxomethyl cytosine (5hmC) and even further oxidize 5hmC to 5-formyl cytosine (5fC) and 5-carboxy cytosine (5caC). TET proteins are responsible for DNA demethylation by either passive or active mechanisms [137–142].

In normal cells CpG dense regions (CpG islands) are often located at gene promoters as well as the untranslated region and exon 1 of genes. These CpG islands are often unmethylated and therefore allow active transcription. Approximately 6-8% of genes have hypermethylated promoter regions that silence these genes and maintain tissue-specific gene expression. In contrast, hypomethylated promoters allow active gene transcription. Regions with low CpG contend are often found in repetitive sequences and are normally highly methylated. This contributes to genome stability by silencing endoparasitic sequences and transposons and therefore prevents chromosomal instability, translocations and gene disruption. Furthermore, methyl-CpG-binding domain containing proteins (MeCPs) can specifically bind to methylated DNA sequences and recruit co-repressors such as histone lysine methyl transferases (HMTs) and histone deacetylases (HDACs). If DNA methylation occurs at transcription factor (TF) binding sites, these sites may be protected from TF binding, therefore preventing or down-regulating transcription of certain genes [89–92].

In addition to their mutation profile, tumors have a distinct DNA methylation pattern that is different from the DNA methylation landscape in normal cells [90,143,144]. Global DNA hypomethylation in cancer cells contributes to genome instability and the expression of aberrant transcripts from repetitive sequences that contribute to chromosomal rearrangements, mitotic recombination and aneuploidy. Furthermore, loss of DNA methylation at gene promoter regions can activate expression of oncogenes, genes involved in DNA repair, cell proliferation, angiogenesis or migration associated genes that may contribute to metastasis [89,91,145]. Despite the general global DNA hypomethylation found in cancer, promoters of tumor suppressor genes are often hypermethylated and therefore silenced in cancer. Prominent tumor suppressors like retinoblastoma (Rb) [146,147], $p16^{INK4a}$ and Breast cancer type 1 susceptibility protein (BRCA1) [148] have been shown to be silenced by promoter

hypermethylation in cancer and just like a mutation profile, different cancer types have a specific DNA methylation profile [91].

Interestingly, normally ubiquitously expressed housekeeping genes, can be silenced by promoter hypermethylation. Furthermore, promoters of tissue-specific genes can lose their hypermethylated state in cancer, therefore re-activating these previously silenced genes and contributing to cell de-diffentiation [90,91,149].

1.3.2 Mechanisms of DNA demethylation: Ten-eleven-translocases

As discussed before, DNA methylation is a dynamic and reversible process. This means that cells need a mechanism by which they can convert methylated cytosines back to an unmethylated state. Although there is evidence that DNMT3a and 3b are able to convert 5hmC back to 5mC *in vitro*, it is still unknown if this occurs *in vivo* [150,151]. In 2009 the first member of the TET enzyme family, Tet1, was demonstrated to hydroxylate 5mC to 5hmC and shortly after, Tet2 and Tet3 were discovered and shown to carry out similar reactions [152–154].

The three TET proteins contain a C-terminal catalytic domain with a cysteine rich region and a double-stranded β-helix. This catalytic domain is characteristic for the family of Fe(II) and 2-oxoglutarate (2-OG)-dependent dioxygenase superfamily and is responsible for binding two Fe(II)-ions and 2-OG that are required as co-factors for the reaction. Tet1 and Tet3 further contain an N-terminal CXXC zinc finger domain (~ 60 AA) that has high affinity for clusters of unmethylated CpGs. Tet2 has lost its CXXC domain but interestingly the domain still exists as the separate gene CXXC4, suggesting that Tet2 lost this part of the gene during evolution. CXXC4 negatively regulates Tet2 by caspase-mediated cleavage and is also a reported inhibitor of WNT signalling (reviewed in [137,138,140–142]).

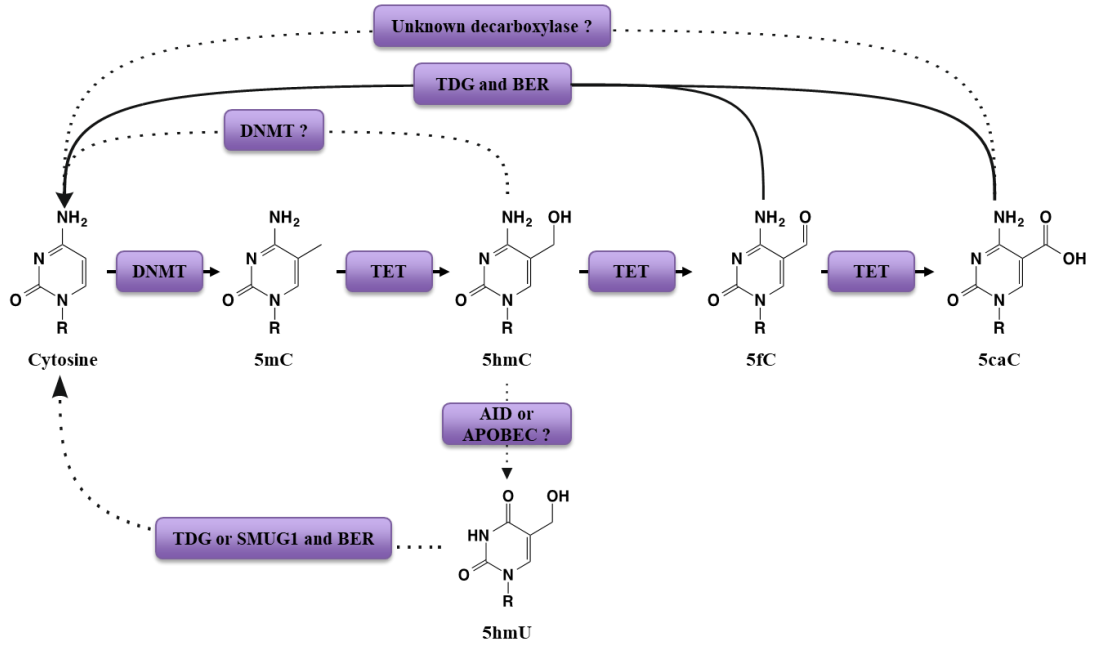

Figure 5: Conversion reactions carried out by DNMTs and TETs as well as mechanisms of DNA demethylation. Cytosine is methylated at the 5C position by DNMT enzymes. Methylated Cytosines can be demethylated by various mechanisms. TET proteins oxidize methylated Cytosines in multiple steps from 5hmC to 5fC to 5caC. These oxidize methyl Cytosines are not recognised by DNMTs during cell division leading to passive DNA demethylation. Active forms of DNA demethylation include removal of 5fC and 5caC by TDG and the BER as well as proposed mechanisms (dotted lines). **5mC:** 5-methyl-Cytosine, **5hmC:** 5-hydroxymethyl-Cytosine, **5fC:** 5-formyl-Cytosine, **5caC:** 5-carboxyl-Cytosine, **5hmU:** 5-hydroxymethyl-Uracile. **DNMT:** DNA methyl transferase, **TET:** Ten-eleven translocase, **TDG:** thymine DNA glycosylase, **BER:** base excision repair, **AID:** activation induced deaminase, **APOBEC:** apolipoprotein B mRNA editing enzyme complex, **SMUG1:** Single-strand selective monofunctional uracil DNA glycosylase. Figure adapted from Pastor *et al.* 2013 [141].

The TET proteins are the counterparts of DNMTs. First, 5hmC is not recognized by some MeCPs, therefore reversing the normally inhibitory effect of DNA methylation. Other DNA binding proteins on the other hand are specifically recruited by 5hmC and recruit chromatin remodelling factors, suggesting that 5hmC might be an epigenetic mark on its own. Furthermore, the maintenance DNA methylase DNMT1, that methylates the newly synthesized DNA strand after DNA replication, does not recognize 5hmC as methylated cytosine, therefore leading to passive DNA demethylation in proliferating cells. The content of 5hmC is highest in the brain, where the number of proliferating cells is relatively low. The process of passive DNA methylation is relatively slow but energy conserving, suggesting a role for demethylation on a larger scale. Active DNA demethylation would provide a faster

and more precise mechanism. Besides being demonstrated, the importance and contribution of active DNA demethylation is still controversial. Active DNA demethylation mechanisms require further oxidation of 5hmC to 5fC and 5caC. Indeed, thymine DNA glycosylase (TDG) is able to excise 5fC and 5caC, therefore creating an abasic site that will be repaired, resulting in unmodified cytosine. Interestingly, TDG is faster in removing 5fC from 5fC:T base pairs that removing G:T mismatches and has virtually no activity on 5mC:T base pairs (reviewed in [138–141]).

Another active demethylation mechanism involves AID/APOBEC (activation induced deaminase, apolipoprotein B mRNA editing enzyme complex) mediated deamination of 5hmC that would produce 5-hydromexyl uracil (5hmU). This would result in a 5hmU:T mismatch that could be repaired by base excision repair mechanisms, therefore restoring the normal, unmethylated C:T base pair. Indeed, DNA glycosylases (e.g. TDG and SMUG1) have robust activity for 5hmU:T mismatches and low activity for 5hmC:T base pairs [155]. In mammalian cells, 5hmU is not accumulating to detectable levels, suggesting that either the repair of 5hmU:T mismatches is extremely fast, or this pathway is only demethylating a minority of the methylated CpGs in mammals [156,157].

The DNA demethylating mechanisms mentioned above are too complex to account for the large-scale demethylation that can be observed during certain stages of development. Wu and Zhang [158] proposed a simple mechanism that would require TET proteins to oxidize 5hmC further to 5fC or 5caC followed by decarboxylation, therefore restoring unmethylated cytosine. This would allow simple and fast, active large scale DNA demethylation, but the putative carboxylase has not yet been discovered [158].

1.3.3 Studying DNA methylation

Methods to study the DNA sequence are well established. Polymerase chain reaction (PCR) techniques are now being performed even at the school level. They are fast, inexpensive and easy, although they can be tricky for regions with a high degree of secondary structures. Sequencing has become fast, relatively inexpensive and reliable and is an integral part of biological research. However, conventional PCR and sequencing techniques are unable to distinguish between methylated and

unmethylated cytosine. A simple way to solve this problem is the use of sodium bisulfite (BS), a reagent that deaminates cytosine, therefore converting it into uracil that become thymines in subsequent PCR amplification. In contrast, 5mC (as well as the much rarer 5hmC) is resistant to bisulfite conversion. Bisulfite conversion-based methods are considered the gold standard of analysing DNA methylation [159].

By using bisulfite-treated DNA (btDNA) and btDNA-specific primers in PCR methods, one can determine if methylation at certain loci is present. By using quantitative PCR, a semi-quantitative estimation of the percentage of DNA methylation can be made. By sequencing both, a bisulfite-treated DNA sample and an untreated one, the two sequences can be compared, and position specific methylation data may be generated. The approach may even be expanded, to not only analyse methylated cytosines, but also hydroximethylated cytosines. In order to achieve this, the input DNA has to be subjected to a special oxidization step that converts 5hmC to 5fC, which in contrast to 5hmC is not protected from bisulfite conversion. After the oxidation step, bisulfite conversion and sequencing can be carried out. By comparing results to sequences from normal DNA and btDNA, information on the positions of 5hmC may be obtained [160].

Utilizing next generation sequencing (NGS) methods, the whole methylome (the DNA methylation across the entire genome) can be analysed. For these methods, it is critical to ensure full conversion of the DNA in the samples, as the results directly depend on it. It is also worth noting, that when analysing data from bisulfite sequencing, the sample degree of heterogeneity should be considered, as analysing samples from mixed cell populations (including heterogenic tumors) can “dilute” the obtained results.

In the following section, a few selected methods to analyse DNA methylation will be discussed.

1.3.3.1 PCR-based methods

The simplest way to investigate DNA methylation at a given site is by using btDNA in a simple PCR reaction. By designing primers, which only bind to the specific sequence if the input DNA (prior to bisulfite conversion) is methylated, one can determine if methylation in present at a given locus. The disadvantage of this method is, that the throughput is low, and the obtained results are not quantitative. It is possible

to obtain semi-quantitative data from this method, if instead of conventional PCR, quantitative PCR (qPCR) is used.

1.3.3.2 Whole genome bisulfite sequencing

Whole genome bisulfite sequencing (WGBS) is the most comprehensive of all methods, as it theoretically provides data on all potential methylation sites in a given sample. WGBS is similar to whole genome sequencing with only one additional step: bisulfite conversion of the input DNA. However, WGBS data analysis can be challenging, as bisulfite conversion reduces the genomic complexity to essentially three nucleotides (compared to cytosine, 5mC, that remains cytosine after conversion, is relatively rare). This makes alignment of the sequences more challenging. Furthermore, btDNA is more fragmented, thus amplification of longer reads is difficult and can lead to chimeric products. The data analysis also requires a considerable amount of bioinformatic expertise and resources because of the difficulties in sequence alignment and the huge amounts of data produced.

Because only a small fraction of the genome has the potential to be differentially methylated, WGBS may not be required for some, if not most, studies. There are other methods that enrich the methylated DNA fraction of the genome that are cheaper and may be sufficient for the specific research question.

1.3.3.3 Reduced Representation Bisulfite Sequencing

Reduced Representation Bisulfite Sequencing (RRBS) in principle follows the same protocol as WGBS, the difference is in the input DNA. Before library preparation, the CpG rich fraction of the genome is enriched by isolating short fragments that are generated by digestion with the restriction enzyme MspI (recognizing CCGG sites). RRBS allows for isolation of about 85% of CpG islands (CGIs) in the human genome and enriches such sequences, that have moderate or high CpG density and allows for analysis of mostly CGIs, promoters and enhancer sites.

Data processing and analysis is very similar to WGBS, although not as intensive as the amount of generated data is smaller. Lastly, when interpreting the data, the fact that the results are based on an enriched subfraction of the genome must be taken into consideration.

In this study, I used oxidative RRBS (oxRRBS) to analyse the methylomes in a preclinical mouse model of cSCC. **Figure 6** shows an overview of the oxRRBS method.

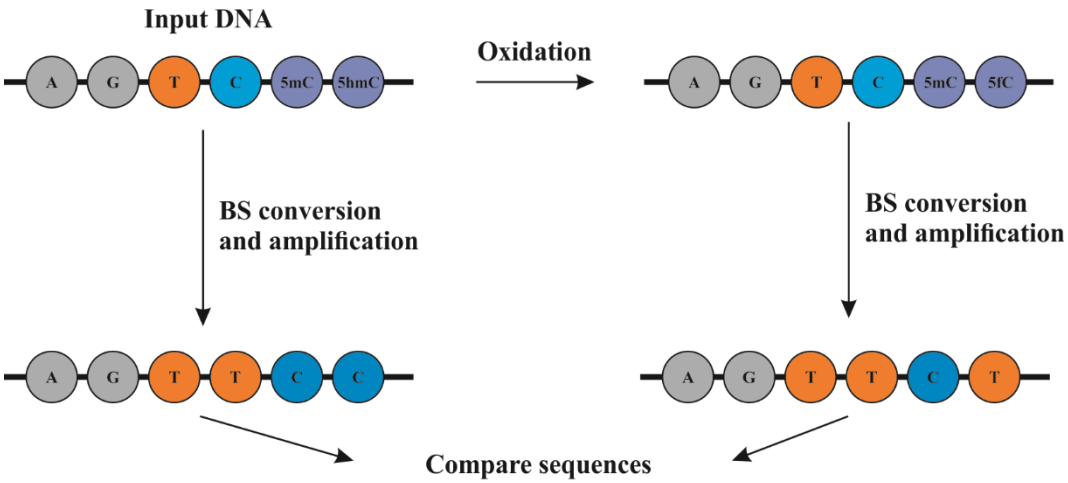

Base	Sequence	BS Sequence	oxBS Sequence
C	C	T	T
5mC	C	C	C
5hmC	C	C	T

Figure 6: Principle of the oxRRBS method. Input DNA is either directly bisulphite (BS) converted or oxidized and then BS converted. Following amplification and sequencing, the sequences can be compared and positions of 5mC and 5hmC can be analysed.

1.3.3.4 Affinity enrichment-based methods

Another way to enrich input DNA for CpG rich sequences, is immunoprecipitation of methylated DNA (MeDIP) with monoclonal antibodies against 5mC [161] or affinity capture of methylated sequences by members of the methyl-CpG binding domain (MBD) family proteins (collectively termed MBDCap) [162]. Different MBDCap methods use different MBD proteins (e.g. MeCP2 in the case of MethylCap assay or MBD2 and MBD3L1 in the case of methylated-CpG island recovery assay (MIRA)). [163,164].

Although MeDIP and MBSCap methods are in principle very similar, the choice of method has a huge influence on the results. The antibodies used in MeDIP bind to DNA fragments that contain a small number of methylated cytosines, while MBD proteins capture DNA fragments with multiple methylated cytosines with increasing affinity [165]. This can be turned into an advantage: By serially eluting methylated

DNA sequences with increasing salt concentrations, one can generate different fractions with increasing CpG density. This can allow to get an overview on the methylation changes at regions with different CpG density or, if the fraction eluded by the highest salt concentration is being analysed, an enrichment for CGIs can be achieved [166]. When interpreting the results, it is crucial to take into account which fraction of the genome is being analysed [165].

1.3.3.5 Illumina Beadchip arrays

Illumina 27k and 450k beadchip arrays provide an alternative to sequencing-based methods but are only available for human samples. While the 27k array covers 27,578 CpGs and over 14,475 annotated genes, the 450k array covers 99% of all annotated genes with an average of 17 CpGs per gene. With probes for more than 450,000 CpGs on the chip, 96% of all CGIs can be analysed [167].

The principle of both arrays is simple: Bisulfite treated DNA is being hybridized to bead-bound probes on the chip. While one probe is designed to bind the methylated CpG, the other probe binds the unmethylated CpG. After hybridization, single base extension with fluorescently labelled nucleotides is used for means of detection. Illumina 450k arrays are used in large international projects like TCGA (The Cancer Genome Atlas, see https://cancergenome.nih.gov/).

Illumina 27k and 450k arrays allow for a fast and cost-efficient quantitative analysis of genome-wide DNA methylation. Furthermore, these arrays allow usage of DNA, isolated from archival samples such as FFPE embedded tissues, that can be problematical in sequencing-based methods. It is worth mentioning, that the Illumina arrays, as hybridization-based methods, are susceptible to small nucleotide polymorphisms (SNPs) in the input DNA, as they may affect hybridization efficiency [168].

1.3.3.6 EpiTYPER MassARRAY

The EpiTYPER MassARRAY system (Agena Bioscience, San Diego USA) provides a method to get quantitative DNA methylation data at specific loci with high throughput. The locus of interest is amplified from btDNA and a T7 promoter is added. In the next step, the amplicon is *in vitro* transcribed into a single stranded RNA molecule. Depending on the methodology used, the *in vitro* transcription mixes use either deoxyribose cytosines or uracils. In the next step, RNase A is used to cleave the

RNA molecules and because RNase A is not able to cleave after deoxyribose nucleotides, cleavage only happens after cytosines or uracils (again, depending on the methodology used). The cleaved RNA can then be analysed using a MALDI-TOF mass spectrometer. Because of the previous steps, unmethylated cytosines will appear as adenines in the mass spectrometry, while methylated cytosines will appear as guanines. As there is a mass difference of 16 Daltons between the two bases, methylated and unmethylated cytosines will appear as separate peaks in the spectrogram that can be quantified.

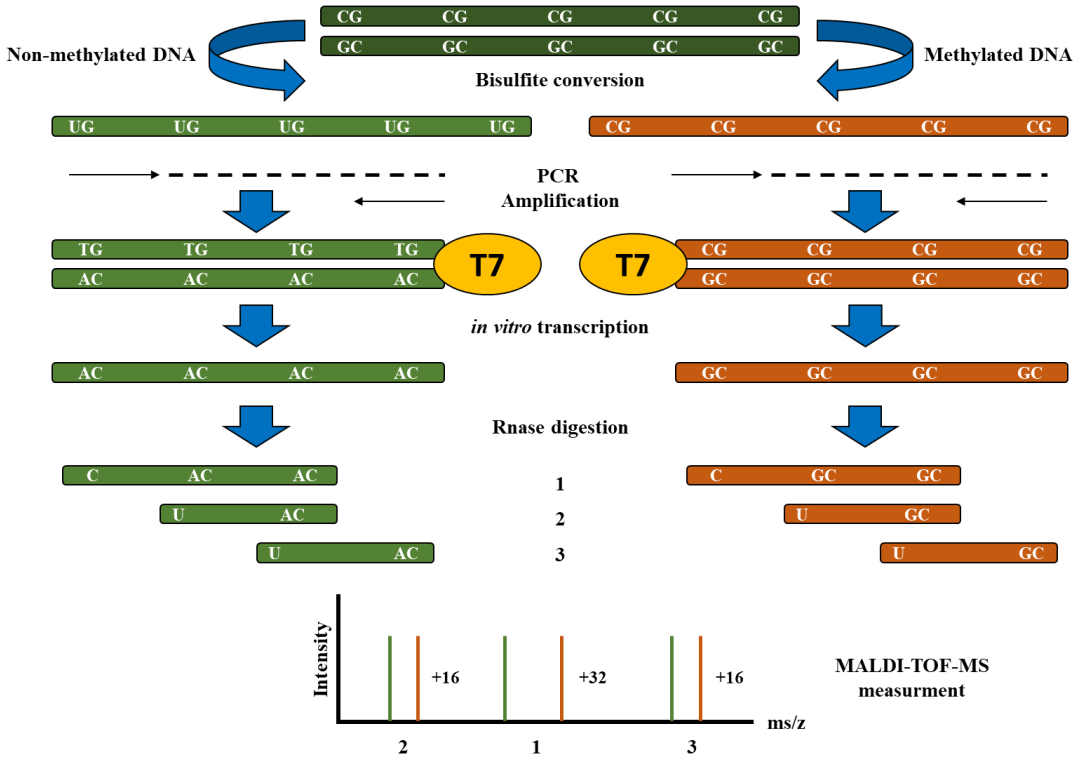

Figure 7: Schematic overview of the EpiTYPER MassARRAY technology. Figure adapted from Busó and Iborra 2016 [169].

One advantages of MassARRAY is that, in contrast to other methods that analyse DNA methylation at specific loci, the method is high throughput. After MassARRAY primers have been established, the required PCRs and following reactions are all performed in a 386 well format. This allows for analysis of a high number of samples and loci in a relatively short amount of time.

During method development, it has been realized that calibration for peaks of fragments below 1700 Da is not ideal and those fragments often produce non-reliable data. The same is true for high mass fragments and therefore, it is recommended that

data from these fragments is not included in analysis. Furthermore, it is possible that different fragments have the exact same mass. In this case, one has to carefully analyse the results from those fragments and if multiple fragments have the same mass, these results also have to be excluded [169].

In this study, I used MassARRAY to validate differentially methylated regions (DMRs) that were identified by RRBS.

1.3.4 DNA methylation in cutaneous squamous cell carcinoma

UV radiation is known to influence DNA methylation and UV-induced changes in the methylome of normal skin cells may contribute to skin carcinogenesis [170–173]. On the other hand, CpG methylation itself changes the absorption spectrum of cytosine (non-methylated C: max at 270 nm, methylated C: max 280 nm) and therefore makes hypermethylated DNA sequences prone to UV-induced DNA damage. This phenomenon has been demonstrated for the coding sequence of p53 [173–175].

In most cases, cancer is associated with global hypomethylation and locus specific hypo- or hypermethylation [90]. A few studies have demonstrated an increase in DNA methylation in human cSCC, murine skin exposed to UVB radiation and skin cancer cell lines, such as A431 and SCC13 [170,172,176], and Lin *et al.* suggested a link of this increase in global DNA methylation with TET proteins [170]. Interestingly, TET proteins have been found to be mutated in human cSCCs (see supplemental information in South *et al.* 2014 [58]). TET proteins also appeared as frequent mutations in murine ssUVR induced cSCCs [59].

Several studies have focused on differentially methylated regions (DMRs) in promoter regions of genes. However, the multitude of different models and methods used makes it difficult to compare the results from those studies. Early investigations used methylation specific PCR (MSP). MSP utilizes bisulfite treated genomic DNA, where unmethylated cytosines are converted to thymines whereas methylated cytosines are protected from this conversion. This allows the design of specific primers for methylated and unmethylated DNA regions. While this method is highly specific for methylated CpGs, it remains a qualitative method that is not able to provide quantitative methylation data. With next generation sequencing techniques becoming more advanced and the cost for these techniques getting lower, more recent studies have utilized genome-wide methods that will be discussed below.

Takeuchi *et al.* used MSP to investigate promoter methylation of the *T-cadherin* gene in human primary tumors. T-cadherin is involved in cell adhesion and may play a role in intracellular signalling. Takeuchi *et al.* demonstrated that the T-cadherin promoter is methylated in invasive human cSCCs as well as in the A431 skin cancer cell line. Treatment with the demethylating agent 5'-aza-2'-deoxycytidine (DAC), a DMNT inhibitor, restored T-cadherin expression in A431 cells [177].

Similar to T-cadherin, E-cadherin is involved in cell adhesion. E-cadherin is a major marker for epithelial cells and is down-regulated when cells undergo epithelial-mesenchymal transition (EMT), a mechanism important for tumor metastasis [178–182]. In their 2003 study, Chiles *et al.* from the Smoller lab (Department of Pathology and Dermatology, University of Arkansas) utilized MSP to investigate methylation at the E-cadherin promoter in human non-neoplastic skin, actinic keratosis, an early pre-stage of cSCC, cSCC *in situ* and invasive cSCC. Despite relatively small sample cohorts, they found that the E-cadherin promoter is un-methylated, and therefore active, in 7 out of 9 cases in non-neoplastic skin samples. In actinic keratosis as well as cSCC *in situ*, the E-cadherin promoter is methylated in approximately 50% of cases (actinic keratosis: 5 un-methylated, 4 methylated; cSCC in situ: 4 un-methylated, 4 methylated). For 6 of 7 cases of invasive cSCC the E-cadherin promoter was methylated, suggesting silencing of the E-cadherin gene and up-regulated EMT mechanisms [183]. Both studies by Takeuchi *et al.* and Chiles *et al.* suggest that in invasive human cSCC, cell-adhesion proteins may be down-regulated by promoter methylation, therefore contributing to increased metastatic potential.

In a publication by Tyler *et al.*, Smoller and co-workers analysed promoter methylation of death-associated protein kinase (DAPK) and the tumor suppressor p16, again using MSP and the same sample cohort as in their E-cadherin study. They found that both promoter regions are mostly un-methylated in nonneoplastic skin samples, actinic keratosis, cSCC *in situ* and invasive cSCC, suggesting that these genes are regulated by different mechanisms in cSCC [184].

Table 4: Overview of differentially methylated genes and global methylation in cSCC. Further explanation is given in **Section 1.3.462**.

GENE	GENE REGION	METHYLATION	EXPRESSION	SAMPLE ORIGIN	TECHNIQUE	SOURCE
T-cadherin	Promoter	hyper	down	invasive human cSCC	MSP	Takeuchi 2002 [185]
T-cadherin	Promoter	hyper	down	A431	MSP	Takeuchi 2002 [185]
E-cadherin	Promoter	hypo 7/9 (78%)		non-neoplastic skin	MSP	Chiles 2003 [183]
E-cadherin	Promoter	hypo 5/9 (56%)		AK	MSP	Chiles 2003 [183]
E-cadherin	Promoter	hypo 4/8 (50%)		cSCC *in situ*	MSP	Chiles 2003 [183]
E-cadherin	Promoter	hyper 6/7 (86%)		invasive human cSCC	MSP	Chiles 2003 [183]
$p14^{ARF}$	Promoter	hyper 16/38 (42%)		human cSCC	MSP	Brown 2004 [108]
$p16^{INK4a}$	Promoter	hyper 13/36 (36%)		human cSCC	MSP	Brown 2004 [108]
$p16^{INK4a}$	Promoter	hyper 2/8 (25%)		human cSCC	MSP	Arbiser 2004 [186]
E-cadherin	Promoter	hyper 4/10 (40%)		TPA/DMBA mouse	btDNA seq	Fraga 2004 [187]
Snail	Promoter	hyper 6/10 (60%)		murine skin cancer cells	btDNA seq	Fraga 2004 [187]
global		250% of normal skin		UVB irradiated mouse skin	Methylamp	Nandakumar 2011 [172]
global		300% of normal skin		UVB induced mouse skin tumors	Methylamp	Nandakumar 2011 [172]
global		350% of normal skin		human cSCC	Methylamp	Nandakumar 2011 [172]
global		325% of NHEK		A431	Methylamp	Nandakumar 2011 (2) [176]
$p16^{INK4a}$	Promoter	hyper	down	UVB induced mouse skin tumors	MSP	Nandakumar 2011 [172]
RASSF1A	Promoter	hyper	down	UVB induced mouse skin tumors	MSP	Nandakumar 2011 [172]
Cip1/p21	Promoter	hyper	down	UVB induced mouse skin tumors	MSP	Nandakumar 2011 (2) [176]
$p16^{INK4a}$	Promoter	hyper	down	13 human cSCC cell lines	MSP	Nandakumar 2011 [172]
RASSF1A	Promoter	hyper	down	13 human cSCC cell lines	MSP	Nandakumar 2011 [172]
Cip1/p21	Promoter	hyper	down	13 human cSCC cell lines	MSP	Nandakumar 2011 (2) [176]
$p16^{INK4a}$	Promoter	hyper	down	A431	MSP	Lin 2014 [170]
Cip1/p21	Promoter	hyper	down	A431	MSP	Lin 2014 [170]

The *CDKN2A* locus encodes for the $p16^{INK4a}$ and $p14^{ARF}$ tumor suppressor genes. The *CDKN2A* gene, as previously mentioned, is also frequently mutated in cSCCs. Brown *et al.* found promoter methylation of the $p16^{INK4a}$ promoter in 13 of 36 (36%) and $p14^{ARF}$ promoter in 16 of 38 cases of human cSCC, again using MSP [108].

Another study that investigated promoter methylation at the $p16^{INK4a}$ promoter was conducted by Arbiser *et al.* 2004, again using the MSP method. They found $p16^{INK4a}$ promoter methylation in 2 of 8 primary human cSCC samples [186], which is consistent with the data from Brown et al [108].

Fraga *et al.* compared methylation of various gene promoters in human primary tumors, tumors that form in the DMBA/TPA mouse multistage skin carcinogenesis model [188,189] as well as human and murine skin cancer cell lines. Most notably, the promoter of E-cadherin was only methylated in 4 out of 10 murine skin cancer cell lines, whereas Chiles *et al.*, as previously discussed, found the E-cadherin promoter to be methylated in 67% of cases in human primary tumors. Concordantly, the promoter of Snail, an EMT promoting transcription factor and negative regulator of E-cadherin, was methylated in 6 out of 10 murine skin cancer cell lines [186], suggesting that regarding to regulation of EMT by DNA methylation, murine cancer cell lines and human primary tumors are different, likely because of differences in cancer drivers (reviewed in [173]). Other gene promoters show similar methylation when comparing human primary tumors and human or murine cancer cell lines. For example, the cysteine and glycine-rich protein 2, involved in the JAK/STAT signalling pathway shows similar methylation patterns. The same is true for the chemokine receptor CXCR4 and the antioxidant enzyme peroxiredoxin 1. In contrast insulin-like growth factor binding protein 3 is mostly unmethylated in human primary tumors but mostly methylated in human and murine skin cancer cell lines [187]. The differences between human primary tumors, human skin cancer cells and murine skin cancer cells highlights the importance of choosing the right and most accurate model system.

In a more recent study from 2011, Nandakumar *et al.* used a variety of methods to address methylation changes in UVB-exposed skin and UVB-induced skin tumors of SKH-1 hairless mice. First, they demonstrated, using Methylamp global methylation quantification kit, that global DNA methylation levels are significantly higher in UVB-irradiated skin and UVB-induced skin tumors. This was also observed in

13 human cSCC samples. This is likely to be caused by elevated expression and activity of DNMTs. Nandakumar *et al.* also found transcriptional silencing of $p16^{INK4a}$ and RASSF1A by promoter methylation and histone deacetylation using a combination of MSP, methylated DNA immunoprecipitation (MeDIP), methyl-CpG-binding domain capture (MCDCap) and western blotting [172].

The methylation specific PCR method used in the studies described so far is an easy and specific method to analyse DNA methylation at small regions. However, this method does not provide any insight in the grade of DNA methylation. An advanced version of MSP was used in a second publication by Nandakumar *et al.* 2011. By using qPCR instead of regular PCR, they created semi-quantitative data for methylation changes in the $p16^{INK4a}$ and Cip1/p21 promoters in A431 skin cancer cells. First Nandakumar *et al.* showed that global methylation levels are higher in A431 cells compared to NHEK keratinocyte cells, and that EGCG, a green tea polyphenol, reduces global methylation levels in a time- and dose-dependent manner. Again, the effect was linked to decreased expression and activity of DNMTs. The effects of EGCG on global DNA methylation levels was also observed in the human SCC 13 cell line, but unfortunately, global methylation levels of A431 and SCC 13 cells were not compared. Furthermore, EGCG was able to up-regulate expression of the silenced tumor suppressor genes $p16^{INK4a}$ and Cip1/p21 by reduced methylation levels at their promoters [176].

More recent techniques make use of next generation sequencing (NGS) to produce quantitative or semi-quantitative genome-wide methylation data. Tony Kong and co-workers (Yang *et al.* 2014 [171]) used methylated DNA immunoprecipitation (MeDIP) coupled with NGS to screen for differentially methylated genes in UVB- or DMBA/TPA-induced murine skin cancers. This approach utilizes monoclonal antibodies specific for 5mC, followed by crosslinking and pulldown of the methylated DNA fragments, followed by NGS. MeDIP is a biased method because it preferentially enriches regions with low and intermediate 5mC contend [167]. Yang *et al.* found 6003 genes to be differentially methylated (≥ 2-fold change in methylation) in the UVB-induced tumors, 4140 of which were hyper- and 1863 were hypomethylated. Regarding the DMBA/TPA-induced mouse skin tumors, 5424 genes showed an at least 2-fold change in DNA methylation levels. The methylation percentage was higher for 3781 and lower for 1643 genes compared to the control.

Unfortunately, there is no comprehensive data for all differentially methylated genes available. But comparing the 50 most hyper- or hypomethylated genes from both models, only TSN1 (tensin1) is hypermethylated and GRIA1 (Glutamate receptor, ionotropic, AMPA 1) is hypomethylated in both models, suggesting that regarding DNA methylation, the two models are not comparable. Yang *et al.* performed Ingenuity Pathway Analysis (IPA) with differentially methylated genes from UVB- and DMBA/TPA-induced murine tumors. Results shows that the differentially methylated genes are enriched in different pathways, with only "molecular mechanisms of cancer" showing up as a pathway enriched in both models. This however is not surprising as Yang *et al.* compared skin tumors with other skin tumors. The lack of shared pathways further suggests that DNA methylation patterns are not comparable between the models [171] and also increases doubts, that the DMBA/TPA model is suitable to investigate cSCC (as discussed in **Section 1.2.3.6**).

While Nandakumar *et al.* 2011 demonstrated that silencing of the p16 and p21 genes in A431 cells can be reversed with EGCG through inhibition of DNMTs, Lin *et al.* 2014 showed that the p16 and p21 are also re-expressed in A431 cells after treatment with vitamin C. Similar to EGCG treatment, vitamin C is able to reduce DNA methylation at the p16 and p21 promoters, therefore up-regulating the expression of both genes. Interestingly, although 5mC levels at the promoters drop, 5hmC levels significantly increase after vitamin C treatment. This suggests a TET-dependant mechanism, as the conversion of 5mC to 5hmC is carried out by TET proteins. Although Lin *et al.* had established shRNA knockdown of Tet1 and Tet2 in A431 cells, they did not test if the accumulation of 5hmC at the p16 and/or p21 promoters is impaired in Tet1/2 knockdown A431 cells after vitamin C treatment, and therefore did not provide direct evidence for a TET-dependant mechanism [170].

The most comprehensible data for DNA methylation in cSCC comes from a recent paper by Rodríguez-Paredes *et al.* [190]. They performed global methylation analysis of 12 normal epidermis samples (taken from healthy volunteers), 16 AK samples and 18 cSCCs using Infinium MethylationEPIC 850k methylation array. Great care was taken to ensure tissue homogeneity by separating the epidermis from the dermis. When principal component analysis (PCA) was performed, normal epidermis samples clearly separated from AK and cSCC samples, and a high overlap between AK and cSCC was observed. Interestingly, methylation between normal epidermis samples

showed high homogeneity, while AK and cSCC samples distributed with greater heterogeneity. Between normal epidermis and AK, pairwise comparison resulted in identification of 372,213 significantly differentially methylated probes, and 310,102 probes were significantly differentially methylated between normal epidermis and cSCC. Between AK and cSCC, no significantly differentially methylated probes were detected (in agreement with PCA). This suggests, that there are profound methylation changes when normal epidermis becomes diseased (AK and cSCC) but also high similarity in methylation between AK and cSCC. When Rodríguez-Paredes *et al.* analysed cancer specific features, they found that AK samples already display these cancer specific features, and that this is conserved in cSCC [191]. These cancer associated features included hypomethylation of open sea regions (CpGs not associated with a CGI), hypermethylation of CGIs and their shores (CpGs in proximity to CGIs) and hypermethylation at lamina-associated domains (LADs) in both, AK and cSCC [192].

Furthermore, when predicting the chronological age of AK and cSCC samples, the calculated methylation age was significantly lower than the chronological age of the patient from whom the sample originated, an effect similar to the one observed for stem cells [193]. In mammalian stem cells, DNA methylation can also be observed outside of a CpG context [194,195]. Rodríguez-Paredes *et al.* were able to detect significantly increased non-CpG methylation in AK and cSCC samples, reminiscent of features observed in stem cells. Furthermore, they showed that expression of the DNA methyltransferase enzyme associated with non-CpG methylation, DNMT3b which is also an important epidermal stem cell gene [196], was increased in AK and cSCC samples compared to controls.

Expression of keratins correlates with the differentiation stage of keratinocytes and the keratin genes are located in gene clusters on chromosomes 12 and 17 [197]. Rodríguez-Paredes *et al.* observed major DNA methylation changes at these clusters between AK, cSCC and healthy samples. Moreover, inspection of DNA methylation at the individual keratin genes (while also confirming their previous findings), indicated that there were two separate keratin gene methylation patterns in AK and cSCC samples. When they performed a similar analysis of keratin gene methylation patterns in datasets from The Cancer Genome Atlas (TCGA, 7824 cancer data sets, 26 different tumor entities), PCA revealed the presence of two subgroups in AK and

cSCC samples. Interestingly, while one group clustered together with the cancer samples, the other one was closely related to healthy epidermis. The Infinium MethylationEPIC also allows for analysis of enhancer regions, a particularly important target of DNA methylation [198]. When analysing over 75,000 enhancers of H1 embryonic stem cells (ESC) line and normal human keratinocytes and clustering samples in a PCA, they identified the same two subclasses, one related to ESCs and one related to keratinocytes. Together, this strongly suggest that cSCC in humans arises from distinct progenitor cell types, undifferentiated epidermal stem cells and more differentiated keratinocytes.

I will compare the data from Rodríguez-Paredes *et al.* with the findings obtained by RRBS in ssUVR induced murine cSCC later in this thesis.

1.4 FILIP1L

When I was analysing DNA methylation in mouse cSCC, *Filip1l* was the most differentially methylated gene, as an intronic region of the gene showed a highly significant difference in methylation in tumors compared to matched healthy skin.

In humans, the *FILIP1L* gene lies on chromosome 3. The gene has 6 exons of varying length (118 bp to 2776 bp) with exon 5 being the longest. In mouse, the *Filip1l* gene has a similar structure compared to humans. It only has 5 exons, but exon and intron lengths are similar. Interestingly, the intron harbouring the differentially methylated region (DMR) identified during my study is extraordinarily long (human: 183,022 bp, mouse: 153,140 bp). FILIP1L has 8 known isoforms. The full-length isoform is isoform 202 (1135 bp, 130 kDa) but isoform 201 has the same molecular weight and only misses the short exon 6 (1133 bp, 130 kDa). Alternative transcription start sites (TSSs) and splicing of exon 6 allow for different N- and C-termini of the different isoforms. Currently, it is not known if FILIP1L isoforms have different biochemical functions or display tissue specific expression. There are only 3 known mouse isoforms of Filip1l. An overview of the FILIP1L isoforms in mouse and human are depicted in **Figure 8**. Information on the *FILIP1l* gene and isoforms is available at Ensemble (http://www.ensembl.org) [199]. The nomenclature to name the FILIP1L isoforms is confusing. I will use the isoform names from Ensemble during this thesis.

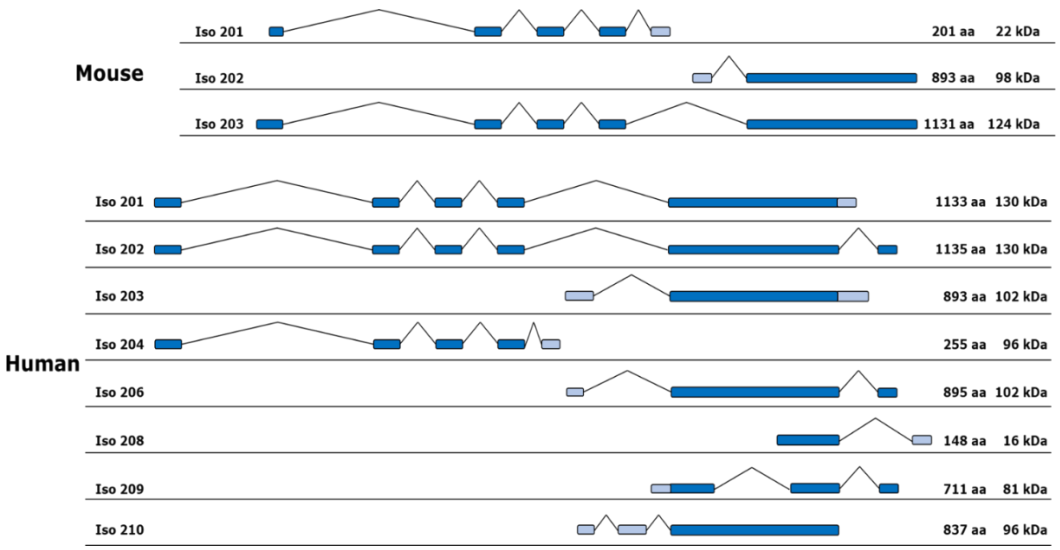

Figure 8: FILIP1L isoform structure in mouse and human. Exons are depicted in blue, alternative TSSs and 3' untranslated regions (UTRs) are depicted in light blue. Size correlates with sequence length but is not scaled. aa = amino acids, kDa= kilo Dalton.

The FILIP1L protein consists of a coiled-coil region (residues 3-542), two leucin zipper motifs (83-111 and 218-253) and a potential nuclear localization sequence (NLS) domain (168-183). Using NCBI conserved domain search (https://www.ncbi.nlm.nih.gov/Structure/cdd/wrpsb.cgi) Kwon *et al.* also found other conserved domains of FILIP1L are: CortBP2 (cortactin-binding protein 2, residues 57-249), SbcC (an ATPase involved in chromosome segregation, residues 15-576), ApoLP-III like (apolipophorin-III and similar insect proteins, residues 383-507) and DHC-N1 (dynein heavy chain N-terminal region 1, residues 392-665). The C-terminus is an unstructured region with a Herpes-BLLF1 (Herpes virus major outer envelope glycoprotein, residues 875-1115) conserved domain (the FILIP1L protein structure is also reviewed in [200]).

Alignment of the human FILIP1L isoform 202 and mouse isoform 203 using NCBI protein Blast (https://blast.ncbi.nlm.nih.gov/Blast.cgi) shows that proteins are very similar between human and mouse (Query cover 99%, percentage identity 88.40%).

1.4.1 Discovery of FILIP1L

Before we were able to perform screens of entire genomes, epigenomes, transcriptomes or proteomes, scientists had to go through great struggles to identify differentially expressed genes, especially when comparing multiple samples. One technique used for this purpose was RNA-based arbitrary primed PCR (RAP). In principle, this technique uses one or two arbitrary primers to amplify multiple sequences from total RNA. By separation of the PCR products on an acrylamide gel, differences in expression between individuals can be observed [201,202]. Using RAP, Mok *et al.* were able to identify two transcripts, which were expressed in human ovarian surface epithelial (HOSE) primary cell cultures but absent in nine ovarian carcinoma cell lines. They termed those transcripts down-regulated in ovarian cancer 1 and 2 (DOC-1 and -2), with DOC-1 later being renamed filamin A interacting protein 1 like (FILIP1L, I will be using this name through this thesis) [203], but the function of the gene remained unknown. In 2002, the down-regulation of FILIP1L was confirmed in primary cell lines, derived from epithelial ovarian carcinomas using an Affymetrix genechip expression array [204]. Although mutations in FILIP1L are common in ovarian cancer, in their 2011 study, Notaridou *et al.* found, that SNPs in FILIP1L most likely do not contribute to ovarian cancer risk [205], other means of gene regulation (for example DNA methylation) were not investigated.

Since then, multiple studies have linked FILIP1L to different cellular processes in both, normal and cancer cells and tissues. For example, Schwarze *et al.* demonstrated, that FILIP1L expression is up-regulated in human prostate epithelial cells (HPECs) when they become senescent, but expression then is down-regulated once the cells are immortalized (using HPV15 E6 and E7 genes) [206]. They also showed, that FILIP1L expression is induced when HPECs as well as the prostate cancer cell lines DU145 and LNCaP are forced into a senescent-like phenotype using doxorubicin, Docetaxel or the DNMT inhibitor 5-aza-2'-deoxycitidine (DAC) [207]. It is however unclear, if FILIP1L expression is involved in inducing or maintaining a senescent phenotype, or simply is a result of cells becoming senescent.

Mazzanti *et al.* found that treatment of human endothelial cells with the angiogenesis inhibitors endostatin or fumagillin, induced expression of FILIP1L after only 1h of treatment using human cDNA 10k array in human umbilical vein endothelial cells (HUVECs). They speculated, that FILIP1L could be involved in cytoskeleton organisation as it shares similarities with the mouse myosin heavy-chain smooth muscle isoform, and that FILIP1L could have a tumor suppressor role [208]. In a similar study, Tandle *et al.* from the same lab reported similar results in HUVECs using the tumor derived cytokine endothelial monocyte activating polypeptide-II (EMAP-II) [209]. In both studies, the authors used siRNA mediated knock-down of FILIP1L to show, that FILIP1L is involved in early signaling in response to angiogenesis inhibitors and that FILIP1L lies upstream of other genes with altered expression.

Stangeland *et al.* found by microarray analysis, that FILIP1L is expressed in glioblastoma stem cells (GSCs) but not in neuronal stem cells (NSCs) from adult brains [210,211]. However, they were not able to validate differential expression of FILIP1L in an independent sample set, but upon closer inspection found, that expression is low in the glioblastoma neural subtype, but consistently up-regulated in mesenchymal tumors. It is interesting to note, that in an earlier study using the same initial microarray data, Sandberg *et al.* noticed that compared to NSCs, GSCs have dysregulate WNT-signaling [211], a pathway FILIP1L has been linked to (data on the function of FILIP1L will be discussed later in this chapter).

1.4.2 Characterization of function and expression of FILIP1L

In two studies, Mazzanti *et al.* [208] and Tandle *et al.* [209] from the Steven K. Libutti group found that FILIP1L expression is upregulated in HUVECs after treatment with angiogenic inhibitors. Kwon *et al.* from the same lab aimed to functionally characterize FILIP1L. First, they made a monoclonal FILIP1L antibody using mice. This antibody was then used to confirm that in HUVECs within two hours, FILIP1L protein is up-regulated after treatment with endostatin. FILIP1L predominantly was localized in the cytoplasm, with lower levels in the membrane and nucleus. Furthermore, Kwon *et al.* used immunohistochemistry to show, that in normal colon tissue, FILIP1L is expressed in the vasculature and muscularis mucosa, while in colon cancer, FILIP1L was strongly expressed in the vasculature as well as the stroma. When trey transfected HUVECs with FILIP1L expressing plasmid, HUVECs displayed decreased proliferation (measured by BrdUrd ELISA after 24 h) and increased apoptosis (increased Caspase-3 and -7 activity). Kwon *et al.* created different truncation mutants of FILIP1L and expressed them in HUVECs in order to determine which part of FILIP1L mediates the antiproliferative effect in those cells. All truncation mutants, except the three shortest ones (residues 1-369, 369-893, 512-893) significantly inhibited cell proliferation and apoptosis, with FILIP1LΔC103 (residues 1-790) being more potent than the full-length protein. When they over-expressed the FILIP1LΔC103 truncation mutant in HUVECs, migration was significantly slower. Using DU145 prostate cancer cells, that have low FILIP1L expression, doxorubicin induced FILIP1L expression had significantly slower migration. Finally, they showed that targeted expression of FILIP1LΔC103 in tumor vasculature in an M21 xenograft model significantly reduced tumor growth and tumors showed extensive apoptosis.

Using a yeast two-hybrid system, Yangzhou and Mivechi discovered FILIP1L isoform 203 (termed version 2 in their publication) as an interaction partner of heat shock factor 1 (HSF1). This interaction was also observed in H1299 (human small cell lung carcinoma) cells using immunoprecipitation. Interestingly, in heat treated (43°C for 1 h) HEK293 (human embryonic kidney epithelial) cells the interaction was weakened. Furthermore, the N-terminal region of FILIP1L (residues 1-230) alone also was able to bind HSF1, suggesting that the N-terminus of FILIP1L that contains the two leucine zipper domains is essential for HSF1 binding. Under physiological conditions, HSF1 exists as a heterodimer with HSP72. Using a series of GST pulldown

assays, Yangzhou and Mivechi also were able to show that full-length HSF1 interacts with both, FILIP1L and HSP72. Furthermore, GST pull-down using FILIP1L residues 1-288 (containing the leucine zipper domains) were able to co-immunoprecipitate FILIP1L, suggesting that FILIP1L exists as a dimer or oligomer. Overexpression of fluorescently labelled FILIP1L reduced expression of endogenous HSF1 in both, physiological conditions and after heat shock, reduced HSF1 nuclear granules following heat shock and reduces HSF1 transcriptional activity. Using overexpression of HA-ubiquitin and HA-HSF1, Yangzhou and Mivechi tested if FLAG-FILIP1L influences HSF1 ubiquitination. Indeed, using proteasome inhibitor MG132, FILIP1L overexpression lead to a significant increase in HSF1 polyubiquitination. They also tested the if the ubiquitin adapter protein HhR23A interacts with FILIP1L. The FILIP1L leucine zipper domains interacted with the ubiquitin associated domains (UBA) of HhR23A and both, FILIP1L and HSF1 can be pulled down together with GST-HhR23A, while HSF1 alone could not. This indicates, that FILIP1L could be an adapter protein for ubiquitinated HSF1 [212].

Following up on the initial discovery, that FILIP1L is not expressed in ovarian cancer, Xie *et al.* investigated, if delivery of FILIP1LΔC103 by biodegradable cationic heparin-polyethyleneimine (HPEI) nanogels is able to inhibit ovarian cancer growth [213]. They established, that delivery of FILIP1L by the HPEI nanogel to an intraperitoneal ovarian carcinoma xenograft model (using SKOV3 human ovarian carcinoma cells) was possible. FILIP1L expression reduced tumor weight by almost 72% and while control group tumors spread to the liver and mice developed ascites, none of the mice harbouring FILIP1L expressing tumors developed ascites and all tumors were in the pelvis area. Staining frozen tumor section with CD31 antibody revealed, that microvessel density (MVD) was significantly reduced in FILIP1L expressing tumors, suggesting that angiogenesis is inhibited in these tumors. This was supported by alginate-encapsulated tumor cell assay and FITC-dextran uptake. Furthermore, FILIP1L expression reduced tumor proliferation by at least 50% (measured by Ki-67 staining) and TUNEL-assay revealed a significant increase in apoptosis. The findings of this study suggest, FILIP1L is a valid therapeutic target in ovarian cancer [213]. In a follow-up study, Xie *et al.* [214] combined delivery of FILIP1L via HPEI nanogels with low-dose cisplatin (3 mg/kg). FILIP1L HPEI nanogels were approximately as effective in inhibiting tumor growth, proliferation and

angiogenesis as cisplatin treatment and induced apoptosis at similar rates. Combination treatment was more effective than either of the treatments alone [214].

As mentioned before, Notaridou *et al.* [205] found, that SNPs in FILIP1L most likely does not contribute to ovarian cancer risk however, Xie *et al.* [214] found that re-expressing FILIP1L in an ovarian cancer xenograft model slowed tumor growth significantly. Taken together, it appears that in ovarian cancer, FILIP1L is repressed on a transcriptional level, but the mechanism was unknown. Using a series of ovarian cancer cell lines as well as both, immortalized and primary human ovarian surface epithelial cells (IOSE and HOSE), Burton *et al.* [215] from the Libutti lab first determined, that FILIP1L expression is high in HOSE cells, but low or absent in all tested ovarian carcinoma cell line (OVCAR8, OV90, SKOV3, OVCA429, OCC1 and ES2). Interestingly, FILIP1L expression was also significantly lower in IOSE cells compared to HOSE cells, but higher than in ovarian carcinoma cell lines. Using immunoblotting, these findings were confirmed on a protein level. Expression levels of FILIP1L were shown to inversely correlate with the invasive potential of the different cell lines. Furthermore, transfecting ES2 and SKVO3 cells, that express no FILIP1L, with the truncation mutant FILIP1LΔC103 reduced invasion significantly. To test if FILIP1L expression inversely correlates with invasiveness in vivo, Burton *et al.* tested FILIP1L mRNA levels in FFPE imbedded clinical ovarian carcinoma specimen. Indeed, FILIP1L expression and protein levels were significantly lower in invasive serous carcinomas compared to serous borderline tumors (low malignant potential tumors).

There is a 407 base pair (59 individual CpGs) CpG island at the promoter controlling FILIP1L isoform 203 expression [215]. The 29 CpGs in the core of the CpG island were highly methylated in ES2 and OCC1 cells (that have no FILIP1L expression) and partially methylated in OVCA429 and SKOV3 cells (having medium and low FILIP1L expression). Interestingly, in HOSE and IOSE the CpG island was almost unmethylated (<10%) and the percentage of methylation inversely correlated with FILIP1L expression. Treatment of cell lines with the DNMT inhibitor DAC resulted in decrease methylation levels at the *FILIP1L* promoter and an increase in FILIP1L expression [215]. The histone deacetylase inhibitor TSA had no effect on FILIP1L expression and treatment of OVCAR8 cells (having medium FILIP1L expression) with DAC did not increase FILIP1L expression significantly. A similar effect was

observed in clinical ovarian carcinoma specimen, where methylation was lower in non-invasive and increased in invasive samples, and FILIP1L expression inversely correlated with percentage methylation of the promoter region, however, the inverse correlation was not as significant as it was in cell lines. Taken together, these findings suggest that promoter methylation mediates FILIP1L expression in ovarian cancer [215].

In an attempt to identify genes, involved in mediating doxorubicin resistance, Lu and Hallstrom [216] used a pooled shRNA screening approach in U2OS human osteosarcoma cells. They found, that shRNA mediated knock-down of FILIP1L significantly decreased doxorubicin induced apoptosis in U2OS cells. Furthermore, doxorubicin treatment increased FILIP1L expression 150-fold and inhibition of ataxia telangiectasia mutated (ATM) and ataxia telangiectasia and Rad3-related (ATR) with caffeine reduced FILIP1L induction by 90%, suggesting ATM or ATR induction or both by doxorubicin induced DNA damage mediates FILIP1L induction. Because U2OS cells carry a wild type *Trp53* gene, Lu and Hallstrom tested if in mutant p53 SAOS-2 cells induction of FILIP1L could also be observed. Interestingly, FILIP1L was not induced in SAOS-2 cells, suggesting ATM/ATR and p53 are required for FILIP1L induction following DNA damage. Doxorubicin is a so-called DNA topoisomerase 2 (TOP2) poison. Agents of this class increase TOP2-DNA complexes and eventually lead to DNA strand breaks and cell death. In contrast, TOP2 catalytic inhibitors do not elevate TOP2-DNA complex levels. FILIP1L expression was only increased after treatment with TOP2 poisons, but not by TOP2 catalytic inhibitors or UV damage, suggesting that up-regulation of FILIP1L is specific to DNA damage cause by TOP2 poisons. It is worth noting, that the results from experiments by Lu and Hallstrom testing the effect on UVR on FILIP1L expression were performed with UV-C radiation and may not produce reliable data (check methods section of Lu and Hallstrom [216]). To test if FILIP1L alone is able to induce apoptosis, Lu and Hallstrom ectopically expressed FILIP1L in U2OS cells and observed that apoptosis was increase 5-fold compared to controls. Similarly, in SAOS-2 cells (that do not upregulate FILIP1L in response to doxorubicin, FILIP1L expression also led to a 4-fold increase in apoptosis. The FILIP1L promoter harbours three potential OCT1 (POUF2F1) binding sites, OCT1 is known to mediate DNA induced cellular stress. Knock-down of OCT1 with shRNA in U2OS cells, while only 60% effective, did not

affect baseline expression of FILIP1L. However, when cells were treated with doxorubicin, FILIP1L induction was reduce by 65% and apoptosis was reduced by 45%. Furthermore, doxorubicin treatment lead tom increased binding of OCT1 to the FILIP1L promoter. Taken together these findings suggest, that doxorubicin induces DNA damage, which then induces OCT1 and subsequently up-regulates FILIP1L expression and apoptosis [216].

In order to elucidate the role of FILIP1L in various human cancers, Kwon *et al.* [217] investigated FILIP1L expression in human cell lines of different tumor origin, namely colon cancer (HT-29, HCT116, HCT-15, SW620, T84, Caco-2, SW480), lung cancer (H23, H322, H1299, H460, A549, H661), pancreas cancer (MIA Paca-2, PANC-1, Hs766T, HPAC, HPAF-II, SU.86.86, Panc 02.03, Capan-1) and breast cancer (BT-549, Hs578T, MDA-MB-468, BT-474, ZR-75-1,MDA-MB-231, MCF7). As controls, they used immortalized colon cell line NCM460, primary small airway epithelial cells (SAEC) and mammary epithelial cells (HMEC). FILIP1L mRNA and protein levels correlated well, except for HMEC and SAEC cell line, that both showed robust FILIP1L expression, but no FILIP1L protein. In general, FILIP1L expression and protein were high in normal cells, nut low in most cancer cell lines. Interestingly in the breast cell line panel, non-invasive MCF7 cancer cells highly expressed FILIP1L. Methylation at the *FILIP1L* promoter inversely correlated with FILIP1L expression in all four cancer entities and treatment of BT549, HT29, H1299 and MIA PaCa2 cells with DAC restored FILIP1L expression. Taken together, this further suggests promoter methylation mediates FILIP1L expression.

When Kwon *et al.* tested the invasive potential of the cell lines using Matrigel, they demonstrated that FILIP1L expression inversely corelates with Matrigel invasion. Re-expression of FILIP1L (or truncation mutant FILIP1LΔC103) in low expressing cells significantly reduced invasion, while siRNA mediated knock-down in high expressing cells significantly increased invasive potential. These data suggest, that FILIP1L expression inversely correlates with invasive potential and the invasive phenotype can be reversed by overexpression of FILIP1L [217].

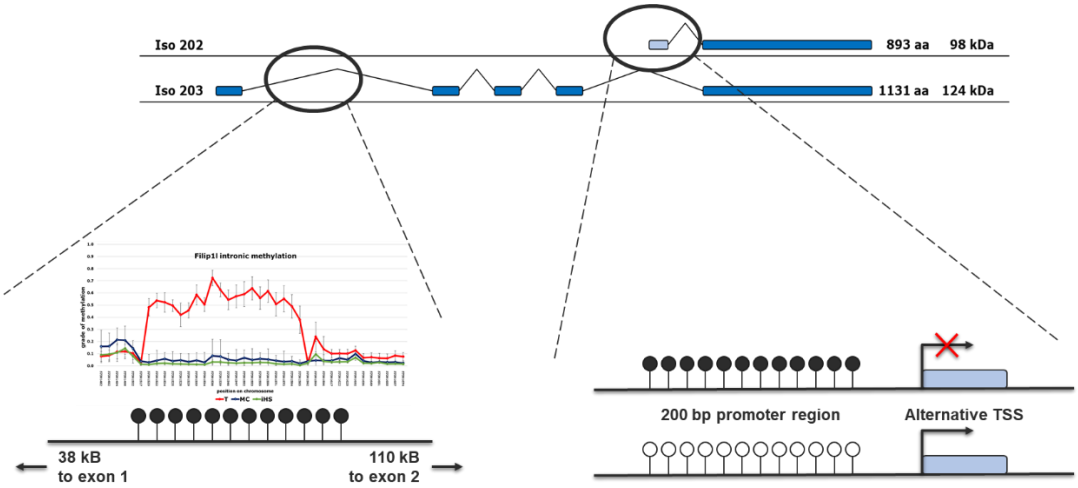

Figure 9: Regulation of FILIP1L expression: Left: An intronic CGI in the mouse *Filip1l* gene could potentially be involved in Filip1l expression. **Right:** Methylation at the human *FILIP1L* promoter has been shown to inversely correlate with FILIP1L expression.

As previously discussed, the *FILIP1L* gene encodes 8 known isoforms (see **Figure 8**). Desostelle *et al.* [218] used isoform specific primers to determine which isoforms are expressed in prostate cancer and normal prostate. They used primers that are able to distinguish between isoforms 202 (full length, termed isoform 1 in their publication) and 203 (termed isoform 2 in their publication). Since their study was published, more FILIP1L isoforms were reported. The primers used to amplify isoform 202 also amplify isoforms 206 and 209 and the primers used to amplify isoform 203 also amplify isoform 206. In human prostate epithelial cells (HPECs) FILIP1L isoform 203 was predominantly expressed, with isoform 202 only showing very low expression. FILIP1L was not expressed in prostate carcinoma cell line DU145, PC3, LNCaP and 22Rv1 cell lines. Furthermore, FILIP1L isoform 203 was up-regulated when HUVECs were cultured to senescence and was down-regulated in 5 of 11 prostate tumors compared to matched controls. Using a tissue microarray and a FILIP1L specific antibody, Desostelle *et al.* found that FILIP1L levels are 15 to 30 times higher in the stroma compared to the epithelium. Furthermore, FILIP1L expression was higher in the cytoplasm. In benign samples, there was no significant difference in FILIP1L levels in the cytoplasm in both, stroma and epithelium. However, in the nucleus FILIP1L levels were significantly lower in nuclei of cancer tissue (highly significant ($p=0.006$) in epithelium, significant ($p=0.045$) in stroma). FILIP1L expression was not associated with Gleason score (level of differentiation), tumor stage or metastasis. Using bisulfite treatment and pyrosequencing, it was shown that the promoter CpG

island controlling isoform 203 expression (called exon 5 in the publication) is hypermethylated in prostate cancer cell lines DU145, PC3, LNCap and 22Rv1, while in HPECs the CpG island was mostly unmethylated. The same was true for benign prostate tissue and prostate cancer samples. When the effect was quantified, the difference, while significant, was below 10% [218]. This could be because the effect in tumors was diluted as DNA samples was not taken from pure tumor, and may have included large amounts of benign surrounding tissue.

Another study from the Libutti group was published in 2014, when Kwon *et al.* further investigated the functional significance of FILIP1L in ovarian cancer [219]. Kwon *et al.* previously showed that out of all ovarian cancer cell lines tested, FILIP1L expression is lowest in ES2 cells [217]. They generated ES2 cells, that express FILIP1LΔC103 and mCherry in a doxycyclin (DOX) inducible manner. Interestingly, FILIP1L expression in ES2 cells did not have an effect on proliferation. When these cells were injected into ovaries of SCID mice, the mice developed very aggressive ovarian cancer. Within 19 days, 90% of mice died with significant ascites by day 17, metastasis into the peritoneum, intra-abdominal organs, pelvic lymph nodes and liver as well as spontaneous lung metastasis by day 14. Expression of FILIP1L induced by DOX did not affect growth of primary tumors, but significantly inhibited metastatic spread to the lungs. Cancer metastasis is a multi-step process, requiring cancer cells to invade surrounding tissue, intravasation into the blood stream and extravasation as well as tumor growth at the secondary site [220]. By injecting ES2 cells in the tail-vein, Kwon *et al.* bypassed the initial invasion and extravasation step. FILIP1L expression did not affect tumor development in lungs, suggesting that FILIP1L is involved in invasion or intravasation and not extravasation. This finding was confirmed *in vitro* with electric cell-substrate impedance sensing. When performing *in vivo* invasion assay in the orthotopic model, it became clear that FILIP1L expression inhibits the early invasion steps of ovarian cancer metastasis. Interestingly, invasion was completely blocked by using pan-MMP (matrix metalloproteinase) inhibitor GM6001 in control cells (not expressing FILIP1L). Expression of MMP3, -7 and -9 were significantly reduced in FILIP1L expressing tumors. Furthermore, gelatine degradation also was significantly lower in tumors expressing FILIP1L. Transfection of a MMP9 expression plasmid restored invasive potential in ES2 cells expressing FILIP1L *in vitro*, suggesting FILIP1L inhibits invasion by down-

regulation of MMPs. MMPs 3, 7 and 9 are transcriptionally controlled by the canonical Wingless/Integrated (WNT) signaling pathway [221]. To test, if WNT signaling is influenced by FILIP1L expression, Kwon *et al.* tested expression of several components of the WNT signaling pathway. WNT ligands WNT-2, -3A, -4, -5A, -7A and -11 were highly expressed in tumors, but not in cultured cells and significantly down-regulated in FILIP1L expressing tumors. Expression of WNT receptors frizzled (FZD) and low-density lipoprotein receptor-related protein (LRP) were not influenced by expression of FILIP1L. Treatment of ES2 cells with WNT3A resulted in induction of MMPs but this was significantly reduced in FILIP1L expressing cells. The WNT pathway can be induced by either WNT agonists of by inhibiting glycogen synthase kinase (GSK) -3β. WNT activity was significantly reduced in ES2 cells that express FILIP1L compared to controls when WNT signaling was activated. Canonical WNT signaling relies on transcriptional activation via β-catenin, that normally is repressed by N-terminal phosphorylation that marks it for ubiquitination and proteasomal degradation. Phospho-β-catenin was reduced by WNT activation, but interestingly remained unchanged in FILIP1L expressing cells. Inhibiting proteasomal degradation with inhibitor MG132 increased phospho-β-catenin levels regardless or FILIP1L expression, suggesting that FILIP1L supresses canonical WNT-signaling by proteasome-mediated β-catenin degradation [217].

Following up on their 2013 study, Kwon *et al.* [222] used an ovarian cancer tissue microarray, where clinical outcomes of patients were available, to test the implications of FILIP1L expression on ovarian cancer outcome. They found, that FILIP1L levels decrease with tumor progression, with a significant difference when comparing normal to metastatic tissue. Levels of the WNT mediator β-catenin and epithelial to mesenchymal transition (EMT) transcription factor SLUG showed an inverse trend. In metastatic tissue, FILIP1L expression was significantly lower than in the primary tumor from the same patient. Strikingly, in tumors that were resistant to platinum/paclitaxel combination therapy, FILIP1L levels were significantly lower compared to sensitive tumors, while SLUG, showed an inverse expression pattern. Indeed, FILIP1L levels inversely correlated with β-catenin and SLUG, while β-catenin and SLUG positively correlated. Expression of another EMT transcription factor, SNAIL, also increased with tumor progression, but did not differ between chemo-resistant and -sensitive tumors and did not inversely correlate with FILIP1L

expression. Patients with high FILIP1L had a significantly improved prognosis and did not yet reach median overall and disease-free survival in a 120-month follow-up period, while patients with low FILIP1L had an overall survival of 60 month and disease-free survival of 16 months. In the Cox proportional hazards model [223], high β-catenin or high SLUG in combination with low FILIP1L levels, high β-catenin in combination with high SLUG expression or low FILIP1L expression alone were independent negative prognostic markers for disease-free survival, suggesting FILIP1L expression is a useful prognostic marker for ovarian cancer. Kwon *et al.* engineered ovarian cancer cells OVCA429 and SKOV3 cells that normally do not express FILIP1L, to express FILIP1L to similar levels as immortalized normal ovarian epithelial cells. When these cells were injected into ovaries of nude mice, there were 16- (OVCA429 cells) and 7-fold (SKOV3 cells) fewer peritoneal metastasis, respectively. Together with previous finding, where similar effects were observed for ES2 cells [217], this suggests that FILIP1L is a potent tumor suppressor in ovarian cancer. Kwon *et al.* previously showed, that in ovarian cancer, FILIP1L expression negatively correlates with the EMT transcription factor SLUG and is lower in tumors that are resistant to platinum and paclitaxel therapy [217]. To test if chemoresistance is regulated by FILIP1L, Kwon *et al.* decreased FILIP1L expression in serous ovarian carcinoma cells using siRNA. FILIP1L suppression increased SLUG expression and cytotoxicity assay revealed, that cisplatin, paclitaxel and doxorubicin efficacy was markedly decreased. Simultaneous siRNA knock-down of SLUG alongside FILIP1L rescued the chemosensitive phenotype. Additionally, FILIP1L expression levels in ovarian cancer cell lines correlated with chemoresistance. WNT signaling activity can be monitored by comparing active (unphosphorylated), inactive (N-terminally phosphorylated, marked for degradation) and total β-catenin. Activation of WNT signaling by LiCl in OVCA429 and SKOV3 cells increased active and decreased inactive β-catenin, while total β-catenin remained relatively constant. Engineered cells, expressing FILIP1L, had reduced active and increase inactive β-catenin levels compared to parental cells. When proteasomal activity was blocked with MG132, inactive β-catenin levels increased independently of FILIP1L expression. Similar effects of FILIP1L were observed, when FILIP1L was knocked down in HEY and OVCAR8 cells that express high levels of FILIP1L, suggesting that FILIP1L controls the canonical WNT signaling pathway, by mediating β-catenin availability upstream of the proteasome.

Previously, Kwon *et al.* detected FILIP1L at centromeres, which serve as proteolytic centres. In OVCA429 and SKOV3 cells expressing FILIP1L, FILIP1L co-localized with inactive β-catenin, proteasomes and the centromere marker γ-tubulin, suggesting FILIP1L facilitates proteasomal degradation of phospho-β-catenin at centromeres, thus blocking WNT signaling.

A key feature of EMT is the loss of epithelial markers (e.g. E-cadherin) and induction of mesenchymal transcription factors (e.g. SLUG), MMPs and adhesion molecules [224]. As EMT is controlled by WNT in ovarian cancer, Kwon *et al.* tested if WNT activation leads to differential expression of EMT markers in FILIP1L^{+} and FILIP1L^{-} cells. Before WNT activation, FILIP1L^{-} cells (OVCAR429 and SKOV3) expressed high levels of mesenchymal markers N-cadherin and vimentin as well as SNAIL, but low levels of epithelial marker E-cadherin. FILIP1L^{+} cells expressed more E-cadherin and less N-cadherin, vimentin and SLUG. Activation of WNT with LiCl in FILIP1L^{-} cells induced mesenchymal markers and repressed epithelial markers. The effects of LiCl were abrogated in FILIP1L^{+} cells, suggesting that FILIP1L supresses EMT through down-regulation of WNT signaling.

In mouse xenograft tumors from FILIP1L^{+} cells, mesenchymal markers were decreased, and E-cadherin was increased compare to tumors from FILIP1L^{-} cells. The FILIP1L^{+} tumors trended towards EMT inhibition, but there was no consistent correlation with data from cultured cells. When FILIP1L was knocked down in HEY and OVCAR8 cells (high FILIP1L), mesenchymal markers increased, and E-cadherin decreased. SLUG was consistently up-regulated when FILIP1L was knocked down or WNT was activated. Furthermore, FILIP1L knockdown changed cell morphology to a more mesenchymal phenotype and interestingly, this could be rescued by additional knockdown of SLUG. Taken together, these findings suggest, that loss of FILIP1L leads to an increase in WNT signaling, thereby promoting tumor progression by SLUG-mediated activation of EMT [222].

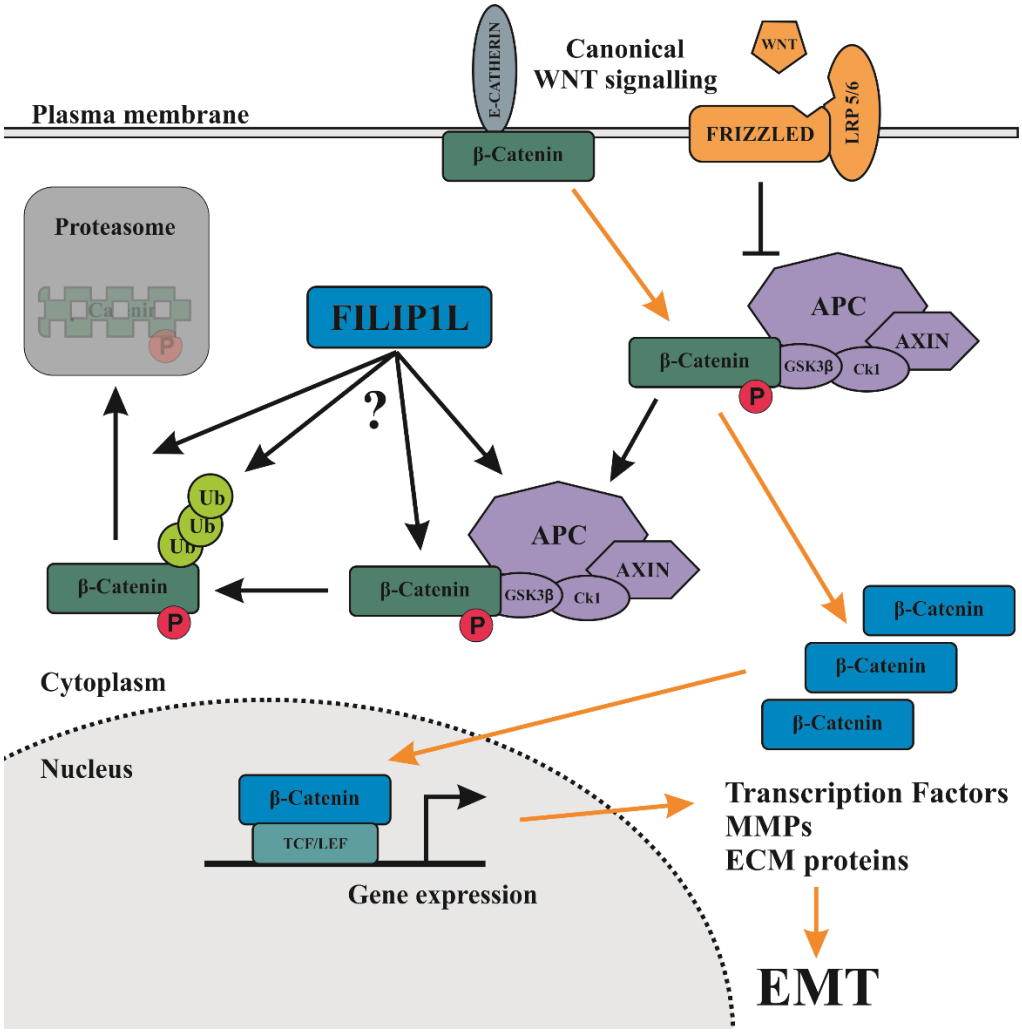

Figure 10: The proposed role of FILIP1L in regulating WNT signaling and cancer metastasis according to Kwon *et al.*: Activation of the WNT signaling pathway by WNT ligands inhibits binding of β-catenin to the destruction complex (purple), which under inactive conditions phosphorylates β-catenin and marks it for proteasomal degradation. Unphosphorylated β-catenin transitions to the nucleus and, in concert with TCF/LEF transcription factors, induces gene expression of EMT promoting transcription factors and MMPs. While MMPs facilitate cancer cell invasion, activation of EMT aids cancer metastasis and chemoresistance. **The exact mechanism how FILIP1L enhances β-catenin degradation is unclear**. Proposed mechanisms are either inactivation of the β-catenin destruction complex (e.g. GSK3β), recruitment of phospho-β-catenin to centromeres or facilitating poly-ubiquitinated β-catenin destruction. Figure adapted from Kwon *et al.* [222].

Most of the functional data on FILIP1L comes from ovarian cancer, but FILIP1L has been demonstrated to be down-regulated in other cancer entities as well. Park *et al.* [225] investigated the role of FILIP1L in colorectal cancer. First, they tested FILIP1L protein levels in various human colorectal cancer cell lines (SW480, DLD1, DKO1, HCT116, HT29 and COLO205). Levels were highest in COLO205 cells and lowest in HCT116. For further experiments, they overexpressed FILIP1L in HCT116 cells and knocked-down expression in COLO205 cells using siRNA. In COLO205 cells, FILIP1L knock-down reduced migration and invasion and increased expression of MMP-2 and -9. Conversely, FILIP1L overexpression in HCT116 cells decreased migration and invasion and decreased MMP-2 expression, while MMP-9 expression did not change. Furthermore, FILIP1L overexpression increased apoptosis, cleaved caspase-3 and -7 and induced sub-G1 cell cycle arrest in HCT116 cells, while FILIP1L knock-down had the opposite effect on COLO205 cells. Park *et al.* used conditioned medium (CM) from either HCT116 cells overexpressing FILIP1L or FILIP1L knock-down COLO205 cells to evaluate the effects of FILIP1L on angiogenesis. When HUVECs were cultured using CM from FILIP1L knock-down COLO205 cells, HUVEC invasion was significantly increased in comparison to CM from control COLO205 cells. Vice-versa, CM from FILIP1L overexpressing HCT116 cells reduced HUVEC invasion in comparison to CM from control HCT116 cells. Angiogenic inducers VEGF-A and HIF-1α were up-regulated and angiogenic inhibitor angiostatin was reduced in FILIP1L knock-down COLO205 cells, while in FILIP1L overexpressing HCT116 cells expression of VEGF-A and -D was reduced and expression of angiostatin and endostatin was increased. Park *et al.* tested if FILIP1L mediates WNT signaling in colorectal cancer, and indeed, FILIP1L expression (either knock-down or overexpression) correlated with levels of phospho-β-catenin and negatively correlated with levels of phosphorylated AKT and GSK3β levels. In fixed colorectal cancer tissues (n=354), FILIP1L was primarily located in the cytoplasm and expression was lower in colorectal cancer compared to colorectal epithelial cells. TUNEL assay revealed, that apoptotic index (AI) did not correlate with FILIP1L expression. However, proliferation (as measured by Ki-67 staining) and angiogenesis (CD34) were significantly reduced in FILIP1L positive tumors. Furthermore, FILIP1L positive tumors were significantly smaller, more differentiated, showed less lymphovascular invasion, were lower in cancer stage, had a lower depth of invasion and less lymph node metastasis. Patients with FILIP1L positive tumors had

significantly longer overall survival than patients with FILIP1L negative tumors. The Cox proportional hazard model revealed, that low FILIP1L expression was independently associated with poor overall survival, suggesting FILIP1L may have an important role in colorectal cancer [225].

Unrelated to the function of FILIP1L in cancer, FILIP1L was found by Liu *et al.* [226] when they examined the effect of melatonin on pig granulosa cells. Exogenous melatonin promotes the maturation of oocytes by granulosa cells (GCs) as in pigs, low melatonin doses cause GCs to produce estradiol. Using transcriptome sequencing, they found 78 differentially expressed genes when pig GCs were treated with melatonin. Among those genes, FILIP1L was upregulated. When Liu et al. knocked down FILIP1L using siRNA, estradiol production in GCs was reduced [226].

Pan *et al.* [227] found that circular RNA (circRNA) Filip1l is expressed in spinal cords of mice with chronic inflammation pain. CircRNAs arise from alternative splicing and are highly stable. Several different modes of action have been proposed for circRNAs, including regulation of micro RNAs (miRNAs), e.g. the interaction of ciRS-7 and miRNA-7 in cancer [228]. When chronic inflammatory pain was induced by subcutaneous injection of carrageenan- and complete Freund's adjuvant (CFA), circRNA-Filip1l was induced in spinal cords after 1 day, peaked at 3 days and came down to baseline levels after 14 days. Circ-Filip1l was located in spinal nuclei. Expression of circ-Filip1l in mouse spinal cords using lentivirus mimicked the nociception-like behaviour. As miRNAs have been shown to influence circRNA expression, Pan *et al.* used the miRBase (http://www.mirbase.org/) miRNA database to search miRNAs that could bind circ-Filip1l and identified miRNA-1224 as a potential regulator. Indeed, CFA decreased miRNA-1224 expression in spinal cords from 2 h to 7 d after injection. Expression of miRNA-1224 in spinal cords decreased levels of circ-Filip1l expression and miRNA-1224 inhibitor had the opposite effect. Interestingly, both treatments had no effect on precursor circ-Filip1l. Injecting miRNA-1225 mimics into spinal cords also attenuated nociceptic effects of CFA. Regulation of circRNAs has been shown to be Ago2 dependant manner. Using AGO2 antibody, Pan *et al.* were able to pull down both, pre-cic-Filip1l and miRNA-1224. Silencing of Ago2 in mouse spinal cords did significantly upregulate circ-Filip1l following CFA treatment, but did not have an influence on prec-circ-Filip1l, suggesting circ-Filip1l is controlled by miRNA-124 in an Ago2 dependant manner.

They used in silico prediction to identify genes that could be regulated by circ-Filip1l and found *ubiquitin protein ligase E3 component η-recognin* (*Ubr5*) as a potential target. Ubr5 is associated with neuronal plasticity and pathological processes of the central neural system. Indeed, Ubr5 was upregulated in spinal cords of CFA treated mice and circ-Filip1l overexpression also induced Ubr5. The nociceptic effects of circ-Filip1l overexpression were significantly reduced when Ubr5 was silenced using siRNA. Taken together, this results suggest a model, in which pre-circ-Filip1l splicing is prevented by miRNA-1244 in an Ago2 dependant manner under normal conditions, but under conditions of inflammatory pain, due to miRNA-1244 down-regulation, pre-circ-Filip1l is spliced into circ-Filip1l that in turn promotes Ubr5 expression and downstream signaling [227].

1.4.3 FILIP1L as novel tumor suppressor gene

Although the number of studies on FILIP1L is limited, the fact that this novel tumor suppressor gene is consistently down-regulated in many cancers, correlates with tumor grade and the risk of metastasis in ovarian and colorectal cancer, and is an independent prognostic marker for survival, highlights that FILIP1L is an important mediator of tumor progression and could be a promising prognostic marker as well as a target for treatment.

2 Materials and Methods

2.1 Materials

2.1.1 Plastics

Table 5: Plastics and other disposable equipment.

	Supplier
0.45 µm syringe filter	Thermo Scientific
96 Well MicroampTM Optical 96-Well Reaction Plates	Thermo Scientific
ABsolute qPCR Plate Seals	Thermo Scientific
Cell Scrapers	Sarstedt
Coolcell® Cell Freezing Container	Biocision
Coverslip	Marienfeld
Cryotubes	Nunc
Eppendorfs	Sarstedt
Falcons	Corningcentristar
Flask	Thermo Scientific
Petri Dish	Thermo Scientific
Qiashredder	Qiagen
Tips (20, 100 and 1000 µl)	Starlab
Tissue culture plates (6, 12, 96 well)	Thermo Scientific

2.1.2 Chemicals

Table 6: Chemicals used for buffers, reactions and other experiments.

	Supplier
2-Mercaptoethanol	Sigma
2-Propanol	VWR
Acetic Acid	Bio Rad
Acrylamide–Bis-Acrylamide Stock	Invitrogen
Agarose	Sigma
Ammonium Persulfate	Sigma
Ampicillin	Sigma
Bovine Serum Albumin	Chemometec
Bromophenol Blue	Sigma
Chloroform	Sigma
DNA Gel Loading Dye	Sigma
DTT	Sigma
EDTA	Sigma
Ethanol	VWR
Fugene HD Transfection Reagent	Promega
Gelatin porcine skin	Sigma
Glycerol	VWR

Glycine	Fisher Biolegends
Guanidine Hydrochloride	Sigma
HEPES	Sigma
Membrane Amersham Protran Supported 0.45µm	GE Healthcare Life
Methanol	VWR
MgCl2	Sigma
MOPS Running Buffer	Invitrogen
NaCl	Sigma
NaOH	Sigma
Non-fat milk powder	Marvel
Nupage™ 4-12% Bis-Tris Protein Gel	Novex, Life
PBS Tablets	Oxoid
Ponceau S Solution	Sigma
Potassium chloride	VWR
Puregene Proteinase K	Qiagen
SDS	Sigma
Seeblue Pre-Stained Protein Standard	Invitrogen
Sodium Azide	Sigma
Sybr Safe	Invitrogen
T4 DNA Ligase & buffer	NEB
TaqmanTM Universal PCR Master Mix	Thermo Scientific
TEMED	Sigma
TRI Reagent	Sigma
Tris Base	Sigma
Tris-HCL	Sigma
Triton X-100	Merck
Tween 20	Sigma

2.1.3 Kits

Table 7: Kits used for isolation and protein quantification.

	Supplier
AllPrep DNA/RNA/Protein Mini Kit	Qiagen
Maxiprep	Qiagen
Miniprep Kit	Qiagen
Omniscript Reverse Transcriptase	Qiagen
Pierce™ BCA Protein Assay Kit	Thermo Scientific
RNAse-Free DNAse Set	Qiagen
Rneasy Kit	Qiagen

2.1.4 Tissue Culture

Table 8: Media and reagents used for tissue culture.

	Supplier
Dulbecco's Modified Eagle Medium (DMEM)	Gibco
Ham's F-12 Nutrient Mix	Gibco
Keratinocyte-SFM	Gibco
Keratinocyte-SFM Medium Kit	Gibco
RPMI 1640	Gibco
Opti-MEM Media	Gibco
AlamarBlue cell viability reagent	Thermo
Cholera Toxin	Sigma
Fetal Bovine Serum	Labtech
Human Keratinocyte Growth Supplement (HKGS)	Gibco
Hydrocortisone	Sigma
Insulin	Sigma
Lipofectamine RNAiMAX reagent	Invitrogen
Mycoalert® Mycoplasma Detection Kit	Lonza
Penicillin-Streptomycin (10,000 U/mL)	Gibco
Plenticrispr V2	Addgene
pMD2.G	Addgene
Polybrene	Santa Cruz
psPAX2	Addgene
Puromycin	Santa Cruz
Recombinant Mouse EGF	Gibco
Transferrin	Sigma
Trypsin 0.05% EDTA, Phenol Red	Gibco

2.2 Solutions

2.2.1 10x PBS

100 PBS Tablets

Sodium Chloride 137 mM

Phosphate Buffer 10 mM

Potassium Chloride 2.7 mM (pH 7.4)

dH_2O up to 1 L

2.2.2 1x PBS

100 mL of 10x PBS

900 mL of dH_2O

Autoclaved

2.2.3 RM^- Medium

2 mg Cholera toxin

1 g hydrocortisone

500 mg insulin

500 mg transferrin

100 mg 3,3’5-Triiodo-L-thyronine sodium salt

100 mL of Ham’s F12 nutrient mixture

300 mL of DMEM (Dulbecco’s Modified Eagle Medium)

40 mL of FBS (Fetal bovine serum)

2.2.4 RM^+ Medium

2 mg Cholera toxin

1 g hydrocortisone

500 mg insulin

500 mg transferrin

100 mg 3,3’5-Triiodo-L-thyronine sodium salt

1 mg mouse Epidermal Growth factor

100 mL of Ham’s F12 nutrient mixture

300 mL of DMEM

40 mL of FBS

2.2.5 Protein wash solution

0.3 M guanidine hydrochloride

In 95% ethanol

2.2.6 2x SDS protein buffer

100 mM Tris-HCl

4% SDS (w/v)

20% glycerol (v/v)

50 mM EDTA

10% β-ME (added after protein quantification)

Bromophenol blue (added after protein quantification)

2.2.7 BCA Protein Assay Reagent B

4 g copper (II) sulphate pentahydrate

100 mL dH_2O

2.2.8 Subcellular Fractionation (SF) buffer

20 mM HEPES pH 7.4

10 mM KCl

2 mM $MgCl_2$

1 mM EDTA

1 mM EGTA

2.2.9 10 x Transfer Buffer

30.3 g Glycine

144 g Tris Base

dH_2O up to 1 L

2.2.10 1x Transfer Buffer

200 mL of methanol

100 mL of 10x Transfer buffer

0.1 % SDS

dH_2O up to 1 L

2.2.11 10x TBS

24.23 g Tris-HCL

80.6 g NaCl

dH_2O up to 1 L

Adjust pH to 7.6 using HCl

2.2.12 1x TBS and TBS-T

100 mL 10x TBS

900 mL dH_2O

1 mL Triton X-100 for TBS-T

2.2.13 Ampicillin (stock 100 mg/ml)

1 g Ampicillin dH_2O up to 10

mL

Filter, aliquot and freeze at -20 °C

2.2.14 Ampicillin LB Agar

LB Agar

Ampicillin stock solution 1:1000 (final concentration 100 µg/mL)

2.2.15 50x TAE Buffer

242 g Tris base

57.1 mL Glacial

Acetic Acid 100

mL 0.5M EDTA

dH_2O up to 1 L

Adjust pH to 8.0

2.2.16 1x TAE Buffer

20 mL 50x TAE buffer

980 mL dH_2O

2.2.17 Agarose gels

1x TAE buffer

x g Agarose/L (where x is the percentage of gel)

2.2.18 Stripping Buffer

334.4 g Guanidine Hydrochloride (7 M)

1.88 g glycine (50 mM)

0.05 mM EDTA

20 mM β-ME

3.73 g KCl (0.1 M)

dH_2O up to 500 mL

pH adjusted to 10.8 using NaOH

2.2.19 Cell culture freezing medium

FBS

5% v/v DMSO

Freezing medium was prepared fresh before usage

2.2.20 2x NTERT freezing medium

9 mL DMEM

9 mL Ham’s F12 nutrient mixture

2 mL FBS

Sterile filtrate with a 0.2 µm filter

2 mL DMSO

NTERT freezing medium was aliquoted and store at -20 °C

2.3 DNA, RNA and Protein Isolation

DNA for reduced representation bisulphite sequencing (RRBS) was isolated prior to the start of this project using the protocol described in [59]. In brief, mouse skin tumors were harvested and snap frozen in liquid N_2. Tumor tissue was enriched using laser capture microdissection and genomic DNA was isolated using the QIAmp DNA micro kit (Qiagen) according to the manufacturers protocol. Genomic DNA was then used for RRBS library preparation as described in **Section 2.4.1**.

For all following experiments, DNA, RNA and protein were isolated from fresh frozen tissue or cell pellets using a combination of TRI reagent (Sigma Aldrich) and the Qiagen AllPrep DNA/RNA kit. The manufacturers' protocol was modified in order to increase DNA and RNA yield and quality as well as meeting the requirements to the usage of TRI reagent. All used buffers were obtained from Qiagen.

2.3.1 Tissue processing and DNA, RNA, Protein separation

Fresh frozen samples were pulverized using a mortar. Sample integrity was ensured by pre-cooling the mortar and pestle with liquid N_2 and the sample was cooled throughout pulverization using liquid N_2. If DNA, RNA or protein was isolated from cell lines, cells were first pelleted using a microcentrifuge. Cell pellets were then washed using cold PBS and pelleted again before isolation. Cell suspensions and pellets were placed on ice throughout harvest.

For isolation, 20 – 50 mg of tissue powder or cell pellets were lysed with 500 µL RLT Plus buffer, supplied with 1% v/v β-mercaptoethanol (β-ME). After complete lysation, samples were centrifuged (3 min, 10000 rpm) in order to remove non-soluble components. For DNA binding, residual liquid was transferred to an AllPrep DNA spin column and flow through was collected in 2 mL reaction tubes. AllPrep DNA spin columns were washed with 500 µL buffer AW1 in order to remove β-ME and DNA isolation was carried out as described in **Section 2.3.2**.

In order to separate RNA and protein, 1 mL of TRI reagent was added to the flow through from the previous step, followed by vortexing. After incubation for 5 min at RT, 200 µL chloroform were added followed by vortexing and incubation for 15 min at RT. Phase separation was achieved by centrifugation (15 min, 13000 rpm, 4 °C). The colourless, aqueous phase, containing the RNA, was transferred to a new 2 mL reaction tube and incubated for 15 mins at RT after addition of 500 µL 2-propanol and

used for RNA isolation as described in **Section 2.3.3**. The red, organic phase was used for protein isolation following the protocol in **Section 2.3.4**.

2.3.2 DNA isolation

DNA was bound to AllPrep DNA spin columns as described in **Section 2.3.1**. Columns were inverted during initial washing with 500 µL buffer AW1 in order to remove β-ME completely. DNA was eluded from columns in 40 µL PBS and 10 µL RNAse (Plasmid Maxi kit, Qiagen) was added. RNA was digested for 30 min at 56 °C before the eluate was transferred to the AllPrep DNA spin column again, following RNAse on-column digestion for additional 15 min at 56 °C. Columns were washed using buffer AW1 and flow though was pipetted on the columns again in order to ensure complete DNA binding. Protein was digested on-column using 20 µL proteinase K solution (Qiagen) mixed with 60 µL buffer AW1 for 30 min at RT. Columns were washed twice with buffer AW1 before two final washing steps with buffer AW2. Columns were inverted during both washing steps in order to remove residual contaminates from buffer AW1. Columns were dry centrifuged (5 min, 13000 rpm) and DNA was eluted using 50 µL buffer EB. The eluate was pipetted back on the column in a second elution step in order to concentrate DNA.

DNA concentration and purity were measured using the NanoDrop ND-1000 Spectrophotometer and DNA was stored at 4 °C with tubes being sealed with parafilm to prevent evaporation.

2.3.3 RNA isolation

All centrifugation steps for RNA isolation were carried out at 4 °C. The RNA containing aqueous phase was handled as described in **Section 2.3.1**. Protein digestion was achieved by adding 15 µL proteinase K solution (Qiagen) to every tube and incubation for 15 min at RT. In order to ensure RNA binding to columns, 400 µL buffer RW1 was added and mixed briefly by inverting the tubes. AllPrep RNA spin columns were primed using 200 µL buffer RW1. The entire solution then was transferred to spin columns in steps of 700 µL using a vacuum manifold. After washing the columns with 400 µL buffer RW1, remaining DNA was digested on column using 10 µL DNAse I in 70 µL buffer RDD (RNAse-free DNAse Set, Qiagen) for 15 min at RT. Columns were washed using 500 µL buffer RW1 and flow through was pipetted on the spin columns again in order to ensure complete RNA binding. Columns were washed twice with buffer RPE and inverted in both washing steps to

ensure removal of residual contaminations from buffer RW1. Columns were dry centrifuged (5 min, 13000 rpm) and RNA was eluted using 30 µL RNAse-free water. The eluate was pipetted back on the column in a second elution step in order to concentrate RNA.

RNA concentration and purity were measured using the NanoDrop ND-1000 Spectrophotometer and RNA was stored at -80 °C.

2.3.4 Protein isolation

Protein was precipitated from the red, organic phase from **Section 2.3.1** by adding 1 mL 2-propanol and incubation for 1 h at RT. Protein was pelleted by centrifugation (10 min, 13000 rpm, 4 °C). Protein pellets were washed twice using 1 mL wash solution (**Solution 2.2.5**) for 20 min. Between washing steps, washing solution and protein pellets were centrifuged for 5 min at 13000 rpm at 4 °C.

After the final washing step, protein pellets were stored in washing solution at -20 °C.

For usage in further experiments, protein pellets were resuspended in 2 x SDS buffer (**Solution 2.2.6**). To ensure complete lysis, protein was heated to 50°C and temperature was increased to 100°C in a shaking heat block. Once heated to 100°C, proteins were boiled for 5 mins and then sonicated (2x 10 s, 20% amplitude, Ultrasonic processor, Cole-Parmer instruments, Illinois, USA). Protein was boiled for an additional 5 mins in a shaking heat block.

Protein concentration was measured in triplicates using BCA protein assay (Thermo Scientific) using albumin standard (Thermo Scientific). Protein samples were diluted 1:10 with water and 10 µL of dilution was mixed with 200 µL of BCA solution, previously prepared by mixing Reagent A with 1:50 volumes of Reagent B. After incubation for 30 mins at room temperature on a shaker, absorbances were measured using the Spectromax M2 microplate reader (Molecular devices) at 562 nm. Protein concentration was determined according to BSA standards and protein subsequently was diluted to a suitable concentration and reducing agent 10% β-ME v/v and bromophenol blue were added.

2.4 Analysis of global DNA methylation in solar simulated UV induced mouse cutaneous squamous cell carcinoma

The goal of this study was to examine DNA methylation in cutaneous squamous cell carcinoma (cSCC) in mice and the feasibility to use solar simulated UV (ssUV) induced mouse cSCC as a model for the human disease. Therefore, we studied global methylation in 7 mouse cSCC tumors, alongside matching control samples from ventral skin of the same mouse, that has not been exposed to UV radiation. A technical replicate was included for one of the controls as well as one of the tumor samples. Additionally, two independent dorsal skin control samples were obtained from mice of the same age as the study group, living under the same conditions, but not exposed to UV-treatment. All samples were subjected to (oxidative) reduced representation bisulphite sequencing ((ox)RRBS).

RRBS was performed at the Ghent University NXTGNT sequencing facility, Belgium. Data was analysed in collaboration with the group of Professor Tim de Meyer (Cancer Research Institute Ghent, Belgium).

2.4.1 Library preparation and Sequencing

DNA for library preparation was isolated following the protocol described in **Section 2.3**. Library preparation and sequencing were performed by NXTGNT. Upon arrival, DNA samples were subjected by Quant-iT™ PicoGreen™ dsDNA Assay Kit (P7589, ThermoFischer) for quality assessment. No aberrations were detected, and 1 µg DNA was used for MSP1 digestion. Digestion was performed overnight for 16 h at 37°C in a volume of 30 µL and stopped with 5 µL 0.5 M EDTA. Subsequently, the digestion product was purified with the GeneJET PCR Purification Kit (K0701, ThermoFischer), eluted in 50 µL elution buffer and quality was checked again on E-Gel™ EX Agarose Gels, 1% (G401001, ThermoFischer). NEBNext Ultra DNA Library Prep Kit for Illumina (E7370, New England Biolabs) and TrueMethyl seq kit (Feb 2015, Cambridge Epigenetix) were used for library preparations. For both kits, the protocol was followed according the manufacturers recommendations. Samples were split into two aliquots (each 275 ng) of which one was oxidized for oxRRBS. After bisulfite conversion and subsequent clean up reaction, polymerase chain reaction (PCR) amplification was performed according the PCR protocol that can be found in **Table 9**.

Table 9: PCR protocol for amplification of (ox)RRBS libraries.

Name	Temp	Time	Cycles
Denaturation	95°C	1 min	1
Cycling			
	95°C	15 sec	15
	61°C	30 sec	
	72°C	1 min	
Final			
Extension	72°C	7 min	1
Hold	4°C	∞	

Agencourt AMPure XP Bead Clean-up 1:1 (E6260) was performed for cleanup and DNA fragment length selection. Finally, a DNA high sensitivity chip on the Bioanalyzer (Agilent technologies) and measurements of qPCR quantification according to the Illumina protocol ("qPCR quantification protocol guide") concluded the last quality control steps.

Sequencing was performed on the NextSeq500 using 7 dark cycles on single read fragments with a length of 76 bp. A concentration of 1.8 pM was loaded with a 15% PhiX spike-in.

The Mouse reference genome as provided by Ensembl (GRCm38/mm10) was used for mapping of (ox)RRBS sequencing reads. Quality control and filtering of low-quality reads was performed using "Trim Galore!" (Babraham Bioinformatics). Quality control indicated no major problems, so Bismark (v.0.16.3, Babraham Bioinformatics) was used in Bowtie2-mode [229], for mapping. Seed length, mismatches and interval during multiseed alignment were set to the default values.

2.4.2 Differential methylation analysis

The differential methylation analysis was performed in R (v. 3.3.1) using Bioconductor (v. 2.34.0). The aligned data was imported using the BiSeq-package (v. 1.14.0) in R. Comparison between average methylation percentages of different states (e.g. cases vs controls) was performed using anova analysis and subsequent Tukey post hoc analysis if more than two groups were compared. Additionally, for correlation calculations, Pearson correlation was performed.

The raw counts were used to calculate methylation percentages per CpG (β-values, (1)) and subsequently M-values (2), with constant equal to 0.01. M-values were demonstrated to have superior statistical properties for Infinium HumanMethylation BeadArray data [230], but can also be applied on methylation sequencing data [231], and yield more appropriate data to be used with the R Bioconductor limma package (v. 3.30.13).

$$\beta = \frac{\#\,Methylated\ reads}{\#\,Total\ reads} \quad (1)$$

$$M = \log_2\left(\frac{\beta + C^{te}}{1 - \beta\ + C^{te}}\right) \quad (C^{te} = 0.01) \quad (2)$$

The calculation of β- and M-values implies intrinsic normalization (i.e. biases are largely equal for methylated and unmethylated reads), therefore no additional normalization between samples was performed. Data was however filtered to improve quality: (i) all loci that have a minimal coverage lower than 8x were considered insufficiently informative and were removed from the dataset, (ii) a minimum of 6 methylated reads over all samples was required to be retained in the dataset for further analysis (i.e. at least some methylation should be present). Finally, after statistical analysis with limma (per CpG), the Benjamini-Hochberg procedure was used to calculate false discovery rates (FDR), and set at a threshold of 10% to indicate significance.

For analysis of differentially methylated regions. the clusterSites function of the BiSeq package was used to search for agglomerations of CpG sites. A minimum of 15 CpGs in maximum 200 bp found in at least 75% of all samples are considered a potential differentially methylated region (DMR). The BiSeq package uses beta binomial regression to estimate p-values for each potential DMR [232].

2.4.3 Comparison with independent data

To evaluate the relevance of the mouse model in a human context, results were compared with human cSCC Infinium HumanMethylation BeadArray data created by Rodriguez-Paredes *et al.* [190]. The data were downloaded via the ArrayExpress database (accession: EGAS00001002670) and imported using the wateRmelon package (v. 1.18.0). Data was analysed using the same strategy that previously was used to analyse the RRBS data from mouse cSCCs, i.e. linear models of the M-values

by means of limma. Due to the high sample size (n=46), and thus more power, compared to the RRBS dataset (n=16) a more conservative FDR cutoff (5%) was consider for the human dataset. Next to assess differentially methylated loci, we also evaluated the identification by Rodriguez-Paredes *et al.* of stem-cell like and keratocyte like tumor samples. The authors kindly provided sample annotation with respect to both tumor groups.

Finally, genes were coined to be of major relevance when they were found in both, murine RRBS data and human Infinium data, and contained at least two significantly differentially methylated CpGs (RRBS) or probes (Infinium) with at least a 20% difference in average methylation between tumor vs. control.

2.4.4 Human-mouse orthologs

For establishing a human-mouse ortholog gene set the biomaRt package (v. 2.30.0) for R was used. Ensembl annotation is broadly used and contains homology information to be used for paralog or ortholog identification. The human genome, assembly GRCh37, was used in combination with the latest reference genome for mouse (assembly GRCm38/mm10), since this version is the most complete for gene symbol annotation [233]. BiomaRt gives an indication whether there is a high or low likelihood of two genes (one human, one murine) being orthologous. In case multiple genes with a high likelihood were found, the gene with the highest degree of homology was selected. Also, in case no gene with a high likelihood was found, the gene with the highest percentage of homology was selected. For both cases, if homology percentages were equal, genes with an identical gene symbol were preferred over their fellow candidates. If the latter still resulted in redundant candidates, all were kept as candidate human-mouse orthologs.

2.4.5 Building UCSC bed tracks

For visualization, results were compiled as a BedGraph file (https://genome.ucsc.edu/goldenpath/help/bedgraph.html). For all significant probes, the methylation percentage is displayed as a positive value (between 0 and 1) whereas for non-significant probes, the methylation percentage is displayed as a negative value and in a different colour. Significance of a probe is defined as was mentioned before (RRBS: FDR<0.10; Infinium: FDR<0.05). This definition for significance is retained respectively for both analyses throughout this manuscript.

2.4.6 Clustering

Clustering was achieved by using the 10,000 most variant loci over all samples, thereby excluding noise and low informative loci. As a measure for the equality of samples the Euclidian distance based on the covariance of the M-values was used.

2.5 Generation of FILIP1L isoform 203 expression vector

To investigate the effect of overexpressing FILIP1L isoform 203 (referred to just FILIP1L) in cell lines that have low expression, FILIP1L isoform 203 coding sequence was cloned into the mammalian expression vector pcDNA 3.1 V5/His A.

2.5.1 FILIP1L coding sequence amplification

FILIP1L coding sequence (CDS) was amplified from genomic DNA isolated from NTERT immortalized human keratinocytes using KOD Hot Start DNA polymerase (Merck) using the primers depicted in **Table 10**. Each 50 µL PCR contained the following reagents: 5 µL 10x Buffer, 3 µL $MgSO_4$ (25 mM), dNTP Mix (5 mM each, Invitrogen), primer mix (10 µM forward and reverse each), 200 ng genomic DNA, 1.5 µL DMSO (Thermo), 1 µL KOD Hot Start polymerase and water to a final volume of 50 µL. PCR was performed with an initial denaturation and enzyme activation step at 95°C for 2 min, 40 cycles of 95°C (20 s), 59°C (10 s) and 70°C (1 min 20 s), followed by a final elongation step at 70°C for 10 min. PCRs were run on a 0.7% agarose gel in TAE buffer (see **Solution 2.2.15**). DNA of the correct size (2814 bp) was cut out and isolated from the agarose gel using the NEB Monarch DNA gel extraction kit using the manufacturers protocol.

Table 10: Primers used for FILIP1L CDS amplification. Primer annealing sequence in bold, restriction enzyme cutting sequence (purple) as well as spacer and overhang (grey) were added in the PCR amplification.

PRIMER	SEQUENCE	ENZYME
FILIP1L_203_FOR	CGCCGC **GGATCC** AAG **TGATGGTGGTGGATGAACAG**	BamHI
FILIP1L_203_REV	CGCTCA **CTCGAG** CCG **GTACGAGTTCAGTCAGTCTTGG**	XhoI

2.5.2 FILIP1L CDS expression vector cloning

Both, FILIP1L CDS (insert) and pcDNA 3.1 V5/His A (vector), were digested with BamHI and XhoI in Fast digest buffer (Thermo). Either 1 µg of insert or vector were mixed with 2 µL 10x Fast Digest buffer, 1 µL BamHI, 1 µL XhoI and water in a total volume of 20 µL and digested for 30 min at 37°C. Restrictions were run on a 0.7 % agarose gel and DNA of the correct size (insert 2801 bp, vector 5441 bp) were cut out and isolated from the agarose gel using the NEB Monarch DNA gel extraction kit using the manufacturers protocol.

Expression plasmid was created by mixing 60 fmol of insert and 20 fmol of vector with T4 ligation mix (4 µL 5x T4 buffer, 1 µL T4 ligase (1 U/µL), water to 20 µL) and incubated at room temperature over-night. Ligations (5 µL) were transfected in competent *E. coli* DH5α. Bacteria were plated on LB agar plates containing 100 µg/mL ampicillin and allowed to grow at 37°C over-night. Colonies were picked and used to inoculate 5 mL of LB ampicillin medium and were grown over night at 37°C. Bacterial plasmid DNA was then isolated using the QIAprep Spin Miniprep kit applying the manufacturers protocol. In order to ensure the FILIP1L expression vector contained the correct insert, 1 µg of plasmid DNA was digested with BamHI and XhoI and digestion was analysed on a 0.7 % agarose gel. Plasmids that showed the correct DNA fragment sizes (insert 2801 bp, vector 5441 bp) were sequenced with the help of the Tayside Centre for Genomic Analysis using the primers listed in **Table 10** and used for overexpression experiments.

2.6 Tissue culture

Human cells, primary and cell lines, were cultured under sterile condition in flasks and maintained at 37°C in a humidified incubator with 5% CO_2 (HERAcellTM incubator). Cells were ensured to be free of mycoplasma contamination by routine testing using MycoAlert® Mycoplasma Detection Kit (Lonza).

2.6.1 Cutaneous squamous cell carcinoma cells

Cutaneous Squamous Cell Carcinoma cells (cSCC) were isolated from tumour tissue obtained from patients after written and informed consent. Details for the human cSCC cell lines as well as references for cell line isolation can be found in **Table 11**.

Before plating, cell stocks were rapidly thawed in a 37 °C water bath, suspended in 10 mL warm RM^- medium (see **Solution 2.2.3**), centrifuged at 1000 rpm for 3 mins and resuspended in warm RM^- medium to remove DMSO. Cells were cultured for 24-48 h in RM^- until all cells adhered to culture flasks. After that, medium was changed to RM^+ (see **Solution 2.2.4**). Culturing and all subsequent experiments were performed in RM^+ medium.

The cSCC cell lines contain a population of feeder fibroblasts that are required during first passages after cell isolation. Fibroblast population was kept as low as possible during all experiments by removing fibroblasts during cell passaging. Cells were first washed with PBS and then incubated with 1:3 0.05% Trypsin in EDTA in PBS at 37 °C until fibroblasts detached. Fibroblast were aspirated, and cells were washed with PBS. cSCC cells were removed from flask by incubation with 0.05% Trypsin in EDTA for a further 3-4 mins at 37 °C. Trypsin was inactivated by adding fresh RM^+ medium and removed by centrifugation of cell suspension for 3 mins at 1000 rpm. Cells were resuspended in fresh RM^+ medium and plated in a new flask. cSCC cells were splitted to a maximum of 1:5 and maintained to a maximum passage of 30.

A list of all cSCC cell lines can be found in **Table 11**.

Table 11: Origin and characteristics of cSCC cell line panel.

	Category	Age	Sex	Tumour site	Tumour histology	Ref.
IC1	Primary tumour	77	M	Right temple	Moderately differentiated	[83]
IC1 met	Metastasis primary tumour	77	M	Right preauricular lymph node	Regional metastasis	[83]
MET1	Renal transplant progression series: primary tumour	55	M	Dorsum left hand	Moderately differentiated	[83, 234]
MET2	Renal transplant progression series: recurrence tumour	55	M	Dorsum left hand	Moderately differentiated recurrence	[83, 234]
MET4	Renal transplant progression series: metastasis tumour	56	M	Left axillary lymph node	Metastasis	[83, 234]
T9	Renal transplant progression series: unrelated primary tumour	55	M	Right hand	Well differentiated	[83]
IC8	Immuno-competent	51	F	Buttock	Poorly differentiated, spindle cells	[83]
IC12	Immuno-competent	87	F	Left calf	Poorly differentiated	[83]
IC18	Immuno-competent	81	M	Right ear	Moderately differentiated	[83]
IC19	Immuno-competent	81	M	Scalp	Well differentiated	[83]
T2	Immunosuppressed: Cardiac transplant	66	M	Hand	Well differentiated	[83]
T8	Immunosuppressed: Renal transplant	67	M	Ear	Poorly differentiated	[83]
T10	Immunosuppressed: Renal transplant	60	M	Left Shin	Moderately differentiated	[83]
T11	Immunosuppressed: Renal transplant	48	M	Back	Poorly differentiated	[83]

2.6.2 NTERT immortalized keratinocytes

NTERT cells are human keratinocytes, that have been immortalized by telomerase activity [235]. NTERT cells were maintained in Keratinocyte serum free medium (K-sfM, Gibco), supplied with ½ volume bovine pituitary extract (Keratinocyte kit, Gibco), 0.2 ng/ml of human EGF (GIBCO) and 0.4 mM of $CaCl_2$, at 37°C in 5% CO_2. EGF was added to K-sfM fresh before use. NTERT cells were passage by washing cells 3x with PBS, before incubation with 0.05% Trypsin EDTA at 37 °C until cell

detached. Trypsin was inactivated by adding fresh K-sfM and removed by centrifugation of cell suspension for 5 mins at 400 rpm. Cells were resuspended in fresh K-sfM and plated in a new flask. NTERTs were splitted to a maximum of 1:5 and maintained to a maximum passage of 40.

2.6.3 A431 epidermoid carcinoma cells

A431 human epidermoid carcinoma cells were used in establishing siRNA knock-downs and initial experiments.

A431 cells were cultured in DMEM supplied with 10% FBS. For passaging, cells were washed with PBS and then incubated with 0.05% Trypsin in EDTA at 37 °C until all cells detached. Trypsin was inactivated with fresh DMEM medium and removed by centrifugation (1000 rpm, 3 min). Cells then were resuspended in fresh DMEM medium and plated with a maximum dilution of 1:5 and maintained to a maximum passage of 40.

2.6.4 Kera308 mouse keratinocyte cells

Mouse keratinocyte cell line Kera308 were maintained in DMEM supplied with 10% FBS. For passaging, cells were washed trice with PBS and then incubated with 0.05% Trypsin in EDTA at 37 °C until all cells detached. Trypsin was inactivated with fresh DMEM medium and removed by centrifugation (1000 rpm, 3 min). Cells then were resuspended in fresh DMEM medium and plated with a maximum dilution of 1:5 and maintained to a maximum passage of 40.

2.6.5 Generation and storage of cell stocks

In order to store cells, cell stocks were generated using the following protocol. Cells were first detached from flasks and trypsin was removed using the same procedure that was used during passaging. Cells (with the exception of NTERT cells) were then resuspended in freezing medium (see **Solution 2.2.19**). NTERT cells were resuspended in K-sfM and mixed 1:1 with 2x NTERT freezing medium (see **Solution 2.2.20**). Cells were stored over-night in cryotubes (Nunc) at -80 °C in a CoolCell® cell freezing container to ensure a standardised controlled freezing rate of -1°C/minute. The next day, cell vials were transferred to liquid nitrogen tanks for long-term preservation.

2.6.6 Knockdown using siRNA

Reverse transfection with siRNA was used to achieve gene knockdowns. Alongside each knockdown, a negative control using non-targeting siRNA was performed, using the maximum amounts of siRNA and transfection reagent used in the experiment. Optimal amounts of RNAiMAX and siRNA were determined in preliminary experiments and were based on knockdown efficiency determined by immunoblot and RT-qPCR.

Lipofectamine RNAiMAX mix for 6 well plate:

2-7µl/well of Lipofectamine RNAiMAX (Invitrogen) in 100 µl/well of Opti-MEM (Life Technology)

siRNAs mix for 6 well plate:

10-40 nM of siRNA in 100 µl/well of Opti-MEM (Life technology)

Lipofectamine RNAiMAX mix for 96 well plate:

0.1-0.2 µl/ well Lipofectamine RNAiMAX (Invitrogen) in 9.8 µl/well of Opti-MEM

siRNAs mix for 96 well plate:

10-40 nM/well of siRNA in 9.8 µl/well of Opti-MEM

Lipofectamine RNAiMAX and siRNA mix were incubated at room temperature for 5 minutes before being combined and vortexed. For 96 well plates, 80 µL cell suspensions containing 1.5 x 10^3 cells or 1800 µl containing 2 x 10^5 cells for 6 well plates were plated, respectively. Cells were maintained under normal growth conditions before analysis.

Isoform specific siRNAs were designed using the RNAi design tool from integrated DNA technologies (https://eu.idtdna.com/Scitools/Applications/RNAi/RNAi.aspx). siRNA specificity was ensured using BLAST algorithm (see https://blast.ncbi.nlm.nih.gov/Blast.cgi).

A list of all used siRNAs can be found in **Table 12** and **Table 13**.

Table 12: Isoform specific siRNAs designed to perform isoform specific knock-down of FILIP1L in cells lines.

NAME	SPECIES	ISOFORMS	SEQUENCE
Hs_FILIP1L_iso201/2_1	**human**	**201 / 202**	GCUCAGUAUGGGUUUGUCA
Hs_FILIP1L_iso201/2_2	**human**	**201 / 202**	CACACAGUGGUAAUGGCCA
Hs_FILIP1L_iso201/3_1	**human**	**201 / 203**	CUAACUGUUGCCUGCAUAG
Hs_FILIP1L_iso201/3_2	**human**	**201 / 203**	UUGACUGCAACUUGUCUUG
Hs_FILIP1L_iso203_1	**human**	**203**	UCGCAUUGUUCGGGCGACU
Hs_FILIP1L_iso203_2	**human**	**203**	CUCGCAGCGCGGCACUACA
Hs_FILIP1L_iso202/6_1	**human**	**202 / 206**	CCACUUCUUCUGCCUCAUU
Mm_Filip1l_iso201/3_1	**mouse**	**201 / 203**	CCAAUGAAUGAGUUGGAUA
Mm_Filip1l_iso201/3_2	**mouse**	**201 / 203**	AGACCUCUCAAGAGAUGAC
Mm_Filip1l_iso202/3_1	**mouse**	**202 / 203**	CAAGAATGCTACTCTCTGA
Mm_Filip1l_iso202/3_2	**mouse**	**202 / 203**	GAGAAGATGTACAGTGTAA

Table 13: Purchased siRNA pools.

DESCRIPTION	REFERENCE	SUPPLIER
ON-TARGETplus Non-targeting Pool	D-001810-10-50	Dharmacon
ON-TARGETplus Human FILIP1L siRNA - SMARTpool	L-019458-00-0005	Dharmacon

2.6.7 Overexpression using plasmid vectors

Overexpression experiments were used in order to restore expression in non-expressing cells.

Optimal concentrations of Lipofectamine and expression plasmid were determined in preliminary experiments. Alongside each overexpression experiment, a negative control using empty vector was performed, using the maximum amounts of plasmid and transfection reagent used in the experiment

Cells were seeded in 6 well plates one day before transfection at a concentration of 2×10^5 cells per well. Cell confluency was checked, and transfections were only performed, if confluency was between 70-90%. Cell medium was replaced with 1.7 mL fresh medium and Lipofectamine mix was prepared by mixing 150 µL Opti-MEM with 2-15 µL Lipofectamine 3000 and DNA mix was prepared by mixing 150 µL Opti-MEM with 1-10 ng/well of plasmid. After mixing, both solutions were combined, briefly vortexed and incubated at room temperature for 5 min.

DNA-Lipofectamine mixture (300 µL total volume) was dropwise added to cells and incubated at 37 °C. Transfection medium was replaced with fresh medium 6 h after transfection and effects of overexpression were analysed using RT-qPCR and immunoblotting.

2.6.8 Cell viability assay

Cell viability was measured using alamarBlue™ cell viability reagent (Thermo). Cells were harvested as described before and plated into 96 well plates at either 1500 or 3000 cells/well. Cells were treated with siRNA (reverse transfection at time of plating, see **Section 2.6.6**) or overexpressing plasmid (the day after plating, see **Section 2.6.7**). As controls, a corresponding number of cells were plated into 6 well plates and treated with the same transfection mix used for the 96 well plates. At the end of the experiment, treatment efficacy was controlled by harvesting cells from 6 well plates, isolating protein and RNA and checking expression levels via RT-qPCR and immunoblotting.

At time of measurement, cell medium was aspirated and replaced with fresh medium supplied with 10% (v/v) alamarBlue reagent. Cells were incubated for 4 h at 37 °C and absorbance was measured using the Spectromax M2 microplate reader (Molecular devices) at 570 nm. All samples were normalized to control wells containing no cells.

2.6.9 Cell proliferation

Cell proliferation was measured using the IncuCyte Live-Cell Imaging System (Sartoris). In brief, cells were plated at appropriate densities in 6 well plates. Cells were transfected using the protocols described in **Sections 2.6.6** and **2.6.7**. Images of cells were taken every 24 h for 96 h, with 16 images per well per time point. Confluency analysis with performed using the IncuCyte Zoom Software. Confluency masks were controlled manually in order to ensure all cells were correctly identified and false positive signals (e.g. debris) were minimal. Mean confluency measurements of all 16 images of a well were taken as the readout and used for subsequent analysis.

As an independent measurement, additional 6 well plates were set up in the same way as described above. Cells were harvested after 96 h, while great care was taken to ensure all cells were removed from plates. Cells were counted using the Countess II automated cell counter (Thermo).

Efficacy of overexpression or knockdown were controlled by treating cells with the same transfection mix used in the experiment, isolating RNA and protein and checking expression levels via RT-qPCR and immunoblotting.

2.7 Nuclear-cytoplasmic separation

Nuclear cytoplasmic separation was achieved by first washing cells twice with ice cold PBS before resuspension in 1 mL subcellular fractionation buffer (SF buffer, see **Solution 2.2.8**). Cells were pushed through a 27G needle 20 to 25 times using a 2 mL syringe. To ensure complete lysis, 10 µL of cell suspension was mixed with 10 µL of trypan blue and lysis was checked using a light microscope. Additional lysis using the syringe and needle was performed if lysis was incomplete.

Lysed cells were incubated on ice for 20 min. Nuclei were pelleted by centrifugation at 720 g for 5 min. The supernatant, containing the cytoplasmic fraction, was transferred to a fresh tube and placed on ice. Nuclei were washed by resuspending the nuclear pellet in 1 mL SF buffer, incubated for 5 min on ice and pelleted again by centrifugation at 720 g for 5 min. Supernatant was discarded and pellet was directly dissolved in an appropriate amount of 2x SDS sample buffer, sonicated and boiled at 100°C for 5 min. Protein concentration was measured using BCA assay.

Cytoplasmic fraction was centrifuged again at 720 g for 5 min to remove remaining nuclear particles. Supernatant was mixed with 2 mL TRI reagent. Protein and RNA were isolated following the protocol described in **Section 2.3.**

2.8 Immunoblotting

Protein samples were prepared using the protocol described in **Section 2.3**.

Proteins were separated using precast polyacrylamide (10% or 4-12%) Bis-Tris gels (Invitrogen), and MOPS (Invitrogen) as running buffer. Suitable amounts of protein were loaded on the gel alongside 3 µL of Seeblue protein standard (Invitrogen). Stacking was achieved by gel electrophoresis at 100 V for 15 mins and separation was carried out at 120 V and run until samples reached the end of the gel.

Proteins were transferred to a 0.45 µm supported nitrocellulose membrane (Amersham – GE Healthcare Life Sciences). Transfer was completed in 1x Transfer buffer (**Solution 2.2.10**), supplied with 0.1 % SDS at 100 V for 90 mins using a wet transfer system. An ice pack was kept inside the transfer tank and buffer was constantly stirred using a magnetic stirrer to avoid overheating. To ensure that protein was completely transferred, membranes were stained with Ponceau S solution (Sigma). Excess solution was washed off using dH_2O and ponceau S was washed off after transfer quality assessment using PBS.

Membranes were blocked using 5% non-fat milk in 1x TBS-T (**Solution 2.2.12**) for 1 h at room temperature. Primary antibodies were prepared in 0.1 % non-fat milk in 1x TBS-T in appropriate dilutions and incubated with the membrane on a roller at 4 °C over-night. Membranes were washed 3 times for 15 mins using 1x TBS-T. Secondary antibodies were diluted 1:15,000 in 0.1 % non-fat milk in 1x TBS-T and incubated for 1 to 2 h at room temperature. Excess secondary antibody was washed off as described before.

Imaging analysis was done using the Odyssey® CLx image system and Image Studio software (LI-COR).

All antibodies used can be found in **Table 14** and **Table 15**.

Table 14: Primary antibodies used in immunoblotting, including manufacturer, host and dilution used.

Antibody	Manufacturer	Reference	Clone	Host	Dil.
Axin2	Abcam	Ab1093307	EPR2005(2)	Rabbit	1:500
cMyc	Abcam	Ab32072	Y69	Rabbit	1:2000
Cyclin D1	Cell Signaling	2978	92G2	Rabbit	1:500
E-cadherin	Santa Cruz	Sc52327	5H9	Mouse	1:1000
FILIP1L	Sigma	SAB2105835	Polyclonal	Rabbit	1:1000
FILIP1L	Sigma	HPA043133	Polyclonal	Rabbit	1:2000
FILIP1L	Aviva	ARP52360 _P050	Polyclonal	Rabbit	1:500
FILIP1L	Thermo scientific	PA5-32021	Polyclonal	Rabbit	1:1000
Keratin 10	Abcam	Ab76318	EP1607IHCY	Rabbit	1:1000
Keratin 14	Abcam	Ab51054	EP1612Y	Rabbit	1:1000
Keratin 8	Abcam	Ab53280	EP1628Y	Rabbit	1:1000
Active β-catenin (Non-phospho Ser33,37, Thr41)	Cell signaling	8814	D13A1	Rabbit	1:1000
Total β-catenin	Cell signaling	9562	Polyclonal	Rabbit	1:1000
Total β-catenin	BD bioscience	610153	14/Beta-Catenin	Mouse	1:1000
α-tubulin	Sigma	T9026	DM1A	Mouse	1:2000
β-actin	Sigma	**A5316**	AC-74	Mouse	1:5000
GAPDH	Cell Signaling	2118s	14C10	Rabbit	1:2000
H2A.X (Ser139)	Cell signaling	2577	20000	Rabbit	1:500

Table 15: Secondary Antibodies used for immunoblotting. All secondary antibodies were purchased from LI-COR.

Antibody	Reference		Host	Reactivity	Dilution
IRDYE® 800CW GOAT ANTI-MOUSE IGG (H + L)	926-32210	Polyclonal	Goat	Mouse	1:15000
IRDYE® 680RD GOAT ANTI-MOUSE IGG (H + L)	925-68070	Polyclonal	Goat	Mouse	1:15000
IRDYE® 800CW GOAT ANTI-RABBIT IGG (H + L)	926-32211	Polyclonal	Goat	Rabbit	1:15000
IRDYE® 680RD GOAT ANTI-RABBIT IGG (H + L)	925-68071	Polyclonal	Goat	Rabbit	1:15000

2.9 Quantitative real time PCR

Quantitative real time PCR (qRT PCR) was performed on the Quantstudio 5 Real time PCR system from ThermoFischer Scientific. Universal master mix and assays were purchased from Applied Biosystems and if available, exon spanning assays were chosen. For FILIP1L isoform expression analysis, custom assays were designed as described below.

2.9.1 Assay design

In order to distinguish between different FILIP1L isoforms, custom assays were designed using Primer Quest online tool from Integrated DNA technologies (see https://www.idtdna.com/PrimerQuest) and sequence specificity was ensured by BLAST algorithm against the host genome and transcripts (see https://blast.ncbi.nlm.nih.gov/Blast.cgi). Assays were diluted prior to usage and final concentrations were: 18 µM primer (each, forward and reverse) and 5 µM probe. Assay efficiency was tested using samples of cDNA (serial dilutions from 1:1 to 1:10,000). Assays for isoform specific qRT PCR are listed in **Table 16** and **Table 17**.

Table 16: Isoform specific assay design for mouse Filip1l. Fo: forward primer**, Re:** reverse Primer**, Pr:** probe. Probes were fluorescently labelled with 5' FAM as fluorophore and 3'TAMRA as quencher.

Name	Isoforms	Sequence	length	TM
Mm_Filip1l_1_Fo	**201**	GAGAGATGCTTTTCAAGCAAA	21	54
Mm_Filip1l_1_Re		TCCGCCTGTGAGATTCTTTATG	22	58.4
Mm_Filip1l_1_Pr		CAGGAGGACATCTATGAGAAACCAATG	27	63.4
		Amplicon length	**109**	
Mm_Filip1l_2_Fo	**202**	CCGCAGCTCAGATTAAAGAAAC	22	62
Mm_Filip1l_2_Re		CTTCAGGGTCTTGATCCTCTTC	22	62.1
Mm_Filip1l_2_Pr		GATCAAGAAACTGCGTCCCAGGAAAAGA	28	68.6
		Amplicon length	**93**	
Mm_Filip1l_3_Fo	**203**	CACAAAGAATATATGAAGAAGAG	23	53.5
Mm_Filip1l_3_Re		TCCTTCTTTTCCTGGGACGCA	21	59.8
Mm_Filip1l_3_Pr		TGAATTCATAAACTTATTGGAGCAGGA	27	58.9
		Amplicon length	**110**	

Table 17: Isoform specific assay design for human FILIP1L. Fo: forward primer**, Re:** reverse Primer**, Pr:** probe. Probes were fluorescently labelled with 5' FAM as fluorophore and 3'TAMRA as quencher.

Name	Isoforms	Sequence	length	TM
Hs_FILIP1L_3/6_Fo	**203 / 206**	GGCAGTTCAGATTAAAGAAGCTAAT	25	61.8
Hs_FILIP1L_3/6_Re		GCTTGGTCAGCTCCTCTTT	19	61.9
Hs_FILIP1L_3/6_Pr		TCAAGTCTCAGGAGGAGAAGGAGCA	25	68
		Amplicon length	**108**	
Hs_FILIP1L_2/6/9_Fo	**202 / 206 / 209**	ACCAATAAAGTCACCAGCAGTA	22	62
Hs_FILIP1L_2/6/9_Re		TGAGTTCAATGAGGCAGAAGAA	22	62
Hs_FILIP1L_2/6/9_Pr		ACTATCACACCAACAGCCACACCT	24	68
		Amplicon length	**104**	
Hs_FILIP1L_1/3_Fo	**201 / 203**	ACCAATAAAGTCACCAGCAGTA	22	62
Hs_FILIP1L_1/3_Re		GGTGAGCGTGGTCAGTTAT	19	62
Hs_FILIP1L_1/3_Pr		ACTATCACACCAACAGCCACACCT	24	68
		Amplicon length	**102**	
Hs_FILIP1L_3_Fo	**203**	CATTGTTCGGGCGACTCT	18	62
Hs_FILIP1L_3_Re		CTTCTCCTCCTGAGACTTGATTT	23	62
Hs_FILIP1L_3_Pr		CGGCGCAGGCAGTTCAGATTAAAG	24	67
		Amplicon length	**147**	
Hs_FILIP1L_1/2/4_Fo	**201 / 202 / 204**	CAGCATTCTGGAGGGAGAAC	20	62
Hs_FILIP1L_1/2/4_Re		TTTGGAGTGACAAACCCATACT	22	62
Hs_FILIP1L_1/2/4_Pr		AAATGGACCTGGCTTTGCTGGAAG	24	67
		Amplicon length	**111**	

2.9.2 cDNA Synthesis

RNA was isolated using the protocol described in **Section 2.3**. cDNA was generated using the Qiagen Omniscipt RT kit with a modified version of the manufacturers protocol. Each cDNA reaction contained 2 µL 10x buffer RT, 2 µL dNTP mix (5 mM each), 0.5 µL RT enzyme, 0.33 µL random hexamers (50 µM, Invitrogen), 4.67 µL water and 10 µL RNA at a concentration of 100 ng/µL. cDNA conversion was carried out for 90 mins at 37 °C. Before qRT PCR, cDNA was diluted 1:40 with water.

2.9.3 qRT PCR

All reactions using the same assay were set up in one mix to ensure reproducibility. Each reaction contained: 4.5 mL master mix, 4.75 µL water and 0.75 µL assay. For each reaction, 5 µL of cDNA were pipetted in one well of a 386 well plate and 10 µL of master mix were added. Plates were then run using standard qPCR program (50 °C for 2 min, 95 °C for 10 mins, 40-times 95 °C for 15 s and 60 °C for 1 min). Each reaction was carried out in triplicates.

2.9.4 Data analysis

CT values were calculated using the Design and Analysis Application on the Thermo Fischer Cloud (https://www.thermofisher.com/de/de/home/cloud). CT values were exported, and all triplicates were checked for possible pipetting errors. Values that were clear outliers were excluded from further analysis and CT means of triplicates were taken for further analysis. Data was normalized to reference genes and relative expression was calculated using the following formula:

$$relative\ Expression\ = 2^{-CT\ normalized}$$

For certain experiments, fold change was calculated using the following formula:

$$fold\ change\ = 2^{-(CT\ treatment - CT\ control)}$$

All results represent the mean of three individual experiments.

2.10 Methylation analysis: MassARRAY

In order to validate differentially methylated regions, that were previously identified in the analysis of oxRRBS data, we utilized the Sequenome MassARRAY technology in collaboration with the Division of Epigenomics and Cancer Risk Factors of the German Cancer Research Center (DKFZ) in Heidelberg, Germany.

2.10.1 Bisulphite conversion of DNA

During bisulphite conversion, cytosines in the DNA get deaminated to uracil. Because 5-methyl-cytosine (5mC) is protected from this deamination, these cytosines continue to behave as cytosines in subsequent PCR applications, while converted cytosines (now uracils) behave like thymines, allowing to distinguish methylated from unmethylated input DNA.

Bisulphite conversion was carried out using the EZ DNA methylation kit (Zymo Research) using a modified version of the manufacturers protocol. CT conversion reagent was prepared by adding 750 µL water and 210 µL M-dilution buffer to one aliquot of CT conversion reagent. DNA samples were prepared by adding 5 µL M-dilution buffer to 45 µL DNA (1 µg) and incubated at 37°C for 15 mins. Bisulphite conversion was achieved by adding 100 µL of previously prepared CT conversion reagent and incubation for 16 h at 50°C in the dark. Samples were placed on ice for 10 min before being mixed with 400 µL M-binding buffer and transferred to a Zymo-Spin IC column. DNA was bound to columns by centrifugation (10,000 g, 30 s) and then washed with 100 µL M-wash buffer and bisulphite conversion was completed by desulphonation with 200 µL M-desulphonation buffer on column for 15 mins at RT, followed by centrifugation (10,000 g, 30 s). Bisulphite converted DNA was washed twice with 200 µL M-wash buffer and, after dry centrifugation at 10,000 g for 3 min, eluded in two steps with 25 µL 1:1 mixture of M-elution buffer and water each. Converted DNA, which will be referred to as bt (bisulphite treated) DNA from now on, was stored at -20°C.

2.10.2 MassARRAY primer design

In order to design MassARRAY primers, DNA sequences first were *in silico* BS converted using a Microsoft Word macro, kindly provided the Division of Epigenomics and Cancer Risk Factors of the German Cancer Research Center (DKFZ)

in Heidelberg, Germany (see **Section 5.1**). Primers were designed using the Agena Bioscience Epidesigner online tool (https://www.epidesigner.com/start3.html).

Primers performance was tested by PCR using HotStar-Taq polymerase (Qiagen). Each 20 µL reaction contained: 1 µL 1:1 diluted BT DNA, 2 µL 10x PCR buffer, 0.16 µL dNTP mix (10 mM each), 0.5 µL primer mix (10 µM each primer), 0.16 µL HotStar-Taq and 15.18 µL water. PCR was performed with the following steps: initial denaturation and enzyme activation for 15 min at 95°C, 45 cycle of denaturation at 95° for 30 s, primer annealing at 52°C, 56°C or 60 °C for 30 s, elongation at 72°C for 1 min and a final elongation step at 72°C for 10 min. PCRs were analysed on a 1.5% agarose gel and the best performing annealing temperature (either 52°C, 56°C or 60°C), that reliably produced a single PCR product of the expected size, was used for generation of DNA for further usage.

As controls, PCRs were also performed on mouse and human DNA standards of known methylation percentage (100%, 80%, 60%, 40%, 20%, 0%). These controls were handled in parallel to the other samples.

Table 18: Primers used to generate DNA amplicon for further methylation analysis using MassARRAY

Amplicon	Primer forward	Primer reverse
Mouse Intron	GGAGGGAATTAGTTATTAGATGGTT	CTCCAAAAATTATCCTCTAACCTCC
Mouse TSS	TGTTAGTAGAATTGTGAGGGTTTGG	TCCTTTAAATTTCTCAATACCTATAACCA
Human TSS 1	GGATGTGTATTGAAGTTTTTGAAGTAA	TCTAACAACAATACCCCTTAATAAAA
Human TSS 2	AGTTTTAGGGATTTAGAGGGAAAAA	CAACCACCCACAAACTTACTACCTA
forward 10-mer tag	AGGAAGAGAG	used to balance primers TM
reverse T7 tag	CAGTAATACGACTCACTATAGGGAGAAGGCT	needed for in vitro transcription

2.10.3 MassARRAY

MassARRAY amplicons were generated using the same PCR as mentioned in **Section 2.10.2** using the best determined primer annealing temperature and the best performing primers (see **Table 18**). PCRs were again checked on a 1.5% agarose gel to ensure specificity of reactions.

Unincorporated dNTPs were dephosphorylated by adding 2 µL of SAP (shrimp alkaline phosphatase) to 5 µL PCR product from the previous step. Dephosphorylation was achieved by incubation at 37°C for 20 min, followed by enzyme deactivation for 5 min at 85°C.

Amplicons were converted to RNA and cleaved using RNase A, by mixing 2 µL SAP treated PCR product with 5 µL *in vitro* transcription (IVT) mix (containing 3.21 µL water, 0.89 µL 5x T7 buffer, 0.22 µL T cleavage mix, 0.22 µL DTT, 0.4 µL T7 and 0.06 µL RNase A). IVT was carried out at 37°C for 180 min.

As samples need to be salt free to ensure correct flying in the mass spectrometer, samples were treated with Clean Resin. Resin was spread into a dimple plate and dried for 10 min. In the meantime, 16 µL of water was added to IVT products and dried resin was added to each well. Desalting was achieved by rotating the plate with IVT product and resin for 15 min. Resin was pelleted at the bottom of the wells by centrifugation at 3200 g for 5 min.

Samples were dispensed to a SpectroCHIP array using the MassARRAY nanodispenser (Agena Biosciences) and analysed using the MassARRAY analyser.

Methylation standards for all primers were analysed to ensure that previous steps were successful in generating fragmented RNA and expected methylation percentages were measured. Fragments with low or high mass that do not produce reliable data were excluded. Furthermore, fragments with more than one silent methylated or silent non-methylated peaks, where a fragment without analytical value has the same mass than the analysed fragment and therefore adds to either a methylated or non-methylated peak, were also not included in the analysis.

3 Results

3.1 Studies preceding this work

The goal of this study was to characterize the global DNA methylation landscape in cSCC and to determine if the mouse model of cSCC, which was recently developed in our lab, reflects the methylation landscape of the human disease. The development of the solar-simulated UV induced murine cSCC (ssUV cSCC) model will be discussed below.

3.1.1 A new preclinical model of cutaneous squamous cell carcinoma

As discussed in the introduction (see **Section 1.2.3.6**), existing models to investigate cSCC may have deficits in accurately mapping human cSCC. For example, DMBA/TPA induced tumors are almost exclusively papillomas and UVB-induced tumors do not factor in UVA radiation which is a critical carcinogen, especially in immunosuppressed individuals.

In an effort to investigate the effects of transcription factor NF-E2 p45-related factor 2 (Nrf2), the master regulator of the oxidative stress response, on skin carcinogenesis our lab has developed a new murine model for cSCC. The aim was to mimic human cSCC development as closely as possible. The main difference between other UV-induced models and the ssUV cSCC model is the usage of UVA-340 lamps. These lamps emit UV radiation, that closely mimics the energetic portion of the solar UV radiation spectrum (see **Figure 3**). Furthermore, relatively low doses of radiation and a longer exposure period were chosen to allow tumor development. The aim was to simulate exposure to UV radiation early in life, followed by development of cSCC over the course of adulthood.

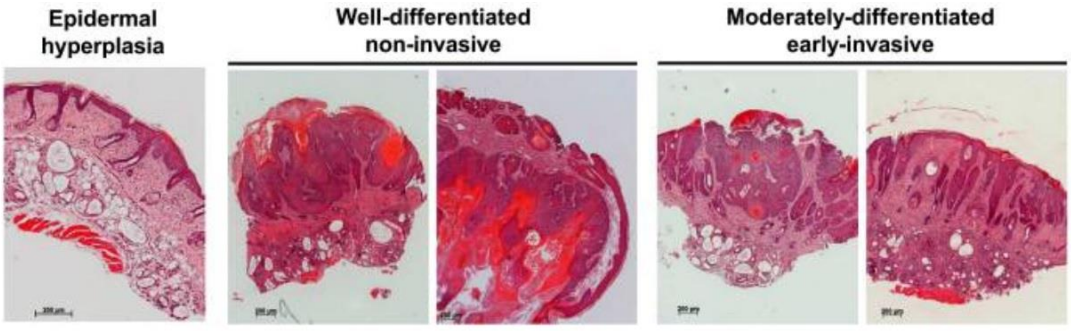

Figure 11: Histopathology of tumors forming in the ssUVR induced mouse cSCC model. Tumors range from pre-malignant epidermal hyperplasia, to well- and moderately differentiated tumors as well as poorly differentiated and invasive cSCCs. Figure taken from Knatko *et al.* 2015 [60].

SKH-1 hairless mice that were subjected to chronic irradiation with ssUVR, showed a “field change”, also known as “field cancerisation”, that is typical for human cSCCs. This suggests that, similar to humans, irradiated mice develop multiple cSCCs in close proximity that arise from dysplastic epithelium. The histopathological spectrum of the ssUV cSCC tumors includes well-, moderately- and poorly-differentiated tumors that histopathologically were very similar to human cSCCs (see **Figure 11**) [60,135]. Thus, by mimicking the carcinogenic process that is known to occur in humans, the resulting mouse tumors are a good model to investigate human cSCC.

3.1.2 Mouse ssUVR induced cSCC resembles the mutation spectrum of human cSCC

As mentioned before, human cSCC is the most highly mutated human cancer, making it difficult to identify drivers of carcinogenesis that could potentially be therapeutically targeted. Having established that the ssUVR-induced mouse tumors are histopathologically similar to human cSCC, our lab aimed to further validate the model using whole exome sequencing. Knatko *et al*. performed sequencing of 18 microdissected tumors, ranging from severely dysplastic actinic keratosis to invasive cSCC. They found a high single nucleotide polymorphism (SNP) rate of 155 mutations per Mb (low of 12 and high of 279), which is even higher than the rate observed in humans (an average of 30 per Mb). The vast majority (78.6 %) of these SNPs were C.G to T.A transitions, consistent with a characteristic UVR mutation signature. Most of these transitions (81.6 %) occurred following a pyrimidine base. Insertion and deletion (INDEL) rate was 23.5 per case, with some cases having no INDELs, and others harbouring 370 INDELs [59].

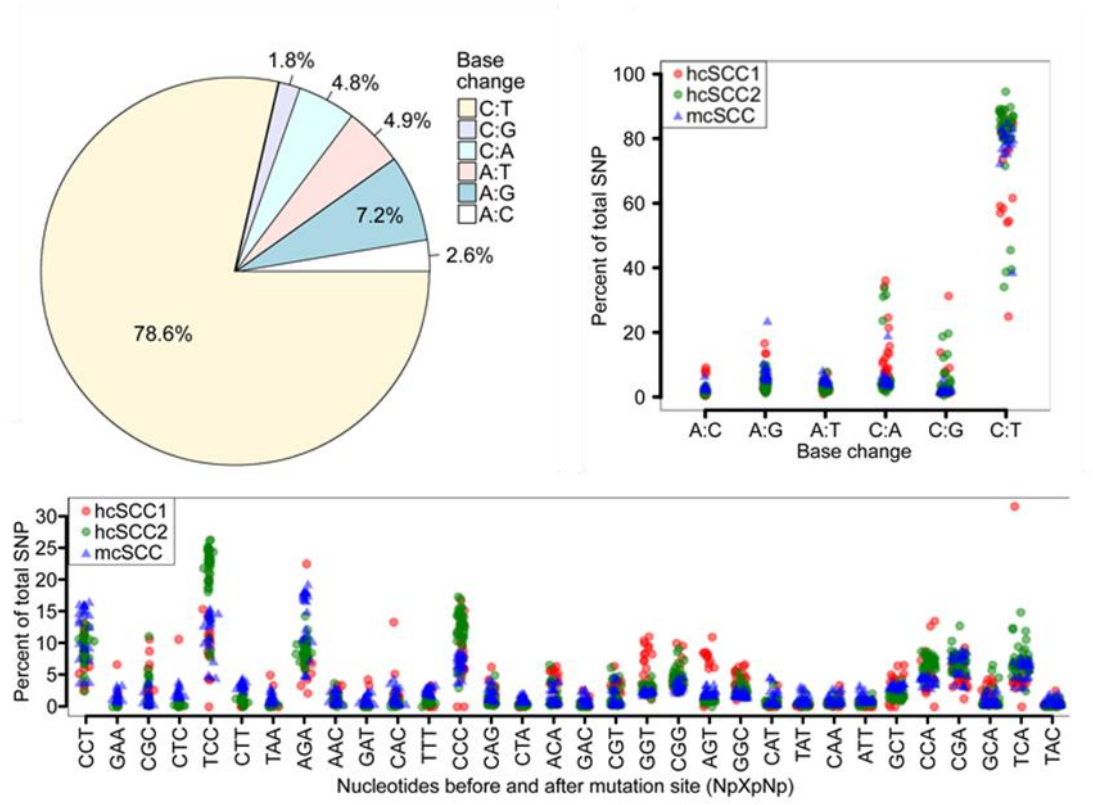

Figure 12: Mutation signature of ssUV induced mouse cSCC and comparison to human cSCC. Top left: SNP distribution occurring in mouse cSCC (mcSCC). The overwhelming majority of SNPs were C.G to T.A transitions, consistent with a typical UV induced mutation signature. **Top right:** Comparison of SNP distribution between mcSCC and human cSCC (hcSCC). The mutation signature observed in mcSCC is very similar to the one present in hcSCC. **Bottom:** The trinucleotide context in which mutations occur in mcSCC is very similar to hcSCC. Figure from Knatko *et al.* 2016 [59].

The observed mutation spectrum is remarkably similar to human cSCC. For example, Pickering *et al.*, South *et al*. and Inman *et al*. reported that the primary mutation in human cSCC are C.G to T.A transitions, the same mutation as in the mouse ssUV cSCCs. Furthermore, there is a correlation between the observed trinucleotide context in ssUV cSCC and human cSCC. Pickering *et al.* and South *et al.* both reported C>T mutations predominantly occurring in a Y(C>T)N context (Y=pyrimidine, N= A/T/G) [58,83,101]. While regions with genes that undergo copy number gains in human cSCC showed significant overlap with ssUV cSCC, regions of loss did not show overlap.

Because of the massive mutation burden in human cSCC, there are a plethora of mutated genes. The most frequently mutated gene is *TP53*. Mutations of the *Trp53* mouse gene were observed in 15 out of 18 samples (83%), similar to the reported 90%

in humans [58]. Most mutations of the *Trp53* gene were located in the DNA binding domain of the protein, suggesting loss of function. *NOTCH* family genes have been shown to be frequently mutated in cSCC [58], with mutations typically being located in the EGF repeat domain. In the mouse cSCCs, genes of the *Notch* family were mutated in 10 out of 18 samples (~ 55%), with 7 out of 16 mutations located in the EGF repeat domain.

3.1.3 The mouse ssUVR induced cSCC model is closely representing human cSCC

Thus, mouse cSCC, which are induced by chronic intermittent exposure to ssUVR, are histopathologically very similar to human cSCC. Furthermore, the complex genetic landscape of human cSCC is represented in the mouse ssUV cSCC, as highlighted by the similarities in frequency, type and context of mutations, as well as the mutations in key tumor suppressor genes. We therefore can conclude, that the model is suitable to investigate the biology and possible treatment strategies for human cSCC.

The whole-exome sequencing revealed frequent mutations in *Tet* genes, which encode Tet proteins that facilitate DNA demethylation. As discussed before, DNA methylation is an important process in cell homeostasis that plays a crucial role in cancer. To further validate our murine model for cSCC, we next aimed to investigate the ssUV cSCC's methylome, to compare it to human cSCC and to identify differentially methylated genes that may play a role in cSCC development.

3.2 Analysis of global DNA methylation in mouse ssUVR induced cSCC

The first goal was to investigate if the methylation landscape of the mouse ssUVR-induced cSCC reflects the methylation changes occurring in human cSCC. Furthermore, we aimed to identify differentially methylated regions (DMRs) that may lead to aberrant gene regulation. In order to achieve this, we used reduced representation bisulphite sequencing (see **Section 2.4**). Because of the initial finding of mutations in *Tet* genes, that are responsible for active DNA demethylation, a special RRBS protocol, termed oxidative RRBS (oxRRBS) was used that not only allows to investigate DNA methylation, but also DNA hydroxymethylation.

3.2.1 oxRRBS data processing

OxRRBS data was analysed as described in **Section 2.4.2**. Figure illustrates the data processing pipeline and the retained CpG sites. Results will be discussed in the following sections.

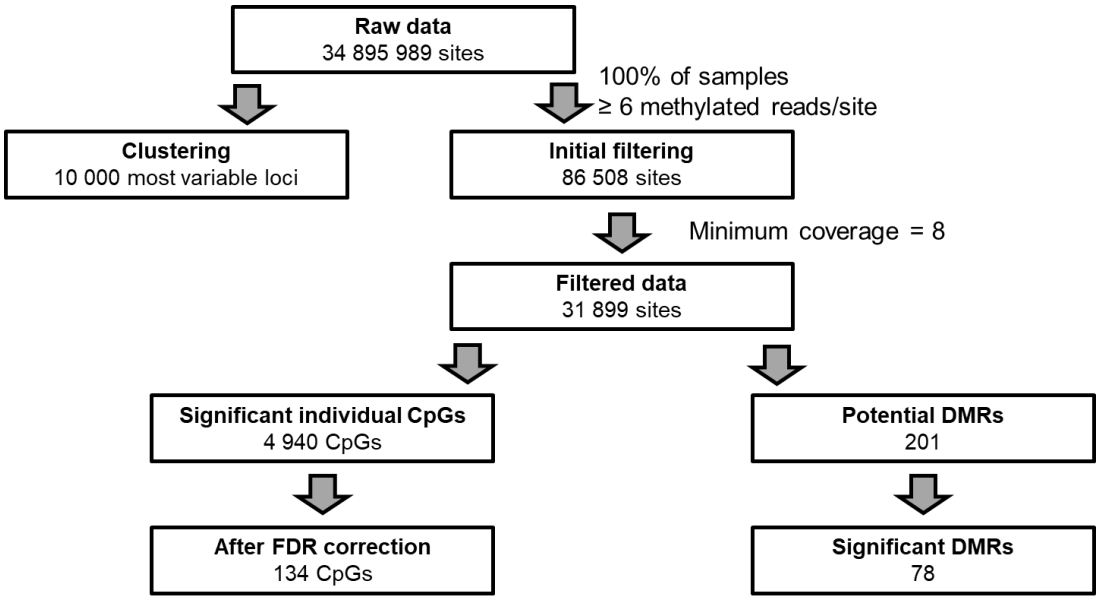

Figure 13: Schematic illustration of oxRRBS data processing. Boxes indicate the filtering steps and the retained CpG loci. oxRRBS yielded information on 34,895,989 loci (**Raw data**) and **Clustering** was performed on the 10,000 most variable loci. In an **Initial filtering** step, only loci were retained that were sequenced in all samples and showed a minimum of 6 methylated reads per site, therefore removing loci with low informatic value (85,508 sites). Further filtering (**Filtered data**) to a minimum coverage of 8 resulted in 31,899 sites. Significance testing for **Significant individual CpGs** resulted in 4,940 CpGs, 134 of which remained **After FDR correction**. We further identified 201 **Potential DMRs**, 78 of with were **Significant DMRs**. Results for differential methylation will be discussed in detail in the following sections.

3.2.2 Quality control of technical replicates

We began by studying duplicate samples for one tumor and one matched control sample as technical replicates. The goal was to have technical replicates that would allow us to evaluate the degree of variance caused by the sequencing reaction. Clustering analysis was performed on all samples for the top 10,000 most variant loci, using the Euclidian distance based on the covariance of the methylation percentages as a measure of equality between samples. After import, the data were filtered by shared regions and coverage. Only those CpGs were included, which (i) were sequenced in all samples and (ii) showed a minimum coverage (number of reads) of 8. These criteria were met by a total of 86,508 CpGs.

The cluster analysis revealed that there was a high degree of similarity between the technical replicates (see **Figure 14**). We therefore concluded that there were no major technical biases present in our data. In order to increase coverage and the number of sequenced CpGs in the technical replicates, the reads were merged over both replicates and henceforth treated as coming from a single sample.

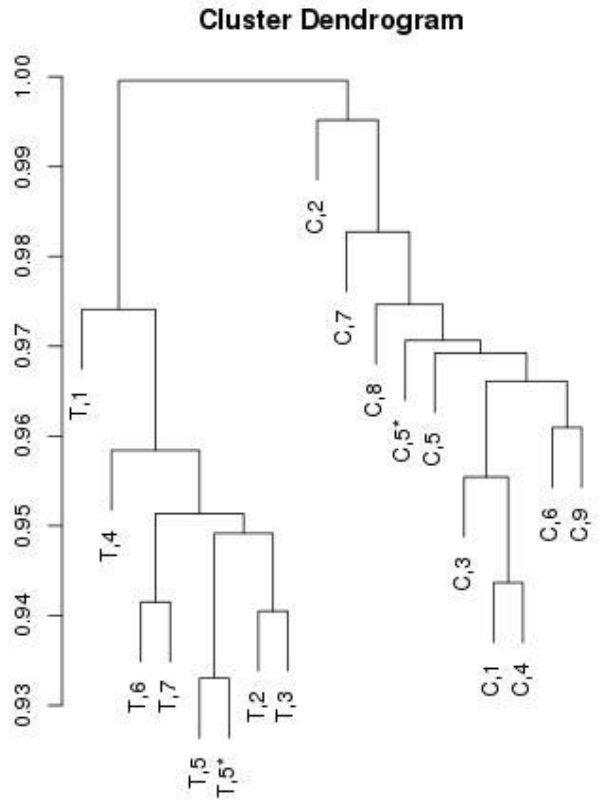

Figure 14: Clustering of sequenced samples based on the 10,000 most variable loci. T and C are tumor and control samples respectively, the number indicates the animal of origin and finally technical replicates are indicated by an "*". Tumor and control samples cluster separately, indicating profound methylation changes between the two groups. Technical replicates cluster closely together, suggesting no major biases in the sequencing reaction. Technical replicates were therefore merged and treated as a single sample in all further analyses.

3.2.3 Hydroxymethylation cannot be distinguished from noise in mouse skin and ssUV cSCC

After the initial finding, that *Tet* genes were frequently mutated in ssUV cSCC, we were especially interested in hydroxymethylation. Tet proteins facilitate active DNA demethylation by oxidizing methylated cytosine (5mC) to hydroximethylated cytosine (5hmC), which subsequently is exchanged for cytosine through active or passive mechanisms (see **Figure 5** in **Section 1.3.2**). We hypothesised, that mutations and possible functional impairment of Tet proteins would lead to changes in the 5hmC content in the DNA. Classic RRBS detects both, 5mC and 5hmC while, by utilizing an additional oxidisation step, in oxidative RRBS (oxRRBS) 5hmC is converted to 5fC which is not detected as a methylated cytosine (see **Figure 6**). Therefore, by

subtracting methylated reads from oxRRBS tracks from classic RRBS tracks, the positions of 5hmC can be analysed.

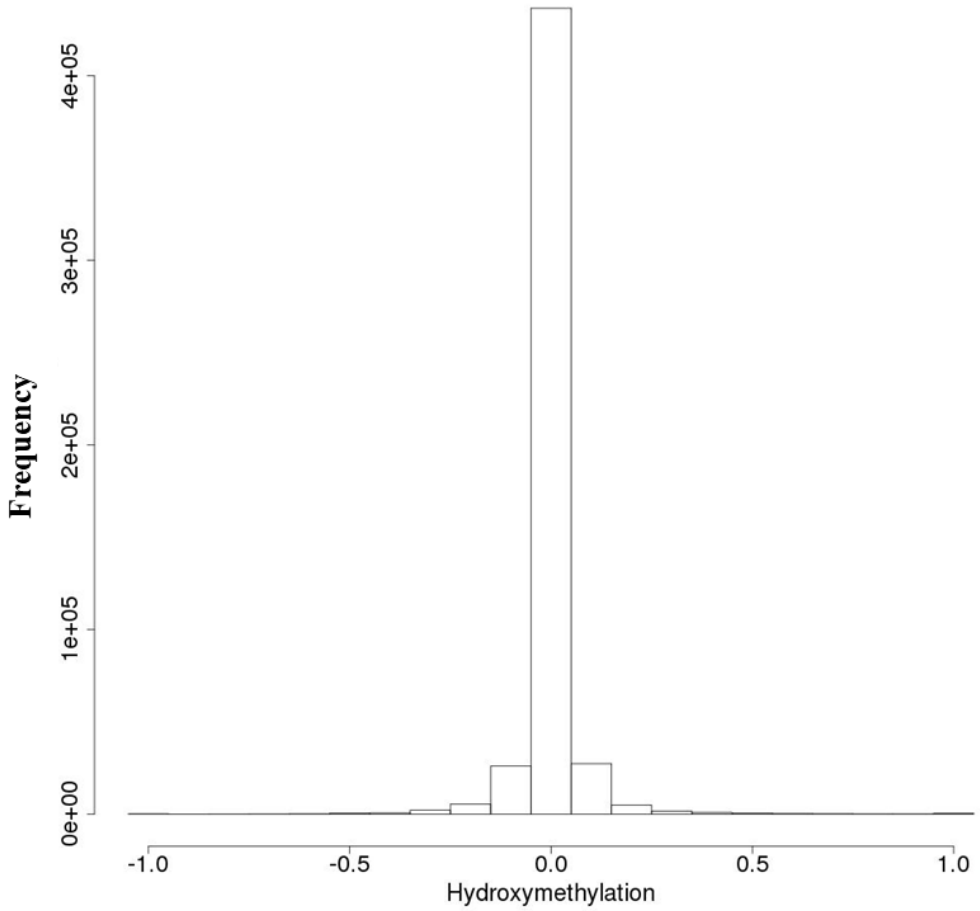

Figure 15: Histogram of frequency of percentage of hydroxymethylation. The vast majority of analysed loci show no hydroxymethylation (see x-axis: 0). Few loci are lowly hydroximethylated. Some loci show negative hydroxymethylation (see x-axis: < 0). This is biologically impossible. The distribution of hydroxymethylation appears to a Gaussian distribution around zero, indicating that hydroxymethylation is not distinguishable from noise.

We therefore filtered oxRRBS data by shared regions (reads present in 100% of samples) and minimum coverage (minCov=8), as well as a minimal methylated read count of at least 6 over all samples. This resulted in a total of 31,899 CpGs. Considering the difference between the result for the oxidative and regular RRBS, it became apparent that 5hmC levels were extremely low and essentially indistinguishable from noise. Additionally, negative values for hydroxymethylation should be treated as noise and distribution of values is virtually symmetrical, further

suggesting hydroxymethylation levels are so low, that they are indistinguishable from noise. A histogram of the distribution of 5hmC levels at all analysed CpGs is shown in **Figure 15**.

Therefore, we cannot draw any conclusions on the effects of mutations in *Tet* genes on global 5hmC content in ssUV cSCC. The low levels of 5hmC suggest that the removal of methylation by means of Tet proteins is either not playing a role in mouse skin, is only of relevance for very few loci, or the exchange of 5hmC to unmethylated cytosine is happening so rapidly, that we are not able to detect it with the used methodology.

Since hydroxymethylation was not distinguishable from noise, the regular (full) RRBS data was used for all subsequent methylation analysis.

3.2.4 General features of the ssUV cSCC methylome

RRBS analysis yielded information on 34,895,989 CpG's, leading to 31,889 variables upon filtering for minimal coverage and a minimal degree of methylation (as overall unmethylated loci are not of interest).

Table 19: Mapping statistics. Columns represent id, coverage (amount of sequenced paired-end fragments), number and fraction of mapped fragments, and final amount of CpGs covered, used for limma-voom statistical analysis. *Technical replicates, replicates with lowest coverage were not considered for statistical analysis (therefore "NA" for library size)

Sample	Coverage	Mapped	Efficiency	Amount of CpGs
B16	50246099	35897072	71.44%	148478473
B168	31208553	11846587	37.96%	20976502
B35	47506596	31168402	65.61%	32953329
B352	59062762	40558384	68.67%	112782255
B44	46671525	37466609	80.28%	214756352
B444	46261104	31338931	67.74%	76641707
B45	52869383	39235006	74.21%	129918624
B54	25497793	15890153	62.32%	55121366
B545	46097634	32793211	71.14%	157000982
B56	55635840	40540911	72.87%	303053855
B56*	34434081	28434250	82.58%	NA
B562	50611092	34949961	69.06%	152969508
B562*	40463535	28614975	70.72%	NA
B77	51857150	41406489	79.85%	203128198
B85	47469589	38480384	81.06%	182230279
B851	49190255	33340159	67.78%	83772331
B87	49688142	32715118	65.84%	52517052
B874	58596499	41893348	71.49%	161520850

3.2.4.1 Average methylation

The methylome of most cancers is characterized by large stretches of non-coding regions of hydroximethylated DNA, while CpG island methylation, especially those that are associated with tumor suppressor gene expression, become hypermethylated. Globally, this results in a decrease in overall methylation. However, there is some evidence that in cSCC, global DNA methylation levels could increase, rather than decrease. For example, Nandakumar *et al.* reported an increase in global methylation after they irradiated SKH-1 hairless mice with UVB radiation as well as in human cSCC samples compared to control skin samples (see **Section 1.3.4**) [172].

We calculated the means of methylation levels across all tumor samples and compared them to the mean methylation levels of matched controls and independent healthy skin. This was done on the 31,889 CpGs as described in **Section 3.2.4**.

Average methylation in ssUV cSCC was significantly higher compared to matched control skin (pairwise t-test, p=0.007, see **Figure 16**). Due to the low number of independent healthy skin samples (n=2) no statistical analysis was performed for this group, but methylation percentage was similar to dorsal skin. A trend for correlation between average methylation and sequencing depth was observed (p=0.0724), but sequencing depth did not differ between control and tumor samples (p=0.314). Although this result is consistent with previously published data, it is important to note that we only analysed a subfraction of the approximately 22 million CpGs present in the murine genome (GRCm38/mm10 assembly). Furthermore, RRBS methodologies enrich for sequences with medium to high CpG density and therefore CGIs, but relatively ignore the parts of the genome that undergo hypomethylation in cancer. We therefore cannot conclude that global methylation increases in ssUV cSCC, but we could say that there might be a trend towards hypermethylation, a pattern that has been reported for human cSCC [172].

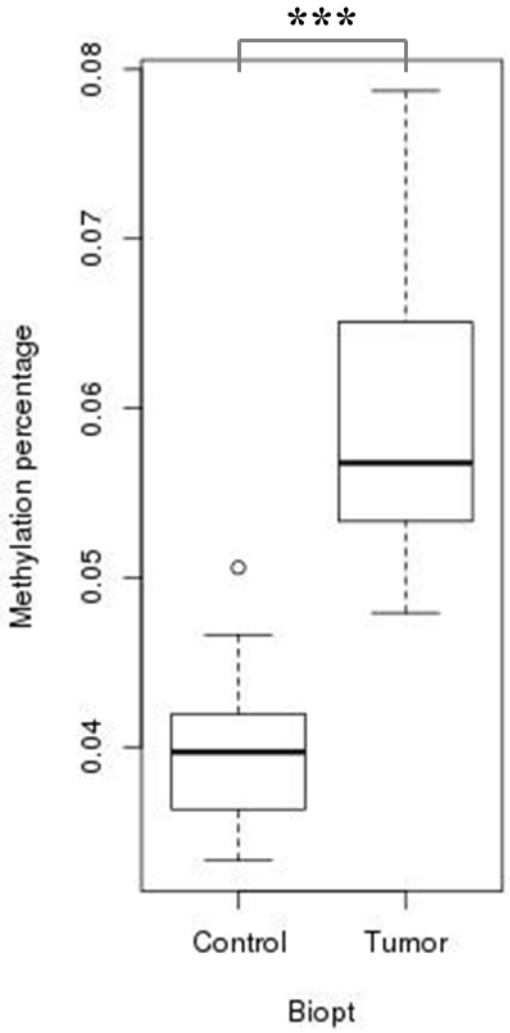

Figure 16: Average methylation is significantly higher in mouse ssUV cSCC compared to matched controls. Average methylation levels are based on the results from 31,899 CpGs. The total number of CpGs in the mouse genome is approximately 22 million CpGs. As only 31,899 CpGs were analysed (< 0.15% of all mouse CpGs), this results should not be confused with global methylation levels.

3.2.5 Visualization of methylation levels in the UCSC genome browser

UCSC tracks were built as described in **Section 2.4.5**. Tracks for both, RRBS and Infinium data by Rodriguez-Paredes *et al.* can be accessed online:

- RRBS:
  http://genome.ucsc.edu/cgi-bin/hgTracks?hgS_doOtherUser=submit&hgS_otherUserName=ljcousse&hgS_otherUserSessionName=Kevin
- Infinium:
  http://genome.ucsc.edu/cgi-bin/hgTracks?hgS_doOtherUser=submit&hgS_otherUserName=ljcousse&hgS_otherUserSessionName=Lyko

3.3 Analysis of differential methylation between ssUV cSCC and normal skin

As discussed before, DNA methylation is a critical process in regulating gene expression and genome stability. DNA methylation patterns can differ massively between cancerous and benign tissue and regulates silencing of tumor suppressor genes and up-regulation of oncogenes. Individual CpGs, even when in a region with multiple other CpGs, can have a profound impact on the ability of transcription factors to bind [236]. On the other hand, some regions are recognised by specialised methyl CpG binding domain (MBD) proteins where the methylation status of all CpGs in the region impacts the regulatory effect [237]. In order to address both, methylation of individual CpGs and methylation across CpG islands (CGIs), two separate analyses were performed.

3.3.1 Differential methylation of individual CpGs

The methylation status of individual CpGs can influence the ability of transcription factors and other regulatory elements to bind specific regulatory regions of DNA and supress gene expression. The RRBS data were filtered by shared regions (100% of samples) and coverage (minCov=8). After exclusion of CpGs not passing the threshold for minimum average methylation (loci that are unmethylated across all samples are not of interest), a total of 31,889 CpGs were considered for differential methylation analysis.

After significance testing and false discovery rate (FDR) correction, we found 134 differentially methylated CpGs in 87 different genes and 10 intergenic CpGs, of which four clustered together in a region on chromosome 17 (36,231,447-36,231,471). All significant CpGs were hypermethylated in tumors, consistent with the fact that regions of medium to high CpG content (that are predominantly picked up by RRBS) become hypermethylated in cancer.

Table 20: Methylation levels of all CpGs at the *Filip1l* locus. Position: Position on chromosome 16, **iHS:** independent healthy skin, **adj. p-Value:** p-value after FDR correction. Significantly differentially methylated CpGs are highlighted in bold.

position	tumor	ventral skin	iHS	adj. p-Value
57391482	0.0784	0.1603	0.0908	0.383665339
57391492	0.0859	0.1613	0.0960	0.367049289
57391494	0.1153	0.2144	0.1091	0.295194978
57391498	0.1185	0.2110	0.1439	0.23858672
57391502	0.1033	0.1432	0.0790	0.321105505
57391517	0.0228	0.0386	0.0142	0.569014216
57391520	**0.4816**	**0.0285**	**0.0100**	**0.027515586**
57391522	**0.5369**	**0.0441**	**0.0197**	**0.027515586**
57391524	**0.5227**	**0.0574**	**0.0223**	**0.027515586**
57391525	**0.4965**	**0.0401**	**0.0170**	**0.027515586**
57391528	**0.4196**	**0.0475**	**0.0156**	**0.032013265**
57391529	**0.4559**	**0.0335**	**0.0132**	**0.027515586**
57391533	**0.5847**	**0.0460**	**0.0119**	**0.027515586**
57391534	**0.5048**	**0.0292**	**0.0105**	**0.027515586**
57391538	**0.7234**	**0.0835**	**0.0320**	**0.027515586**
57391539	**0.6259**	**0.0773**	**0.0318**	**0.027515586**
57391546	**0.5436**	**0.0519**	**0.0252**	**0.027515586**
57391547	0.5724	0.0445	0.0221	0.054320133
57391552	**0.5907**	**0.0663**	**0.0253**	**0.032447585**
57391553	**0.6377**	**0.0492**	**0.0255**	**0.038106479**
57391555	**0.5577**	**0.0583**	**0.0291**	**0.027515586**
57391556	**0.6157**	**0.0534**	**0.0274**	**0.032447585**
57391571	**0.5074**	**0.0436**	**0.0173**	**0.032013265**
57391572	0.5528	0.0349	0.0140	0.054320133
57391584	**0.4891**	**0.0383**	**0.0160**	**0.027515586**
57391585	0.3797	0.0199	0.0049	0.063242775
57391592	0.0221	0.0382	0.0222	0.909063251
57391593	0.2390	0.0456	0.0958	0.681628775
57391596	0.1366	0.0431	0.0369	0.379501469
57391617	0.1010	0.0437	0.0315	0.107375253
57391622	0.1026	0.0638	0.0332	0.152881156
57391625	0.1005	0.0504	0.0339	0.111199584
57391632	0.1269	0.0986	0.0689	0.322642769
57391636	0.0670	0.0405	0.0225	0.24123848
57391649	0.0714	0.0282	0.0210	0.261554549
57391651	0.0642	0.0324	0.0278	0.322642769
57391655	0.0621	0.0300	0.0155	0.231940497
57391657	0.0847	0.0314	0.0168	0.228728963
57391674	0.0759	0.0226	0.0147	0.132937668

Interestingly, 17 of the differentially methylated CpGs clustered in an intronic region of the *Filip1l* gene (and the *Cmss1* gene that is coded on the opposite DNA strand). The CpGs in this region showed one of the highest percentages of differential methylation. The methylation levels of the CpGs at the *Filip1l* locus are summarized in **Table 20** and **Figure 17**. The locus will be discussed in more detail in **Section 3.4.1**.

Methylation changes in individual CpGs are profound in mouse cSCC. In the following sections, we will further analyse differences in methylation and compare these changes with data from human cSCC cases.

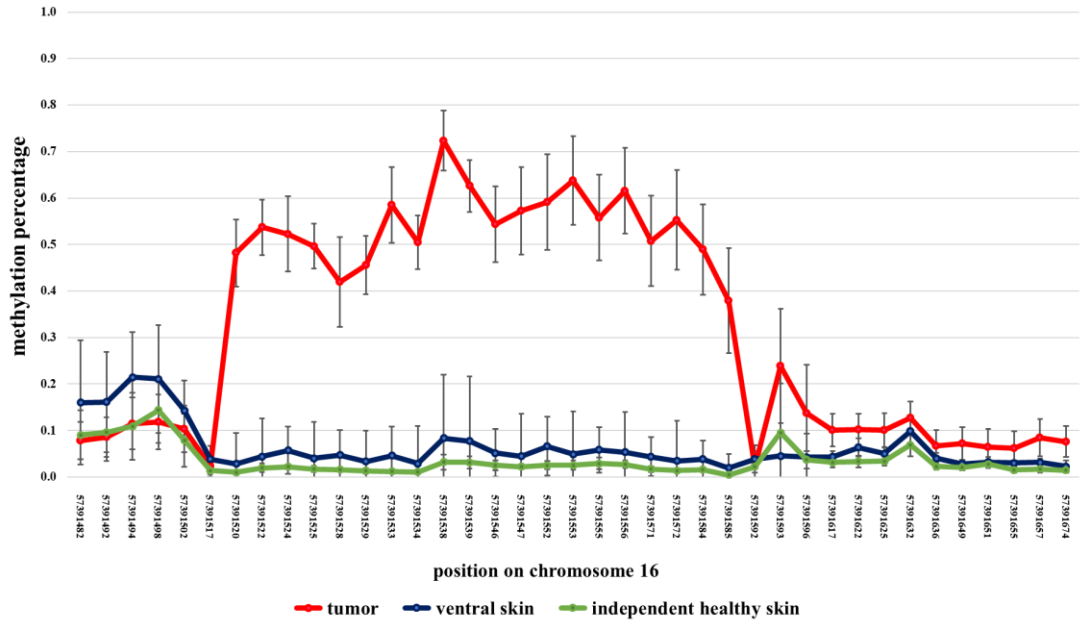

Figure 17: Graphical representation of methylation levels of CpGs at the Filip1l locus. The locus is located on chromosome 16. A cluster of 20 CpGs are hypermethylated in tumors compared to matched controls, 17 of which display significantly higher methylation.

3.3.2 Regions of potential differential methylation

Methylation at CpG islands (CGIs) is associated with inactivation of promoters or other regulatory elements CGIs are frequently differentially methylated in cancer.

A total of 201 regions were found as potential DMRs. Using the BiSeq package and binominal regression, we estimated the p-values for each of those regions. After statistical analysis, 78 DMRs were found to be significantly differentially methylated. The differences in methylation between controls and tumors ranged from -13% to -40% (positive values indicate increased methylation in tumors). Hypermethylation in tumors occurred in 76 DMRs, which was expected, since CGIs tend to become

hypermethylated in cancer. The methylation difference between ventral skin controls and tumors of the 78 significantly differentially methylated regions can be found in **Figure 18**.

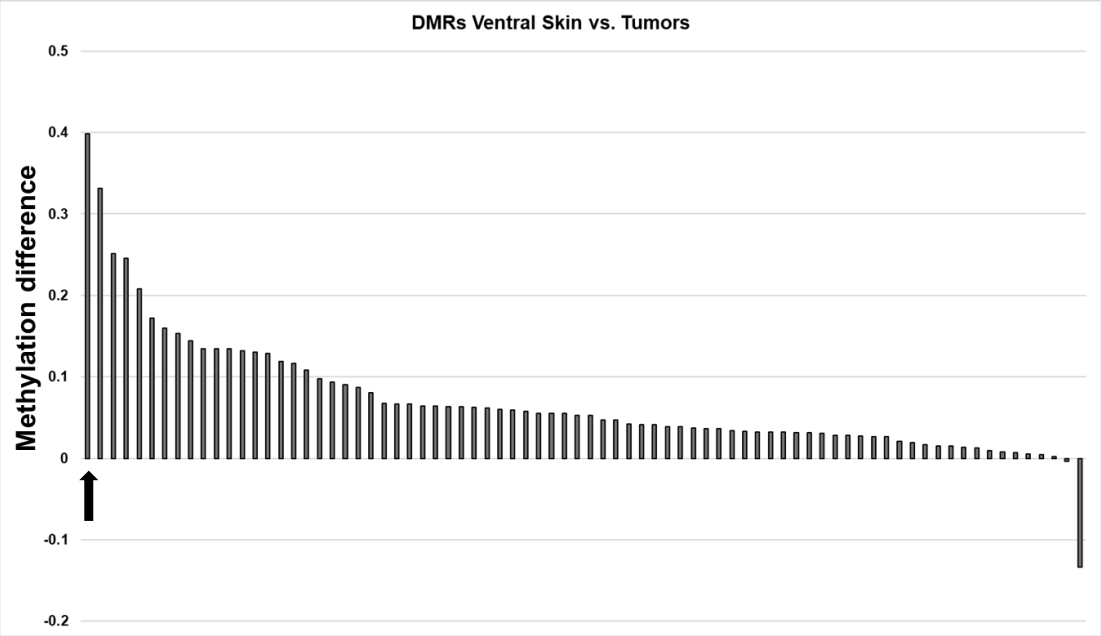

Figure 18: Methylation differences between ventral skin controls and tumors of the 78 significantly differentially methylated regions. A positive methylation difference indicates hypermethylation in tumors compared to ventral skin controls. Methylation differences range from 40% to -13%. The majority of DMRs (76 of 78) are hypermethylated in tumors, consistent with the observation, that average methylation is significantly increased in tumors. The region with the highest difference in methylation is the previously discussed *Filip1l* locus (indicated by the black arrow).

From a biological point of view, DMRs with a high difference in methylation are most likely to be of relevance, whereas very high significances are not as important. We therefore searched for DMRs that showed a high methylation difference between controls and tumors and significant p-values. One region of particular interest is located on chromosome 16, position 57,391,482-57,391,657. The medium methylation difference was -40% (hypermethylation in tumors), making this region the most differential methylated one that we detected. The region overlaps with two genes on opposite strands, *Filip1l* and *Cmss1*.

Selected regions of differential methylation will be discussed in the following section.

3.4 Regions of differential methylation are often associated with regulatory elements

In our previous analysis, we identified 78 significantly differentially methylated regions of which 76 were hypermethylated and 2 were hypomethylated in ssUV cSCC compared to controls. Next, we aimed to investigate genomic features of these regions.

Using the bed tracks built for the UCSC genome browser (https://genome.ucsc.edu/) we visualized methylation at the identified regions. Furthermore, the following tracks were used to display genomic features (from figure top to bottom):

1. Scale

2. Position on chromosome

3. GENCODE annotation, Harrow *et al.* 2006 [238]

   Gene annotation for protein coding and RNA genes

   Annotated genes are displayed as blue arrowed lines (introns) and blue rectangles (exons)

4. Baseline methylation levels in mouse keratinocytes, He *et al.* 2014 [239]

   A reference for DNA methylation in normal mouse keratinocytes, mainly indicating the position of all CpGs in the displayed region

5. UCSC bed tracks showing methylation in controls and tumors (see **Section 2.4.5**)

   Methylation levels in tumors and controls. Scale from (-)1 (100% methylation) to 0 (0% methylation).
   Positive values indicate significantly differentially methylated CpGs, negative values indicate non significantly differentially methylated CpGs.

   VS_CTL: Methylation in ventral skin controls

   Tumor: Methylation in tumors

6. EPD viewer hub, displaying promoters and CAGE sequencing, FANTOM Consortium and the RIKEN PMI and CLST (DGT) and Dreos *et al.* [240]

   CAGE seq measures transcriptional activity and is used to map transcription start sites and gives an indication on the regions regulatory relevance.

7. FANTOM5 TSS activity in adult skin, Noguchi et al. 2017 [241]

   Transcriptional activity at the region.

8. JASPAR 2018 Transcription factor binding sites, Khan *et al.* 2018 [242].

   Predicted transcription factor binding sites, supports the regulatory importance of the region.

3.4.1 Filip1l intronic DMR

The Filip1l intronic DMR that was detected at the *Filip1l* locus (

Figure 19) and is located in the intron between exon 1 and 2. It is 176 bp long and contains 38 individual CpGs (GC content: 76%). The medium methylation in controls is 34 %, while methylation in tumors is 76%.

In both analyses, i.e. individual CpGs and DMRs, the CpG cluster appeared as the top hit, showing both a highly significant methylation difference and a large difference in methylation percentages.

With 153,140 bps, the intron in which the DMR resides is unusually long. The DMR is located approximately 38,000 bp downstream of exon 1. Out of 39, 17 CpGs were identified as significantly differentially methylated and were hypermethylated in tumors compared to controls (see **Section 3.3.1**, **Figure 17** and **Table 20**). Furthermore, the region shows both, a high median methylation difference as well as a highly significant p-value (see **Figure 18**).

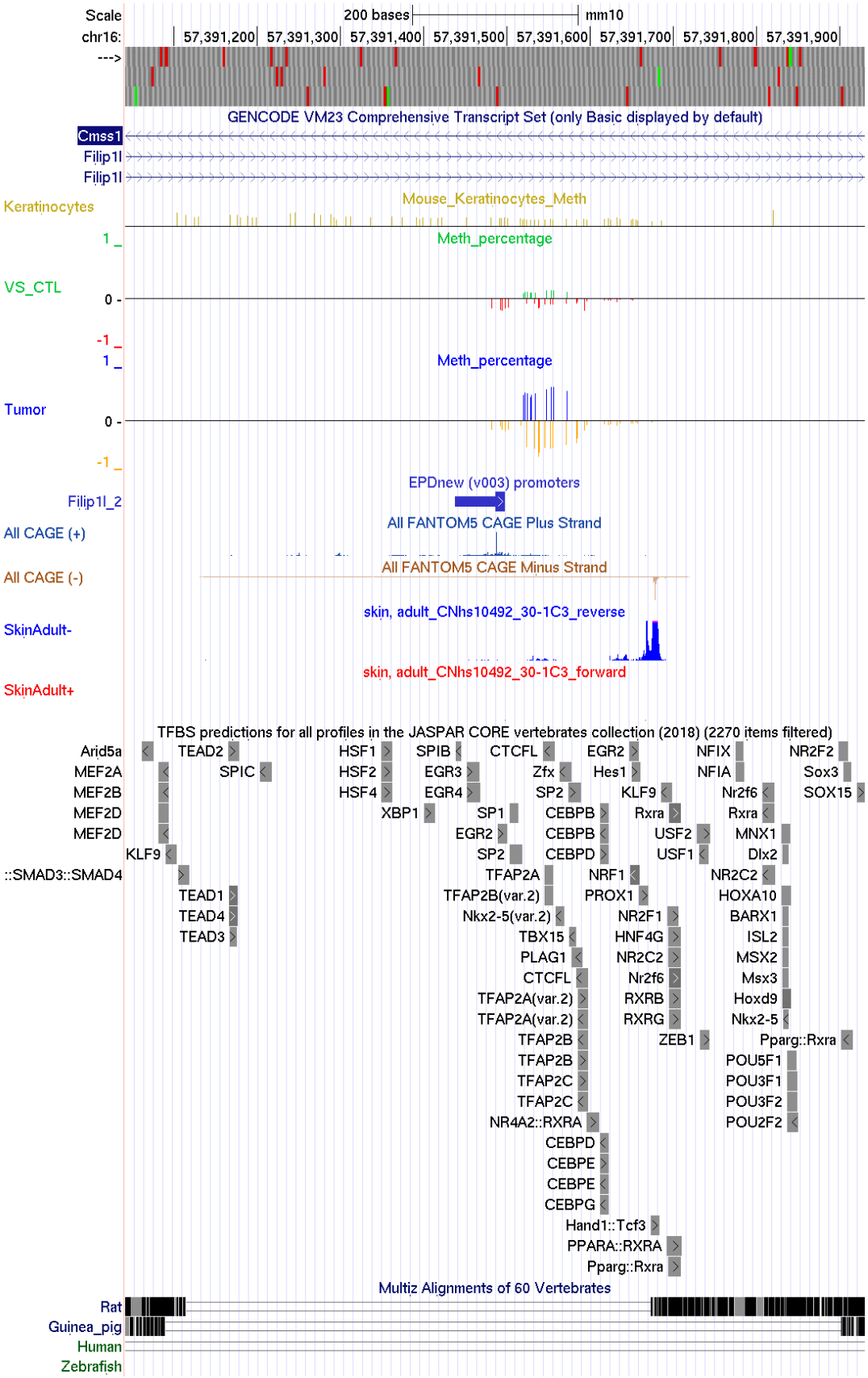
Scale
200 bases
mm10
chr16:
57,391,200
57,391,300
57,391,400
57,391,500
57,391,600
57,391,700
57,391,800
57,391,900
--->
GENCODE VM23 Comprehensive Transcript Set (only Basic displayed by default)
Cmss1
Filip1l
Filip1l
Keratinocytes
Mouse_Keratinocytes_Meth
1 _
Meth_percentage
VS_CTL
0 -
-1 _
1 _
Meth_percentage
Tumor
0 -
-1 _
EPDnew (v003) promoters
Filip1l_2
All CAGE (+)
All FANTOM5 CAGE Plus Strand
All CAGE (-)
All FANTOM5 CAGE Minus Strand
skin, adult_CNhs10492_30-1C3_reverse
SkinAdult-
skin, adult_CNhs10492_30-1C3_forward
SkinAdult+
TFBS predictions for all profiles in the JASPAR CORE vertebrates collection (2018) (2270 items filtered)
Arid5a
MEF2A
MEF2B
MEF2D
MEF2D
KLF9
::SMAD3::SMAD4
TEAD2
SPIC
TEAD1
TEAD4
TEAD3
HSF1
HSF2
HSF4
XBP1
SPIB
EGR3
EGR4
SP1
EGR2
SP2
TFAP2A
TFAP2B(var.2)
Nkx2-5(var.2)
TBX15
PLAG1
CTCFL
TFAP2A(var.2)
TFAP2A(var.2)
TFAP2B
TFAP2B
TFAP2C
TFAP2C
NR4A2::RXRA
CEBPD
CEBPE
CEBPE
CEBPG
Hand1::Tcf3
PPARA::RXRA
Pparg::Rxra
CTCFL
EGR2
Zfx
SP2
CEBPB
CEBPB
CEBPD
NRF1
PROX1
NR2F1
HNF4G
NR2C2
Nr2f6
RXRB
RXRG
ZEB1
Rxra
USF2
USF1
NFIX
NFIA
KLF9
Nr2f6
Rxra
NR2C2
HOXA10
BARX1
ISL2
MSX2
Msx3
Hoxd9
Nkx2-5
Pparg::Rxra
POU5F1
POU3F1
POU3F2
POU2F2
NR2F2
Sox3
SOX15
Dlx2
MNX1
Multiz Alignments of 60 Vertebrates
Rat
Guinea_pig
Human
Zebrafish

Figure 19: Intronic DMR at the *Filip1l* locus. The DMR is 176 bp long and contains 39 individual CpGs. Median methylation level in the controls is 34% while it is 76% in the tumors, a methylation difference of almost 42% between the groups making it the most differentially methylated region we detected. The methylation difference between controls and tumors is also highly significant (median p=0.00014). EPD predicted a promoter sequence at the locus, and FANTOM5 CAGE seq peaks indicate that this region is of regulatory relevance (see All CAGE tracks). Furthermore, FANTOM5 TSS activity (SkinAdult tracks) show transcriptional activity at the intronic region. We suspect this transcriptional activity is due to transcription of enhancer RNAs, strongly indicating that the DMR co-localizes with an enhancer [243]. This is further confirmed by clustering of multiple predicted transcription factor binding sites (TFBS, JASPAR CORE), a common occurrence at enhancer regions [244,245].

We suspected that this region could be an enhancer. The region is almost 200,000 bp upstream of the promoter of Filip1l isoform 202, providing sufficient physical space to allow for regulation of this promoter. Interestingly, mouse isoform 202 is the ortholog of human isoform 203, which has been shown to play an important role in various cancers, most notably in ovarian carcinoma.

Investigation of the DMR shows that there is transcriptional activity at the region. As the DMR is far away from any known protein coding sequence, it is possible, that they are enhancer RNAs. The function of enhancer RNAs is unknown, but their expression is a common occurrence near enhancer regions [243]. Furthermore, predicted transcription factor binding sites are clustering in this region, a common feature of enhancer regions [244,245]. Therefore, strengthening the hypothesis that the region is indeed an enhancer, possibly controlling expression of *Filip1l* isoform 202.

As shown in

Figure 19, the DMR co-localizes with a proposed Filip1l promoter (see EPDnew (v003) promoter track). This finding further suggests a regulatory role of methylation changes at the *Filip1l* DMR.

Although DNA methylation is known to regulate human FILIP1L expression, the human differentially methylated regulatory region is located upstream of exon 5 at the promoter and transcription start site (TSS) of FILIP1L isoform 203, the ortholog of mouse Filip1l isoform 202. The *Filip1l* DMR we detected is not conserved in humans, suggesting that in mice, there could be additional epigenetic mechanisms regulating *Filip1l.*

We will investigate the role of Filip1l in cSCC in further detail later in this thesis.

3.4.2 DMR #2

DMR #2 is located on chromosome 3 at position 5,860,619 to 5,860,741. It is 123 bp long and contains 30 individual CpGs. Methylation in controls skin samples is 25% while the CGI is hypermethylated in tumors with 58% average methylation. The CGI is of unknown function, but the presence of CAGE seq peaks and RNA transcripts in this non-coding region as well as the presence of multiple potential transcription factor binding sites hint at a possible enhancer function. The closest genes of known functions are *Pex2* (approximately 250 kb upstream) and *Zfhx4* (500 kb upstream).

Pex2 (peroxisomal biogenesis factor 2) is involved in peroxisome biogenesis and has been demonstrated to be essential for survival of liver cancer cells [246]. The Human Protein Atlas (https://www.proteinatlas.org/) lists Pex2 as moderately expressed in human skin, but with low to no expression in skin cancer [247]. Zfhx4 (Zinc finger homeobox 4) is highly expressed in both skin and skin cancer, making it an unlikely target for regulation by DMT #2 [247].

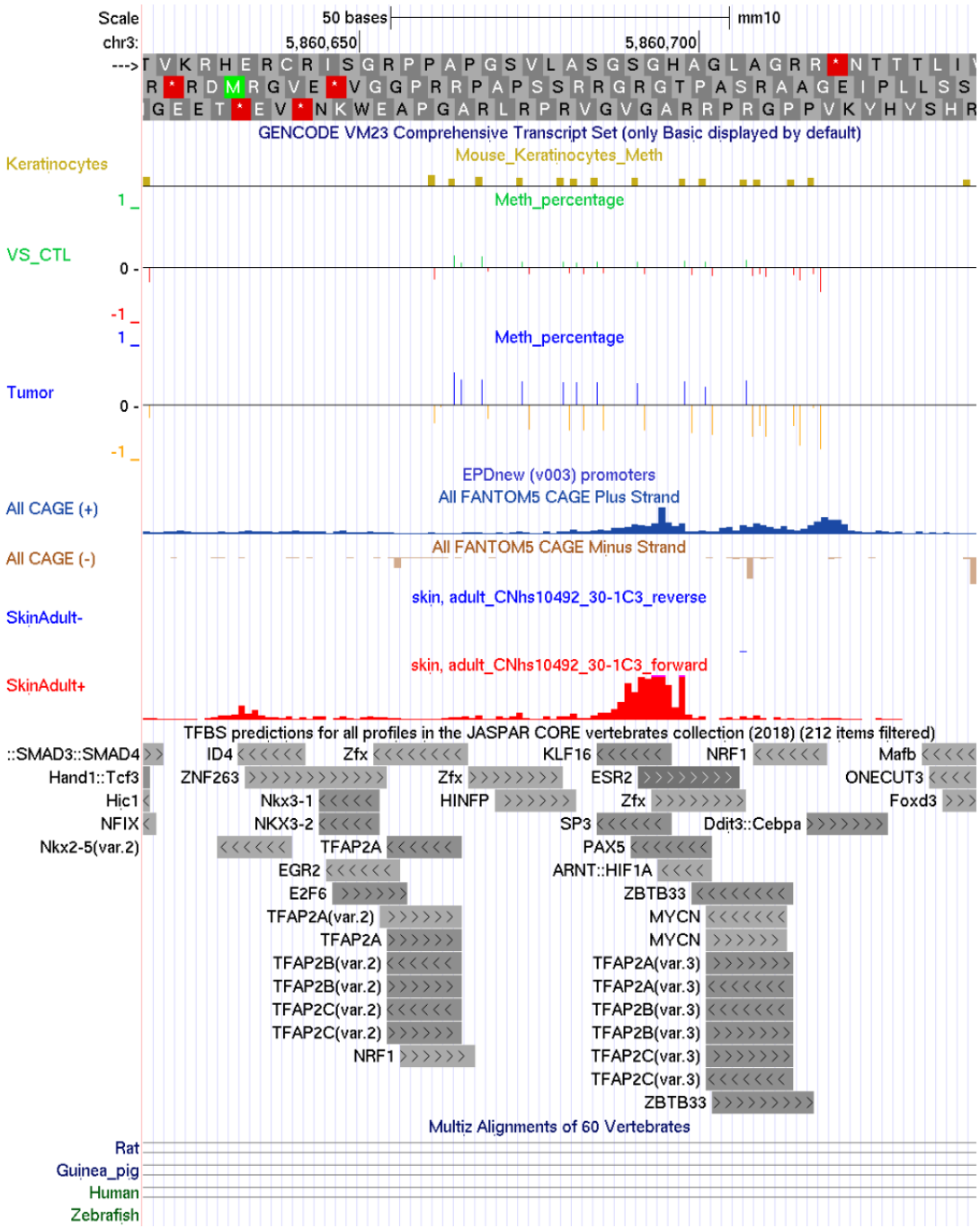

Figure 20: DMR #2 is 123 bp long and contains 27 individual CpGs. Median methylation is 25% in controls and 58% in tumors. Although the region is of unknown function, FANTOM5 CAGE seq peaks indicate that this region is of regulatory relevance (see All CAGE tracks). Furthermore, FANTOM5 TSS activity (SkinAdult tracks) show transcriptional activity at the intronic region. We suspect this transcriptional activity is due to transcription of enhancer RNAs, strongly indicating that the DMR co-localizes with an enhancer [243]. This is further confirmed by clustering of multiple predicted transcription factor binding sites (TFBS, JASPAR CORE), a common occurrence at enhancer regions [244,245].

3.4.3 Gm26917 DMR

The *Gm26917* DMR is the 2nd largest DMR we identified. It spans 838 bp and contains 123 individual CPGs. This intergenic region contains the coding sequence of *Gm26917*, a long intergenic non-coding RNA (lincRNA) gene of unknown function. Similar to long non-coding RNAs (lncRNA), lincRNAs are involved in a multitude of cellular processes, including metabolism, growth, cell maintenance and regulation [248–251]. LincRNAs are conserved across mammalian species and may have conserved function [252].

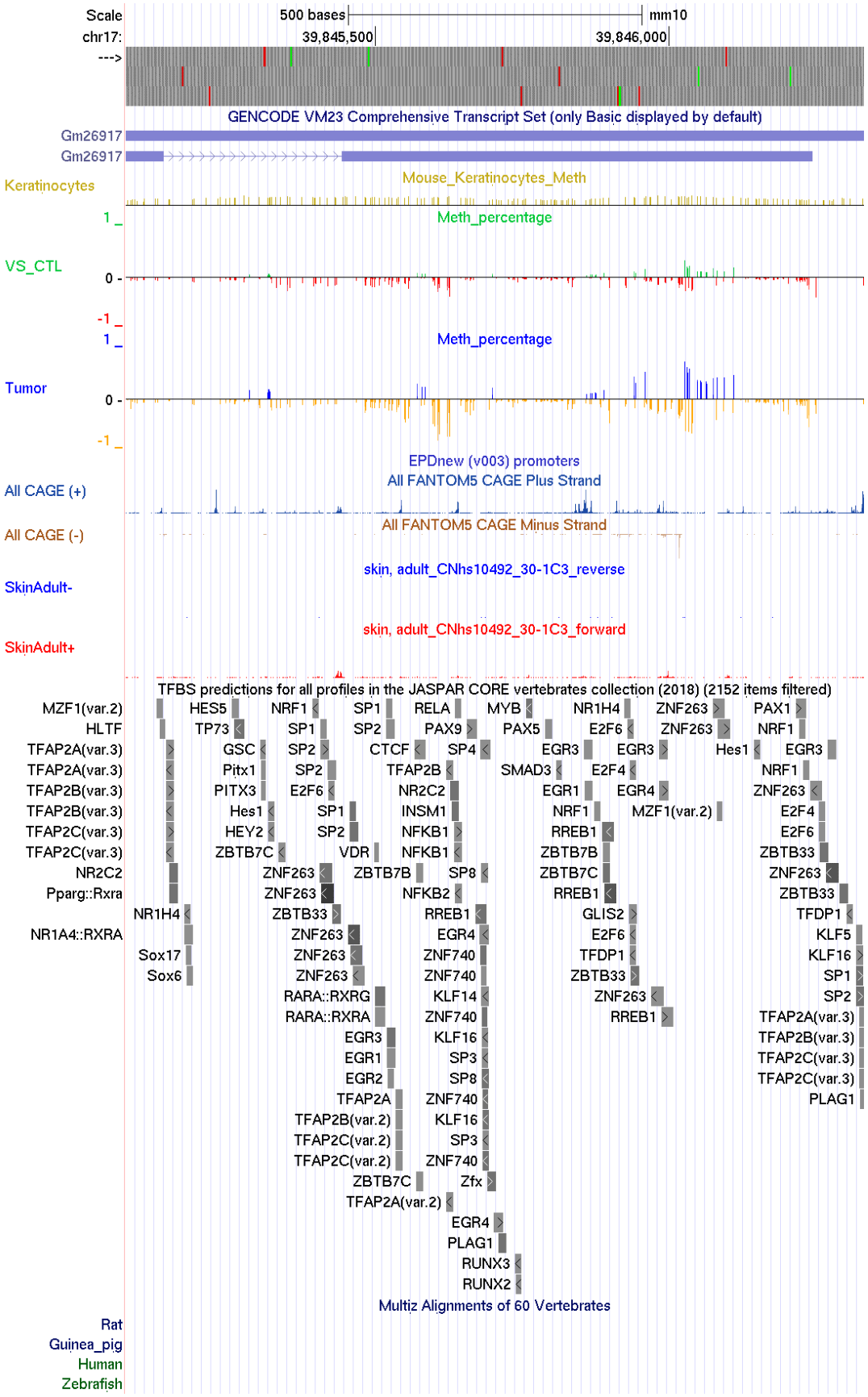
Scale
500 bases
mm10
chr17:
39,845,500
39,846,000
--->
GENCODE VM23 Comprehensive Transcript Set (only Basic displayed by default)
Gm26917
Gm26917
Keratinocytes
Mouse_Keratinocytes_Meth
1
Meth_percentage
VS_CTL
0
-1
1
Meth_percentage
Tumor
0
-1
EPDnew (v003) promoters
All FANTOM5 CAGE Plus Strand
All CAGE (+)
All FANTOM5 CAGE Minus Strand
All CAGE (-)
skin, adult_CNhs10492_30-1C3_reverse
SkinAdult-
skin, adult_CNhs10492_30-1C3_forward
SkinAdult+
TFBS predictions for all profiles in the JASPAR CORE vertebrates collection (2018) (2152 items filtered)
MZF1(var.2)
HLTF
TFAP2A(var.3)
TFAP2A(var.3)
TFAP2B(var.3)
TFAP2B(var.3)
TFAP2C(var.3)
TFAP2C(var.3)
NR2C2
Pparg::Rxra
NR1A4::RXRA
HES5 NRF1 SP1 RELA MYB NR1H4 ZNF263 PAX1
TP73 SP1 SP2 PAX9 PAX5 E2F6 ZNF263 NRF1
GSC SP2 CTCF SP4 EGR3 EGR3 Hes1 EGR3
Pitx1 SP2 TFAP2B SMAD3 E2F4 NRF1
PITX3 E2F6 NR2C2 EGR1 EGR4 ZNF263
Hes1 SP1 INSM1 NRF1 MZF1(var.2) E2F4
HEY2 SP2 NFKB1 RREB1 E2F6
ZBTB7C VDR NFKB1 ZBTB7B ZBTB33
ZNF263 ZBTB7B SP8 ZBTB7C ZNF263
ZNF263 NFKB2 RREB1 ZBTB33
NR1H4 ZBTB33 RREB1 GLIS2 TFDP1
ZNF263 EGR4 E2F6 KLF5
Sox17 ZNF263 ZNF740 TFDP1 KLF16
Sox6 ZNF263 ZNF740 ZBTB33 SP1
RARA::RXRG KLF14 ZNF263 SP2
RARA::RXRA ZNF740 RREB1 TFAP2A(var.3)
EGR3 KLF16 TFAP2B(var.3)
EGR1 SP3 TFAP2C(var.3)
EGR2 SP8 TFAP2C(var.3)
TFAP2A ZNF740 PLAG1
TFAP2B(var.2) KLF16
TFAP2C(var.2) SP3
TFAP2C(var.2) ZNF740
ZBTB7C Zfx
TFAP2A(var.2)
EGR4
PLAG1
RUNX3
RUNX2
Multiz Alignments of 60 Vertebrates
Rat
Guinea_pig
Human
Zebrafish

Figure 21: The Gm26917 DMR is 838 bp long and contains 123 individual CpGs. It is the 2nd largest DMR identified in our analysis. The region codes for the lincRNA Gm26917. Methylation level in controls is 14.5% while it is 31.2% in tumors. Multiple CAGE seq peaks and transcription factor b8inding sites suggest the presence of multiple transcription start sites in the area, but there seems to be only negligible RNA transcription in skin.

Interestingly, the *Gm26971* DMR contains multiple CAGE seq peaks, suggesting multiple transcription start sites. As nothing is known about the Gm26971 lincRNA, the significance of this is unclear. However, there is almost no transcriptional activity in skin in this region, as shown by the lack of FANTOM 5 TSS signal.

3.4.4 Cdk8 intronic DMR

Cyclin dependant kinase 8 (Cdk8) is an important factor of the mediator complex, facilitating the interaction between transcription factors and RNA polymerase II and may be an oncogene, depending on the cell context [253,254]. We detected a DMR approximate 1.7 kb upstream of exon 2 of the *Cdk8* gene. The DMR is 136 bp long and contains 24 individual CpGs. Methylation levels are 8.4% in controls and 21.8% in tumors.

The DMR does not co-localize with any known regulatory element. There are no promoters and transcription is minimal at this region, which is expected for an intronic region. Although there are transcription factor binding sites at the area of the DMR, binding sites do not cluster at the DMR to the same extend as they do for other loci (for example see

Figure 19).

Intronic methylation has been identified as a regulator of translational retention [255,256]. Most transcripts are spliced co-transcriptionally, meaning splicing occurs at the same time as transcription [257]. This opens up the possibility of DNA methylation to regulate alternative splicing as DNA methylation can influence chromatin structure and therefore the elongation rate of RNA polymerase II. Alternatively, methyl CpG binding protein 2 (MeCP2) can bind methylated DNA and recruit RNA binding factors that regulate splicing [256,258].

Indeed, *Cdk8* has multiple splice variants with some retaining introns [259]. It is possible, that in cSCC differential DNA methylation is influencing alternative splicing of *Cdk8*, therefore altering the proteins function. Differential intronic methylation of the *Cdk8* gene in murine cSCC may lead to alternative splicing and altered Cdk8 isoform composition in malignant cells.

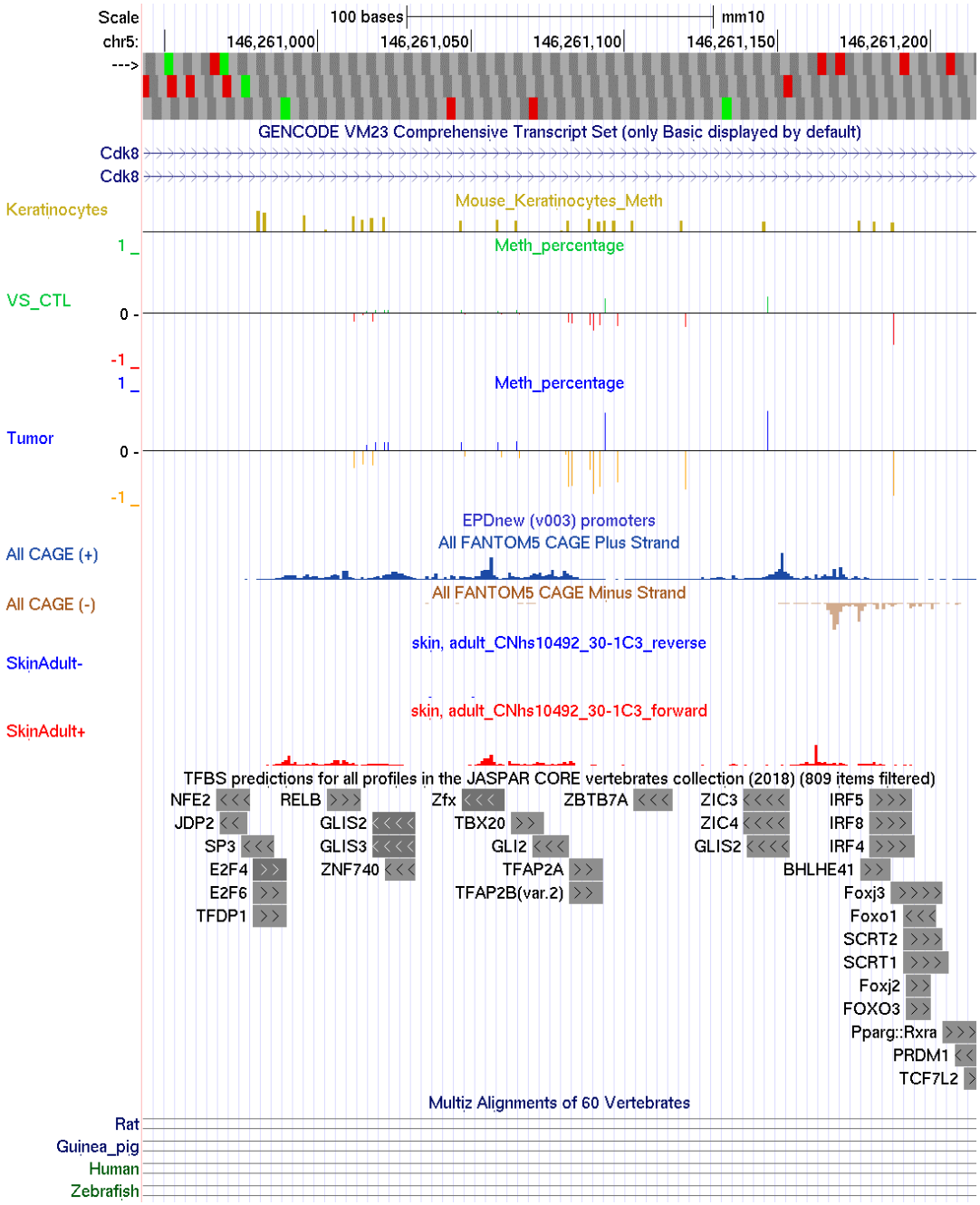

Figure 22: Cdk8 intronic DMR. The DMR is 136 bp long and contains 24 individual CpGs. Methylation levels are 8.4% in controls and 21.8% in tumors. There are no annotated promoters in the area and transcription is minimal. Transcription factor binding sites do not cluster at the area. We are not able to draw direct conclusions on the relevance of the region. However, it is possible, that intragenic methylation may reduce the rate of transcription and therefore alter splicing of the *Cdk8* gene [255].

3.4.5 DMR #12

DMR #12 is located in an intergenic region on chromosome 11 at position 109,011,629 to 109,012,044. The DMR is 277 bp long and contains 37 CpGs. While medium methylation across the region is 17.1% in controls, medium methylation is 31.6% in tumors.

The region is of unknown function, but the presence of multiple predicted transcription factor binding sites and CAGE seq peaks suggests the CGI could have an enhancer function. Furthermore, transcriptional activity at this intergenic DMR could be due to enhancer RNA transcription. The absence of other CAGE seq peaks or transcriptional activity in the proximity of the CGI (within 25 kb of the DMR), further strengthens this hypothesis.

The nearest gene (50 kb upstream) is *Axin2*, which plays a crucial role in controlling β-catenin stability in the Wnt signalling pathway. This pathway is not classically associated with cSCC, but has been proposed to be a potential therapeutic target in human cSCC [260]. However, based on the available data, we cannot conclude that DMR #12 is an enhancer region for *Axin2*.

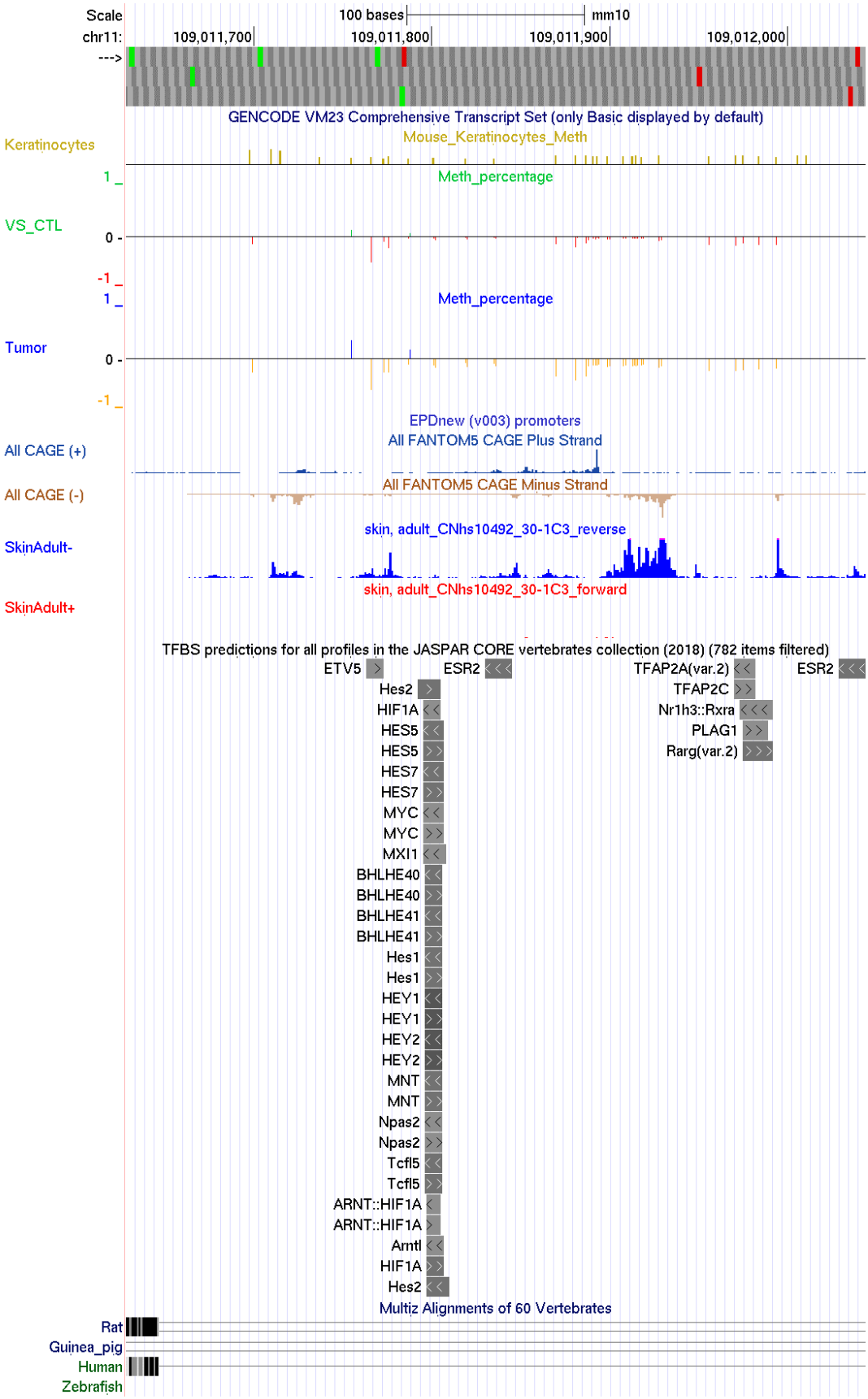
Scale
100 bases
mm10
chr11:
109,011,700
109,011,800
109,011,900
109,012,000
--->
GENCODE VM23 Comprehensive Transcript Set (only Basic displayed by default)
Keratinocytes
Mouse_Keratinocytes_Meth
1
Meth_percentage
VS_CTL
0
-1
1
Meth_percentage
Tumor
0
-1
EPDnew (v003) promoters
All FANTOM5 CAGE Plus Strand
All CAGE (+)
All FANTOM5 CAGE Minus Strand
All CAGE (-)
skin, adult_CNhs10492_30-1C3_reverse
SkinAdult-
skin, adult_CNhs10492_30-1C3_forward
SkinAdult+
TFBS predictions for all profiles in the JASPAR CORE vertebrates collection (2018) (782 items filtered)
ETV5
ESR2
TFAP2A(var.2)
ESR2
Hes2
TFAP2C
HIF1A
Nr1h3::Rxra
HES5
PLAG1
HES5
Rarg(var.2)
HES7
HES7
MYC
MYC
MXI1
BHLHE40
BHLHE40
BHLHE41
BHLHE41
Hes1
Hes1
HEY1
HEY1
HEY2
HEY2
MNT
MNT
Npas2
Npas2
Tcfl5
Tcfl5
ARNT::HIF1A
ARNT::HIF1A
Arntl
HIF1A
Hes2
Multiz Alignments of 60 Vertebrates
Rat
Guinea_pig
Human
Zebrafish

Figure 23: DMR #12 is 277 bp long and contains 37 individual CpGs. Median methylation is 17.1% in controls and 31.6% in tumors. Although the region is of unknown function, FANTOM5 CAGE seq peaks indicate that this region is of regulatory relevance (see All CAGE tracks). Furthermore, FANTOM5 TSS activity (SkinAdult tracks) show transcriptional activity at the intronic region. We suspect this transcriptional activity is due to transcription of enhancer RNAs, strongly indicating that the DMR co-localizes with an enhancer [243]. This is further confirmed by clustering of multiple predicted transcription factor binding sites (TFBS, JASPAR CORE), a common occurrence at enhancer regions [244].

3.5 Comparison of methylation in mouse ssUV cSCC with human cSCC

There is a surprisingly small number of studies investigating DNA methylation in human cSCC. Furthermore, most studies have only focussed on a single or only few regions of differential methylation. In addition, these studies only use qualitative or semi quantitative methods.

One study by Yang *et al.* [171] investigated global DNA methylation in both, DMBA/TPA- and UVB-induced mouse tumors, but found very little overlap between the two models, again highlighting the need for an adequate preclinical model. More recently, Rodriguez-Paredes *et al.* [190] have published their detailed analysis of the methylome of 16 human AK and 18 cSCC cases. This provides an excellent opportunity to test if the ssUVR induced mouse cSCC model, is a good model for the human disease in terms of DNA methylation, in addition to histopathology and genetics.

3.5.1 Methylation of keratin clusters differentiates two subtypes of human cSCC

One of the most important findings from the study by Rodriguez-Paredes *et al.* was that there seem to be two cSCC subtypes. Methylation at keratin gene clusters clearly differentiated that one AK and cSCC subclass was related to healthy epidermis, while the other one was related to cancer. When we examined the corresponding keratin cluster region in the mouse data (chr15:101,343,355-102,046,669), the region was not covered with sufficient detail to perform a subtype analysis. Therefore, we are unable to draw any conclusions if there are any subtypes in the murine ssUV cSCC.

3.5.2 Global methylation levels are higher in stem cell like human cSCC

In the murine ssUV cSCC, the average levels of methylation were significantly higher than in control samples. Although this is in contrast to the hypomethylation pattern in most cancers, this effect has been reported for human cSCC and some skin cancer cell lines.

In order to investigate the global levels of methylation, we performed a similar analysis on the Infinium HumanMethylation BeadArray data from Rodriguez-Paredes *et al.* Cluster analysis of global levels of methylation supported the presence of different subtypes, as the stem cell like tumor samples (as identified by Rodriguez-Paredes *et al.*) compose a single cluster (see **Figure 24**).

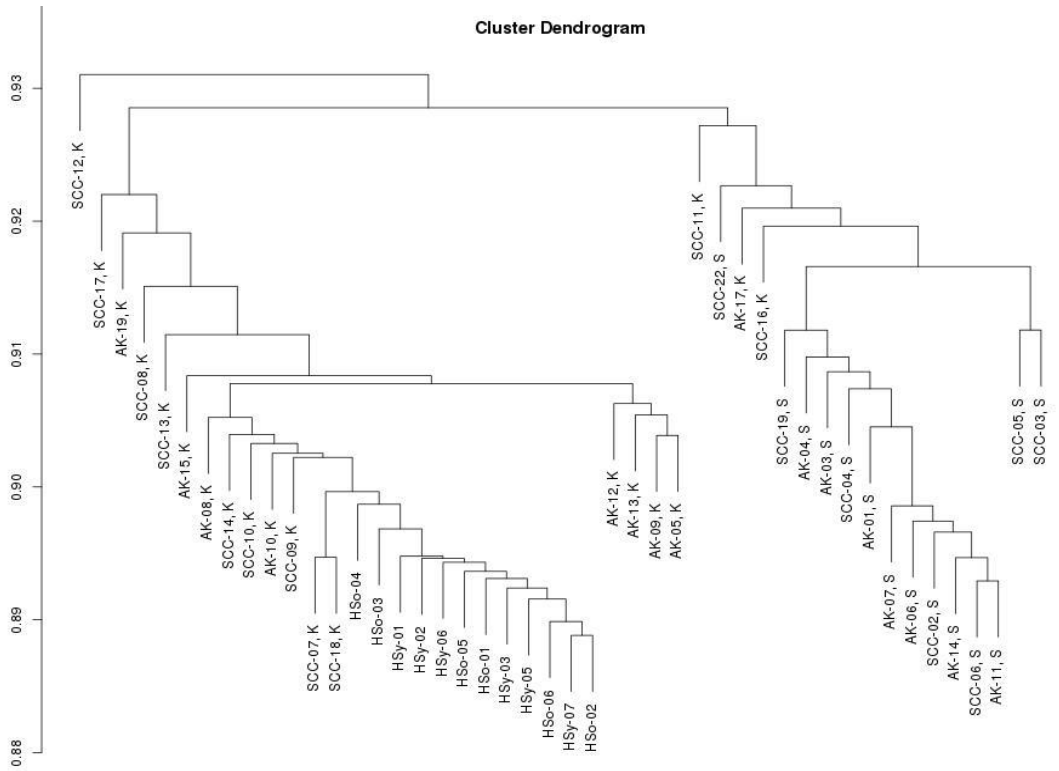

Figure 24: Cluster plot: HSo and HSy are control samples, cSCC and AK are tumor samples; for the latter K and S indicate whether the samples is respectively a keratinocyte like or stem cell like cancer sample. The majority of stem cell like AK and cSCC samples cluster together, indicating that they indeed for a separate subclass.

However, as shown in **Figure 25**, when we compared the average methylation levels between controls, AK samples and cSCC samples, there was no difference between the groups. As the publication by Rodriguez-Paredes *et al.* suggests, in terms of DNA methylation, there are striking similarities between AK and cSCC. We regrouped the samples in controls and keratinocyte-like as well as stem cell-like AK and cSCC samples and analysed average methylation. Here, the control- and keratinocyte-like samples showed no difference in methylation. Differences in global methylation levels between keratinocyte-like samples were higher, which is not surprising since those samples include cSCC samples that are more heterogeneous than the normal skin control samples that are also included in this group (**Figure 25 A**). Interestingly, stem cell-like samples showed significantly higher average methylation levels than both keratinocyte-like ($p=0.002$) and control ($p=0.010$) samples (**Figure 25 B**). This suggests that in addition to methylation at keratin clusters, global methylation levels distinguish keratinocyte- and stem cell-like cSCC subtypes.

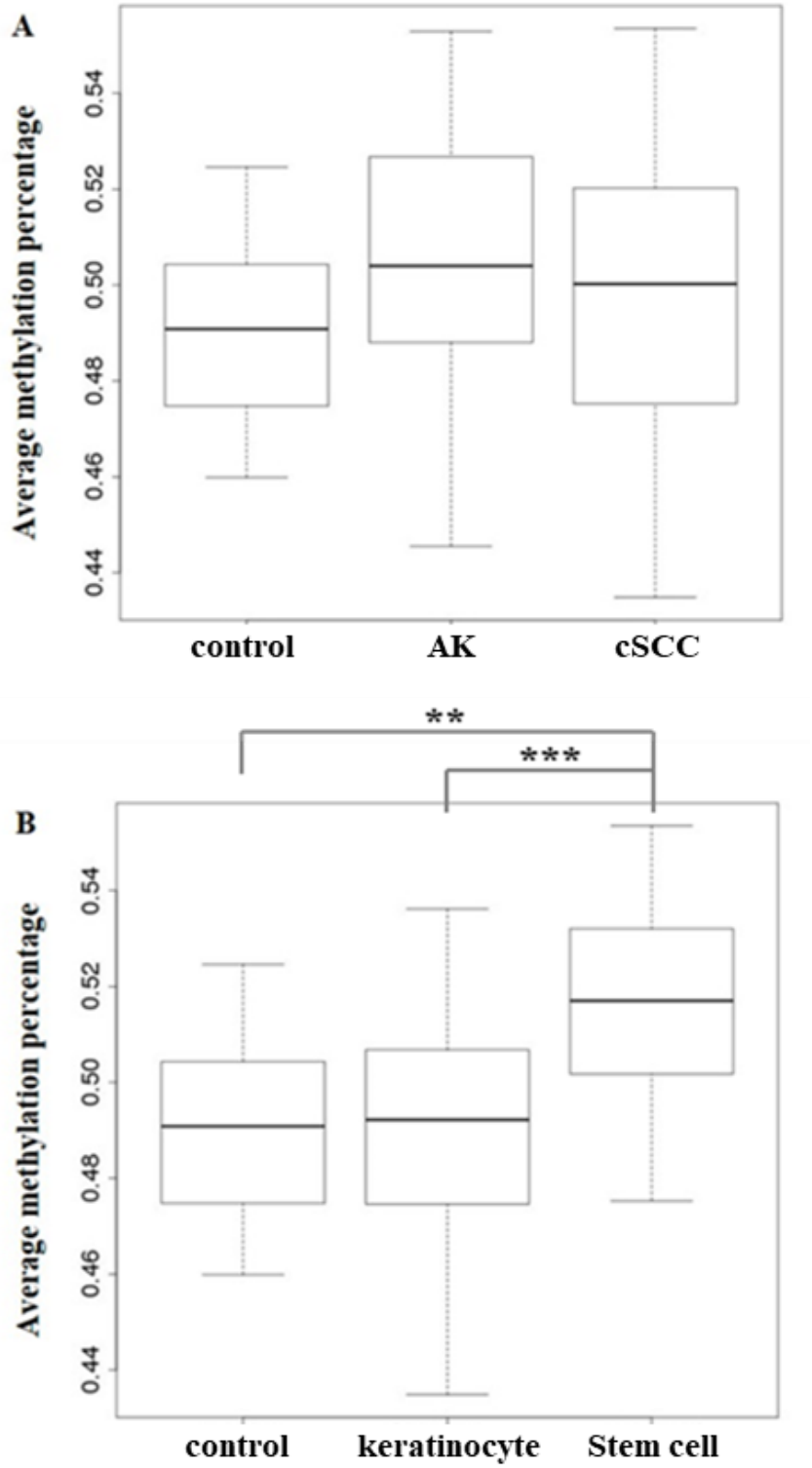

Figure 25: A: Average methylation of human skin samples (control), AK and cSCC. No difference in average methylation between the groups was detected. B: Average methylation of control samples and AK and cSCC samples, identified as keratinocyte like of stem cell like. Average methylation is significantly higher in stem cell like samples compare to both, control and keratinocyte like samples. Significance is indicated by asterisks (* $p<0.05$, ** $p<0.01$, *** $p<0.001$).

3.5.3 Differentially methylated regions overlap between human cSCC and mouse ssUV cSCC

In the analysis by Rodriguez-Paredes *et al.*, out of 859,515 Infinium probes 378,190 (= 44%) were found to be differentially methylated between control and tumor samples (including both, AK and cSCC). The Infinium 850k array covers 31,047 annotated genes, of which at least one differentially methylated probe was found in 26,703 genes (= 86%).

Starting from our RRBS data, we found 214 mouse genes that have at least one differentially methylated CpG. Using Ensemble annotation and the R package biomaRt (as described in **Section 2.4.4**), we found that out of the 214 mouse genes, 153 appear to have a human ortholog. Remarkably, 150 out the 153 (= 98%) mouse genes with a human ortholog were differentially methylated in both, our RRBS mouse data and the human data by Rodriguez-Paredes *et al*. This remarkable overlap suggests that methylation changes in mouse ssUV cSCC reflects the processes in human cSCC.

When we further filtered the gene list to contain at least two differentially methylated probes (Infinium) or CpGs (RRBS) and show a difference in methylation of at least 20%, seven genes were identified: Tspan9, Cmss1/Filip1l, Abr, Drd2, Nrros, Mdga2 and Slc2a10.

3.6 Investigation of methylation of the regulatory elements of FILIP1L in human and mouse cSCC

In collaboration with the German Cancer Research Center, we used MassARRAY (Agena Biosciences) to validate the previously detected DMR in mouse ssUV cSCC. Unfortunately, we were not able to create a PCR product of sufficient quality from the DMR between exon 1 and 2 of the mouse *Filip1l* gene. Therefore, no robust data could be generated for this region.

In the following section, I will compare methylation at the FILIP1L promoter of human cSCC cell lines with expression of FILIP1L in those cell lines. Results for FILIP1L expression can be found in **Section 3.8.2**.

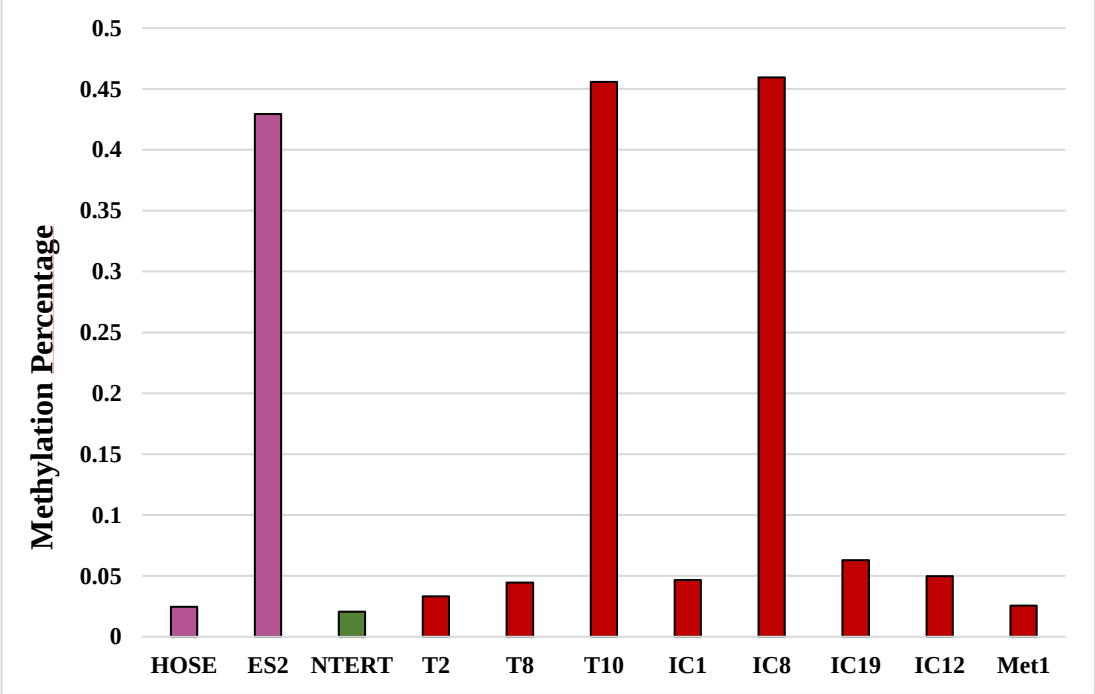

Figure 26: DNA methylation levels in HOSE and ES2 cell lines, NTERT cells and 8 human cSCC cell lines. Results represent the mean of three technical replicates. The FILIP1L promoter is hypermethylated in ES2, T10 and IC8 cancer cells and hypomethylated in the normal cell lines HOSE and NTERT, as well as the cSCC cell lines T2, T8, IC1, IC12, IC19 and Met1.

In humans, FILIP1L expression is controlled by promoter methylation. This promoter is located at an alternative transcription start site upstream of *FILIP1L* exon 5. For example, the promoter is hypomethylated in HOSE cells that express high levels of FILIP1L, while it is hypermethylated in ES2 ovarian cancer cells that express no FILIP1L (see [215,261]). We first tested, if this promoter is differentially methylated in human cSCC cell lines and if the methylation status correlates with FILIP1L

expression. DNA from human cSCC cell lines was BS converted and the MassARRAY protocol was followed as described in **Section 2.10**. As a control, we included DNA from HOSE and ES2 cells (kindly provided by the laboratory of Dr. Gillian Smith), where promoter methylation status is known. The results are displayed in **Figure 26**. As expected, the promoter region is almost un-methylated in HOSE cells, while ES2 cells show methylation levels of over 40%. In NTERT cells, the region is also un-methylated, as expected in a non-cancer cell line with high FILIP1L expression, In T2, T8, IC1, IC19, IC12 and Met1 cells, the promoter region also shows low methylation levels. However, methylation in T10 and IC8 cells is similar to ES2 cells. The high methylation levels in T10 cells correlate well with low FILIP1L expression in the cell line, but IC8 has both, a hypermethylated FILIP1L promoter and high FILIP1L expression. In the cell lines with hypomethylated promoter regions, methylation levels also do not inversely correlate with FILIP1L expression. For example, FILIP1L expression is high in T2 cells and low in T8 cells although both cell lines have similarly low promoter methylation. This suggests, that there are unknown regulatory mechanisms other than DNA methylation controlling FILIP1L expression in human cSCC. **Table 21** summarizes DNA methylation levels at the FILIP1L promoter and FILIP1L expression in the tested cell lines.

Table 21: FILIP1L promoter methylation and FILIP1L expression levels of the tested cell lines. There is no clear inverse correlation between methylation and expression in human cSCC cell lines. Inverse correlations between FILIP1L promoter methylation and expression are highlighted in bold.

Cell line	FILIP1L promoter methylation	FILIP1L expression
HOSE	**low**	**high**
ES2	**high**	**low**
NTERT	**low**	**high**
T2	**low**	**high**
T8	low	low
T10	**high**	**low**
IC1	low	normal
IC8	high	high
IC12	**low**	**high**
IC19	low	low
MET1	low	low

Figure 27 shows the *FILIP1L* promoter methylation levels in 14 human cSCC samples. In all but one sample (cSCC2) methylation levels were < 10%, suggesting that methylation at the *FILIP1L* promoter is not a common feature of human cSCC.

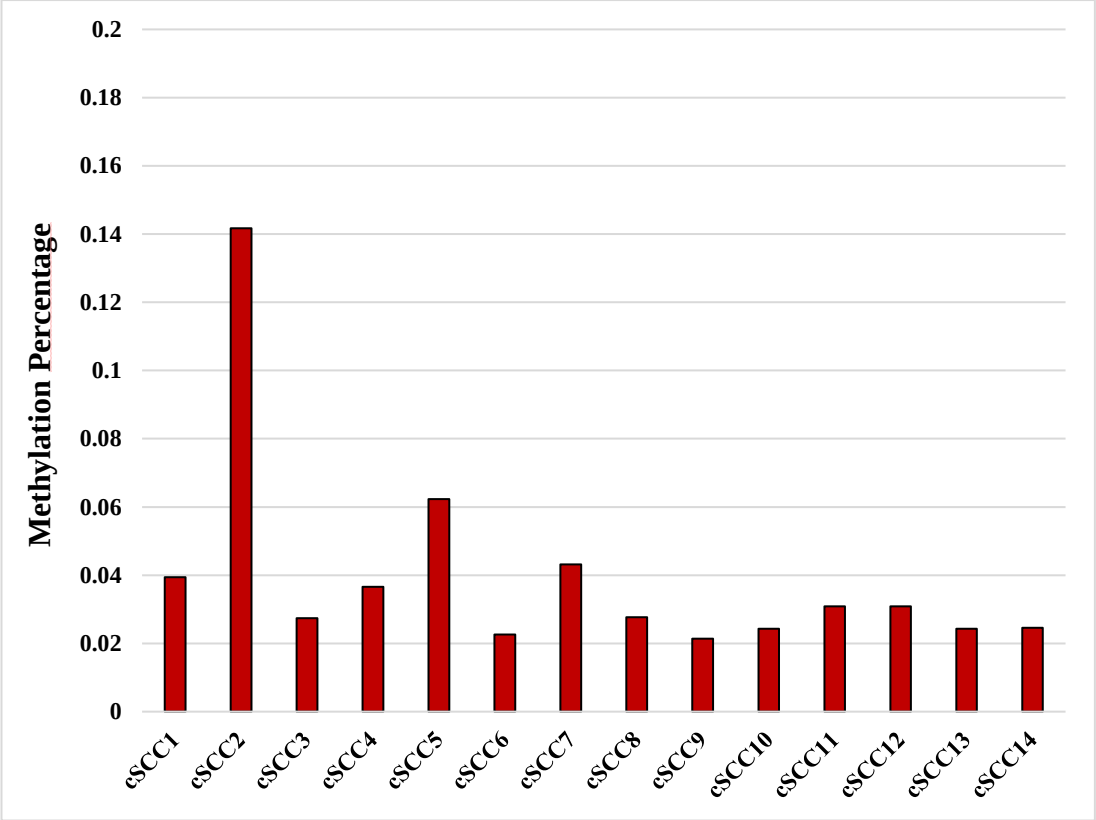

Figure 27: FILIP1L promoter methylation in 14 human cSCCs. Results represent the mean of three technical replicates. Although the promoter controls FILIP1L expression in multiple cancers and is hypermethylated in these cancers compared to controls, the promoter region is almost unmethylated in all tested human cSCC samples.

Using BLAST search, we identified the mouse region that corresponds to the human *FILIP1L* promoter, located upstream This region is also a CGI and may be involved in regulation of mouse Filip1l. **Figure 28** shows the average methylation levels of the mouse *Filip1l* promoter in ventral and dorsal skin controls as well tumors and the mouse keratinocyte cell line Kera308. Methylation levels are < 0.02 % across all tested samples. Furthermore, there are no differences between normal skin and tumors, suggesting that the *Filip1l* promoter, similar to human cSCC, does not play a role in regulation of *Filip1l* in murine skin.

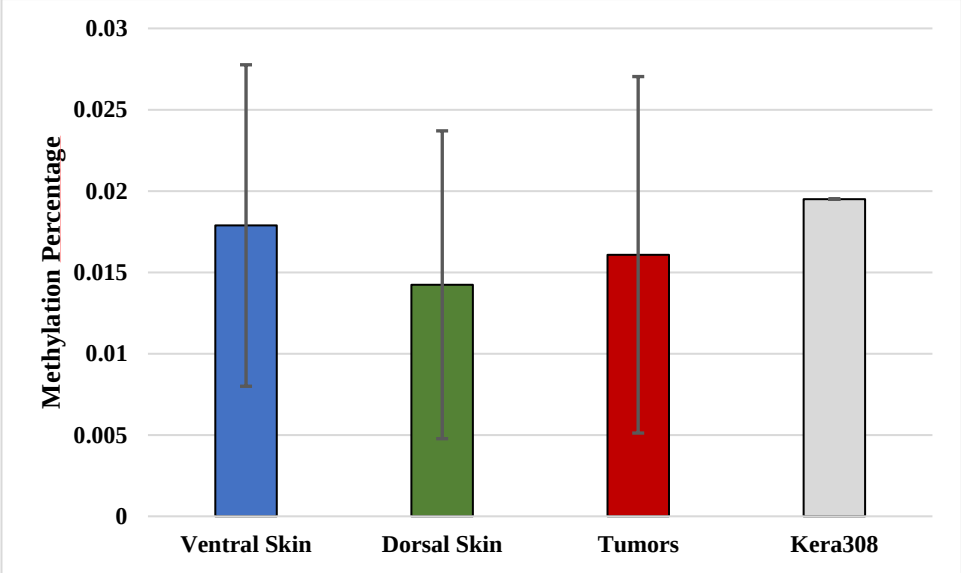

Figure 28: Methylation at the mouse *Filip1l* promoter in ventral skin, dorsal skin, tumors and the mouse keratinocyte cell line Kera308.. Ventral Skin: matched controls; Dorsal Skin: Chronically irradiated but benign skin; Tumors: mouse cSCC. Results represent the mean and standard deviation of 18 VS, DS and Tumor samples and three technical replicates of Kera308 DNA. The promoter shows very low methylation levels across all samples.

3.7 Filip1l in murine cutaneous squamous cell carcinoma

As previously described, we detected a differentially methylated region (DMR) within an intronic region of the *Filip1l* gene. This DMR showed the biggest difference in average methylation between the tumors and the normal skin tissue that we detected in our dataset. Furthermore, inspection of genomic features at the detected DMR suggests that the region is of regulatory relevance. More precisely, we suspected the region could represent an enhancer, possibly controlling the expression of Filip1l isoform 202.

Since there is no published information about the role of Filip1l in the skin, we next characterized the Filip1l isoform composition, the expression of Filip1l in the mouse skin and cSCC, and its functional significance.

3.7.1 Filip1l isoform 202 is the main expressed isoform in mouse skin

Murine Filip1l has three known isoforms (see **Figure 8**). There is nothing known about which isoforms are expressed in mouse skin or if there is any tissue specific expression pattern. Furthermore, it is unknown if the individual Filip1l isoforms may have different cellular functions.

Filip1l isoform 201 contains the shorter exons 1 to 4, isoform 202 has an alternative exon after regular exon 4 and also contains the long and main exon 5, while isoform 203 contains all exons (1 to 5). Exon spanning primers in exons 3 and 4 amplify the mRNA transcripts of isoforms 201 and 203. Isoform 203 is amplified by primers spanning exon 4 and 5, while a forward primer in isoform 202s alternative exon and exon 5 amplify only isoform 202.

We used isoform specific qPCR to determine the expression pattern of different Filip1l isoforms in healthy mouse skin and skin tumors, as well as in the mouse keratinocyte cell line Kera308. The results are shown in **Figure 29** and **Figure 30**. In these figures, VS refers to non-irradiated ventral skin, DS refers to chronically irradiated, but benign dorsal skin and T refers to mouse cSCC tumors, while numbers indicate animals and tumor numbers (e.g 1.10 T1 is tumor 1 of animal 1.10).

In mouse ventral skin (VS), the expression of the full-length isoform 203 is minimal, while the expression of isoforms 203 and 201 combined is slightly higher. The expression of isoform 202 is 15- to 37-fold higher than the expression of the other

isoforms. This clearly shows that isoform 202 is the main expressed isoform in mouse ventral skin (see **Figure 29**).

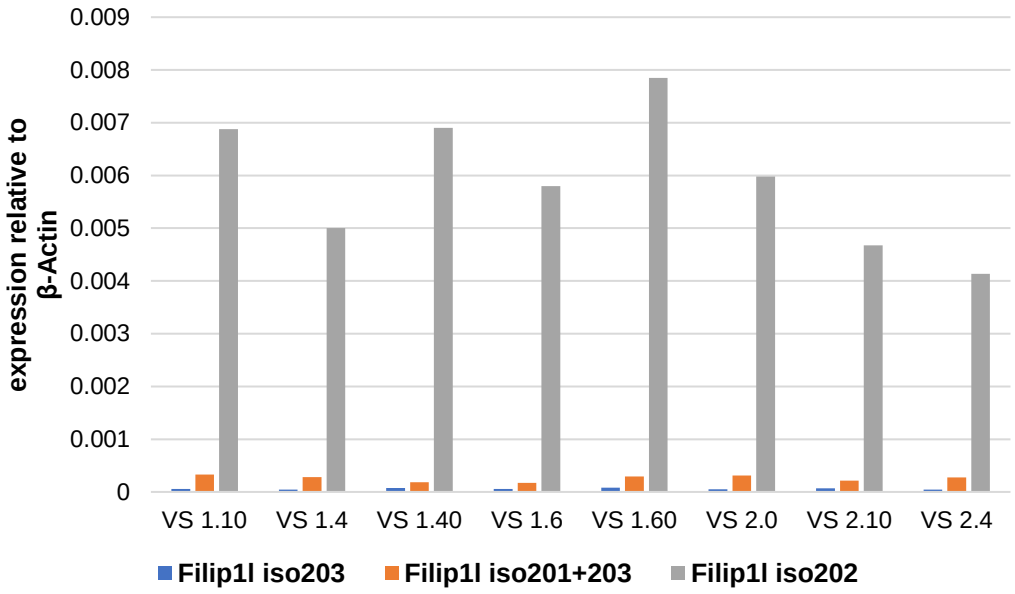

Figure 29: Isoform-specific qPCR for Filip1l in mouse ventral skin (VS). Results represent the mean of three technical replicates. The expression of isoforms 201 and 203 is minimal compared to the expression of isoform 202. We therefore conclude, that isoform 202 is the main expressed isoform in mouse VS.

Similar to VS, Filip1l isoform 202 is the main expressed isoform in dorsal skin (DS) and tumors. In DS, the expression ratio between isoforms 202 and 201+203 are in a similar range as in VS (18-fold, isoform 202 compared to the other isoforms combined). This is also the case for the isoform composition in the mouse keratinocyte cell line Kera308, where isoform 202 is the main isoform, and the ratios between isoforms are similar with those in VS and DS (see **Figure 30**).

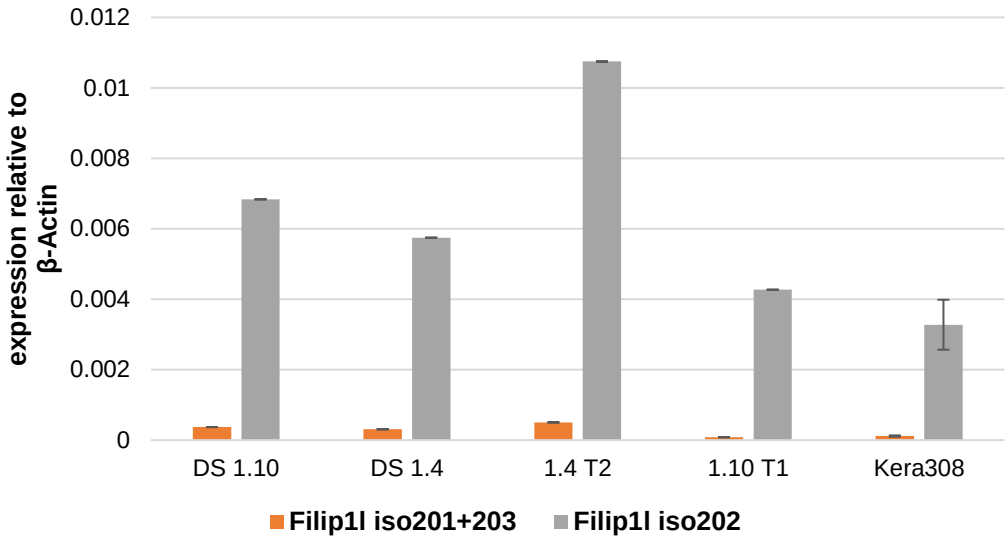

Figure 30: Isoform specific qPCR for Filip1l in mouse dorsal skin (DS) and the mouse keratinocyte cell line Kera308. Results represent the mean of three technical replicates. Similar to VS, isoform 202 is the main expressed isoform in chronically irradiated dorsal mouse skin (DS), Tumors (T) and the Kera308 cell line.

Having determined the expression of Filip1l in mouse skin and Kera308 cells, we assessed the protein levels of Filip1l in Kera308 cells by immunoblotting and confirmed the observed isoform expression using isoform-specific siRNAs. We designed siRNAs to target either isoforms 201 and 203 or isoforms 202 and 203 (see **Table 12**). As shown in **Figure 31,** under these experimental conditions, the Filip1l protein appears as a band at 110 kDa in control cells (i.e. cells transfected with a non-targeting siRNA pool). siRNA knock-down of all isoforms (using a combination of all siRNAs) completely abolishes the Filip1l protein expression at both 24- and 48-hours post-transfection. Treatment with siRNAs targeting isoforms 201 and 203 does not reduce Filip1l protein, while siRNAs targeting isoforms 202 and 203, similar to treatment with all siRNAs, supresses Filip1l protein expression. Furthermore, treatment with siRNAs targeting Filip1l isoforms other than 202, appears to increase Filip1l isoform 202 expression (see **Figure 31**, si 201/203). Treatment with siRNAs targeting isoform 202 is sufficient to compensate for this effect. This could be a compensatory mechanism in response to Filip1l isoform 201 and 203 knock-down, despite both isoforms being expressed at a low level.

This experiment further confirms that, in Kera308 cells, isoform 202 is the main expressed isoform of Filip1l.

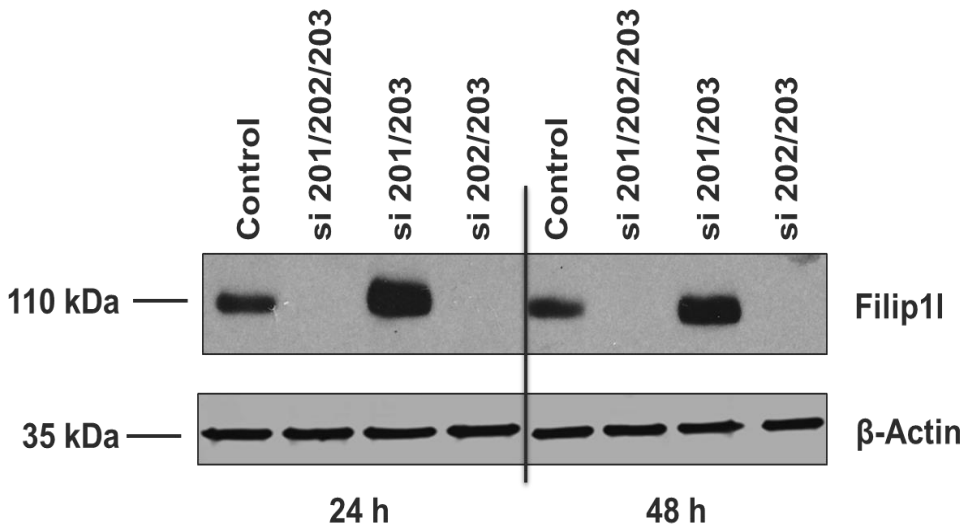

Figure 31: Protein levels of Filip1l after siRNA treatment at 24- and 48-hours post-transfection. The used siRNAs target two isoforms, either 201 and 203, or 202 and 203. si 201/203 and si 202/203 experiments use two siRNAs each, si 201/202/203 use the combination of 4 siRNAs. The combination of siRNAs targeting all Filip1l isoforms completely abolishes Filip1l protein expression, while siRNAs targeting isoforms 201 and 203 do not. Treatment with siRNAs targeting isoforms 202 and 203 also supress Filip1l expression. This confirms the finding from the mRNA analysis that Filip1l isoform 202 is the main expressed isoform in Kera308 cells.

We therefore conclude that Filip1l isoform 202 is the main expressed isoform in mouse skin, and in the keratinocyte cell line Kera308. Interestingly, the mouse Filip1l isoform 202 is very similar to the human isoform 203 (compare **Figure 8**), which seems to be the functional isoform in humans. From this point onwards, we refer to the mouse Filip1l isoform 202 as simply Filip1l, unless otherwise indicated.

3.7.2 Comparison of Filip1l expression in mouse tumors vs. healthy skin is inconclusive

Having established the isoform composition and a methodology to investigate Filip1l expression, we aimed to determine if Filip1l expression is altered in murine cSCCs compared to normal skin. Using the same isoform-specific primer, we utilized RT-qPCR to test the Filip1l expression in tumors as well as matched ventral and dorsal skin samples collected from 18 animals. The results are displayed in **Figure 32**, **Figure 33** and **Figure 34**.

We first used 18S as a reference gene and found, that compared to VS, the expression of Filip1l is significantly lower in DS (p=0.013) and is further reduced in tumors (p<0.001) (**Figure 32**). However, the expression of 18S varied across samples. When the expression analysis was repeated using the genes encoding actin, Gapdh and Hprt1 as reference genes, the expression of Filip1l showed a different pattern. There were no significant differences detected between VS and DS, while expression of Filip1l increased in tumor samples (significant when normalized to actin, p=0.003) as shown in **Figure 33** and **Figure 34**.

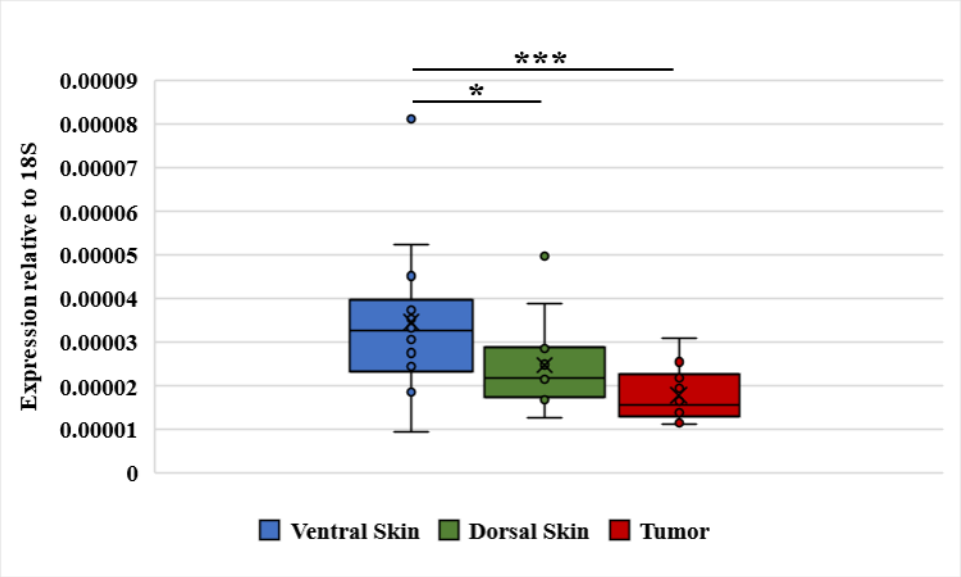

Figure 32: Expression of Filip1l in ventral skin (VS), dorsal skin (DS) and tumors, normalized to 18S. Results represent the means and standard deviations of 18 ventral skin, dorsal skin and tumor samples. Expression is significantly lower in DS and tumors in comparison with VS. The expression of the reference genes displayed considerable variance. Significance is indicated by asterisks (* p<0.05, ** p<0.01, *** p<0.001).

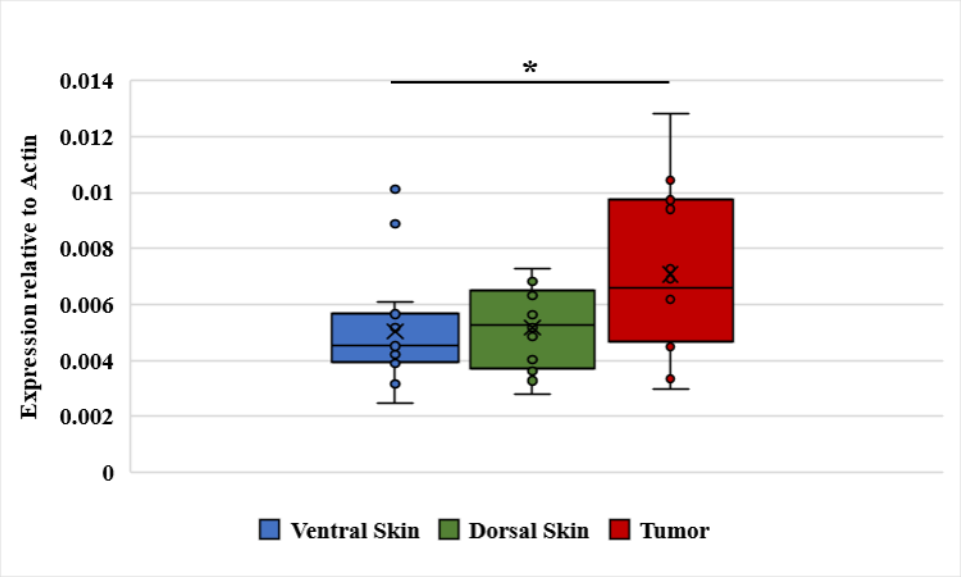

Figure 33: Expression of Filip1l in ventral skin (VS), dorsal skin (DS) and tumors, normalized to Actin. Results represent the means and standard deviations of 18 ventral skin, dorsal skin and tumor samples. Expression is significantly lower in DS and tumors in comparison with VS. The expression of the reference genes displayed considerable variance. Significance is indicated by asterisks (* p<0.05, ** p<0.01, *** p<0.001).

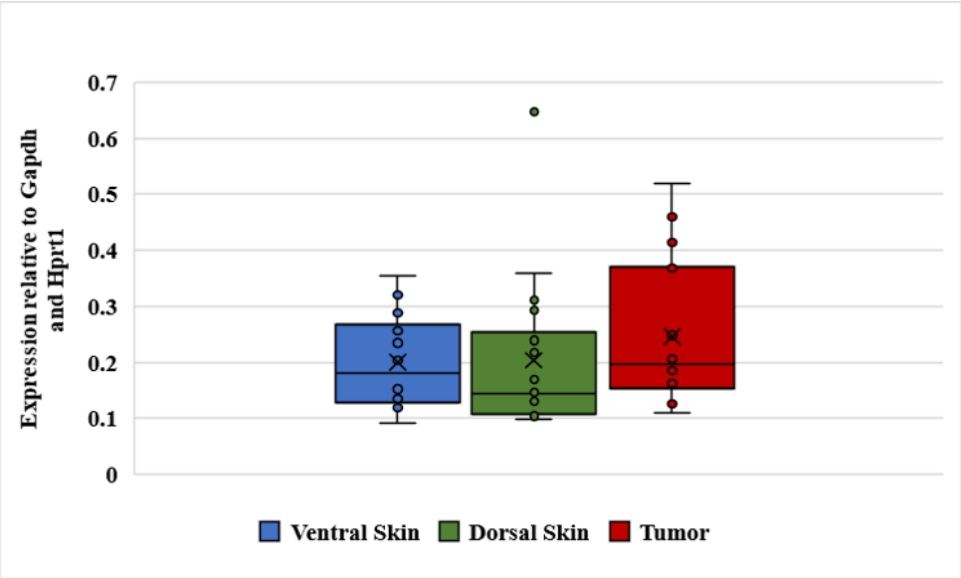

Figure 34: Expression of Filip1l in ventral skin (VS), dorsal skin (DS) and tumors, normalized to Gapdh and Hprt1. Results represent the means and standard deviations of 18 ventral skin, dorsal skin and tumor samples. Expression is significantly lower in DS and tumors in comparison with VS. The expression of the reference genes displayed considerable variance. Significance is indicated by asterisks (* p<0.05, ** p<0.01, *** p<0.001).

Similar to 18S, there was a considerable variance in the expression of actin, Gapdh and Hprt1. Using linear regression, it became apparent that the expression of the chosen reference genes did not display sufficient correlation to be able to determine which reference genes should be used for qPCR normalization (**Figure 35**). Therefore, these qPCR results are not conclusive with regard to potential differences in expression of Filip1l between normal and tumor tissue.

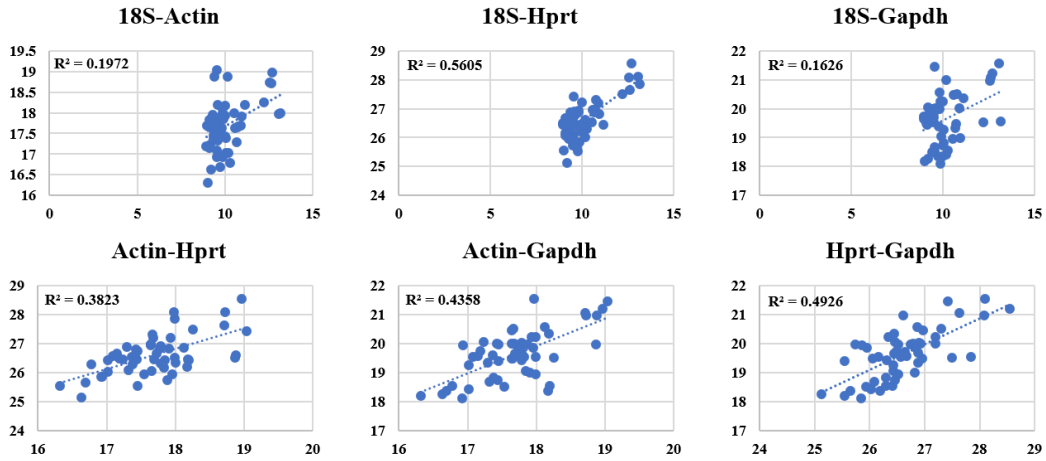

Figure 35: Correlation of CT values between 18S, actin, Gapdh and Hprt1. Correlation between the reference genes is not sufficient to produce conclusive qPCR results. R^2 indicate Pearson correlation coefficients.

3.7.3 Filip1l protein levels are reduced in murine cSCC tumors

The alterations in the expression levels of Filip1l in tumors vs. control skin could not be conclusively determined using RT-qPCR due to variance in reference gene expression. In order to determine the levels of Filip1l protein in mouse cSCC tumors and control skin, immunoblotting was used. A total of 54 samples from 18 animals (three samples per animal: VS, DS and tumor, numbers above this indicate animal designations) were analysed as shown in **Figure 36**. Using fluorescence detection immunoblotting (LiCOR), we were able to quantify the Filip1l protein levels in all samples using α-Tubulin as a loading control. The Filip1l protein levels were significantly reduced in chronically-irradiated DS compared to non-irradiated VS (paired t-test, $p=0.03$). Furthermore, in murine cSCC tumors, the Filip1l protein levels were further reduced compared to VS (paired t-test, $p=0.0026$).

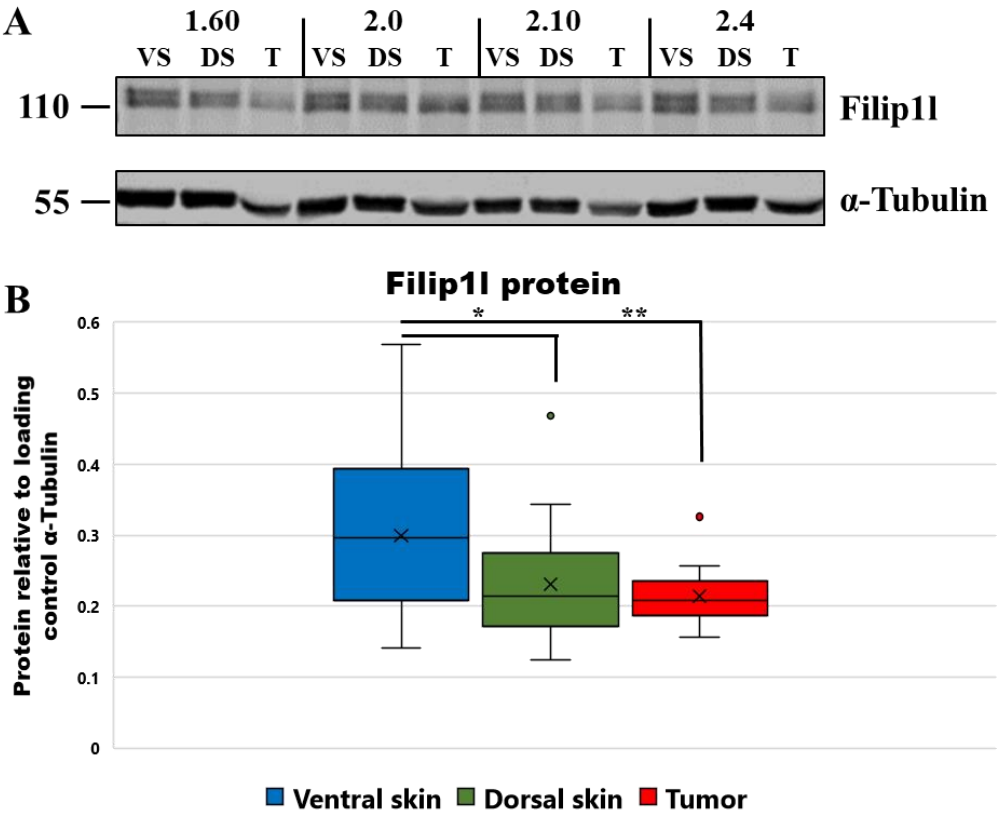

Figure 36: Filip1l protein levels in VS, DS and tumors of SKH-1 hairless mice that had been chronically exposed to UV radiation. A: Representative immunoblot for 4 out of 18 animals. Filip1l is detected as a band at 110 kDa, consistent with its molecular weight of 98 kDa. Filip1l appears as a double band in murine skin**. B: Quantification of Filip1l protein levels in all 18 animals.** Filip1l protein levels are significantly reduced in DS compared to VS and further reduced in tumors compared to VS. Significance is indicated by asterisks (* $p<0.05$, ** $p<0.01$, *** $p<0.001$). The numbers on the top indicate individual animals.

Surprisingly, the Filip1l protein appeared as a double band in the SKH-1 mouse skin samples. As this had not been previously reported, SKH-1 mouse samples were analysed side-by-side with Kera308 samples using different Filip1l antibodies (see **Figure 37**). While the presence of the second (top) Filip1l band in skin homogenates from SKH-1 mice was confirmed irrespective of the antibody used, it was absent in Kera308 cell lysates. Interestingly, the second (top) band was markedly weaker in the tumor samples. The identity of this second band is unknown.

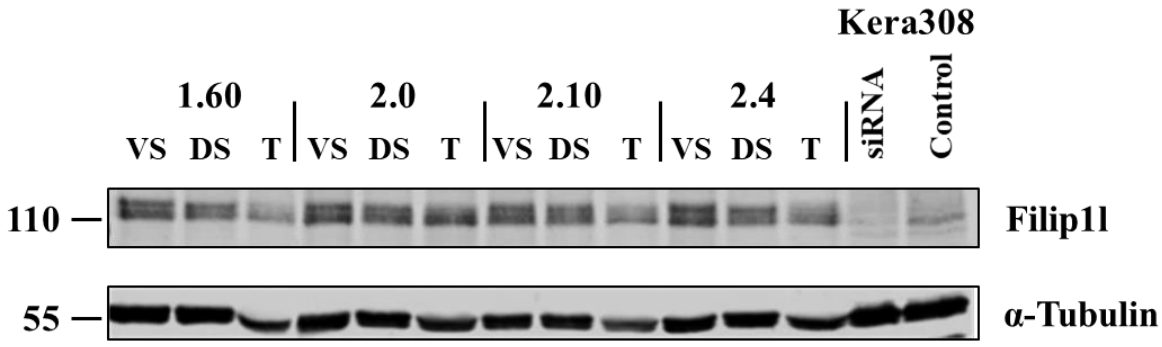

Figure 37: The second (top) Filip1l band was confirmed in SKH-1 mouse samples using different Filip1l antibodies. In Kera308 samples, Filip1l only appears as a single band. The identity of the second band is unknown.

3.7.4 Is Filip1l controlling Wnt signalling in mouse cSCC?

We have observed a reduction in Filip1l protein levels in murine cSCC, possibly through changes in DNA methylation affecting its gene expression. The role of Filip1l is largely unknown, but the strongest evidence of its cellular function has been provided by the laboratory of Steven K. Libutti. In multiple publications, Libutti and co-workers established, that human FILIP1L is a tumor suppressor in various cancers. Their data indicate, that Filip1l is involved in regulating β-catenin stability and thus affecting the canonical WNT/β-catenin signalling pathway [200,215,222,261], although the precise mechanism is unknown.

Using immunoblotting and antibodies against either total β-catenin or non-phosphorylated β-catenin (Ser33, Ser37, Thr41), the active form of β-catenin, we aimed to determine Wnt/β-catenin signalling activity and possibly correlate it to Filip1l protein levels. The results are displayed in **Figure 38** and **Figure 39**.

Active Wnt-signalling would be indicated by an increase in the ratio between active (non-phosphorylated) and total β-catenin. In tumors from 5 out of 18 animals (28%), the ratio between active and total β-catenin was increased in comparison to VS controls, indicating enhanced Wnt/β-catenin signalling. In contrast, tumours from 12 out of 18 animals (67%) showed the opposite trend, and one animal (6%) did not show changes in β-catenin ratio.

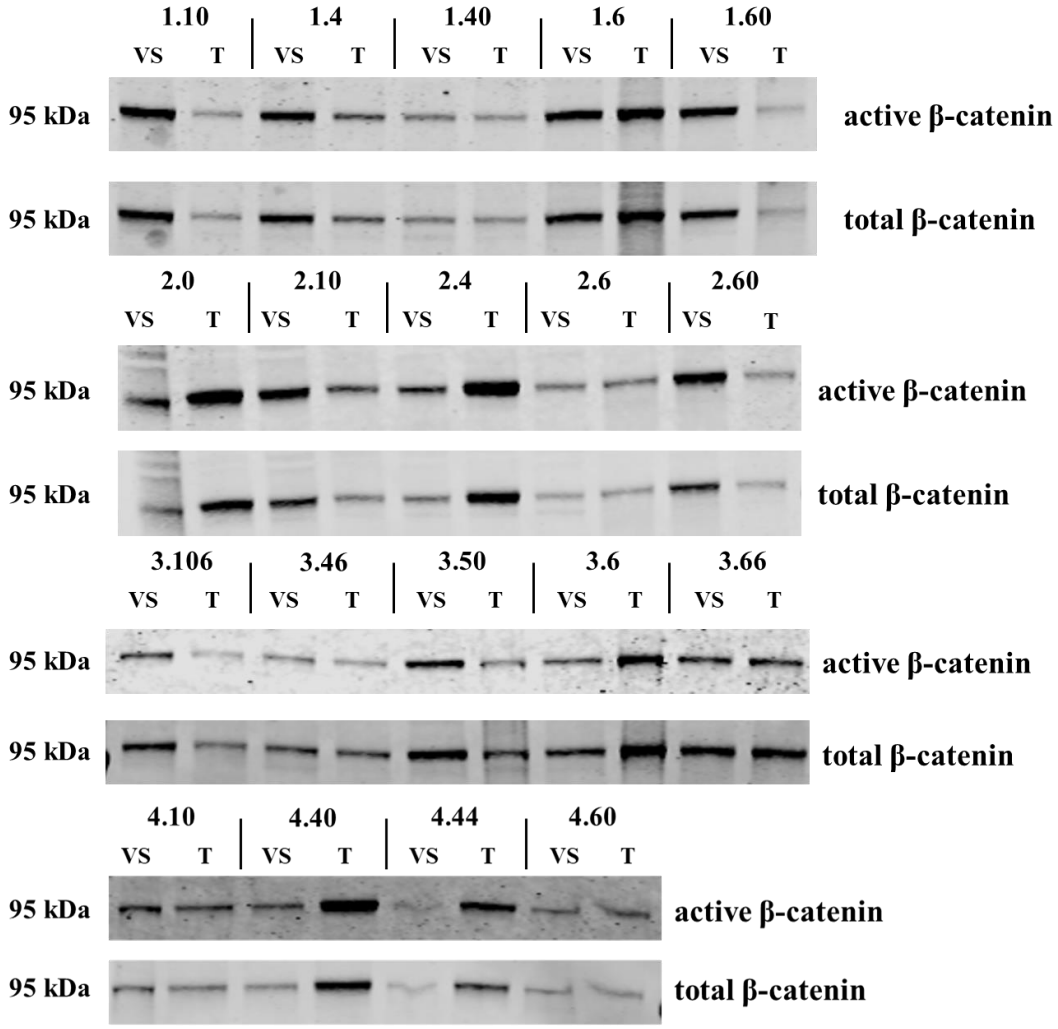

Figure 38: Ratios between active and total β-catenin. Active Wnt/β-catenin signalling would be indicated by an increase in the ratio between active and total β-catenin. The blots were quantified for further analysis

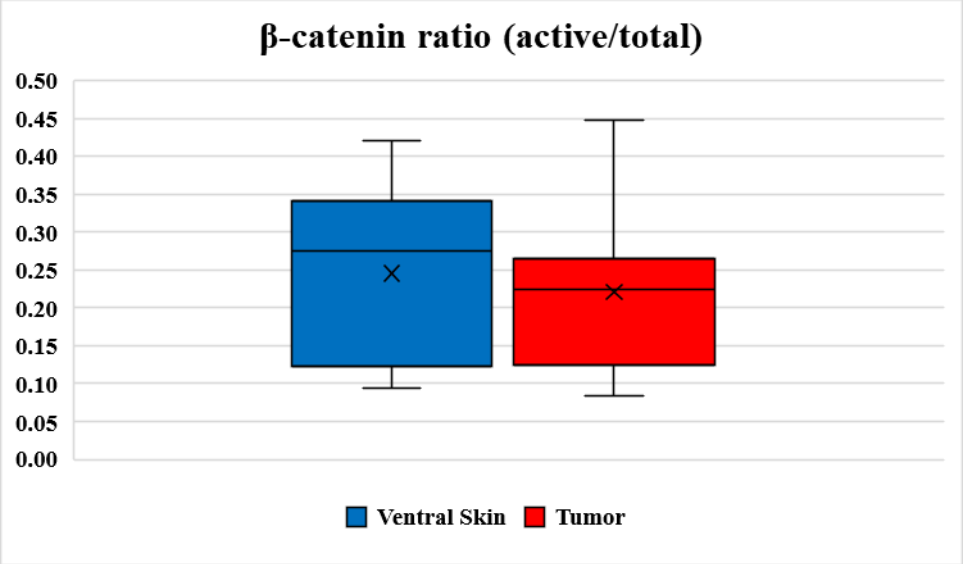

Figure 39: Quantification of the immunoblots shown in Figure 38. The ratio between active and total β-catenin does not differ between VS controls and tumors.

Having previously established, that the Filip1l protein levels are down-regulated in murine cSCC tumors compared to VS controls, we can conclude that, although, as published research suggests, Filip1l may have a role in controlling Wnt/β-catenin signalling in other tumor types, there is no correlation (see **Figure 40**) between active β-catenin and Filip1l protein levels in murine cSCC, suggesting that in this tumor type, Filip1l does not regulate Wnt/β-catenin signalling

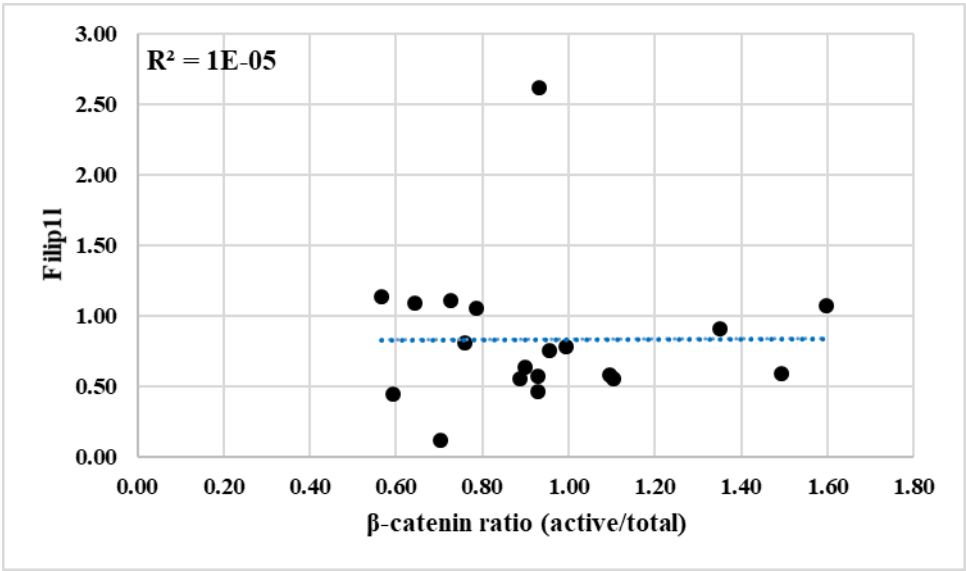

Figure 40: Correlation analysis between Filip1l protein levels and active to total β-catenin ratio. There is no inverse correlation between the tested parameters, suggesting that in murine cSCC tumors, Filip1l does not regulate Wnt-signaling or other factors play a more pivotal role.

3.8 FILIP1L in human cutaneous squamous cell carcinoma

FILIP1L was initially discovered as down-regulated in ovarian cancer 1 (DOC1) and its role in ovarian cancer has been described. To this date, FILIP1L has never been described in a skin context and its role in cSCC is completely unknown. After having established that down-regulation of Filip1l is common in murine cSCC, we aimed to investigate the role of FILIP1L in human cSCC cell lines.

3.8.1 The isoform expression in human cSCC is more complex compared to mouse

While mouse Filip1l has three known isoforms, of which only isoform 202 is expressed in murine skin and tumors, in humans, there are eight known isoforms. Similar to mouse, it is unknown if the different isoforms serve distinct cellular functions. Everything that is known about the function of FILIP1L focuses on isoform 203 and an artificially created truncation mutant lacking 103 amino acids at the C-terminus (FILIP1LΔC103) that is based on isoform 203.

We first wanted to examine the expression levels of the different FILIP1L isoforms in a panel of 15 cSCC cell lines and 3 cultures of primary human keratinocytes. Similar to the experiments carried out in mouse samples (see **Section 3.7.1**), isoform specific qPCR probes were designed in order to distinguish between expression of the eight isoforms. Due to the more complex nature and greater overlap between human compared to mouse isoforms, most probes unfortunately target multiple isoforms. A list of primer target sites can be found in **Table 22**.

Table 22: Primer binding sites for human FILIP1L isoform specific primers.

TARGETED ISOFORMS	BINDING SITE 1	BINDING SITE 2
201, 202, 203, 206, 210	Exon 5	Exon 5
203, 206	alternative TSS 203/206	Exon 5
210	alternative TSS 210	Exon 5
202, 206, 209	Exon 5	Exon 6
204	Exon 4	alternative end 204
209	alternative TSS 209	Exon 5
Exon 5	Exon 5	Exon 5

Figure 41 shows the means of expression of different FILIP1L isoforms in 15 human cSCC cell lines and 3 primary cultures of normal human keratinocytes (NHK). The main detected isoforms are isoforms containing exon 5 (exon 5 probe, isoforms 201, 202, 203, 206, 210), isoforms 203 and 206 (iso 203/206 probe) and isoforms 201 and 203 (iso 201/203 probe). As indicated by the low expression values of their respected probes, isoforms 210 (iso 210 probe), isoforms 202, 206 and 209 (iso 202/206/209 probe), isoform 209 (iso 209 probe) and isoform 204 (iso 204 probe), only show marginal expression in the tested cell lines. As expression of isoform 206 is marginal, we can conclude, that CT values of the iso 203/206 probe are a good approximation of isoform 203 expression.

We therefore can conclude, that FILIP1L isoforms 201 and 203 are the main expressed isoforms in human cSCC cell lines and NHK primary cultures.

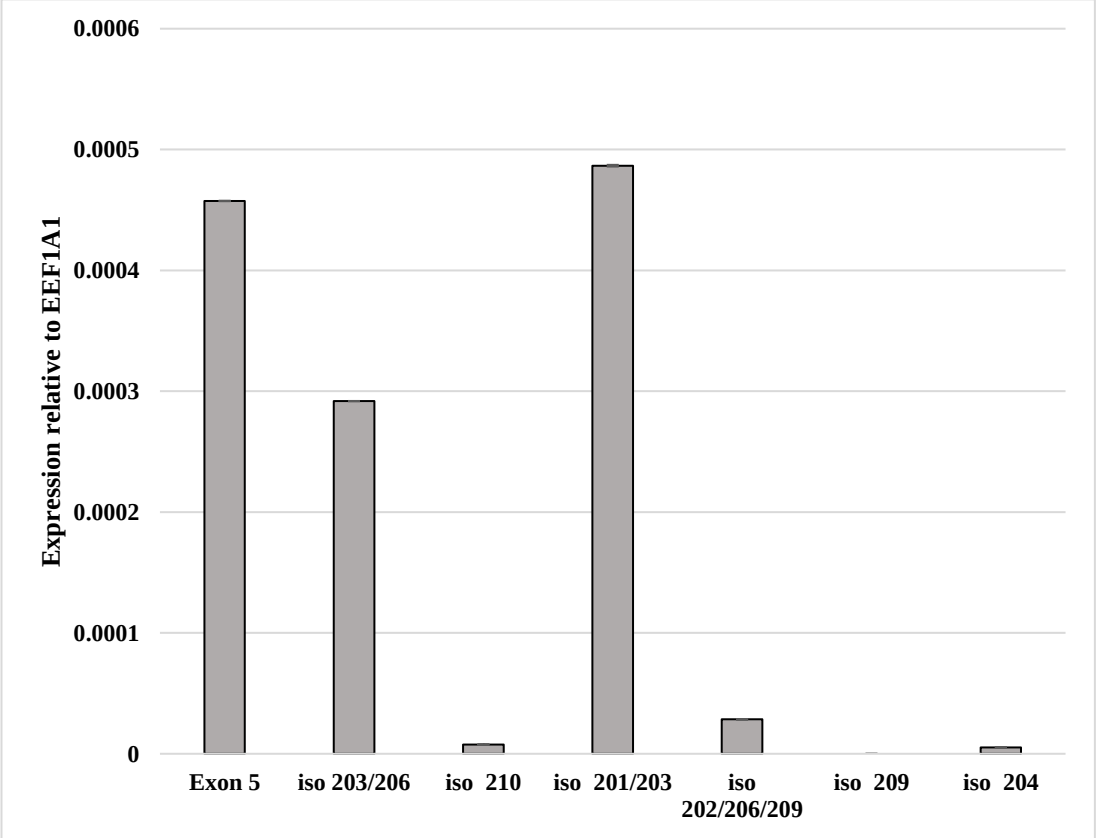

Figure 41: Means of expression of different Filip1l isoforms in 15 human cSCC cell lines and 3 primary cultures of normal human keratinocytes (NHK).Error bars indicate the variance between the different cell lines. Expression of isoforms 210, 202, 206, 209 and 204 are negligible. The main expressed isoforms are isoforms 201 and 203.

Isoform specific qPCR results are displayed in Error! Reference source not found.. In both, normal human keratinocytes (NHK) and all tested cSCC cell lines, FILIP1L isoforms 204 and 209 are expressed at either low or undetectable levels. Isoform 210 is not expressed in most cell lines, but interestingly it is expressed at high levels in IC1 met cells. Isoforms 202, 206 and 209 are expressed at very low levels in NHK cells, but expression is higher in some cSCC cell lines, most notably IC8. As expression for isoform 206 is negligible in most cell lines, probes detecting isoforms 203 and 206, can be considered isoform 203 specific. This isoform, that is most similar to mouse Filip1l isoform 202, accounts for the majority of expressed FILIP1L isoforms. Isoforms 201, 202, 203, 206 and 210 are all amplified by the Exon 5 probe. As we established that isoforms 202 and 206 are lowly expressed, while isoform 210 is only expressed in IC1 met cells, we can conclude, that the majority of the Exon 5 probe amplification comes from isoform 201 and 203.

Having established that isoforms 201 and 203 are the main expressed isoforms in human cSCC cell lines and NHKs, we used the same isoform specific qPCR probes to determine the expression levels of both isoforms and compare expression in cancer cell lines to NHKs. The results are displayed in **Figure 42**. FILIP1L isoform 203 is considered the functional isoform in humans and expression of this isoform is reduced in 9 out of 15 cSCC cell lines compared to NHKs (IC18, IC19, IC, Met1, Met4, PM1, T8, T10 and T11). Conversely, in 6 out of 15 cSCC cell lines. FILIP1L isoform 203 expression is increased compared to NHKs.

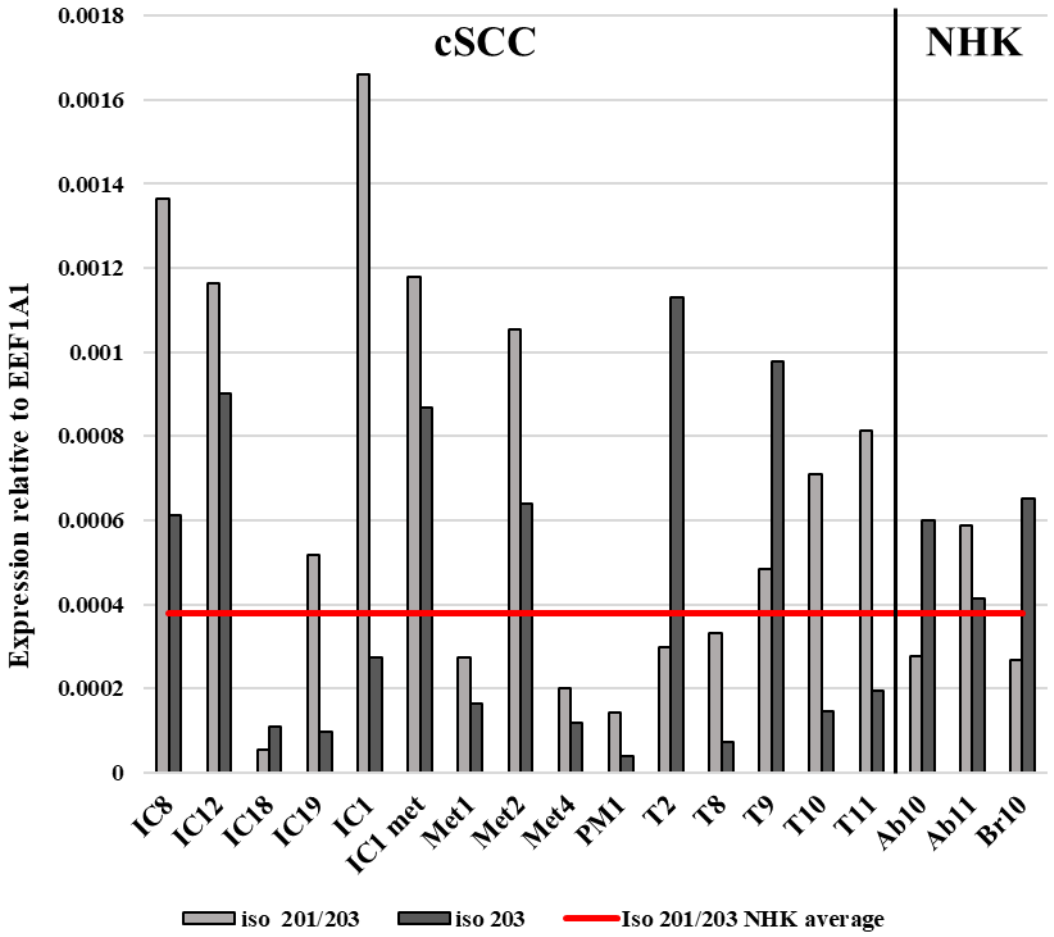

Figure 42: Expression of FILIP1L isoforms 201 and 203 in 15 cSCC cell lines (cSCC) and 3 primary cultures of normal human keratinocytes (NHK). The red line indicates the average expression of isoform 201 and 203 in NHKs. Expression of isoform 203 is reduced in 9 out of 15 and increased in 6 out of 15 human cSCC cell lines compared to NHKs.

To our knowledge, this is the first time the FILIP1L isoform composition has been determined in human cell lines. Interestingly, in NHK and human cSCC cells, isoform 203 is the main expressed isoform alongside isoform 201. It is currently unknown, if the two different isoforms serve different cellular function. We therefore decided to focus on FILIP1L isoform 203, which will be simply referred to as FILIP1L unless indicated otherwise.

3.8.2 FILIP1L protein levels are reduced in some cSCC cell lines

On the mRNA level, FILIP1L expression is reduced in 9 out of 15 human cSCC cell lines compared to NHKs. In order to test if the expression changes translate to a reduction in FILIP1L protein levels, we analysed protein samples from 3 NHK cultures and 11 cSCC cell lines. The results are displayed in **Figure 43**.

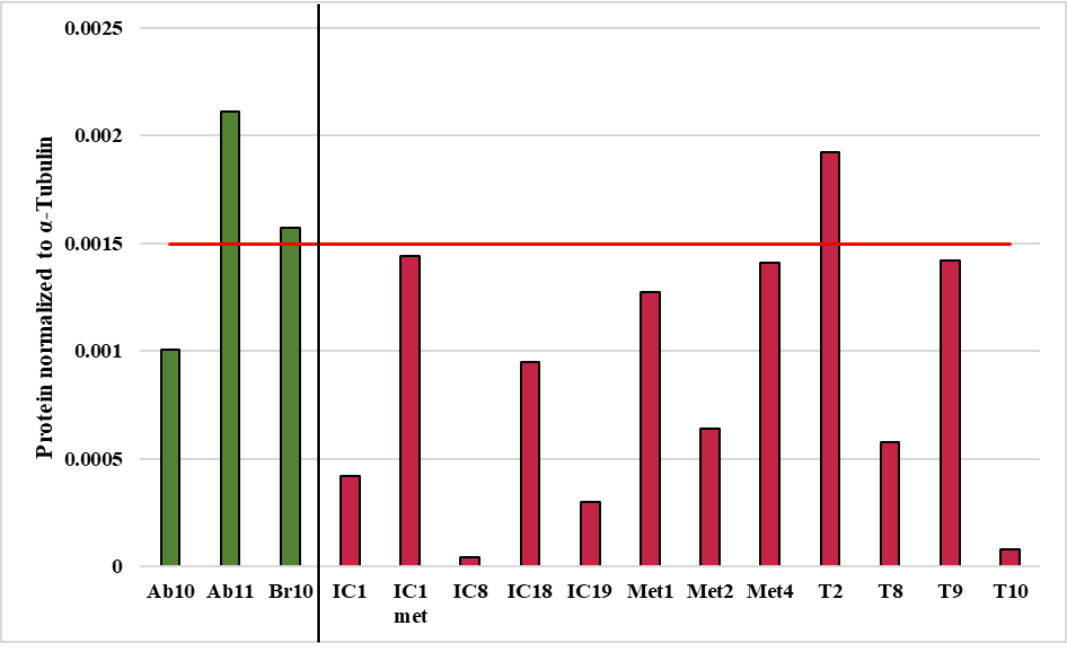

Figure 43: FILIP1L Protein levels in NHK cultures and human cSCC cell lines. The red line indicates the mean FILIP1L protein levels in NHKs. FILIP1L protein levels are reduced in 7 out of 11 cSCC cell lines compared to NHKs. Protein expression levels correlate with mRNA expression data.

When comparing FILIP1L mRNA expression with FILIP1L protein levels, the results do not necessarily correlate. For example, Ab10 shows higher expression than Ab11, yet FILIP1L protein levels are higher in Ab11. Despite that, all cell lines that show decreased FILIP1L expression, also have reduced FILIP1L protein levels (IC1, IC18, IC19, Met1, T8 and T10). Met4 and T9 cells have low FILIP1L expression but show no reduction in protein levels. This suggests, that there could be a post-transcriptional control of FILIP1L protein expression.

Most importantly, FILIP1L protein levels are markedly reduced in 7 out of the 12 cSCC lines tested (IC1, IC8, IC18, IC19, Met2, T8 and T10), suggesting that, similar to murine cSCC, reduced FILIP1L levels are a common feature of human cSCC. Therefore, it is important to investigate the role that FILIP1L plays in human skin and how reduced FILIP1L levels may benefit tumors. This knowledge will broaden our understanding about the complex biology of cSCC and may lead to the development of treatment strategies.

Interestingly, IC1 and IC1 met cells have different levels of FILIP1L protein. The IC1 cell line has been derived from a primary cSCC tumor, while the IC1 met cell lines

comes from a metastasis in the same patient. We choose IC1 and IC1 met cell lines to investigate the function of FILIP1L in human cSCC.

In a parallel study, our lab has found that under standard cell culture conditions, primary human keratinocytes have highly active WNT/β-Catenin-signalling (Daniela Nobre Salvador, PhD thesis). As we suspect that FILIP1L may influence WNT/β-Catenin-signalling, we decided to use the immortalized human keratinocyte cell line NTERT as a control, where WNT/β-Catenin activity is more uniform.

3.8.3 The role of FILIP1L in the immortalized human keratinocyte cell line NTERT

As previously discussed, the majority of available data on FILIP1L suggest a role as a tumor suppressor by aiding destruction of β-Catenin and suppression of WNT/β-Catenin signalling activity (see **Figure 10**).

In order to test, if FILIP1L itself may be a target of WNT/β-Catenin signalling, we utilized the human keratinocyte cell line NTERT. NTERT cells were either untreated, or grown for 2 h, 4 h, 8 h or 24 h in the presence of LiCl. LiCl inhibits glycogen synthase kinase 3 β (GSK 3β) activity and therefore the phosphorylation and subsequent destruction of β-Catenin. As a control, NaCl treatment was used. The results are displayed in **Figure 44**, **Figure 45, Figure 46** and **Figure 47**.

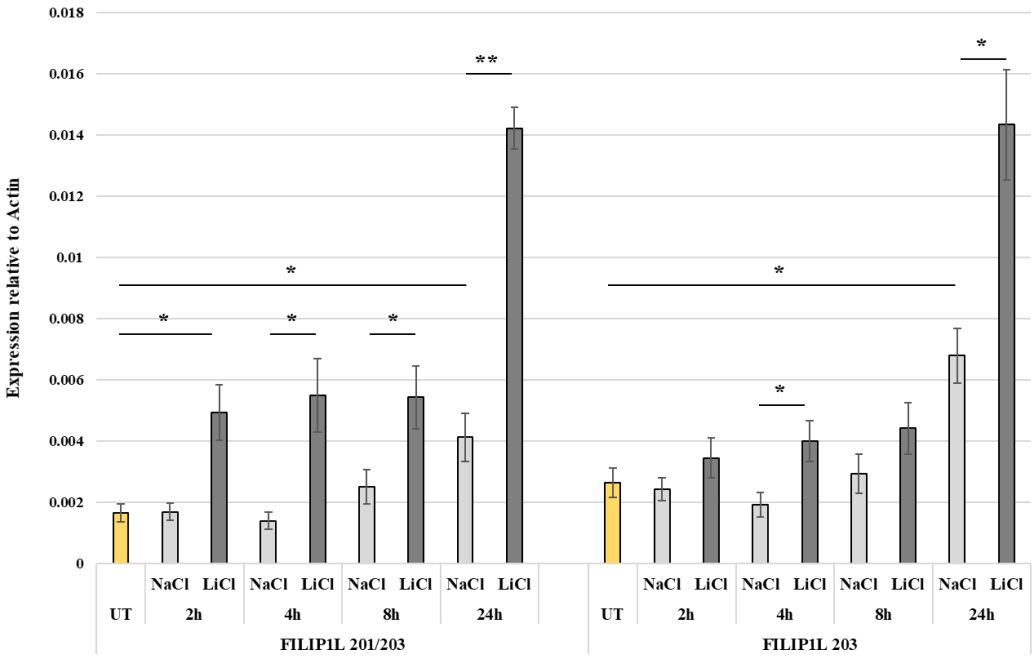

Figure 44: FILIP1L levels in NTERT cells treated with 10 mM LiCl, equal amounts of NaCl or were left untreated. Results represent the quantification results from immunoblots and three biological replicates. UT: Untreated control. LiCl was used to inhibit GSK 3β FILIP1L levels are up-regulated by LiCl treatment after 2 h and are highest after treatment for 24 h. Expression also increases with time, possibly due to a response to increased confluency. Significance is indicated by asterisks (* $p<0.05$, ** $p<0.01$, *** $p<0.001$).

In response to treatment with 10 mM LiCl, FILIP1L expression is significantly up-regulated after 2 h and remains stable at 4 and 8 h timepoints. Expression is highest after 24 h treatment. In NaCl-treated control cells, FILIP1L expression is not significantly altered (except for the 24 h timepoint compared to untreated controls. However, FILIP1L expression increases with time, possibly through increased confluency.

There are few known direct target genes for WNT/β-Catenin activation in skin. We investigated the expression of the WNT/β-Catenin target genes *AXIN2* [262], *CCND1* (Cyclin D1) [263] and *MYC* [264] (**Figure 45, Figure 46** and **Figure 47**). The expression of AXIN2 is increased in NaCl controls after 2 and 4 h but is significantly up-regulated after 8 and 24 h of NaCl treatment in comparison to untreated controls. Upon treatment with LiCl, AXIN2 expression is significantly increased compared to NaCl controls at all time points. Although AXIN2 is a known target gene of the WNT/β-Catenin signalling pathway, we do not have evidence, that this is through this pathway, as other effects of LiCl may play a role.

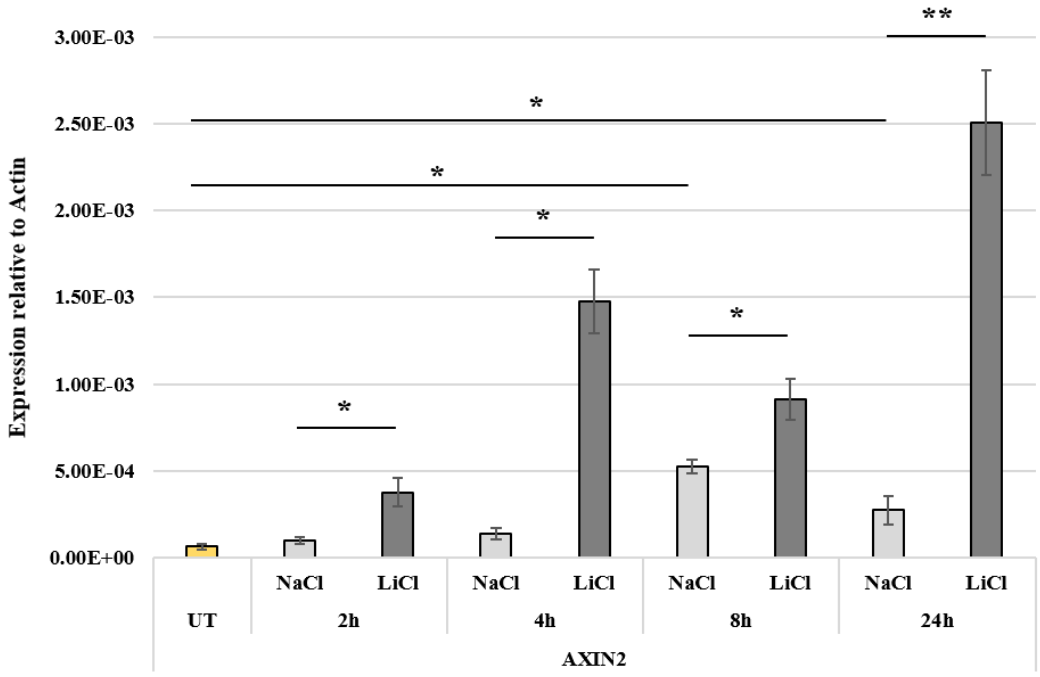

Figure 45: Expression of AXIN2 after stimulation of WNT/β-Catenin signalling with 10 mM LiCl. Results represent the quantification results from immunoblots and three biological replicates. AXIN2 expression is not affected by NaCl controls at 2 and 4 h but is up-regulated after 8 and 24 h compared to untreated controls. Compared to NaCl controls, expression of AXIN2 is significantly up-regulated at all timepoints. This suggests that WNT/β-Catenin activation with LiCl increases AXIN2 expression. Significance is indicated by asterisks (* $p<0.05$, ** $p<0.01$, *** $p<0.001$).

CCND1 (Cyclin D1) is up-regulated upon WNT/β-Catenin activation in various tissues [263]. In NTERT cells, there are no significant changes in CCND1 expression after 2 and 4 h of LiCl or NaCl treatment (**Figure 46**). After 8 and 24 h, CCND1 expression is significantly increased in NaCl controls compared to untreated control. At the 8 and 24 h timepoints, LiCl treatment has no significant effect on CCND1 expression. There is no clear pattern of CCND1 expression changes after treatment with LiCl, suggesting that CCND1 may not be a suitable WNT/β-Catenin reporter gene in NTERT cells or other effects of LiCl overshadow the activation of the *CCND1* gene.

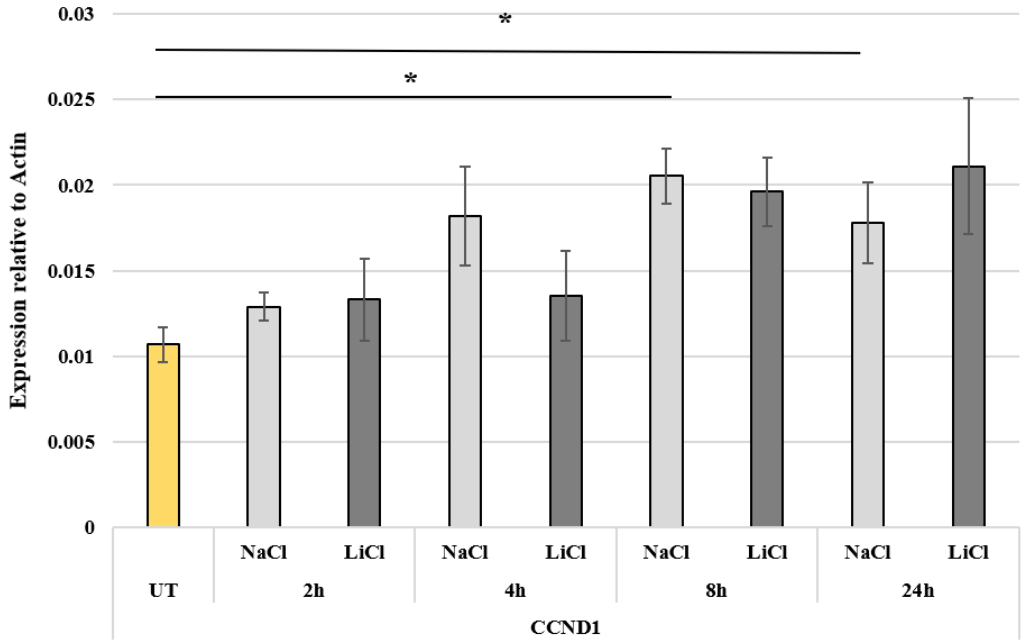

Figure 46: Expression of CCND1 after stimulation of WNT/β-Catenin signalling with 10 mM LiCl. Results represent the quantification results from immunoblots and three biological replicates. There is no clear pattern of CCDN1 expression changes in response to LiCl stimulation. At 2 and 4 h, no significant changes can be observed, but CCDN1 expression is significantly increased in NaCl controls compared to untreated controls after 8 and 24 h. No significant changes between NaCl controls and LiCl treatments were detected. Significance is indicated by asterisks (* $p<0.05$, ** $p<0.01$, *** $p<0.001$).

Similar to CCND1, MYC can be used as a WNT/β-Catenin reporter. While there is an increase in MYC expression at all timepoints in NaCl controls compared to untreated controls, the increase is not significant. LiCl treatment non-significantly reduces MYC expression at 2 h and significantly after 4, 8 and 24 h (**Figure 47**). This suggests, that MYC expression is reduced upon LiCl treatment in NTERT cells.

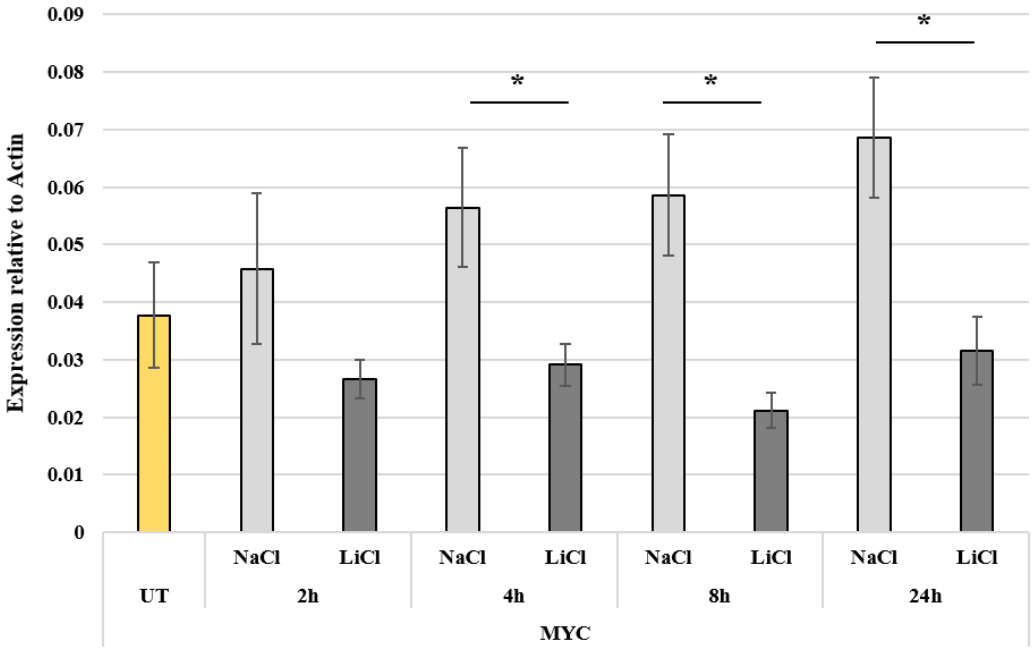

Figure 47: Expression of MYC after stimulation of WNT/β-Catenin signalling with 10 mM LiCl. Results represent the quantification results from immunoblots and three biological replicates. Expression of MYC is not significantly affected in the NaCl controls compared to untreated controls. However, there is a tendency for increased MYC expression at later timepoints. At 4, 8 and 24 h, MYC expression is significantly decreased compared to NaCl controls, suggesting WNT/β-Catenin activation with LiCl reduces MYC expression. Significance is indicated by asterisks (* $p<0.05$, ** $p<0.01$, *** $p<0.001$).

3.8.4 FILIP1L levels do not correlate with markers of WNT/β-Catenin activity

It was interesting to see that the expression of FILIP1L and AXIN2 was increased after treatment with LiCl (**Figure 44**). To investigate, if FILIP1L expression influences the expression of the WNT/β-Catenin signalling target genes *AXIN2* and *MYC*, we performed FILIP1L siRNA knock-down in NTERT cells and examined the AXIN2 and MYC protein levels; the results are displayed in **Figure 48** and **Figure 49**.

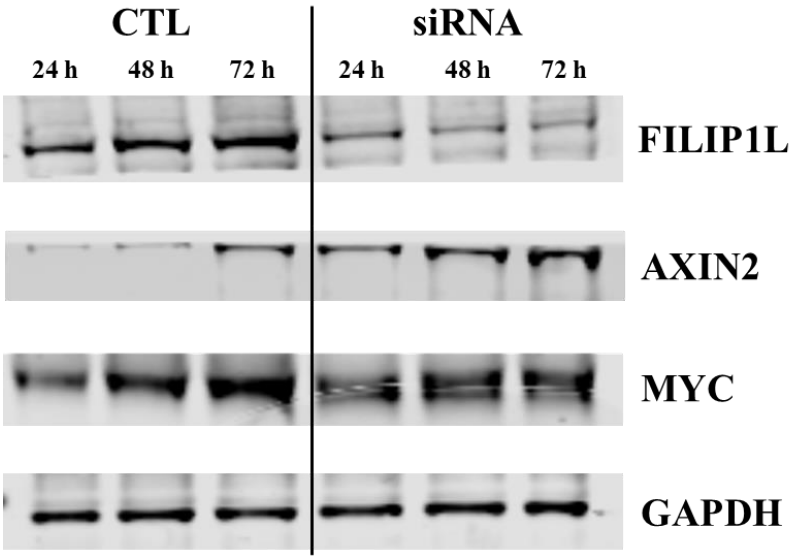

Figure 48: Representative blot of markers of WNT/β-Catenin activity in NTERT cells. FILIP1L siRNA knock-down decrease FILIP1L protein levels at all timepoints. AXIN2 levels increase at all timepoints, while MYC levels appear to be unaffected by FILIP1L knock-down. This suggest, that FILIP1L knock-down activates WNT/β-Catenin signalling in NTERT cells, therefore increasing expression of target genes, such as AXIN2.

Unfortunately, we were unable to achieve a complete knock-down of FILIP1L in NTERT cells. As shown in Figure 32 and **Figure 49 A**, the FILIP1L protein levels are markedly reduced in siRNA-transfected cells compare to scrambled siRNA-transfected control cells (CTL) at 24, 48 and 72 h post-transfection. The reduction is not statistically significant, most likely due to the small sample size and large variations between experiments. The AXIN2 protein levels are increased in siRNA-transfected cell compared to control cells after 24, 48 and 72 h of transfection (see **Figure 49 B**). Similar to FILIP1L results, the increase is not statistically significant. Nonetheless, there is a clear trend in AXIN2 levels increasing when FILIP1l is knocked down and cells are treated with LiCl. MYC protein levels do not change with FILIP1L siRNA knock-down. Western blots for the above mentioned figures can be found in the appendix.

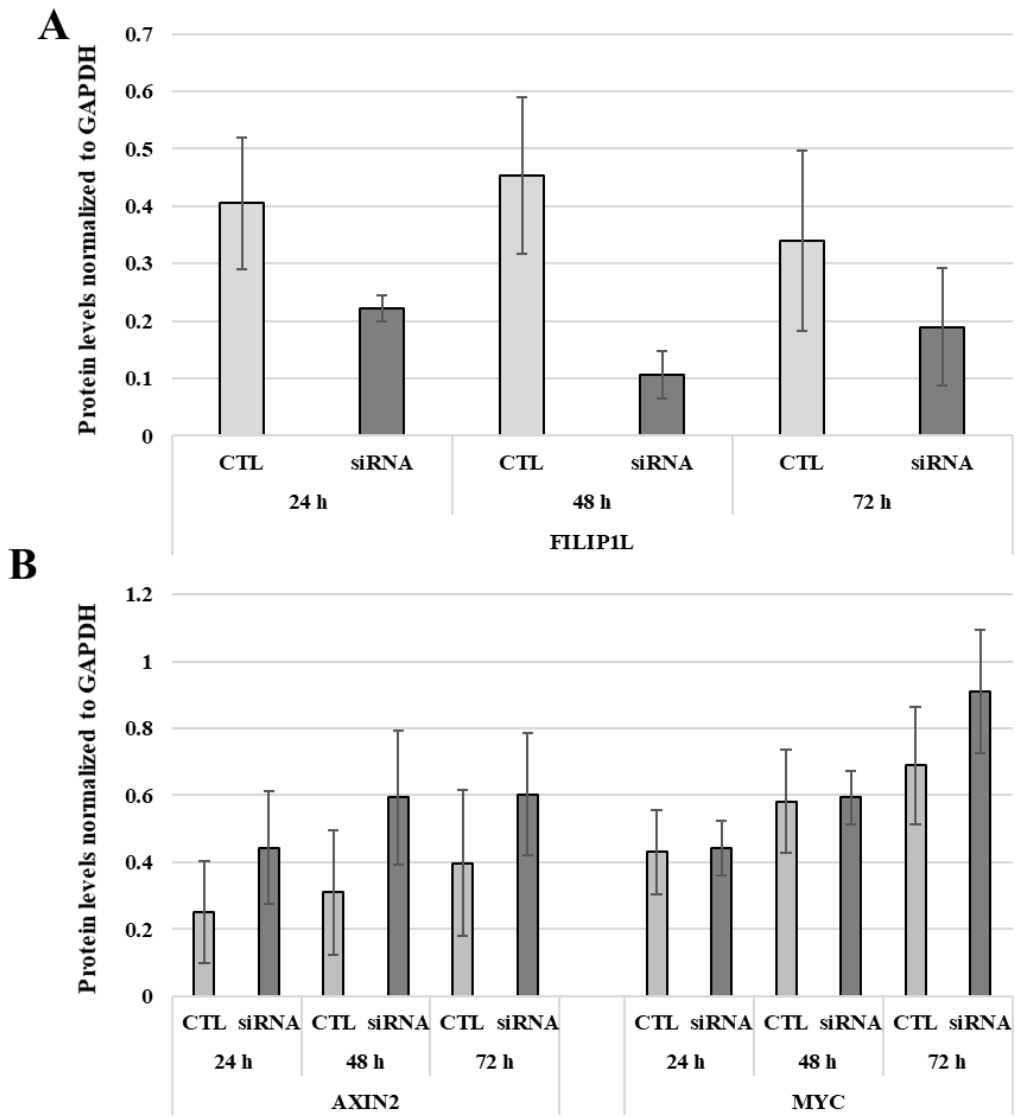

Figure 49: A: FILIP1L protein levels in NTERT cells after transfection with either non-targeting siRNA (CTL) or siRNA pool targeting FILIP1L (siRNA) after 24, 48 and 72 h post transfection. FILIP1L protein levels are reduced in siRNA transfected cells, but reduction is non-significant due to inter experimental variation. **B: AXIN2 and MYC protein levels after transfection with either non-targeting siRNA (CTL) or siRNA pool targeting FILIP1L (siRNA) after 24, 48 and 72 h post transfection.** Contrary to FILIP1L, AXIN2 protein levels increase in siRNA transfected cells. Results represent the quantification results from immunoblots and three biological replicates.

3.8.5 FILIP1L knock-down does not affect nuclear levels of β-Catenin in NTERT cells

As shown in **Figure 49**, siRNA knock-down of FILIP1L induces AXIN2 protein expression in NTERT cells, although this effect was not statistically significant. A more direct approach to access WNT/β-Catenin signalling activity is to determine the

nuclear levels of unphosphorylated β-Catenin, as this is the factor that drives transcription with the help of the co-activators T-Cell Factor (TCF) or lymphoid enhancer factor (LEF). We performed siRNA knock-down of FILIP1L in NTERT cells. The nuclear and cytoplasmic fractions were then separated (as described in **Section 2.7**) and the levels of FILIP1L, unphosphorylated (active) β-Catenin as well as nuclear and cytoplasmic loading controls Histone H3 and α-Tubulin were measured using immunoblotting. The results are displayed in **Figure 50** and **Figure 51**.

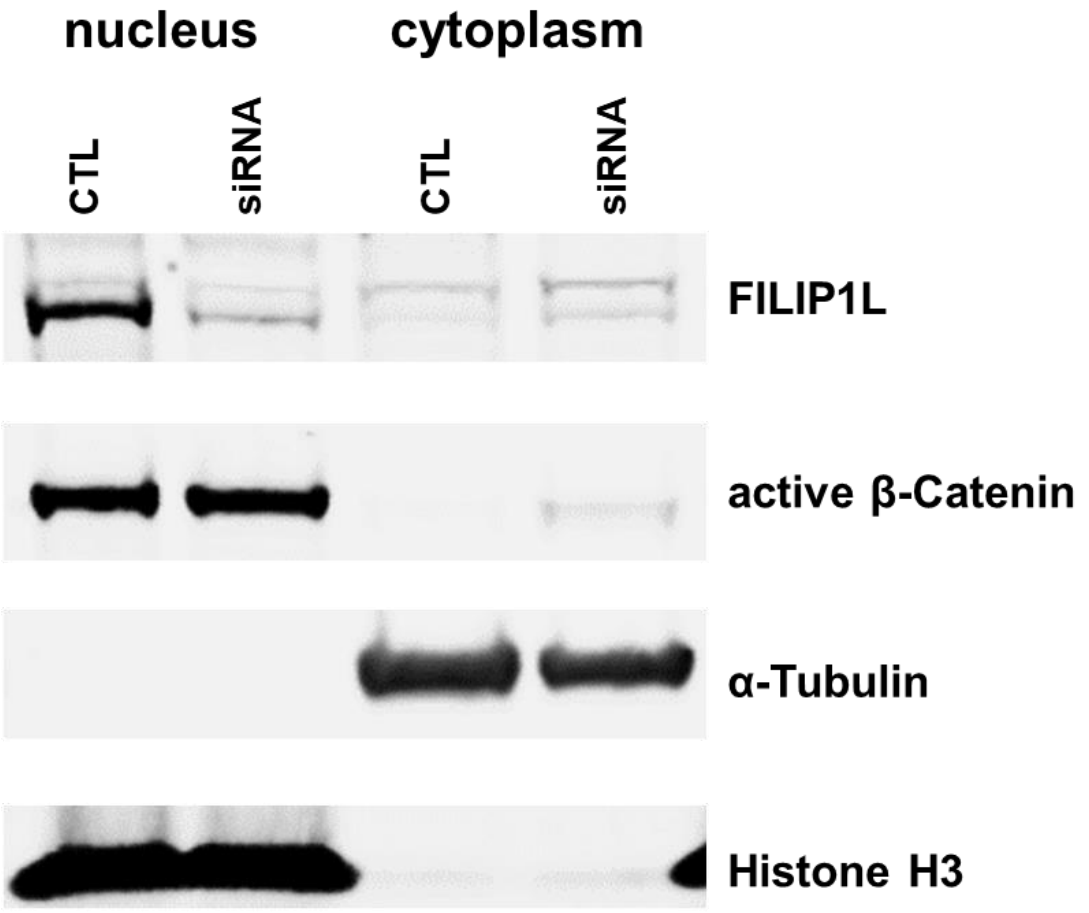

Figure 50: Representative blot of nuclear and cytoplasmic levels of FILIP1L and active β-Catenin. FILIP1L protein is predominantly located in the nucleus. Knock-down of FILIP1L using siRNA reduces nuclear protein levels but has no effect on the cytoplasmic fraction. As FILIP1L, β-Catenin is located in the nucleus. FILIP1L knock-down is slightly increasing nuclear β-Catenin.

The majority of FILIP1L protein is located in the nucleus and significantly reduced in siRNA-treated cells compared to controls, indicating that the siRNA knock-down was successful. In the cytoplasm, FILIP1L levels do not change. As expected, active β-Catenin is almost exclusively located in the nucleus. In other cell origins, such as prostate, ovarian or lung, FILIP1L controls β-Catenin stability by aiding its

destruction. In NTERT cells, FILIP1L knock-down does not significantly increase nuclear β-Catenin levels.

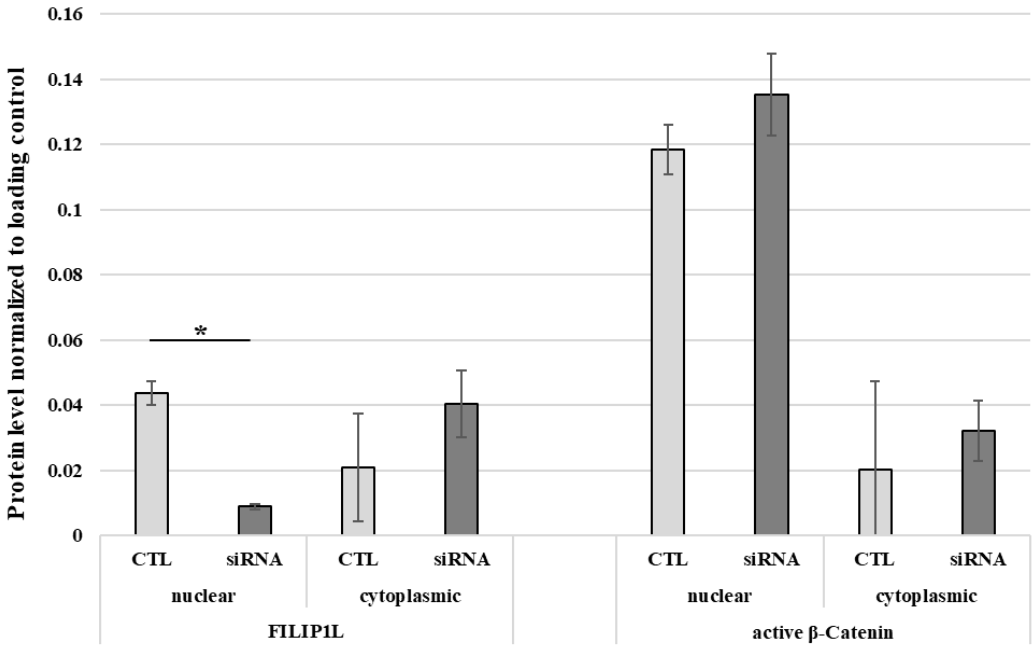

Figure 51: Quantification of blot shown in Figure 50 and independent repetition of the experiment. Results represent the quantification results from immunoblots and three biological replicates. FILIP1L protein levels significantly decrease after transfection with siRNA after 48 h in the nuclear fraction, but there is no effect on cytoplasmic FILIP1L levels. There is a slight increase in nuclear levels of active β-Catenin, but significance was not reached (p=0.1845), suggesting that factors other than FILIP1L are more important in controlling WNT/ β-Catenin signalling in NTERT cells. Significance testing was performed on 3 individual experiments and is indicated by asterisks (* $p<0.05$, ** $p<0.01$, *** $p<0.001$).

3.8.6 Functional significance of FILIP1L in cSCC cells

In order to investigate the functional significance of FILIP1L levels, we decided to knock-down or re-express FILIP1L in IC1 met and IC1 cells respectively. IC1 met cells express FILIP1L at a level similar to NHK cells, while IC1 cells have reduced FILIP1L levels. Both cell lines are derived from the same donor. IC1 represents the primary tumor, while IC1 met cells come from a metastasis.

The coding sequence for FILIP1L isoform 203 was cloned into a standard pcDNA vector under control of a T7 promoter. The identity of the plasmid and the correct sequence and positioning of the FILIP1L insert were confirmed by sequencing with the help of the Tayside Centre for Genomic Analysis. As siRNA knock-down of FILIP1L in NTERT cells using an siRNA pool was only about 50% effective, we used pools of individual siRNAs and additional siRNAs in order to knock-down FILIP1L more efficiently IC1 cell line

3.8.6.1 Overexpression of FILIP1L in IC1 met cells

Expression and protein levels of FILIP1L are reduced in the human cSCC cell line IC1 compared to NTERT cells and normal human keratinocytes (see **Figure 43**). Using the protocol described in **Section 2.6.7**, we aimed to over-express FILIP1L in IC1 cells. The results are displayed in **Figure 52**. Untreated (UT) IC1 cells have low FILIP1L levels. However, there is a significant 3-fold increase in FILIP1L protein expression after transfection, even in empty vector (EV) controls. Transfection for 48 h with vector containing FILIP1L significantly increases FILIP1L protein compared to EV, with expression being highest when using 2 µg plasmid. Expression does not differ between empty vector controls and FILIP1L containing plasmid after 72 h of transfection. However, FILIP1L protein levels are significantly higher compared to untreated control. This suggests, that the transfection procedure by itself induces FILIP1L expression. Although FILIP1L levels are further and significantly increased when transfection is carried out with FILIP1L expression vector, the increase in EV controls disqualifies overexpression of FILIP1L in IC1 cells from further investigating the functional significance of FILIP1L in this cell line. Additional means of IC1 transfection were tested, however neither resulted in a sufficient transfection efficiency while also not causing increased expression of FILIP1L in negative controls (data not shown).

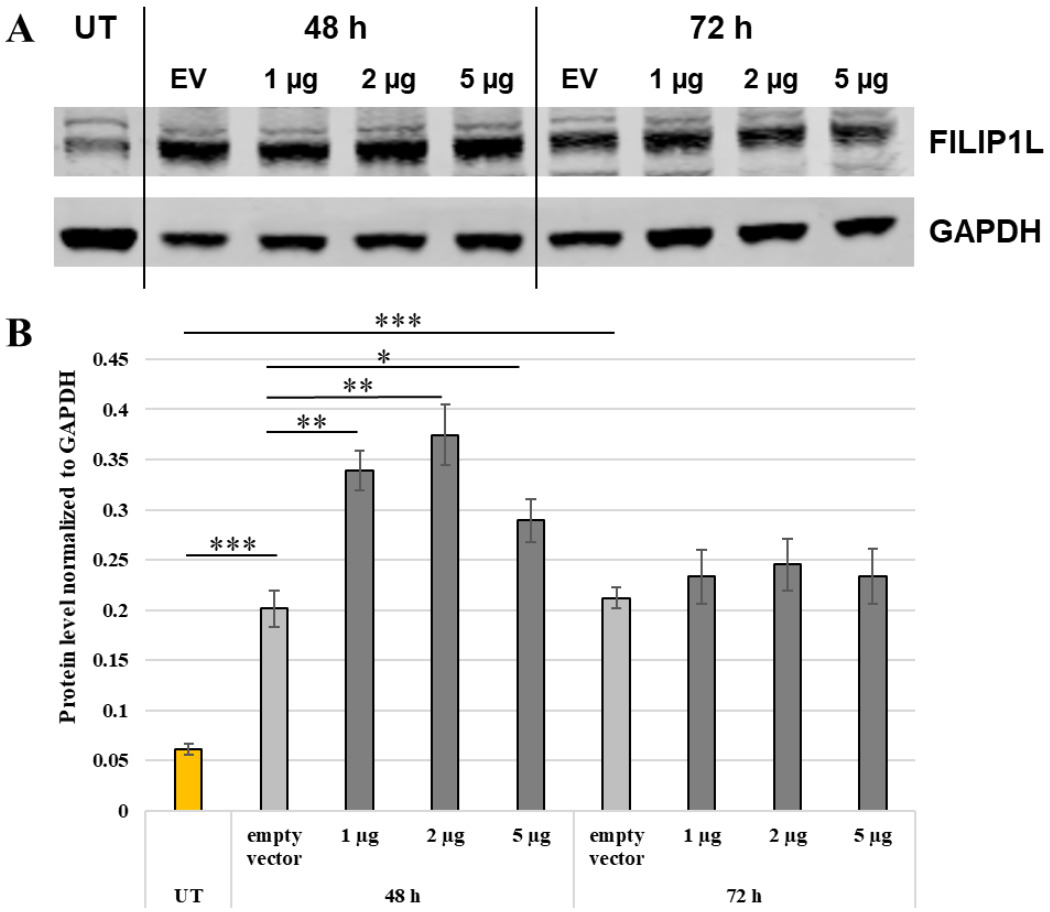

Figure 52: A: Representative blot of FILIP1L overexpression in IC1 cells. FILIP1L protein levels are increased in empty vector (EV) controls compared to untreated (UT) control after 48 h. In cells transfected with FILIP1L expression vector, FILIP1L levels further increase at the 48 h timepoint. After 72 h, FILIP1L is increased in EV controls compared to UT controls, but there is no further increase in cells transfected with FILIP1L expression vector. **B: Quantification of FILIP1L overexpression experiments (three biological replicates).** Compared to UT controls, FILIP1L levels are significantly higher in EV controls after both, 48 and 72 h, suggesting that the transfection procedure alone induces FILIP1L expression. Although FILIP1L protein levels significantly increase in cells transfected with FILIP1L expression vector after 48 h, the protocol is not suitable to investigate the functional significance of FILIP1L in IC1 cells. Significance is indicated by asterisks (* $p<0.05$, ** $p<0.01$, *** $p<0.001$).

3.8.6.2 siRNA knock-down of FILIP1L in IC1 met cells

The expression and protein levels of FILIP1L in IC1 met cells are comparable to NTERT cells and normal human keratinocytes (see **Figure 43**). FILIP1L was knocked-down in IC1 met cells using siRNA, as described in **Section 2.6.6**. The results are shown in **Figure 53**. FIIP1L siRNA knockdown in IC1 met cells is successful, using either siRNA 1 or a combination of siRNAs 2 and 3 from the smart

pool. Similar to IC1 cells, treatment with transfection agents up-regulates FILIP1L expression (data not shown) in IC1 met cells, suggesting, that FILIP1L expression could be a response to agents that weaken cell membranes. Nevertheless, siRNA knock-down is sufficient to compensate for the effect.

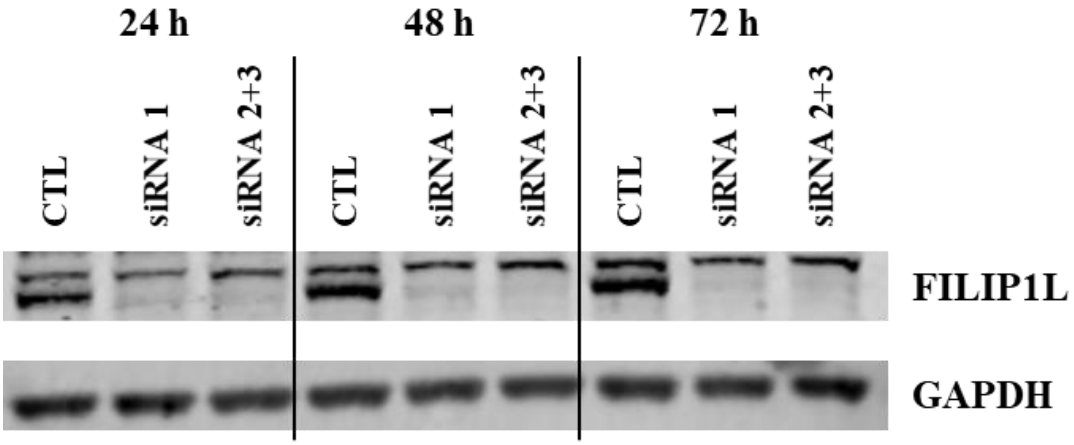

Figure 53: FILIP1L siRNA knock-down in IC1 met cells. FILIP1L protein levels are markedly reduced in FILIP1L targeting siRNA transfected cells compare to non-targeting control (CTL).

Having established a working protocol to knock-down FILIP1L in IC1 met cells, we tested if FILIP1L knock-down in this cell line affects the levels of active and total β-catenin and therefore WNT/β-catenin signalling activity. The results are displayed in **Figure 54**.

FILIP1L protein levels are significantly reduced in IC1 met cells after 48 and 72 h of transfection with targeting siRNA compared to non-targeting controls (CTL). The knock down efficiency was ~90% and therefore considerably higher than in NTERT cells (~50%).

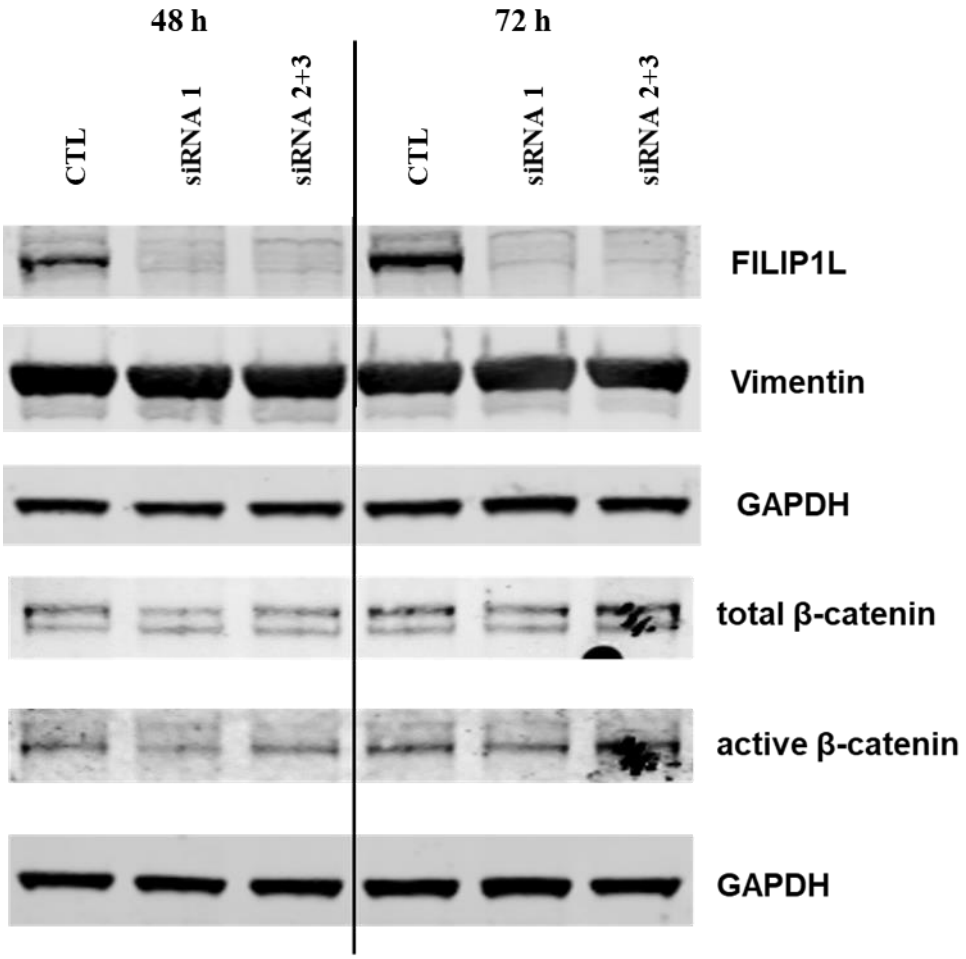

Figure 54: Representative blot of FILIP1L, Vimentin as well as total and active β-catenin in IC1 met cell, transfected with siRNA targeting FILIP1L. FILIP1L knock-down was successful. The high levels of **Vimentin** confer that the tested cells are IC1 met cells and not feeder fibroblasts. The change in **total** and **active β-catenin** appear to very little.

Total β-catenin levels do not change after 48 h of FILIP1L knockdown compared to controls (CTL). However, after 72 h, there is a significant decrease in total β-catenin levels. Interestingly, the decrease is more pronounced in IC1 cells transfected with siRNA 1 although FILIP1L levels are lower in cells transfected with siRNAs 2 and 3, suggesting there is no direct correlation between FILIP1L and total levels of β-catenin. In contrast to total β-catenin, active β-catenin levels are significantly reduced in IC1 met cells after 48 h of FILIP1L siRNA knock-down. This is the opposite of what we would expect if FILIP1L would negatively regulate WNT/β-catenin signalling. After 72 h of FILIP1L knock-down, while total β-catenin levels are significantly reduced, active β-catenin levels significantly increase. There is no clear pattern of the interaction between FILIP1L and levels of active β-catenin.

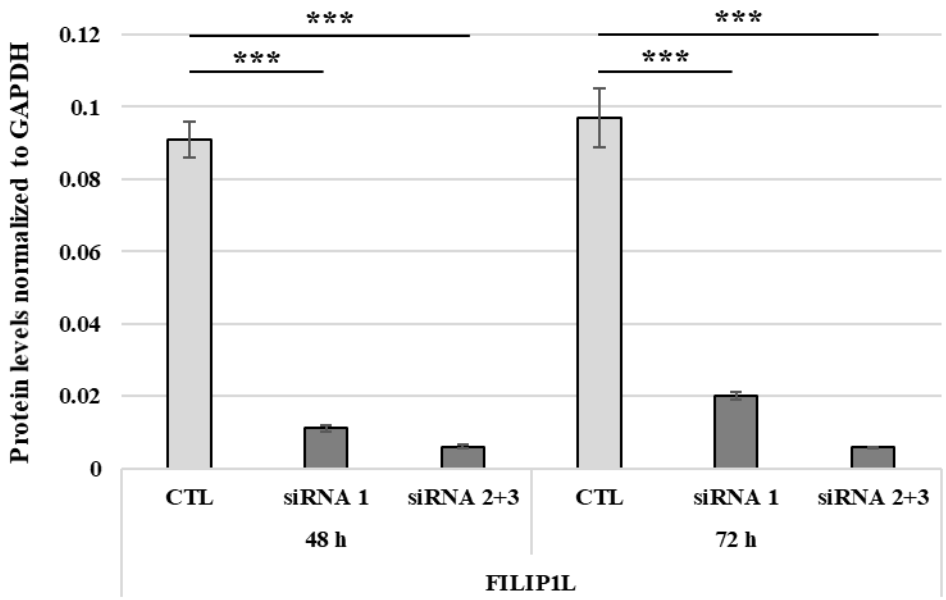

Figure 55: Quantification of FILIP1L protein levels in IC1 met cells after knock-down of FILIP1L after 48 and 72 h. Results represent the quantification results from immunoblots and three biological replicates. FILIP1L protein levels are significantly reduced after 48 and 72 h. Significance is indicated by asterisks (* $p<0.05$, ** $p<0.01$, *** $p<0.001$).

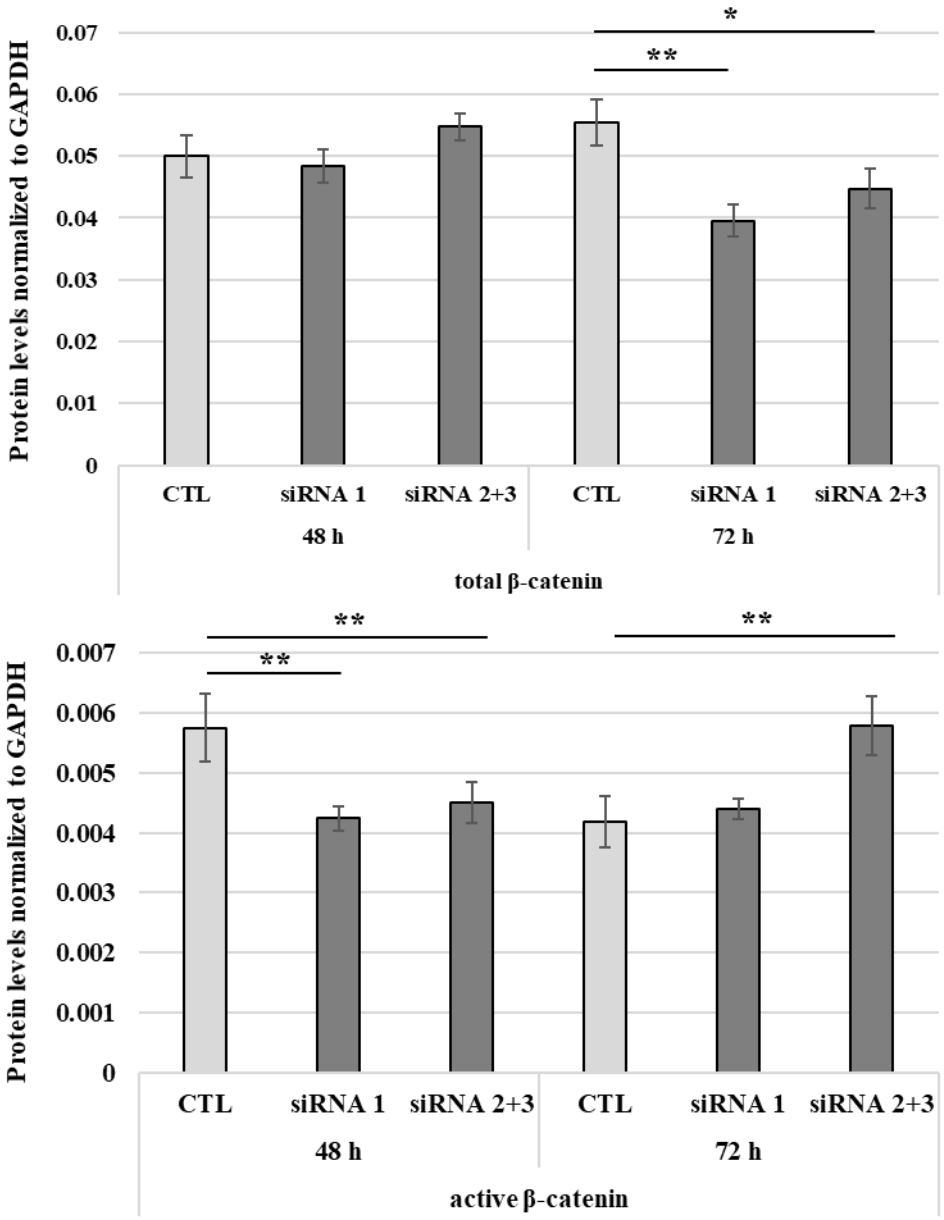

Figure 56: Quantification of total and active β-catenin in IC1 met cells transfected with siRNA targeting FILIP1L or non-targeting siRNA control (CTL). Results represent the quantification results from immunoblots and three biological replicates. Total β-catenin levels do not significantly change after 48 h of siRNA treatment. However, total β-catenin levels are significantly lower after 72 h of FILIP1L knock-down. In contrast to total β-catenin, active β-catenin levels significantly decrease after 48 h of FILIP1L knock-down. This is the opposite of what is expected, if FILIP1L would negatively regulate WNT/ β-catenin in IC1 met cells. However, active β-catenin levels significantly increase after 72 h of FILIP1L knock-down. There is no clear pattern how or if FILIP1L is influencing total and active β-catenin levels in IC1 met cells. Significance is indicated by asterisks (* $p<0.05$, ** $p<0.01$, *** $p<0.001$).

Next, we investigated if FILIP1L knock-down has an effect on the behaviour of the cells. IC1 met cells were plated into 6 well plates at $5*10^5$ cells/well and reverse transfected with either siRNA targeting FILIP1L, non-targeting control siRNA or were left untreated. The efficacy of FILIP1L knockdown was ensured in control experiment, using the same transfection mix as used in the proliferation experiment. Cell confluency was then measured over the course of 96 h using the IncuCyte (Satorius) imaging system as described in **Section 2.6.9**. The results are displayed in **Figure 57**.

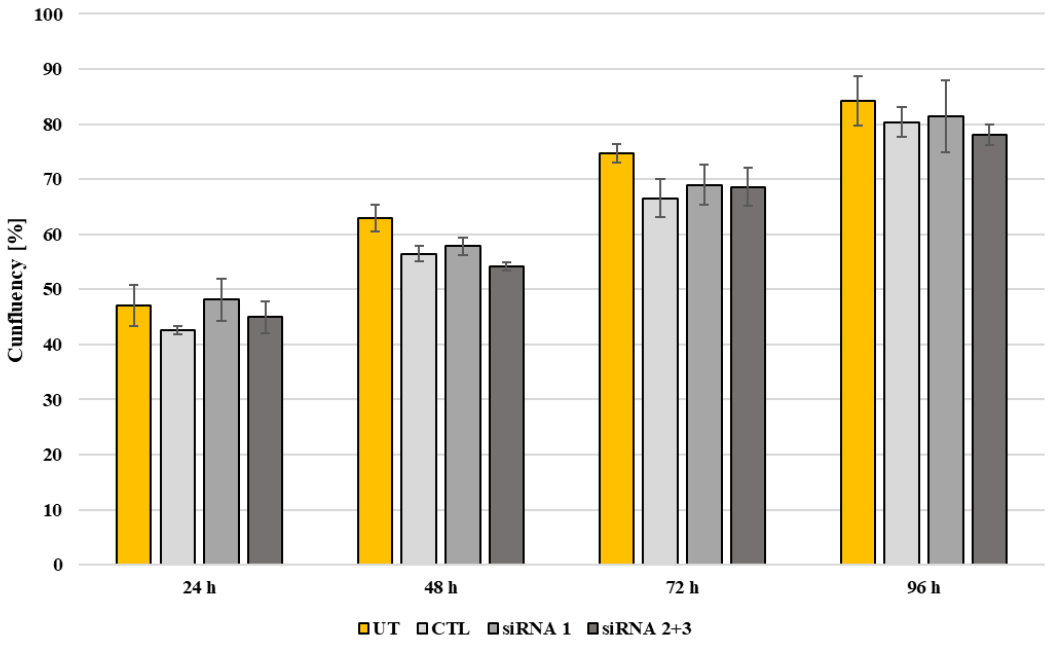

Figure 57: Measurement of confluency of IC1 met cells transfected with non-targeting siRNA (CTL) of siRNA targeting FILIP1L (siRNA 1 and 2+3) of untreated (UT) cells as a measurement of cell proliferation. Results represent the means and standard deviations from three biological replicates. No difference in confluency between FILIP1L knock-down and controls was observed. Untreated cells tended to have a higher confluency, but the effect was not significant.

Untreated IC1 met cells show similar percentages of confluency compared to non-targeting siRNA controls (CTL). Overall, the confluency did not significantly differ among any of the treatments. This suggests, that FILIP1L knock-down has no effect on IC1 met cells proliferation.

We next assessed the viability of IC1 met cells after FILIP1L knock-down using Alamar Blue reagent. The results are displayed in **Figure 58**.

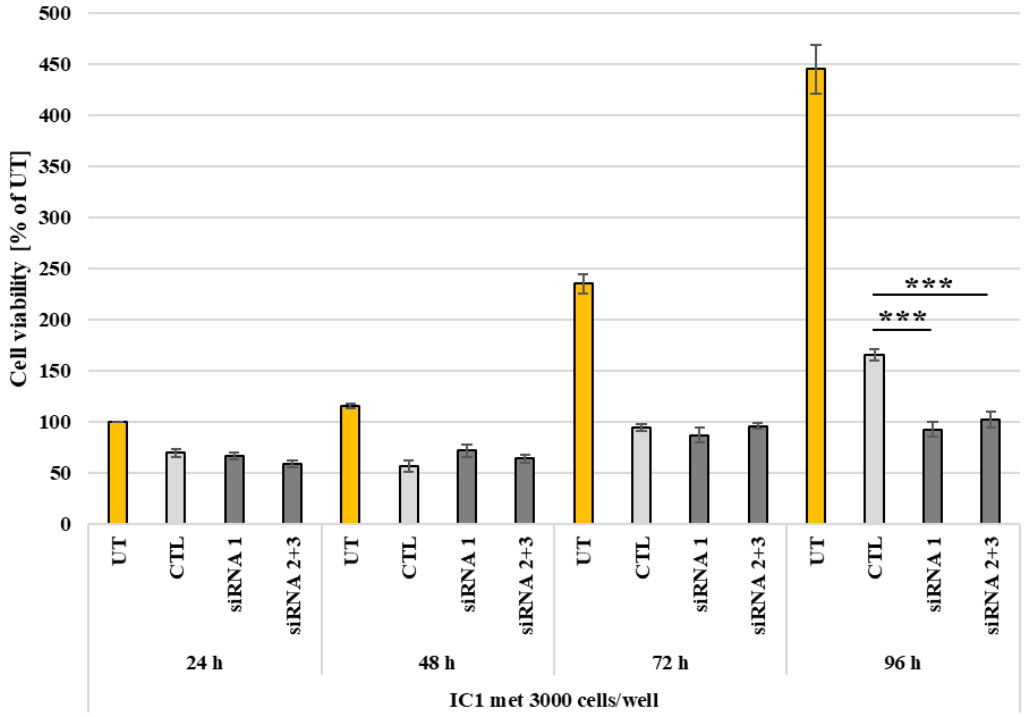

Figure 58: Cell viability of IC1 met cells after 24, 48, 72 and 92 h of siRNA mediated FILIP1L knock-down. Results represent the means and standard deviations from three biological replicates. Cell viability is reduced in transfected cells compared to untreated (UT) cells. FILIP1L knock-down does not affect cell viability after 24, 48 and 72 h compared to non-targeting controls (CTL). However, IC1 met viability is significantly lower in FILIP1L knock-down cells compared to CTL after 96 h. Significance is indicated by asterisks (* $p<0.05$, ** $p<0.01$, *** $p<0.001$).

In contrast to proliferation, as measured by cell confluency (see **Figure 57**), cell viability is significantly reduced in IC1 met cells transfected with siRNA, regardless of the FILIP1L expression status. Cell viability is not affected by FILIP1L knock-down after 24, 48 and 72 h. However, cell viability significantly decreases in FILIP1L knock-down cells after 96 h of siRNA knock-down, although the effect is smaller in comparison to the much more pronounced decrease in cell viability between untreated and siRNA treated cells.

Taken together, FILIP1L knock-down has no clear effect on WNT/ β-catenin signaling in IC1 met cells and no effect on proliferation as measured by confluency. There was no effect on IC1 met viability after 24, 48 and 72 h of FILIP1L knock-down. However, a significant reduction of cell viability was observed after 96 h of knock-down, but this effect was small in comparison to the reduction observed between untreated and siRNA (targeting and non-targeting) transfected cells.

4 Discussion

4.1 DNA methylation in solar simulated UV induced cSCC

The first goal of the work presented in this thesis was to characterize the methylome of murine cSCC tumors, generated by chronic exposure to solar simulated UV radiation.

There were frequent mutations in *Tet* genes that facilitate DNA demethylation. This led us to hypothesise, that there could be changes in the distribution of 5hmC. Therefore, we chose oxidative RRBS, a methodology that allows for analysis of both 5mC and 5hmC. Unfortunately, during analysis of the oxRRBS data it became clear, that the amount of detected 5hmC was not sufficient to distinguish it from data noise. Therefore, we cannot draw any conclusions if mutations in the *Tet* genes have an effect on the methylation landscape of mouse ssUV cSCC. Recently, in addition to being a by-product DNA demethylation by TET proteins, 5hmC has been shown to regulate many cellular and developmental processes (e.g. pluripotency of stem cells and tumorigenesis, summarized in [265]). The high turnover of skin cells and therefore quick passive removal of 5hmC may be the reason we only detected very low amounts of 5hmC. It would be interesting to see how 5hmC levels change in response to the mutations in *Tet* genes in skin. This would require creating e.g. Kera308 cell lines with inducible CRISPR and sgRNAs targeting the *Tet* genes and monitor the changes with oxRRBS or pull-down of 5hmC rich DNA using 5hmC antibodies with subsequent sequencing. Additionally, the global changes in 5hmC content could be measured using a 5hmC ELISA assay.

It has been suggested, that UVR leads to an increase in global DNA methylation in both irradiated mouse skin as well as cell lines. Because the used methodology (RRBS) induces bias as the method enriches for regions of medium to high CpG density and excludes large parts of the genome (e.g. open sea regions with low CpG density), analysis of the global content of 5mC was not possible. Analysis of the subfraction of the genome covered by our method, we found that methylation was significantly higher in tumors, consistent with previously published data. Unfortunately, a colorimetric ELISA assay to determine the global levels of 5mC in mouse ssUV cSCC failed to produce reliable data (data not shown).

Analysis of genomic features, such as TSS activity, transcription factor binding sites and CAGE seq, at differentially methylated regions revealed that most DMRs colocalize with regions of potential regulatory function. This suggests that the methylation changes in mouse ssUV cSCC are important for cancer development or progression. In cSCC, most mutations do not occur within oncogenes, but within tumor suppressor genes. Our findings highlight, that in addition to mutations, changes in DNA methylation could have a crucial role in silencing of tumor suppressor genes in cSCC. This is supported by the significant increase in average methylation in the murine tumors. RRBS enriches for CGI and most CGIs (especially at promoter regions) are unmethylated in normal cells. It is possible that the increase in average methylation across the analysed CGIs could indicate that the corresponding genes are silenced via DNA methylation. The importance of silencing of tumor suppressor genes is critical when considering potential therapeutic approaches. Oncogenes often have similar functions across all tissues of the body. For example, receptor tyrosine kinases are cell surface proteins that sense growth stimulating signals in many cell types. By contrast, tumor suppressor genes often have cell-specific roles and may be better candidates for treatment, especially in cSCC where many tumor suppressors are involved in cancer progression.

Although we show that DMRs often can be found at regions of potential regulatory function, we did not actually investigate if the regions have indeed regulatory function. Unrevealing the function of differentially methylated regions can be challenging. We do not have sufficient understanding how cells ‘decide’ which CGIs they methylate, and which regulatory elements should be silenced by DNA methylation. In the past, investigating the function of distinct DMRs involved treating cells with drugs that inhibit DNA methyl transferases (DNMT), such as 5- azacytidine, that result in DNA demethylation on a genome wide scale and then accessing expression changes of the gene of interest (or transcriptome analysis). However, reducing DNA methylation using DNMT inhibitors leads to demethylation of a multitude of regulatory elements and activation of normally silenced transcription start sites and therefore does not allow for functional assessment of a single region. Furthermore, DNA methylation in cell lines tends to be rather stable at certain regions. More recently, methods have been developed to modulate DNA methylation in a targeted manner. The most promising is using the CRISPR-Cas9 system. By fusing a dead Cas9 enzyme with DNMT or

TET enzymes, it is possible to methylate or demethylate DNA at a specific locus. However, this technology has not been extensively used and it is unsuitable to change methylation at larger regions. It would be interesting to change methylation at selected regions of proposed regulatory function, especially the Filip1l locus, and observe the effects on gene expression. This would allow us to further elucidate the role of DNA methylation changes in cSCC.

A second goal of this work was to compare methylation in the ssUV cSCC with methylation in human cSCC. We compared general features of the human and mouse cSCC methylome such as average/global methylation. While initially we did not find a difference in global methylation between normal and neoplastic human skin, when we grouped the data by Rodriguez-Paredes *et al.* into control, keratinocyte like and stem cell like, global methylation was significantly higher in the stem cell like samples. The RRBS method we used does not cover the whole genome, therefore we were not able to draw conclusions on genome wide DNA methylation levels. The Infinium 850K array, used by Rodriguez-Paredes *et al.,* covers a much larger portion of the genome and our analysis of the data found a significant increase in global DNA methylation in stem cell like cSCCs. We have performed an assay to determine the global DNA methylation levels in the murine ssUV cSCCs and controls, the human cSCC cell line panel and NHKs as well as human cSCCs and normal skin. Unfortunately, this assay did not produce reliable data. Repeating the experiment or using an equivalent assay, will be crucial to validate if global methylation levels increase in murine ssUV cSCC, as suggested by the RRBS analysis, and allow further comparison of the mouse ssUV cSCC model to human cSCCs.

One of the most important findings by Rodriguez-Paredes *et al.* was the identification of two sub-types of human AK and cSCC, one keratinocyte like and one stem cell like. The differentiation was mainly made by analysing the methylation at the keratin gene cluster. Unfortunately, the mouse keratin genes were not sufficiently covered by RRBS in our dataset. It would be very interesting, if these two subclasses also exist in mouse ssUV cSCC. Investigating this would probably include targeted bisulfite sequencing of the mouse keratin clusters. Furthermore, including more tumor samples as well as chronically irradiated AK-like mouse skin would be crucial. This could further validate the ssUV cSCC model.

The differences in the method used by Rodriguez-Paredes *et al.* and us to investigate DNA methylation make it difficult to directly compare methylation at specific regions. We chose to compare the genes in both datasets, that either contain at least one significantly differentially methylated probe (Rodriguez-Paredes *et al.*) and at least one significantly methylated CpG (oxRRBS). In our data, these criteria were met by 214 genes, 153 of the genes had a human ortholog. A staggering 150 of those genes (98%) were also differentially methylated in human cSCC. The remarkable similarities in the methylomes of human and ssUV cSCC suggest that the ssUV cSCC model, in addition to histopathology and genetics, is similar to human cSCC on the DNA methylation level and may be advantageous over other preclinical models. It would be interesting, to analyse the ssUV cSCC in more detail, for example by using WGBS instead of RRBS. This would allow for a more detailed comparison of the ssUV cSCC methylome to the human cSCC methylome. Rodriguez-Paredes *et al.* used the Infinium 850k array and ideally, the same methodology should be used in order to allow for the best possible comparison. Unfortunately, the Infinium arrays are designed for humans and usage for murine samples is limited.

4.2 Filamin A interacting protein 1 like

The top hit in our CpG and DMR analyses was an intronic region of the *Filip1l* gene. *Filip1l* is an interesting new tumor suppressor gene that has never been investigated in skin. In mice, the *Filip1l* gene encodes for 3 isoforms.

Unfortunately, we were not able to validate the *Filip1l* intronic methylation in an independent sample set using MassARRAY because we were not able to amplify the region with sufficient quality. Design of new primers, possibly at the minus strand, could solve the amplification problems. However, MassARRAY revealed, that although in human, methylation at the *FILIP1L* promoter CGI controls FILIP1L expression, the promoter is virtually unmethylated in mouse control skin as well as tumors.

For the first time, we have shown that Filip1l isoform 202 is the main expressed isoform in the murine skin. Remarkably, Filip1l isoform 202 is very similar (91% identity) to human isoform 203, the functional isoform in humans. Our first efforts to compare Filip1l expression in murine skin and cSCC tumors by qPCR was not successful due to problems with finding a suitable reference gene. However, the

analysis of the Filip1l protein levels by immunoblotting revealed that the protein is significantly down-regulated in murine cSCC tumors compared to VS control tissue. The function of Filip1l is incompletely understood. The strongest evidence points to a role in regulating β-catenin stability and Wnt/β-catenin signalling. To test if Wnt/β-catenin signalling is dysregulated in the mouse cSCC, we examined the ratios between the active form of β-catenin and the total β-catenin levels. These ratios were lower in the majority of tumor samples compared to VS controls (12 out of 18 animals, 67%) and higher in 5 animals (28%), while no correlation between Filip1l levels and β-catenin ratios could be detected. While down-regulation of Filip1l is a common feature of UV radiation-induced murine cSCC, up-regulation of the Wnt/β-catenin signalling is not. This suggests, that in contrast to other tumor types, Filip1l does not regulate Wnt/β-catenin signalling in murine cSCC.

In humans, the *FILIP1L* gene encodes for 8 isoforms. It is assumed, that isoform 203 is the main isoform. Nothing is known about the FILIP1L isoform expression pattern and if different FILIP1L isoforms serve different biological function. The majority of functional data on FILIP1L has focused on its role in modulating the WNT/β-catenin signalling pathway. FILIP1L has been shown to facilitate the destruction of β-catenin and therefore supress canonical WNT/β-catenin signalling, but the exact mechanism remains unknown.

In various cancers, such as ovarian, prostate and pancreatic cancer, FILIP1L expression is controlled by promoter methylation, with hypermethylation silencing FILIP1L expression in the cancers. We tested 8 human cSCC cell lines and found promoter hypermethylation in 2 using MassARRAY. However, there was no clear inverse correlation between promoter methylation and FILIP1L expression levels. Furthermore, the promoter was lowly methylated in 14 human cSCC samples. Together this suggests, that unknown factors other than promoter methylation control FILIP1L expression in human cSCC.

We investigated both the levels of FILIP1L and its isoform composition in a panel of 15 human cSCC cell lines as well as normal human keratinocytes (NHK). We found that FILIP1L isoform 203 is the main expressed isoform in all cell lines with other isoform's expression varying between cell lines. Furthermore, FILIP1L expression was reduced in 9 out of 15 cSCC cell lines compared to NHKs. For the first time, we

have shown that FILIP1L isoform 203 is the main expressed isoform in human skin. In fact, this thesis, to our knowledge, is the first investigation if FILIP1L in skin.

We chose the immortalized keratinocyte cell line NTERT to investigate the function of FILIP1L in human skin. Both the levels and the isoform composition of FILIP1L were similar in NTERT cells compared to NHK cultures. When we treated NTERT cells with LiCl, a GSK3β inhibitor, this resulted in induction of FILIP1L expression and induced expression of the WNT/β-catenin target gene AXIN2. However, we do not have evidence that this induction is through activation of the WNT/β-catenin pathway. Knock-down of FILIP1L using siRNA did not induce AXIN2 expression in NTERT cells. Furthermore, FILIP1L knock-down did not affect the levels of active β-catenin in the nucleus, but the efficiency of the knock-down was only about 50% and the variation between repetitions of experiments was high. Establishing a better knock-down, a more reliable supply of cells and reducing variations would be required to draw definitive conclusions.

We chose to investigate the role of FILIP1L using the human cSCC cell lines IC1 and IC1 met. While IC1 was derived from a primary tumor and FILIP1L expression is low (compared to NHKs) in this cell line, IC1 met is from a metastasis of the same patient and has normal levels of FILIP1L expression. We cloned the coding sequence for FILIP1L isoform 203 into a pcDNA3.1 expression vector. Unfortunately, when we transfected IC1 cells with the pcDNA vector, FILIP1L expression was significantly induced in empty vector controls, suggesting, that the transfection procedure alone is inducing FILIP1L expression. This is supported by the fact, that transfection of IC1 met cells with siRNA is also slightly inducing FILIP1L. While reducing the amount of transfection reagent (Lipofectamine 3000) did reduce FILIP1L induction, transfection efficiency was not sufficient. We also tested other transfection reagents, but the results were similar.

Knock-down of FILIP1L in IC1 met cells was successful and efficiency was higher than in NTERT cells (90% compared to 50%). However, FILIP1L knock-down did not lead to a significant increase in the levels of active β-catenin in IC1 met cells. This suggests, that FILIP1L does not control WNT/β-catenin signalling in skin or that other factors have a bigger role.

Last, we tested the effect of FILIP1L knock-down on the proliferation of IC1 met cells, using confluency measurements with the IncuCyte imaging system. FILIP1L knock-down had no effect on IC1 met proliferation, suggesting that in contrast to e.g. ovarian cancer, the role of FILIP1L in skin is not as profound.

4.3 Conclusion

In this study, we present a comprehensive analysis of DNA methylation in mouse cSCC and propose, that the most significant changes occur at regions of regulatory importance. Remarkably, the changes in the methylome of murine cSCC show high degrees of similarity to human cSCC in terms of both general features and the genes affected. Therefore, we conclude that the murine cSCC model developed in our lab recapitulates human cSCC, as shown by the remarkable similarities in histopathology, mutation spectrum and DNA methylation. The model may be advantageous over other currently used preclinical models.

FILIP1L is a novel tumor suppressor gene that is potentially involved in WNT/β-catenin signalling. Especially in ovarian cancer, FILIP1L is an important regulator of aggressiveness and an independent prognostic marker. We found the *Filip1l* gene to be differentially methylated in ssUV cSCC, and the Filip1l protein to be down-regulated in the tumors compared to control skin. Furthermore, FILIP1L expression and protein levels are reduced in 9 out of 15 of the tested human cSCC cell lines. However, we did not find evidence, that FILIP1L regulates WNT/β-catenin signalling in skin. Further investigation will be necessary to determine if down-regulation of FILIP1L is important in human cSCC and which pathways are involved.

Evidence is increasing that in cSCC, inactivation of tumor suppressor genes plays a major role. The mutation burden of completely normal appearing skin can exceed that of aggressive cancers in other tissues, suggesting that skin is especially resilient to mutations in oncogenes. Silencing of tumor suppressor genes is frequently mediated by DNA hypermethylation of tumor suppressor promoters and other regulatory elements. In this work, we provide evidence that tumor suppressor genes, e.g. FILIP1L, can be silenced by DNA methylation in cSCC. Epigenetic regulation of gene expression plays a major role in cSCC. For example, cSCC cells are very sensitive to drugs that target histone deacetylase and histone demethylase [266]. Targeting DNA methylation in cSCC may have similar effects and could provide new approaches for the therapy of cSCC.

5 Appendix

5.1 *In silico* bisulfite conversion macro for word

The *in silico* BS conversion macro includes a clean-up function to remove unnecessary characters and line breaks. It was kindly provided by the Division of Epigenetics and Cancer Risk Factors of the German Cancer Research Center.

```
Sub AUTOEXEC()
   Set MYBAR = CommandBars _
   .Add(Name:="CpG", Position:=msoBarFloating, TEMPORARY:=True)
   MYBAR.Visible = True
   MYBAR.Left = 1000
   MYBAR.Top = 130

   Set CLEANUPBUTTON = MYBAR.Controls _
   .Add(Type:=msoControlButton)
   CLEANUPBUTTON.OnAction = "CLEANUP"
   CLEANUPBUTTON.TooltipText = "Clean up sequence"
   CLEANUPBUTTON.FaceId = 2174

   Set REVCOMPBUTTON = MYBAR.Controls _
   .Add(Type:=msoControlButton)
   REVCOMPBUTTON.OnAction = "REVCOMP"
   REVCOMPBUTTON.TooltipText = "Reverse complement"
   REVCOMPBUTTON.FaceId = 1977

   Set BISTREATBUTTON = MYBAR.Controls _
   .Add(Type:=msoControlButton)
   BISTREATBUTTON.OnAction = "BISTREAT"
   BISTREATBUTTON.TooltipText = "Bisulfite treatment"
   BISTREATBUTTON.FaceId = 625
End Sub
Sub CLEANUP()
   With Selection.Font
      .Name = "COURIER"
```

```
    .AllCaps = True
End With
Selection.Find.ClearFormatting
Selection.Find.Replacement.ClearFormatting
With Selection.Find
    .Text = "^p"
    .Replacement.Text = ""
    .Forward = True
    .Wrap = wdFindStop
    .Format = False
    .MatchCase = False
    .MatchWholeWord = False
    .MatchWildcards = False
    .MatchSoundsLike = False
    .MatchAllWordForms = False
End With
Selection.Find.Execute Replace:=wdReplaceAll
With Selection.Find
    .Text = "^t"
    .Replacement.Text = ""
    .Forward = True
    .Wrap = wdFindStop
    .Format = False
    .MatchCase = False
    .MatchWholeWord = False
    .MatchWildcards = False
    .MatchSoundsLike = False
    .MatchAllWordForms = False
End With
Selection.Find.Execute Replace:=wdReplaceAll
With Selection.Find
    .Text = "^#"
```

```
        .Replacement.Text = ""
        .Forward = True
        .Wrap = wdFindStop
        .Format = False
        .MatchCase = False
        .MatchWholeWord = False
        .MatchWildcards = False
        .MatchSoundsLike = False
        .MatchAllWordForms = False
    End With
    Selection.Find.Execute Replace:=wdReplaceAll
    With Selection.Find
        .Text = " "
        .Replacement.Text = ""
        .Forward = True
        .Wrap = wdFindStop
        .Format = False
        .MatchCase = False
        .MatchWholeWord = False
        .MatchWildcards = False
        .MatchSoundsLike = False
        .MatchAllWordForms = False
    End With
    Selection.Find.Execute Replace:=wdReplaceAll
End Sub
Sub REVCOMP()
    Dim STARTSTRING
    Dim ENDSTRING
    Dim THISBASE
    STARTSTRING = UCase(Selection.Text)
    For BASEPOSITION = Len(STARTSTRING) To 1 Step -1
    THISBASE = Mid(STARTSTRING, BASEPOSITION, 1)
```

```
    Select Case THISBASE
    Case "A"
    ENDSTRING = ENDSTRING & "T"
    Case "T"
    ENDSTRING = ENDSTRING & "A"
    Case "C"
    ENDSTRING = ENDSTRING & "G"
    Case "G"
    ENDSTRING = ENDSTRING & "C"
    Case Else
    ENDSTRING = ENDSTRING & LCase(THISBASE)
    End Select
    Next
    Selection.Text = ENDSTRING
End Sub
Sub BISTREAT()
    With Selection.Font
        .Name = "COURIER"
        .AllCaps = True
    End With
    Selection.Find.ClearFormatting
    Selection.Find.Replacement.ClearFormatting
    With Selection.Find
        .Text = "CG"
        .Replacement.Text = "XG"
        .Forward = True
        .Wrap = wdFindStop
        .Format = False
        .MatchCase = False
        .MatchWholeWord = False
        .MatchWildcards = False
        .MatchSoundsLike = False
```

```
        .MatchAllWordForms = False
    End With
    Selection.Find.Execute Replace:=wdReplaceAll
    With Selection.Find
        .Text = "C"
        .Replacement.Text = "T"
        .Forward = True
        .Wrap = wdFindStop
        .Format = False
        .MatchCase = False
        .MatchWholeWord = False
        .MatchWildcards = False
        .MatchSoundsLike = False
        .MatchAllWordForms = False
    End With
    Selection.Find.Execute Replace:=wdReplaceAll
    With Selection.Find
        .Text = "XG"
        .Replacement.Text = "CG"
        .Forward = True
        .Wrap = wdFindStop
        .Format = False
        .MatchCase = False
        .MatchWholeWord = False
        .MatchWildcards = False
        .MatchSoundsLike = False
        .MatchAllWordForms = False
    End With
    Selection.Find.Execute Replace:=wdReplaceAll
End Sub
```

5.2 NTERT FILIP1L siRNA KD Western blots

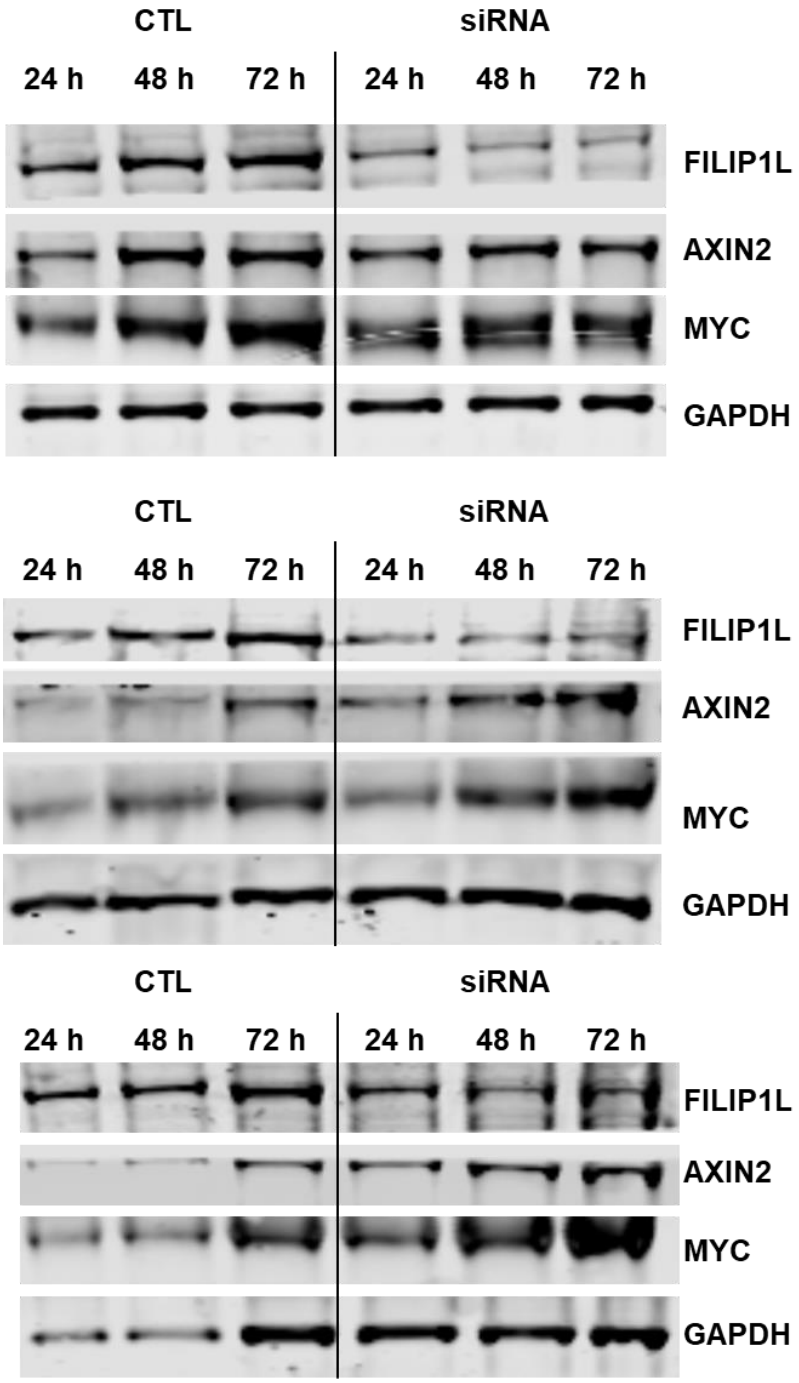

Figure 59: NTERT cells, FILIP1L siRNA knock-down. Quantifications see Figure 44: FILIP1L levels in NTERT cells treated with 10 mM LiCl, equal amounts of NaCl or were left untreated. Results represent the quantification results from immunoblots and three biological replicates. UT: Untreated control. LiCl was used to inhibit GSK 3β FILIP1L levels are up-regulated by LiCl treatment after 2 h and are highest after treatment for 24 h. Expression also increases with time, possibly due to a response to increased confluency. Significance is indicated by asterisks (* $p<0.05$, ** $p<0.01$, *** $p<0.001$).**Figure 44, Figure 45, Figure 46, Figure 47.**

5.3 NTERT FILIP1L siRNA knock-down with LiCl treatment blots (preliminary)

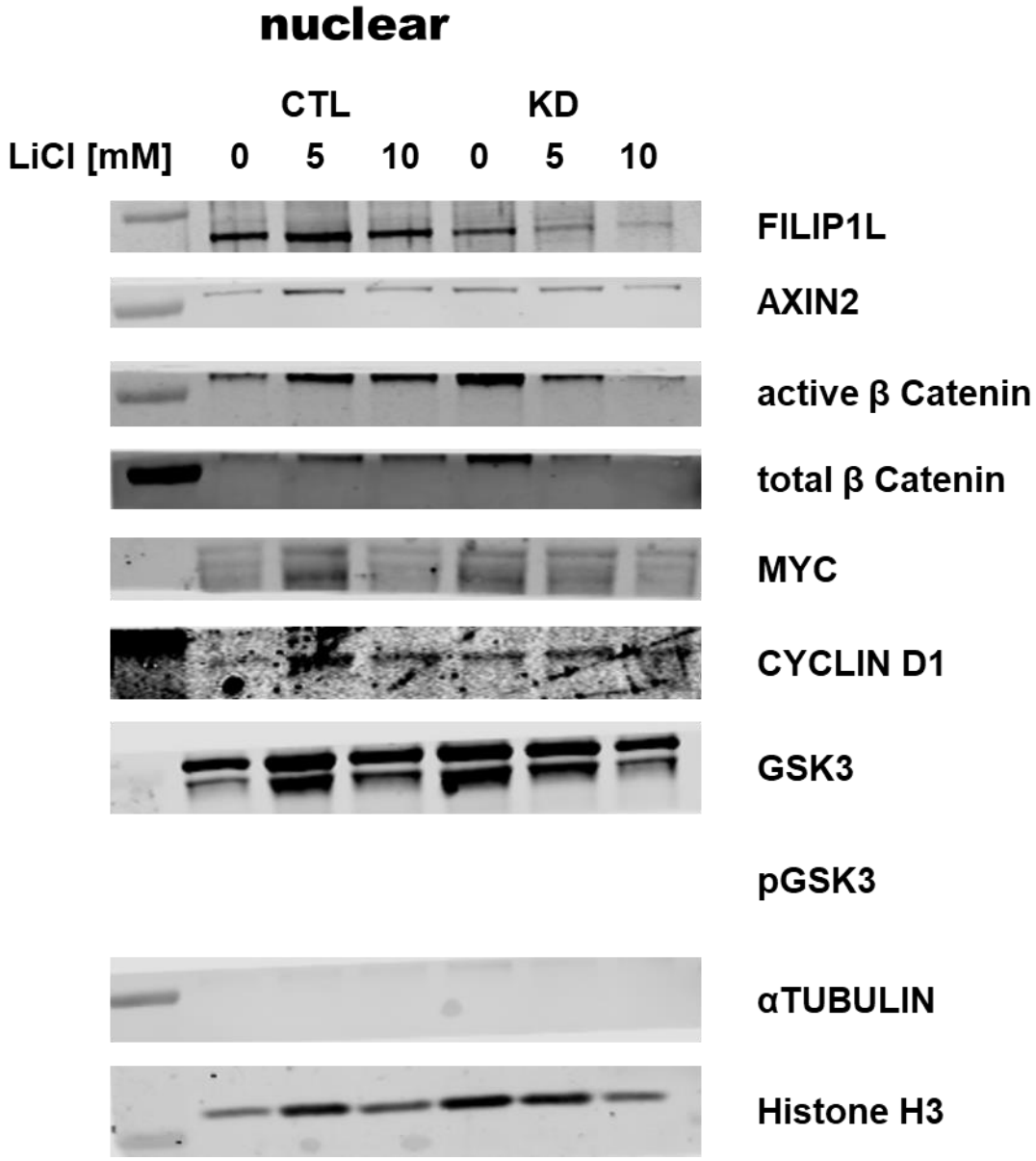

Figure 60: NTERT cells, FILIP1L siRNA knock-down for 48 h, nuclear fraction.

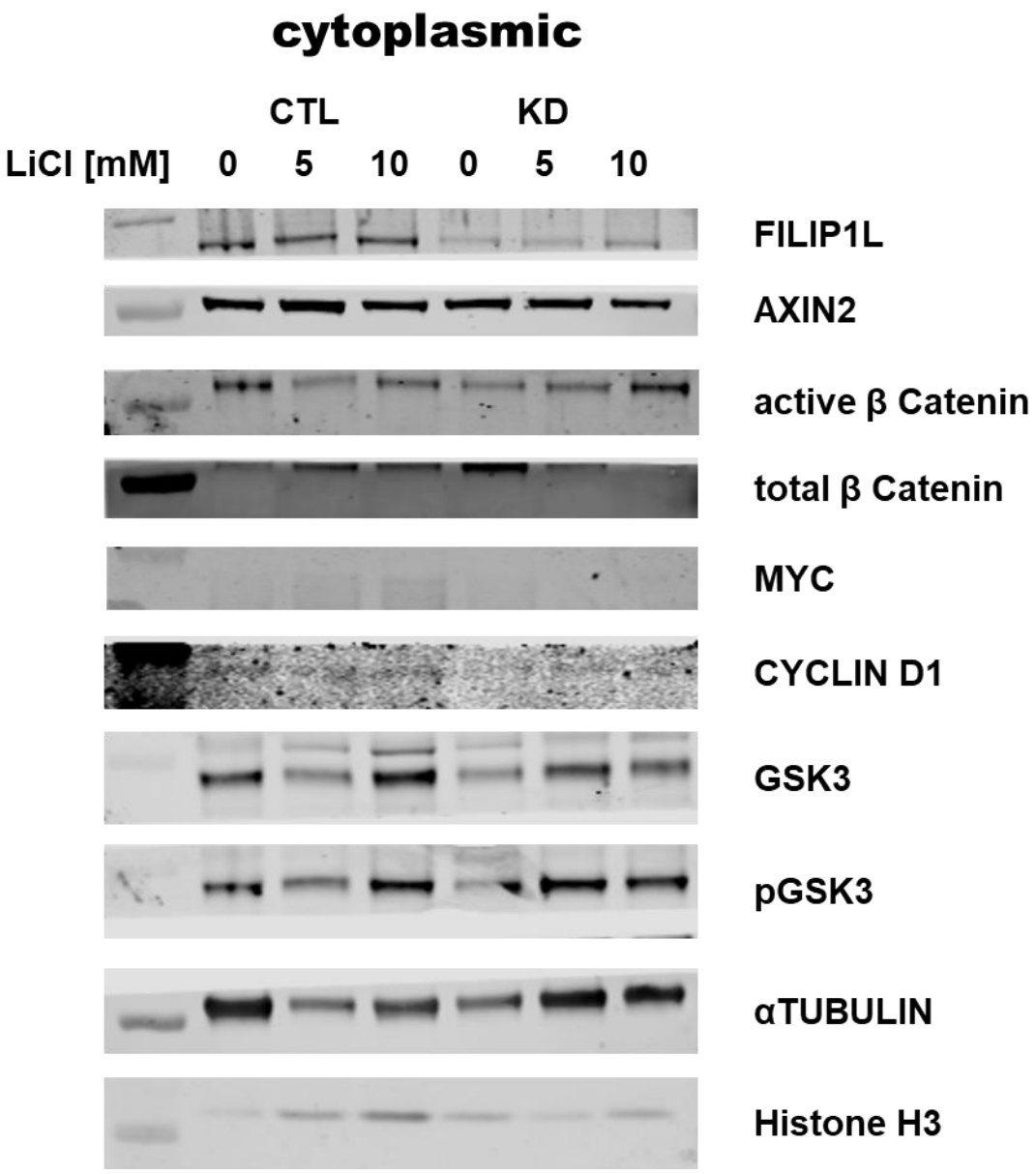

Figure 61: NTERT cells, FILIP1L siRNA knock-down for 48 h, cytoplasmic fraction.

References

1. Wright F, Weller RB. Risks and benefits of UV radiation in older people: More of a friend than a foe? Maturitas. 2015;81: 425–31. doi:10.1016/j.maturitas.2015.05.003

2. Weller RB. Sunlight Has Cardiovascular Benefits Independently of Vitamin D. Blood Purification. S. Karger AG; 2016. pp. 130–134. doi:10.1159/000441266

3. Nagarajan P, Asgari MM, Green AC, Guhan SM, Arron ST, Proby CM, et al. Keratinocyte Carcinomas: Current Concepts and Future Research Priorities. Clin Cancer Res. American Association for Cancer Research; 2019;25: 2379–2391. doi:10.1158/1078-0432.CCR-18-1122

4. Cancer Research UK. Melanoma incidence [Internet]. 2019 p. Accessed August 2019. Available: https://www.cancerresearchuk.org/health-professional/cancer-statistics/statistics-by-cancer-type/melanoma-skin-cancer#heading-Zero

5. Cancer Research UK. No Title [Internet]. 2019 p. Accessed August 2019. Available: https://www.cancerresearchuk.org/health-professional/cancer-statistics/statistics-by-cancer-type/non-melanoma-skin-cancer#heading-Zero

6. Diao DY, Lee TK. Sun-protective behaviors in populations at high risk for skin cancer. Psychology Research and Behavior Management. 2013. pp. 9–18. doi:10.2147/PRBM.S40457

7. Redlarski G, Palkowski A, Krawczuk M. Body surface area formulae: An alarming ambiguity. Sci Rep. Nature Publishing Group; 2016;6. doi:10.1038/srep27966

8. Lam TK, Leung DT y., Mosteller RD. More on Simplified Calculation of Body-Surface Area. New England Journal of Medicine. 1988. p. 1130. doi:10.1056/NEJM198804283181717

9. Pasparakis M, Haase I, Nestle FO. Mechanisms regulating skin immunity and inflammation. Nature Reviews Immunology. Nature Publishing Group; 2014. pp. 289–301. doi:10.1038/nri3646

10. Rittié L, Fisher GJ. Natural and sun-induced aging of human skin. Cold Spring Harb Perspect Med. 2015;5: a015370. doi:10.1101/cshperspect.a015370

11. Khavkin J, Ellis DAF. Aging skin: histology, physiology, and pathology. Facial Plast Surg Clin North Am. 2011;19: 229–34. doi:10.1016/j.fsc.2011.04.003

12. Nestle FO, Di Meglio P, Qin J-Z, Nickoloff BJ. Skin immune sentinels in health and disease. Nat Rev Immunol. 2009;9: 679–91. doi:10.1038/nri2622

13. Menon GK. New insights into skin structure: scratching the surface. Adv Drug Deliv Rev. 2002;54 Suppl 1: S3-17. Available: http://www.ncbi.nlm.nih.gov/pubmed/12460712

14. Ross A, Allison G. Anatomy and Physiology in health and Illness. Anatomy and Physiology in health and Illness. 12th editi. 2014. pp. 362–373.

15. Truong AB, Kretz M, Ridky TW, Kimmel R, Khavari PA. p63 regulates proliferation and differentiation of developmentally mature keratinocytes. Genes Dev. 2006;20: 3185–97. doi:10.1101/gad.1463206

16. Nguyen B, Lefort K, Dotto GP, Mandinova A, Antonini D, Devgan V, et al. Cross-regulation between Notch and p63 in keratinocyte commitment to differentiation Results p63 expression is down-modulated by Notch1 activation in differentiation. Genes Dev. 2005;20: 1028–1042. doi:10.1101/gad.1406006.whereas

17. Nickoloff BJ, Qin J-Z, Chaturvedi V, Denning MF, Bonish B, Miele L. Jagged-1 mediated activation of notch signaling induces complete maturation of human keratinocytes through NF-kappaB and PPARgamma. Cell Death Differ. 2002;9: 842–55. doi:10.1038/sj.cdd.4401036

18. Lowell S, Jones P, Le Roux I, Dunne J, Watt FM. Stimulation of human epidermal differentiation by delta-notch signalling at the boundaries of stem-cell clusters. Curr Biol. 2000;10: 491–500. doi:10.1016/s0960-9822(00)00451-6

19. Candi E, Schmidt R, Melino G. The cornified envelope: a model of cell death in the skin. Nat Rev Mol Cell Biol. 2005;6: 328–40. doi:10.1038/nrm1619

20. Proksch E, Fölster-Holst R, Jensen J-M. Skin barrier function, epidermal

proliferation and differentiation in eczema. J Dermatol Sci. 2006;43: 159–69. doi:10.1016/j.jdermsci.2006.06.003

21. Alam M, Ratner DD. Cutaneous Squamous-Cell Carcinoma. N Engl J Med. 2001;344: 975–983. doi:10.1056/NEJM200103293441306

22. Bray F, Ferlay J, Soerjomataram I, Siegel RL, Torre LA, Jemal A. Global cancer statistics 2018: GLOBOCAN estimates of incidence and mortality worldwide for 36 cancers in 185 countries. CA Cancer J Clin. American Cancer Society; 2018;68: 394–424. doi:10.3322/caac.21492

23. World Health Organization. Global Cancer Observatory. In: Global Cancer Observatory [Internet]. 2019 [cited 4 Feb 2019] p. Accessed February 2019. Available: http://gco.iarc.fr/

24. Apalla Z, Nashan D, Weller RB, Castellsagué X. Skin Cancer: Epidemiology, Disease Burden, Pathophysiology, Diagnosis, and Therapeutic Approaches. Dermatol Ther (Heidelb). Springer; 2017;7: 5–19. doi:10.1007/s13555-016-0165-y

25. Fahradyan A, Howell A, Wolfswinkel E, Tsuha M, Sheth P, Wong A. Updates on the Management of Non-Melanoma Skin Cancer (NMSC). Healthcare. 2017;5: 82. doi:10.3390/healthcare5040082

26. Weinberg RA. The Biology of Cancer. Garland Science; 2014.

27. Parrish JA, Jaenicke KF, Anderson RR. ERYTHEMA AND MELANOGENESIS ACTION SPECTRA OF NORMAL HUMAN SKIN. Photochem Photobiol. John Wiley & Sons, Ltd (10.1111); 1982;36: 187–191. doi:10.1111/j.1751-1097.1982.tb04362.x

28. Liu J, Zhu H, Premnauth G, Earnest KG, Hahn P, Gray G, et al. UV cell stress induces oxidative cyclization of a protective reagent for DNA damage reduction in skin explants. Free Radic Biol Med. Pergamon; 2019;134: 133–138. doi:10.1016/J.FREERADBIOMED.2018.12.037

29. Kanitakis J. Anatomy, histology and immunohistochemistry of normal human skin. Eur J Dermatol. 12: 390–9; quiz 400–1. Available: http://www.ncbi.nlm.nih.gov/pubmed/12095893

30. Lin JY, Fisher DE. Melanocyte biology and skin pigmentation. Nature. 2007;445: 843–850. doi:10.1038/nature05660

31. CANDIDO S, RAPISARDA V, MARCONI A, MALAPONTE G, BEVELACQUA V, GANGEMI P, et al. Analysis of the B-RAFV600E mutation in cutaneous melanoma patients with occupational sun exposure. Oncol Rep. 2014;31: 1079–1082. doi:10.3892/or.2014.2977

32. Curtin JA, Fridlyand J, Kageshita T, Patel HN, Busam KJ, Kutzner H, et al. Distinct Sets of Genetic Alterations in Melanoma. N Engl J Med. 2005;353: 2135–2147. doi:10.1056/NEJMoa050092

33. Bastian BC. The Molecular Pathology of Melanoma: An Integrated Taxonomy of Melanocytic Neoplasia. Annu Rev Pathol Mech Dis. 2014;9: 239–271. doi:10.1146/annurev-pathol-012513-104658

34. Pollock PM, Harper UL, Hansen KS, Yudt LM, Stark M, Robbins CM, et al. High frequency of BRAF mutations in nevi. Nat Genet. 2003;33: 19–20. doi:10.1038/ng1054

35. Leonardi GC, Accardi G, Monastero R, Nicoletti F, Libra M. Ageing: from inflammation to cancer. Immun Ageing. 2018;15: 1. doi:10.1186/s12979-017-0112-5

36. Shain AH, Bastian BC. From melanocytes to melanomas. Nat Rev Cancer. 2016;16: 345–358. doi:10.1038/nrc.2016.37

37. Gray-Schopfer V, Wellbrock C, Marais R. Melanoma biology and new targeted therapy. Nature. 2007;445: 851–857. doi:10.1038/nature05661

38. Hodis E, Watson IR, Kryukov GV, Arold ST, Imielinski M, Theurillat J-P, et al. A Landscape of Driver Mutations in Melanoma. Cell. 2012;150: 251–263. doi:10.1016/j.cell.2012.06.024

39. Krauthammer M, Kong Y, Ha BH, Evans P, Bacchiocchi A, McCusker JP, et al. Exome sequencing identifies recurrent somatic RAC1 mutations in melanoma. Nat Genet. 2012;44: 1006–1014. doi:10.1038/ng.2359

40. Akbani R, Akdemir KC, Aksoy BA, Albert M, Ally A, Amin SB, et al. Genomic Classification of Cutaneous Melanoma. Cell. 2015;161: 1681–1696.

doi:10.1016/j.cell.2015.05.044

41. Moro N, Mauch C, Zigrino P. Metalloproteinases in melanoma. Eur J Cell Biol. 2014;93: 23–29. doi:10.1016/j.ejcb.2014.01.002

42. Falzone L, Salemi R, Travali S, Scalisi A, McCubrey J, Candido S, et al. MMP-9 overexpression is associated with intragenic hypermethylation of MMP9 gene in melanoma. Aging (Albany NY). 2017;8: 933–944. doi:10.18632/aging.100951

43. Sandri S, Faião-Flores F, Tiago M, Pennacchi PC, Massaro RR, Alves-Fernandes DK, et al. Vemurafenib resistance increases melanoma invasiveness and modulates the tumor microenvironment by MMP-2 upregulation. Pharmacol Res. 2016;111: 523–533. doi:10.1016/j.phrs.2016.07.017

44. Cancer Research UK. Melanoma skin cancer survival statistics. In: https://www.cancerresearchuk.org/health-professional/cancer-statistics/statistics-by-cancer-type/melanoma-skin-cancer/survival. 2019 p. Accessed February 2019.

45. Cancer Research UK. Melanoma skin cancer statistics. In: https://www.cancerresearchuk.org/health-professional/cancer-statistics/statistics-by-cancer-type/melanoma-skin-cancer. 2019 p. Accessed February 2019.

46. Cancer Research UK. Non-melanoma skin cancer statistics [Internet]. 2019 [cited 20 Sep 2002] p. Accessed February 2019. Available: https://www.cancerresearchuk.org/health-professional/cancer-statistics/statistics-by-cancer-type/non-melanoma-skin-cancer

47. Koh D, Wang H, Lee J, Chia KS, Lee HP, Goh CL. Basal cell carcinoma, squamous cell carcinoma and melanoma of the skin: analysis of the Singapore Cancer Registry data 1968-97. Br J Dermatol. 2003;148: 1161–6. Available: http://www.ncbi.nlm.nih.gov/pubmed/12828744

48. Mohan S V, Chang ALS. Advanced Basal Cell Carcinoma: Epidemiology and Therapeutic Innovations. Curr Dermatol Rep. Springer; 2014;3: 40–45. doi:10.1007/s13671-014-0069-y

49. Pellegrini C, Maturo MG, Di Nardo L, Ciciarelli V, Gutiérrez García-Rodrigo C, Fargnoli MC. Understanding the Molecular Genetics of Basal Cell Carcinoma. Int J Mol Sci. Multidisciplinary Digital Publishing Institute (MDPI); 2017;18. doi:10.3390/ijms18112485

50. Christenson LJ, Borrowman TA, Vachon CM, Tollefson MM, Otley CC, Weaver AL, et al. Incidence of Basal Cell and Squamous Cell Carcinomas in a Population Younger Than 40 Years. JAMA. 2005;294: 681. doi:10.1001/jama.294.6.681

51. Wu TP, Stein JA. Nonmelanoma skin cancer in young women. J Drugs Dermatol. 2013;12: 568–72. Available: http://www.ncbi.nlm.nih.gov/pubmed/23652953

52. Memon AA, Tomenson JA, Bothwell J, Friedmann PS. Prevalence of solar damage and actinic keratosis in a Merseyside population. Br J Dermatol. 2000;142: 1154–9. Available: http://www.ncbi.nlm.nih.gov/pubmed/10848739

53. Kempf W, Hantschke M, Kutzner H, Burgdorf WHC. Dermatopathology. Steinkopff Verlag; 2008.

54. Szeimies R-M, Hautschild A, Garbe C, Kaufmann, Roland LM. Tumoren der Haut. Geor Thieme Verlag KG; 2010.

55. Durinck S, Ho C, Wang NJ, Liao W, Jakkula LR, Collisson EA, et al. Temporal Dissection of Tumorigenesis in Primary Cancers. Cancer Discov. American Association for Cancer Research; 2011;1: 137–143. doi:10.1158/2159-8290.CD-11-0028

56. Martincorena I, Roshan A, Gerstung M, Ellis P, Van Loo P, McLaren S, et al. High burden and pervasive positive selection of somatic mutations in normal human skin. Science (80-). 2015;348: 880–886. doi:10.1126/science.aaa6806

57. Wang NJ, Sanborn Z, Arnett KL, Bayston LJ, Liao W, Proby CM, et al. Loss-of-function mutations in Notch receptors in cutaneous and lung squamous cell carcinoma. Proc Natl Acad Sci U S A. 2011;108: 17761–6. doi:10.1073/pnas.1114669108

58. South AP, Purdie KJ, Watt SA, Haldenby S, den Breems NY, Dimon M, et al.

NOTCH1 Mutations Occur Early during Cutaneous Squamous Cell Carcinogenesis. J Invest Dermatol. 2014;134: 2630–2638. doi:10.1038/jid.2014.154

59. Knatko E V., Praslicka B, Higgins M, Evans A, Purdie KJ, Harwood CA, et al. Whole-Exome Sequencing Validates a Preclinical Mouse Model for the Prevention and Treatment of Cutaneous Squamous Cell Carcinoma. Cancer Prev Res. 2016; Available: http://cancerpreventionresearch.aacrjournals.org/content/early/2016/12/15/1940-6207.CAPR-16-0218

60. Knatko E V., Ibbotson SH, Zhang Y, Higgins M, Fahey JW, Talalay P, et al. Nrf2 activation protects against solar-simulated ultraviolet radiation in mice and humans. Cancer Prev Res. Europe PMC Funders; 2015;8: 475–486. doi:10.1158/1940-6207.CAPR-14-0362

61. Purdie KJ, Surentheran T, Sterling JC, Bell L, McGregor JM, Proby CM, et al. Human papillomavirus gene expression in cutaneous squamous cell carcinomas from immunosuppressed and immunocompetent individuals. J Invest Dermatol. Europe PMC Funders; 2005;125: 98–107. doi:10.1111/j.0022-202X.2005.23635.x

62. Wang J, Aldabagh B, Yu J, Arron ST. Role of human papillomavirus in cutaneous squamous cell carcinoma: a meta-analysis. J Am Acad Dermatol. NIH Public Access; 2014;70: 621–629. doi:10.1016/j.jaad.2014.01.857

63. Pfister H. Chapter 8: Human papillomavirus and skin cancer. J Natl Cancer Inst Monogr. 2003; 52–6. Available: http://www.ncbi.nlm.nih.gov/pubmed/12807946

64. Forslund O, Lindelöf B, Hradil E, Nordin P, Stenquist B, Kirnbauer R, et al. High prevalence of cutaneous human papillomavirus DNA on the top of skin tumors but not in "Stripped" biopsies from the same tumors. J Invest Dermatol. Europe PMC Funders; 2004;123: 388–94. doi:10.1111/j.0022-202X.2004.23205.x

65. Weissenborn SJ, Nindl I, Purdie K, Harwood C, Proby C, Breuer J, et al. Human Papillomavirus-DNA Loads in Actinic Keratoses Exceed those in Non-

Melanoma Skin Cancers. J Invest Dermatol. 2005;125: 93–97. doi:10.1111/j.0022-202X.2005.23733.x

66. Nichols AJ, Allen AH, Shareef S, Badiavas E V, Kirsner RS, Ioannides T. Association of Human Papillomavirus Vaccine With the Development of Keratinocyte Carcinomas. JAMA dermatology. American Medical Association; 2017;153: 571–574. doi:10.1001/jamadermatol.2016.5703

67. Nichols AJ, Gonzalez A, Clark ES, Khan WN, Rosen AC, Guzman W, et al. Combined Systemic and Intratumoral Administration of Human Papillomavirus Vaccine to Treat Multiple Cutaneous Basaloid Squamous Cell Carcinomas. JAMA Dermatology. American Medical Association; 2018;154: 927. doi:10.1001/jamadermatol.2018.1748

68. zur Hausen H. Papillomaviruses and cancer: from basic studies to clinical application. Nat Rev Cancer. 2002;2: 342–350. doi:10.1038/nrc798

69. Harwood CA, Toland AE, Proby CM, Euvrard S, Hofbauer GFL, Tommasino M, et al. The pathogenesis of cutaneous squamous cell carcinoma in organ transplant recipients. Br J Dermatol. 2017;177: 1217–1224. doi:10.1111/bjd.15956

70. Ramsay HM, Fryer AA, Hawley CM, Smith AG, Nicol DL, Harden PN. Epidemiology and Health Services Research Non-melanoma skin cancer risk in the Queensland renal transplant population. Br J Dermatol. 2002; 950–956.

71. Harwood CA, Mesher D, McGregor JM, Mitchell L, Leedham-Green M, Raftery M, et al. A Surveillance Model for Skin Cancer in Organ Transplant Recipients: A 22-Year Prospective Study in an Ethnically Diverse Population. Am J Transplant. 2013;13: 119–129. doi:10.1111/j.1600-6143.2012.04292.x

72. Berg D, Otley CC. Skin cancer in organ transplant recipients: Epidemiology, pathogenesis, and management. J Am Acad Dermatol. 2002;47: 1–17. doi:10.1067/mjd.2002.125579

73. Mittal A, Colegio OR. Skin Cancers in Organ Transplant Recipients. Am J Transplant. 2017;17: 2509–2530. doi:10.1111/ajt.14382

74. Noone AM, Howlader N, Krapcho M, Miller D, Brest A, Yu M, Ruhl J,

Tatalovich Z, Mariotto A, Lewis DR, Chen HS, Feuer EJ, Cronin KA (eds)Noone AM, Howlader N, Krapcho M, Miller D, Brest A, Yu M, Ruhl J, Tatalovich Z, Mariotto A, Lewis DR, Chen HS, Feuer EJ CK (eds). SEER Cancer Statistics Review, 1975-2015. Natl Cancer Institute Bethesda, MD. 2018; Available: https://seer.cancer.gov/csr/1975_2015/

75. Hagen JW, Pugliano-Mauro MA. Nonmelanoma Skin Cancer Risk in Patients With Inflammatory Bowel Disease Undergoing Thiopurine Therapy. Dermatologic Surg. 2018;44: 469–480. doi:10.1097/DSS.0000000000001455

76. Ariyaratnam J, Subramanian V. Association Between Thiopurine Use and Nonmelanoma Skin Cancers in Patients With Inflammatory Bowel Disease: A Meta-Analysis. Am J Gastroenterol. 2014;109: 163–169. doi:10.1038/ajg.2013.451

77. van den Reek JMPA, van Lümig PPM, Janssen M, Schers HJ, Hendriks JCM, van de Kerkhof PCM, et al. Increased incidence of squamous cell carcinoma of the skin after long-term treatment with azathioprine in patients with auto-immune inflammatory rheumatic diseases. J Eur Acad Dermatology Venereol. 2014;28: 27–33. doi:10.1111/jdv.12041

78. Zhao H, Shu G, Wang S. The risk of non-melanoma skin cancer in HIV-infected patients: new data and meta-analysis. Int J STD AIDS. 2016;27: 568–575. doi:10.1177/0956462415586316

79. Brewer JD, Habermann TM, Shanafelt TD. Lymphoma-associated skin cancer: incidence, natural history, and clinical management. Int J Dermatol. 2014;53: 267–274. doi:10.1111/ijd.12208

80. Velez NF, Karia PS, Vartanov AR, Davids MS, Brown JR, Schmults CD. Association of Advanced Leukemic Stage and Skin Cancer Tumor Stage With Poor Skin Cancer Outcomes in Patients With Chronic Lymphocytic Leukemia. JAMA Dermatology. 2014;150: 280. doi:10.1001/jamadermatol.2013.6249

81. Hofbauer GFL, Attard NR, Harwood CA, McGregor JM, Dziunycz P, Iotzova-Weiss G, et al. Reversal of UVA Skin Photosensitivity and DNA Damage in Kidney Transplant Recipients by Replacing Azathioprine. Am J Transplant. 2012;12: 218–225. doi:10.1111/j.1600-6143.2011.03751.x

82. O'Donovan P, Perrett CM, Zhang X, Montaner B, Xu Y-Z, Harwood CA, et al. Azathioprine and UVA Light Generate Mutagenic Oxidative DNA Damage. Science (80-). 2005;309: 1871–1874. doi:10.1126/science.1114233

83. Inman GJ, Wang J, Nagano A, Alexandrov LB, Purdie KJ, Taylor RG, et al. The genomic landscape of cutaneous SCC reveals drivers and a novel azathioprine associated mutational signature. Nat Commun. Nature Publishing Group; 2018;9: 3667. doi:10.1038/s41467-018-06027-1

84. Kuschal C, Thoms K-M, Boeckmann L, Laspe P, Apel A, Schön MP, et al. Cyclosporin A inhibits nucleotide excision repair via downregulation of the xeroderma pigmentosum group A and G proteins, which is mediated by calcineurin inhibition. Exp Dermatol. 2011;20: 795–799. doi:10.1111/j.1600-0625.2011.01320.x

85. Wu X, Nguyen B-C, Dziunycz P, Chang S, Brooks Y, Lefort K, et al. Opposing roles for calcineurin and ATF3 in squamous skin cancer. Nature. 2010;465: 368–372. doi:10.1038/nature08996

86. Holdaas H, De Simone P, Zuckermann A. Everolimus and Malignancy after Solid Organ Transplantation: A Clinical Update. J Transplant. 2016;2016: 1–11. doi:10.1155/2016/4369574

87. Rademacher S, Seehofer D, Eurich D, Schoening W, Neuhaus R, Oellinger R, et al. The 28-year incidence of de novo malignancies after liver transplantation: A single-center analysis of risk factors and mortality in 1616 patients. Liver Transplant. 2017;23: 1404–1414. doi:10.1002/lt.24795

88. Ikeya S, Sakabe J, Yamada T, Naito T, Tokura Y. Voriconazole-induced photocarcinogenesis is promoted by aryl hydrocarbon receptor-dependent COX-2 upregulation. Sci Rep. Nature Publishing Group; 2018;8: 5050. doi:10.1038/s41598-018-23439-7

89. Pudenz M, Roth K, Gerhauser C. Impact of soy isoflavones on the epigenome in cancer prevention. Nutrients. 2014;6: 4218–72. doi:10.3390/nu6104218

90. Esteller M. Cancer epigenomics: DNA methylomes and histone-modification maps. Nat Rev Genet. 2007;8: 286–98. doi:10.1038/nrg2005

91. Berdasco M, Esteller M. Aberrant Epigenetic Landscape in Cancer: How Cellular Identity Goes Awry. Dev Cell. 2010;19: 698–711. doi:10.1016/j.devcel.2010.10.005

92. Shen H, Laird PWW. Interplay between the Cancer Genome and Epigenome. Cell. Elsevier Inc.; 2013;153: 38–55. doi:10.1016/j.cell.2013.03.008

93. Hanahan D, Weinberg RA. Hallmarks of cancer: the next generation. Cell. Elsevier Inc.; 2011;144: 646–74. doi:10.1016/j.cell.2011.02.013

94. Hanahan D, Weinberg RA. The hallmarks of cancer. Cell. 2000;100: 57–70. Available: http://www.ncbi.nlm.nih.gov/pubmed/10647931

95. Missero C. The genetic evolution of skin squamous cell carcinoma: tumor suppressor identity matters. Exp Dermatol. 2016;25: 863–864. doi:10.1111/exd.13075

96. Missero C, Antonini D. Crosstalk among p53 family members in cutaneous carcinoma. Exp Dermatol. 2014;23: 143–146. doi:10.1111/exd.12320

97. Yilmaz AS, Ozer HG, Gillespie JL, Allain DC, Bernhardt MN, Furlan KC, et al. Differential mutation frequencies in metastatic cutaneous squamous cell carcinomas versus primary tumors. Cancer. 2017;123: 1184–1193. doi:10.1002/cncr.30459

98. Wikonkal NM, Brash DE. Ultraviolet radiation induced signature mutations in photocarcinogenesis. J Investig dermatology Symp Proc. 1999;4: 6–10. Available: http://www.ncbi.nlm.nih.gov/pubmed/10537000

99. Li Z, Gonzalez CL, Wang B, Zhang Y, Mejia O, Katsonis P, et al. Cdkn2a suppresses metastasis in squamous cell carcinomas induced by the gain-of-function mutant p53(R172H). J Pathol. 2016;240: 224–34. doi:10.1002/path.4770

100. Lin-Shiao E, Lan Y, Coradin M, Anderson A, Donahue G, Simpson CL, et al. KMT2D regulates p63 target enhancers to coordinate epithelial homeostasis. Genes Dev. Cold Spring Harbor Laboratory Press; 2018;32: 181–193. doi:10.1101/gad.306241.117

101. Pickering CR, Zhou JH, Lee JJ, Drummond JA, Peng SA, Saade RE, et al.

Mutational Landscape of Aggressive Cutaneous Squamous Cell Carcinoma. Clin Cancer Res. 2014;20: 6582–6592. doi:10.1158/1078-0432.CCR-14-1768

102. Nicolas M, Wolfer A, Raj K, Kummer JA, Mill P, van Noort M, et al. Notch1 functions as a tumor suppressor in mouse skin. Nat Genet. 2003;33: 416–21. doi:10.1038/ng1099

103. Proweller A, Tu L, Lepore JJ, Cheng L, Lu MM, Seykora J, et al. Impaired notch signaling promotes de novo squamous cell carcinoma formation. Cancer Res. 2006;66: 7438–44. doi:10.1158/0008-5472.CAN-06-0793

104. Kanellou P, Zaravinos A, Zioga M, Stratigos A, Baritaki S, Soufla G, et al. Genomic instability, mutations and expression analysis of the tumour suppressor genes p14ARF, p15INK4b, p16INK4a and p53 in actinic keratosis. Cancer Lett. Elsevier; 2008;264: 145–161. Available: https://linkinghub.elsevier.com/retrieve/pii/S0304383508000645

105. Soufir N, Molès JP, Vilmer C, Moch C, Verola O, Rivet J, et al. P16 UV mutations in human skin epithelial tumors. Oncogene. 1999;18: 5477–5481. doi:10.1038/sj.onc.1202915

106. Soufir N, Daya-Grosjean L, de La Salmonière P, Moles JP, Dubertret L, Sarasin A, et al. Association between INK4a-ARF and p53 mutations in skin carcinomas of xeroderma pigmentosum patients. J Natl Cancer Inst. 2000;92: 1841–7. Available: http://www.ncbi.nlm.nih.gov/pubmed/11078762

107. Kleijer WJ, Laugel V, Berneburg M, Nardo T, Fawcett H, Gratchev A, et al. Incidence of DNA repair deficiency disorders in western Europe: Xeroderma pigmentosum, Cockayne syndrome and trichothiodystrophy. DNA Repair (Amst). 2008;7: 744–750. doi:10.1016/j.dnarep.2008.01.014

108. Brown VL, Harwood CA, Crook T, Cronin JG, Kelsell DP, Proby CM. p16INK4a and p14ARF tumor suppressor genes are commonly inactivated in cutaneous squamous cell carcinoma. J Invest Dermatol. 2004;122: 1284–92. doi:10.1111/j.0022-202X.2004.22501.x

109. Rose AM, Sansom OJ, Inman GJ. Loss of TGF-β signaling drives cSCC from skin stem cells - More evidence. CELL CYCLE. 2017;16: 386–387.

doi:10.1038/ncomms12493

110. Cammareri P, Rose AM, Vincent DF, Wang J, Nagano A, Libertini S, et al. Inactivation of TGFβ receptors in stem cells drives cutaneous squamous cell carcinoma. Nat Commun. Nature Publishing Group; 2016;7: 12493. doi:10.1038/ncomms12493

111. Alexandrov LB, Nik-Zainal S, Wedge DC, Aparicio SAJR, Behjati S, Biankin A V., et al. Signatures of mutational processes in human cancer. Nature. Nature Publishing Group; 2013;500: 415–421. doi:10.1038/nature12477

112. Petljak M, Alexandrov LB. Understanding mutagenesis through delineation of mutational signatures in human cancer. Carcinogenesis. 2016;37: 531–540. doi:10.1093/carcin/bgw055

113. Yanofsky VR, Mercer SE, Phelps RG. Histopathological variants of cutaneous squamous cell carcinoma: a review. J Skin Cancer. 2011;2011: 210813. doi:10.1155/2011/210813

114. Stratigos A, Claus Garbe CL, Malvehy J, Marmol V del, Pehamberger H, Peris K, et al. Diagnosis and treatment of invasive squamous cell carcinoma of the skin: European consensus-based interdisciplinary guideline. Eur J Cancer. 2015;51: 1989–2007. doi:10.1016/j.pestbp.2011.02.012.Investigations

115. Evans HL, Smith JL. Spindle cell squamous carcinomas and sarcoma-like tumors of the skin: a comparative study of 38 cases. Cancer. 1980;45: 2687–97. doi:10.1002/1097-0142(19800515)45:10<2687::aid-cncr2820451034>3.0.co;2-r

116. Breuninger H, Schaumburg-Lever G, Holzschuh J, Horny HP. Desmoplastic squamous cell carcinoma of skin and vermilion surface: a highly malignant subtype of skin cancer. Cancer. 1997;79: 915–9. doi:10.1002/(sici)1097-0142(19970301)79:5<915::aid-cncr7>3.0.co;2-a

117. Nappi O, Wick MR, Pettinato G, Ghiselli RW, Swanson PE. Pseudovascular adenoid squamous cell carcinoma of the skin. A neoplasm that may be mistaken for angiosarcoma. Am J Surg Pathol. 1992;16: 429–38. doi:10.1097/00000478-199205000-00001

118. Venables ZC, Autier P, Nijsten T, Wong KF, Langan SM, Rous B, et al. Nationwide Incidence of Metastatic Cutaneous Squamous Cell Carcinoma in England. JAMA dermatology. 2019;155: 298–306. doi:10.1001/jamadermatol.2018.4219

119. Brodland DG, Zitelli JA. Surgical margins for excision of primary cutaneous squamous cell carcinoma. J Am Acad Dermatol. 1992;27: 241–8. doi:10.1016/0190-9622(92)70178-i

120. Cranmer LD, Engelhardt C, Morgan SS. Treatment of unresectable and metastatic cutaneous squamous cell carcinoma. Oncologist. 2010;15: 1320–8. doi:10.1634/theoncologist.2009-0210

121. Geohas J, Roholt NS, Robinson JK. Adjuvant radiotherapy after excision of cutaneous squamous cell carcinoma. J Am Acad Dermatol. 1994;30: 633–636. doi:10.1016/S0190-9622(94)70073-7

122. Cartei G, Cartei F, Interlandi G, Meneghini G, Jop A, Zingone G, et al. Oral 5-fluorouracil in squamous cell carcinoma of the skin in the aged. Am J Clin Oncol. 2000;23: 181–4. Available: http://www.ncbi.nlm.nih.gov/pubmed/10776981

123. Shao X-H, Xu Y-S, Zhang X-Q, Li W-F. Evidence based analysis of Cisplatin for treating patients with cutaneous squamous cell carcinoma. Asian Pac J Cancer Prev. 2014;15: 9813–5. doi:10.7314/apjcp.2014.15.22.9813

124. Sadek H, Azli N, Wendling JL, Cvitkovic E, Rahal M, Mamelle G, et al. Treatment of advanced squamous cell carcinoma of the skin with cisplatin, 5-fluorouracil, and bleomycin. Cancer. 1990;66: 1692–6. doi:10.1002/1097-0142(19901015)66:8<1692::aid-cncr2820660807>3.0.co;2-y

125. Denic S. Preoperative treatment of advanced skin carcinoma with cisplatin and bleomycin. Am J Clin Oncol. 1999;22: 32–4. Available: http://www.ncbi.nlm.nih.gov/pubmed/10025376

126. Bauman JE, Eaton KD, Martins RG. Treatment of recurrent squamous cell carcinoma of the skin with cetuximab. Arch Dermatol. 2007;143: 889–92. doi:10.1001/archderm.143.7.889

127. Suen JK, Bressler L, Shord SS, Warso M, Villano JL. Cutaneous squamous cell carcinoma responding serially to single-agent cetuximab. Anticancer Drugs. 2007;18: 827–9. doi:10.1097/CAD.0b013e32809ef9e0

128. Que SKT, Zwald FO, Schmults CD. Cutaneous squamous cell carcinoma: Incidence, risk factors, diagnosis, and staging. J Am Acad Dermatol. 2018;78: 237–247. doi:10.1016/j.jaad.2017.08.059

129. Shin DM, Glisson BS, Khuri FR, Clifford JL, Clayman G, Benner SE, et al. Phase II and biologic study of interferon alfa, retinoic acid, and cisplatin in advanced squamous skin cancer. J Clin Oncol. 2002;20: 364–70. doi:10.1200/JCO.2002.20.2.364

130. Brewster AM, Lee JJ, Clayman GL, Clifford JL, Reyes MJTN, Zhou X, et al. Randomized trial of adjuvant 13-cis-retinoic acid and interferon alfa for patients with aggressive skin squamous cell carcinoma. J Clin Oncol. 2007;25: 1974–8. doi:10.1200/JCO.2006.05.9873

131. Nassar D, Latil M, Boeckx B, Lambrechts D, Blanpain C. Genomic landscape of carcinogen-induced and genetically induced mouse skin squamous cell carcinoma. Nat Med. 2015;21: 946–954. doi:10.1038/nm.3878

132. McCreery MQ, Halliwill KD, Chin D, Delrosario R, Hirst G, Vuong P, et al. Evolution of metastasis revealed by mutational landscapes of chemically induced skin cancers. Nat Med. 2015;21: 1514–1520. doi:10.1038/nm.3979

133. Karran P, Attard N. Thiopurines in current medical practice: molecular mechanisms and contributions to therapy-related cancer. Nat Rev Cancer. 2008;8: 24–36. doi:10.1038/nrc2292

134. Brem R, Karran P. Oxidation-Mediated DNA Cross-Linking Contributes to the Toxicity of 6-Thioguanine in Human Cells. Cancer Res. 2012;72: 4787–4795. doi:10.1158/0008-5472.CAN-12-1278

135. Knatko E V., Higgins M, Fahey JW, Dinkova-Kostova AT. Loss of Nrf2 abrogates the protective effect of Keap1 downregulation in a preclinical model of cutaneous squamous cell carcinoma. Sci Rep. Nature Publishing Group; 2016;6: 25804. doi:10.1038/srep25804

136. Esteller M. CpG island hypermethylation and tumor suppressor genes: a booming present, a brighter future. Oncogene. 2002;21: 5427–5440. doi:10.1038/sj.onc.1205600

137. Rawłuszko-Wieczorek AA, Siera A, Jagodziński PP. TET proteins in cancer: Current 'state of the art.' Crit Rev Oncol Hematol. 2015; doi:10.1016/j.critrevonc.2015.07.008

138. Wu H, Zhang Y. Mechanisms and functions of Tet protein- mediated 5-methylcytosine oxidation. 2011; 2436–2452. doi:10.1101/gad.179184.111.genomes

139. Jurkowski TP, Jeltsch A. Burning off DNA methylation: New evidence for oxygen-dependent DNA demethylation. ChemBioChem. 2011;12: 2543–2545. doi:10.1002/cbic.201100549

140. Kohli RM, Zhang Y. TET enzymes, TDG and the dynamics of DNA demethylation. Nature. 2013;502: 472–479. doi:10.1038/nature12750

141. Pastor WA, Aravind L, Rao A. TETonic shift: biological roles of TET proteins in DNA demethylation and transcription. Nat Rev Mol Cell Biol. Nature Publishing Group; 2013;14: 341–356. doi:10.1038/nrm3589

142. Li D, Wu H, Lu Q. TET Family of Dioxygenases: Crucial Roles and Underlying Mechanisms Duo Li. 2015; 1–16. doi:10.1159/000438853

143. Goelz SE, Vogelstein B, Hamilton SR, Feinberg a P. Hypomethylation of DNA from benign and malignant human colon neoplasms. Science. 1985;228: 187–190. doi:10.1126/science.2579435

144. Feinberg AP, Vogelstein B. A technique for radiolabeling DNA restriction endonuclease fragments to high specific activity. Anal Biochem. 1983;132: 6–13. Available: http://www.ncbi.nlm.nih.gov/pubmed/6312838

145. Esteller M. Epigenetics in cancer. N Engl J Med. 2008;358: 1148–59. doi:10.1056/NEJMra072067

146. Greger V, Passarge E, Höpping W, Messmer E, Horsthemke B. Epigenetic changes may contribute to the formation and spontaneous regression of retinoblastoma. Hum Genet. 1989;83: 155–8. Available:

http://www.ncbi.nlm.nih.gov/pubmed/2550354

147. Sakai T, Toguchida J, Ohtani N, Yandell DW, Rapaport JM, Dryja TP. Allele-specific hypermethylation of the retinoblastoma tumor-suppressor gene. Am J Hum Genet. 1991;48: 880–8. Available: http://www.pubmedcentral.nih.gov/articlerender.fcgi?artid=1683063&tool=pmcentrez&rendertype=abstract

148. Herman JG, Baylin SB. Gene silencing in cancer in association with promoter hypermethylation. N Engl J Med. 2003;349: 2042–54. doi:10.1056/NEJMra023075

149. De Smet C, Lurquin C, Lethé B, Martelange V, Boon T. DNA methylation is the primary silencing mechanism for a set of germ line- and tumor-specific genes with a CpG-rich promoter. Mol Cell Biol. 1999;19: 7327–35. Available: http://www.pubmedcentral.nih.gov/articlerender.fcgi?artid=84726&tool=pmcentrez&rendertype=abstract

150. Liutkeviciute Z, Lukinavicius G, Masevicius V, Daujotyte D, Klimasauskas S. Cytosine-5-methyltransferases add aldehydes to DNA. Nat Chem Biol. 2009;5: 400–2. doi:10.1038/nchembio.172

151. Chen C-C, Wang K-Y, Shen C-KJ. The mammalian de novo DNA methyltransferases DNMT3A and DNMT3B are also DNA 5-hydroxymethylcytosine dehydroxymethylases. J Biol Chem. 2012;287: 33116–21. doi:10.1074/jbc.C112.406975

152. Tahiliani M, Koh KP, Shen Y, Pastor WA, Bandukwala H, Brudno Y, et al. Conversion of 5-methylcytosine to 5-hydroxymethylcytosine in mammalian DNA by MLL partner TET1. Science. 2009;324: 930–5. doi:10.1126/science.1170116

153. He Y-F, Li B-Z, Li Z, Liu P, Wang Y, Tang Q, et al. Tet-mediated formation of 5-carboxylcytosine and its excision by TDG in mammalian DNA. Science. 2011;333: 1303–7. doi:10.1126/science.1210944

154. Ito S, D'Alessio AC, Taranova O V, Hong K, Sowers LC, Zhang Y. Role of Tet proteins in 5mC to 5hmC conversion, ES-cell self-renewal and inner cell

mass specification. Nature. 2010;466: 1129–33. doi:10.1038/nature09303

155. Cortellino S, Xu J, Sannai M, Moore R, Caretti E, Cigliano A, et al. Thymine DNA glycosylase is essential for active DNA demethylation by linked deamination-base excision repair. Cell. 2011;146: 67–79. doi:10.1016/j.cell.2011.06.020

156. Globisch D, Münzel M, Müller M, Michalakis S, Wagner M, Koch S, et al. Tissue distribution of 5-hydroxymethylcytosine and search for active demethylation intermediates. PLoS One. Public Library of Science; 2010;5: e15367. doi:10.1371/journal.pone.0015367

157. Pfaffeneder T, Hackner B, Truss M, Münzel M, Müller M, Deiml CA, et al. The discovery of 5-formylcytosine in embryonic stem cell DNA. Angew Chem Int Ed Engl. 2011;50: 7008–12. doi:10.1002/anie.201103899

158. Wu SC, Zhang Y. Active DNA demethylation: many roads lead to Rome. Nat Rev Mol Cell Biol. 2010;11: 607–20. doi:10.1038/nrm2950

159. Kurdyukov S, Bullock M. DNA Methylation Analysis: Choosing the Right Method. Biology (Basel). 2016;5: 3. doi:10.3390/biology5010003

160. Hahn MA, Li AX, Wu X, Pfeifer GP. Single base resolution analysis of 5-methylcytosine and 5-hydroxymethylcytosine by RRBS and TAB-RRBS. Methods Mol Biol. NIH Public Access; 2015;1238: 273–87. doi:10.1007/978-1-4939-1804-1_14

161. Taiwo O, Wilson GA, Morris T, Seisenberger S, Reik W, Pearce D, et al. Methylome analysis using MeDIP-seq with low DNA concentrations. Nat Protoc. 2012;7: 617–636. doi:10.1038/nprot.2012.012

162. Nair SS, Coolen MW, Stirzaker C, Song JZ, Statham AL, Strbenac D, et al. Comparison of methyl-DNA immunoprecipitation (MeDIP) and methyl-CpG binding domain (MBD) protein capture for genome-wide DNA methylation analysis reveal CpG sequence coverage bias. Epigenetics. 2011;6: 34–44. doi:10.4161/epi.6.1.13313

163. Rauch TA, Pfeifer GP. DNA methylation profiling using the methylated-CpG island recovery assay (MIRA). Methods. 2010;52: 213–217.

doi:10.1016/j.ymeth.2010.03.004

164. Rauch T, Li H, Wu X, Pfeifer GP. MIRA-Assisted Microarray Analysis, a New Technology for the Determination of DNA Methylation Patterns, Identifies Frequent Methylation of Homeodomain-Containing Genes in Lung Cancer Cells. Cancer Res. 2006;66: 7939–7947. doi:10.1158/0008-5472.CAN-06-1888

165. Robinson MD, Statham AL, Speed TP, Clark SJ. Protocol matters: which methylome are you actually studying? Epigenomics. 2010;2: 587–598. doi:10.2217/epi.10.36

166. Brinkman AB, Simmer F, Ma K, Kaan A, Zhu J, Stunnenberg HG. Whole-genome DNA methylation profiling using MethylCap-seq. Methods. 2010;52: 232–236. doi:10.1016/j.ymeth.2010.06.012

167. Gerhauser C, Heilmann K, Pudenz M. Genome-Wide DNA Methylation Profiling in Dietary Intervention Studies: a User's Perspective. Curr Pharmacol Reports. 2015;1: 31–45. doi:10.1007/s40495-014-0001-y

168. Stirzaker C, Taberlay PC, Statham AL, Clark SJ. Mining cancer methylomes: prospects and challenges. Trends Genet. 2014;30: 75–84. doi:10.1016/j.tig.2013.11.004

169. Busó EJ, Iborra M. Chapter 7 - Sequenom MassARRAY Technology for the Analysis of DNA Methylation: Clinical Applications. 2016; doi:10.1016/B978-0-12-801899-6.00007-3

170. Lin J, Qin H, Wu W, He S, Xu J. Vitamin C protects against UV irradiation-induced apoptosis through reactivating silenced tumor suppressor genes p21 and p16 in a Tet-dependent DNA demethylation manner in human skin cancer cells. Cancer Biother Radiopharm. 2014;29: 257–64. doi:10.1089/cbr.2014.1647

171. Yang AY, Lee JH, Shu L, Zhang C, Su Z-Y, Lu Y, et al. Genome-wide analysis of DNA methylation in UVB- and DMBA/TPA-induced mouse skin cancer models. Life Sci. Elsevier Inc.; 2014;113: 45–54. doi:10.1016/j.lfs.2014.07.031

172. Nandakumar V, Vaid M, Tollefsbol TO, Katiyar SK. Aberrant DNA

hypermethylation patterns lead to transcriptional silencing of tumor suppressor genes in UVB-exposed skin and UVB-induced skin tumors of mice. Carcinogenesis. 2011;32: 597–604. doi:10.1093/carcin/bgq282

173. van Doorn R, Gruis N a, Willemze R, van der Velden P a, Tensen CP. Aberrant DNA methylation in cutaneous malignancies. Semin Oncol. 2005;32: 479–87. doi:10.1053/j.seminoncol.2005.07.001

174. Denissenko MF, Chen JX, Tang MS, Pfeifer GP. Cytosine methylation determines hot spots of DNA damage in the human P53 gene. Proc Natl Acad Sci U S A. 1997;94: 3893–8. Available: http://www.pubmedcentral.nih.gov/articlerender.fcgi?artid=20538&tool=pmcentrez&rendertype=abstract

175. You YH, Pfeifer GP. Similarities in sunlight-induced mutational spectra of CpG-methylated transgenes and the p53 gene in skin cancer point to an important role of 5-methylcytosine residues in solar UV mutagenesis. J Mol Biol. 2001;305: 389–99. doi:10.1006/jmbi.2000.4322

176. Nandakumar V, Vaid M, Katiyar SK. (-)-Epigallocatechin-3-gallate reactivates silenced tumor suppressor genes, Cip1/p21 and p16INK4a, by reducing DNA methylation and increasing histones acetylation in human skin cancer cells. Carcinogenesis. 2011;32: 537–44. doi:10.1093/carcin/bgq285

177. Takeuchi T, Liang S-B, Matsuyoshi N, Zhou S, Miyachi Y, Sonobe H, et al. Loss of T-cadherin (CDH13, H-cadherin) expression in cutaneous squamous cell carcinoma. Lab Invest. 2002;82: 1023–9. Available: http://www.ncbi.nlm.nih.gov/pubmed/12177241

178. Thiery JP. Epithelial-mesenchymal transitions in tumour progression. Nat Rev Cancer. 2002/08/22. 2002;2: 442–454. doi:10.1038/nrc822

179. Tam WL, Weinberg RA. The epigenetics of epithelial-mesenchymal plasticity in cancer. Nat Med. 2013;19: 1438–49. doi:10.1038/nm.3336

180. De Craene B, Berx G. Regulatory networks defining EMT during cancer initiation and progression. Nat Rev Cancer. 2013;13: 97–110. doi:10.1038/nrc3447

181. Lamouille S, Subramanyam D, Blelloch R, Derynck R. Regulation of epithelial-mesenchymal and mesenchymal-epithelial transitions by microRNAs. Curr Opin Cell Biol. 2013;25: 200–7. doi:10.1016/j.ceb.2013.01.008

182. Nickel A, Stadler SC. Role of epigenetic mechanisms in epithelial-to-mesenchymal transition of breast cancer cells. Transl Res. 2015;165: 126–42. doi:10.1016/j.trsl.2014.04.001

183. Chiles MC, Ai L, Zuo C, Fan C-Y, Smoller BR. E-cadherin promoter hypermethylation in preneoplastic and neoplastic skin lesions. Mod Pathol. 2003;16: 1014–8. doi:10.1097/01.MP.0000089779.35435.9D

184. Tyler LN, Ai L, Zuo C, Fan C-Y, Smoller BR. Analysis of promoter hypermethylation of death-associated protein kinase and p16 tumor suppressor genes in actinic keratoses and squamous cell carcinomas of the skin. Mod Pathol. 2003;16: 660–4. doi:10.1097/01.MP.0000077516.90063.7D

185. Takeuchi T, Liang SB, Matsuyoshi N, Zhou S, Miyachi Y, Sonobe H, et al. Loss of T-cadherin (CDH13, H-cadherin) expression in cutaneous squamous cell carcinoma Recent progress in T-cadherin (CDH13, H-cadherin) research. Lab Invest. 2002;82: 1023–1029. doi:10.1097/01.LAB.0000025391.35798.F1

186. Arbiser JL, Fan C-Y, Su X, Van Emburgh BO, Cerimele F, Miller MS, et al. Involvement of p53 and p16 tumor suppressor genes in recessive dystrophic epidermolysis bullosa-associated squamous cell carcinoma. J Invest Dermatol. 2004;123: 788–90. doi:10.1111/j.0022-202X.2004.23418.x

187. Fraga MF, Herranz M, Ballestar E, Paz MF, Ropero S, Erkek E, et al. A mouse skin multistage carcinogenesis model reflects the aberrant DNA methylation patterns of human tumors. Cancer Res. 2004;64: 5527–34. doi:10.1158/0008-5472.CAN-03-4061

188. Yuspa SH. The pathogenesis of squamous cell cancer: lessons learned from studies of skin carcinogenesis--thirty-third G. H. A. Clowes Memorial Award Lecture. Cancer Res. 1994;54: 1178–89. Available: http://www.ncbi.nlm.nih.gov/pubmed/8118803

189. Balmain A, Harris CC. Carcinogenesis in mouse and human cells: parallels and

paradoxes. Carcinogenesis. 2000;21: 371–7. Available: http://www.ncbi.nlm.nih.gov/pubmed/10688857

190. Rodríguez-Paredes M, Bormann F, Raddatz G, Gutekunst J, Lucena-Porcel C, Köhler F, et al. Methylation profiling identifies two subclasses of squamous cell carcinoma related to distinct cells of origin. Nat Commun. Nature Publishing Group; 2018;9: 577. doi:10.1038/s41467-018-03025-1

191. Baylin SB, Jones PA. A decade of exploring the cancer epigenome - biological and translational implications. Nat Rev Cancer. NIH Public Access; 2011;11: 726–34. doi:10.1038/nrc3130

192. Berman BP, Weisenberger DJ, Aman JF, Hinoue T, Ramjan Z, Liu Y, et al. Regions of focal DNA hypermethylation and long-range hypomethylation in colorectal cancer coincide with nuclear lamina–associated domains. Nat Genet. 2012;44: 40–46. doi:10.1038/ng.969

193. Horvath S. DNA methylation age of human tissues and cell types. Genome Biol. 2013;14: R115. doi:10.1186/gb-2013-14-10-r115

194. Lister R, Pelizzola M, Dowen RH, Hawkins RD, Hon G, Tonti-Filippini J, et al. Human DNA methylomes at base resolution show widespread epigenomic differences. Nature. Nature Publishing Group; 2009;462: 315–322. doi:10.1038/nature08514

195. Schultz MD, He Y, Whitaker JW, Hariharan M, Mukamel EA, Leung D, et al. Human body epigenome maps reveal noncanonical DNA methylation variation. Nature. 2015;523: 212–216. doi:10.1038/nature14465

196. Rinaldi L, Datta D, Serrat J, Morey L, Solanas G, Avgustinova A, et al. Dnmt3a and Dnmt3b Associate with Enhancers to Regulate Human Epidermal Stem Cell Homeostasis. Cell Stem Cell. 2016;19: 491–501. doi:10.1016/j.stem.2016.06.020

197. Moll R, Divo M, Langbein L. The human keratins: biology and pathology. Histochem Cell Biol. 2008;129: 705–733. doi:10.1007/s00418-008-0435-6

198. Wiench M, John S, Baek S, Johnson TA, Sung M-H, Escobar T, et al. DNA methylation status predicts cell type-specific enhancer activity. EMBO J.

2011;30: 3028–3039. doi:10.1038/emboj.2011.210

199. FILIP1L Ensemble [Internet]. 2019 p. Accessed March 2019. Available: http://www.ensembl.org/Mus_musculus/Transcript/Exons?db=core;g=ENSMUSG00000043336;r=16:57353093-57573126;t=ENSMUST00000159816

200. Kwon M, Libutti SK. Filamin A interacting protein 1-like as a therapeutic target in cancer. Expert Opin Ther Targets. 2014;18: 1435–47. doi:10.1517/14728222.2014.957181

201. Welsh J, Chada K, Dalal SS, Cheng R, Ralph D, McClelland M. Arbitrarily primed PCR fingerprinting of RNA. Nucleic Acids Res. Oxford University Press; 1992;20: 4965–70. Available: http://www.ncbi.nlm.nih.gov/pubmed/1383934

202. Liang P, Pardee AB. Differential display of eukaryotic messenger RNA by means of the polymerase chain reaction. Science. 1992;257: 967–71. Available: http://www.ncbi.nlm.nih.gov/pubmed/1354393

203. Mok SC, Wong KK, Chan RK, Lau CC, Tsao SW, Knapp RC, et al. Molecular cloning of differentially expressed genes in human epithelial ovarian cancer. Gynecologic oncology. 1994. pp. 247–252. doi:10.1006/gyno.1994.1040

204. Matei D, Graeber TG, Baldwin RL, Karlan BY, Rao J, Chang DD. Gene expression in epithelial ovarian carcinoma. Oncogene. 2002;21: 6289–6298. doi:10.1038/sj.onc.1205785

205. Notaridou M, Quaye L, Dafou D, Jones C, Song H, Kjaer SK, et al. UKPMC Funders Group Common alleles in candidate susceptibility genes associated with risk and development of epithelial ovarian cancer. Int J Cancer. 2011;128: 2063–2074. doi:10.1002/ijc.25554.Common

206. Schwarze SR, DePrimo SE, Grabert LM, Fu VX, Brooks JD, Jarrard DF. Novel pathways associated with bypassing cellular senescence in human prostate epithelial cells. J Biol Chem. 2002;277: 14877–14883. doi:10.1074/jbc.M200373200

207. Schwarze SR, Fu VX, Desotelle JA, Kenowski ML, Jarrard DF. The Identification of Senescence-Specific Genes during the Induction of

Senescence in Prostate Cancer Cells. Neoplasia. 2005;7: 816–823. doi:10.1593/neo.05250

208. Endothelial H, Mazzanti CM, Tandle A, Lorang D, Mazzanti CM, Tandle A, et al. Early Genetic Mechanisms Underlying the Inhibitory Effects of Early Genetic Mechanisms Underlying the Inhibitory Effects of Endostatin and Fumagillin on Human Endothelial Cells. 2004; 1585–1593. doi:10.1101/gr.2552804

209. Tandle AT, Mazzanti C, Alexander HR, Roberts DD, Libutti SK. Endothelial monocyte activating polypeptide-II induced gene expression changes in endothelial cells. Cytokine. 2005;30: 347–358. doi:10.1016/j.cyto.2005.01.020

210. Stangeland B, Mughal AA, Grieg Z, Sandberg CJ, Joel M, Nygård S, et al. Combined expressional analysis, bioinformatics and targeted proteomics identify new potential therapeutic targets in glioblastoma stem cells. Oncotarget. 2015;6. doi:10.18632/oncotarget.4613

211. Sandberg CJ, Altschuler G, Jeong J, Strømme KK, Stangeland B, Murrell W, et al. Comparison of glioma stem cells to neural stem cells from the adult human brain identifies dysregulated Wnt- signaling and a fingerprint associated with clinical outcome. Exp Cell Res. 2013;319: 2230–2243. doi:10.1016/j.yexcr.2013.06.004

212. Hu Y, Mivechi NF. Promotion of Heat Shock Factor Hsf1 Degradation via Adaptor Protein Filamin A-interacting Protein 1-Like (FILIP-1L). J Biol Chem. 2011;286: 31397–31408. doi:10.1074/jbc.M111.255851

213. Xie C, Gou M, Yi T, Deng H, Li Z, Liu P, et al. Efficient Inhibition of Ovarian Cancer by Truncation Mutant of FILIP1L Gene Delivered by Novel Biodegradable Cationic Heparin-Polyethyleneimine Nanogels. Hum Gene Ther. 2011;22: 1413–1422. doi:10.1089/hum.2011.047

214. Xie C, Gou M, Yi T, Qi X, Liu P, Wei Y, et al. Enhanced antitumor effect of biodegradable cationic heparin-polyethyleneimine nanogels delivering FILIP1LDeltaC103 gene combined with low-dose cisplatin on ovarian cancer. Oncotarget. 2017;8: 76432–76442. doi:10.18632/oncotarget.19464

215. Burton ER, Gaffar A, Lee SJ, Adeshuko F, Whitney KD, Chung J-Y, et al. Downregulation of Filamin A Interacting Protein 1-Like is Associated with Promoter Methylation and Induces an Invasive Phenotype in Ovarian Cancer. Mol Cancer Res. 2011;9: 1126–1138. doi:10.1158/1541-7786.MCR-11-0162

216. Lu H, Hallstrom TC. Sensitivity to TOP2 Targeting Chemotherapeutics Is Regulated by Oct1 and FILIP1L. Tsuji Y, editor. PLoS One. Public Library of Science; 2012;7: e42921. doi:10.1371/journal.pone.0042921

217. Kwon M, Lee SJ, Reddy S, Rybak Y, Adem A, Libutti SK. Down-Regulation of Filamin Ainteracting protein 1-like Is Associated with Promoter Methylation and an Invasive Phenotype in Breast, Colon, Lung and Pancreatic Cancers. Rishi A, editor. PLoS One. 2013;8: e82620. doi:10.1371/journal.pone.0082620

218. Desotelle J, Truong M, Ewald J, Weeratunga P, Yang B, Huang W, et al. CpG island hypermethylation frequently silences FILIP1L isoform 2 expression in prostate cancer. J Urol. NIH Public Access; 2013;189: 329–35. doi:10.1016/j.juro.2012.08.188

219. Kwon M, Lee SJ, Wang Y, Rybak Y, Luna A, Reddy S, et al. Filamin A interacting protein 1-like inhibits WNT signaling and MMP expression to suppress cancer cell invasion and metastasis. Int J cancer. 2014;135: 48–60. doi:10.1002/ijc.28662

220. Bravo-Cordero JJ, Hodgson L, Condeelis J. Directed cell invasion and migration during metastasis. Curr Opin Cell Biol. 2012;24: 277–283. doi:10.1016/j.ceb.2011.12.004

221. Wu B, Crampton SP, Hughes CCW. Wnt Signaling Induces Matrix Metalloproteinase Expression and Regulates T Cell Transmigration. Immunity. 2007;26: 227–239. doi:10.1016/j.immuni.2006.12.007

222. Kwon M, Kim J-H, Rybak Y, Luna A, Hun Choi C, Chung J-Y, et al. Reduced expression of FILIP1L, a novel WNT pathway inhibitor, is associated with poor survival, progression and chemoresistance in ovarian cancer. Oncotarget. 2016;7: 77052–77070. doi:10.18632/oncotarget.12784

223. Breslow NE. Analysis of Survival Data under the Proportional Hazards Model.

Int Stat Rev / Rev Int Stat. International Statistical Institute (ISI); 1975;43: 45. doi:10.2307/1402659

224. Kalluri R, Weinberg RA. The basics of epithelial-mesenchymal transition. J Clin Invest. 2009/06/03. 2009;119: 1420–1428. doi:10.1172/JCI39104

225. Park Y-L, Park S-Y, Lee S-H, Kim R-B, Kim J-K, Rew S-Y, et al. Filamin A interacting protein 1-like expression inhibits progression in colorectal cancer. Oncotarget. Impact Journals, LLC; 2016;7: 72229–72241. doi:10.18632/oncotarget.12664

226. Liu Y, Yang Y, Li W, Ao H, Zhang Y, Zhou R, et al. Effects of melatonin on the synthesis of estradiol and gene expression in pig granulosa cells. J Pineal Res. 2019;66: e12546. doi:10.1111/jpi.12546

227. Pan Z, Li G-F, Sun M-L, Xie L, Liu D, Zhang Q, et al. MicroRNA-1224 Splicing CircularRNA-Filip1l in an Ago2-Dependent Manner Regulates Chronic Inflammatory Pain via Targeting Ubr5. J Neurosci. Society for Neuroscience; 2019;39: 2125–2143. doi:10.1523/JNEUROSCI.1631-18.2018

228. Hansen TB, Kjems J, Damgaard CK. Circular RNA and miR-7 in Cancer. Cancer Res. American Association for Cancer Research; 2013;73: 5609–5612. doi:10.1158/0008-5472.CAN-13-1568

229. Krueger F, Andrews SR. Bismark: A flexible aligner and methylation caller for Bisulfite-Seq applications. Bioinformatics. 2011;27: 1571–1572. doi:10.1093/bioinformatics/btr167

230. Du P, Zhang X, Huang C-C, Jafari N, Kibbe WA, Hou L, et al. Comparison of Beta-value and M-value methods for quantifying methylation levels by microarray analysis. BMC Bioinformatics. 2010;11: 587. doi:10.1186/1471-2105-11-587

231. Sun Z, Cunningham J, Slager S, Kocher JP. Base resolution methylome profiling: Considerations in platform selection, data preprocessing and analysis. Epigenomics. 2015;7: 813–828. doi:10.2217/epi.15.21

232. Hebestreit K, Dugas M, Klein HU. Detection of significantly differentially methylated regions in targeted bisulfite sequencing data. Bioinformatics.

2013;29: 1647–1653. doi:10.1093/bioinformatics/btt263

233. Liao B-Y, Zhang J. Null mutations in human and mouse orthologs frequently result in different phenotypes. Proc Natl Acad Sci. 2008;105: 6987–6992. doi:10.1073/pnas.0800387105

234. Proby CM, Purdie KJ, Sexton CJ, Purkis P, Navsaria HA, Stables JN, et al. Spontaneous keratinocyte cell lines representing early and advanced stages of malignant transformation of the epidermis. Exp Dermatol. 2000;9: 104–17. Available: http://www.ncbi.nlm.nih.gov/pubmed/10772384

235. Dickson MA, Hahn WC, Ino Y, Ronfard V, Wu JY, Weinberg RA, et al. Human keratinocytes that express hTERT and also bypass a p16(INK4a)-enforced mechanism that limits life span become immortal yet retain normal growth and differentiation characteristics. Mol Cell Biol. 2000;20: 1436–47. Available: http://www.ncbi.nlm.nih.gov/pubmed/10648628

236. Watt F, Molloy PL. Cytosine methylation prevents binding to DNA of a HeLa cell transcription factor required for optimal expression of the adenovirus major late promoter. Genes Dev. 1988;2: 1136–43. Available: http://www.ncbi.nlm.nih.gov/pubmed/3192075

237. Lewis JD, Meehan RR, Henzel WJ, Maurer-Fogy I, Jeppesen P, Klein F, et al. Purification, sequence, and cellular localization of a novel chromosomal protein that binds to methylated DNA. Cell. 1992;69: 905–14. Available: http://www.ncbi.nlm.nih.gov/pubmed/1606614

238. Harrow J, Denoeud F, Frankish A, Reymond A, Chen C-K, Chrast J, et al. GENCODE: producing a reference annotation for ENCODE. Genome Biol. BioMed Central; 2006;7: S4. doi:10.1186/gb-2006-7-s1-s4

239. He X, Chatterjee R, Tillo D, Smith A, FitzGerald P, Vinson C. Nucleosomes are enriched at the boundaries of hypomethylated regions (HMRs) in mouse dermal fibroblasts and keratinocytes. Epigenetics Chromatin. BioMed Central; 2014;7: 34. doi:10.1186/1756-8935-7-34

240. FANTOM Consortium and the RIKEN PMI and CLST (DGT), Forrest ARR, Kawaji H, Rehli M, Baillie JK, de Hoon MJL, et al. A promoter-level

mammalian expression atlas. Nature. 2014;507: 462–470. doi:10.1038/nature13182

241. Noguchi S, Arakawa T, Fukuda S, Furuno M, Hasegawa A, Hori F, et al. FANTOM5 CAGE profiles of human and mouse samples. Sci Data. Nature Publishing Group; 2017;4: 170112. doi:10.1038/sdata.2017.112

242. Khan A, Fornes O, Stigliani A, Gheorghe M, Castro-Mondragon JA, van der Lee R, et al. JASPAR 2018: update of the open-access database of transcription factor binding profiles and its web framework. Nucleic Acids Res. 2018;46: D260–D266. doi:10.1093/nar/gkx1126

243. Ding M, Liu Y, Liao X, Zhan H, Liu Y, Huang W. Enhancer RNAs (eRNAs): New insights into gene transcription and disease treatment. Journal of Cancer. Ivyspring International Publisher; 2018. pp. 2334–2340. doi:10.7150/jca.25829

244. Flores MA, Ovcharenko I. Enhancer reprogramming in mammalian genomes. BMC Bioinformatics. 2018;19: 316. doi:10.1186/s12859-018-2343-7

245. Palstra RJ, Grosveld F. Transcription factor binding at enhancers: Shaping a genomic regulatory landscape in flux. Frontiers in Genetics. 2012. doi:10.3389/fgene.2012.00195

246. Cai M, Sun X, Wang W, Lian Z, Wu P, Han S, et al. Disruption of peroxisome function leads to metabolic stress, mTOR inhibition, and lethality in liver cancer cells. Cancer Lett. 2018;421: 82–93. doi:10.1016/j.canlet.2018.02.021

247. The Human Protein Atlas. Zfhx4 The Human Protein Atlas [Internet]. 2019. Available: https://www.proteinatlas.org/ENSG00000164751-PEX2/tissue

248. Ponjavic J, Ponting CP, Lunter G. Functionality or transcriptional noise? Evidence for selection within long noncoding RNAs. Genome Res. Cold Spring Harbor Laboratory Press; 2007;17: 556–65. doi:10.1101/gr.6036807

249. Guttman M, Amit I, Garber M, French C, Lin MF, Feldser D, et al. Chromatin signature reveals over a thousand highly conserved large non-coding RNAs in mammals. Nature. NIH Public Access; 2009;458: 223–7. doi:10.1038/nature07672

250. Ørom UA, Derrien T, Beringer M, Gumireddy K, Gardini A, Bussotti G, et al.

Long non-coding RNAs with enhancer-like function in human. Cell. NIH Public Access; 2010;143: 46. doi:10.1016/J.CELL.2010.09.001

251. Cabili MN, Trapnell C, Goff L, Koziol M, Tazon-Vega B, Regev A, et al. Integrative annotation of human large intergenic noncoding RNAs reveals global properties and specific subclasses. Genes Dev. Cold Spring Harbor Laboratory Press; 2011;25: 1915–27. doi:10.1101/gad.17446611

252. Khalil AM, Guttman M, Huarte M, Garber M, Raj A, Morales DR, et al. Many human large intergenic noncoding RNAs associate with chromatin-modifying complexes and affect gene expression. Proc Natl Acad Sci U S A. National Academy of Sciences; 2009;106: 11667. doi:10.1073/PNAS.0904715106

253. Taatjes DJ, Marr MT, Tjian R. Regulatory diversity among metazoan co-activator complexes. Nat Rev Mol Cell Biol. Nature Publishing Group; 2004;5: 403–410. doi:10.1038/nrm1369

254. Donner AJ, Ebmeier CC, Taatjes DJ, Espinosa JM. CDK8 is a positive regulator of transcriptional elongation within the serum response network. Nat Struct Mol Biol. 2010;17: 194–201. doi:10.1038/nsmb.1752

255. Gelfman S, Cohen N, Yearim A, Ast G. DNA-methylation effect on cotranscriptional splicing is dependent on GC architecture of the exon-intron structure. Genome Res. 2013;23: 789–799. doi:10.1101/gr.143503.112

256. Lev Maor G, Yearim A, Ast G. The alternative role of DNA methylation in splicing regulation. Trends Genet. Elsevier Current Trends; 2015;31: 274–280. Available: http://www.ncbi.nlm.nih.gov/pubmed/25837375

257. Iannone C, Valcárcel J. Chromatin's thread to alternative splicing regulation. Chromosoma. 2013;122: 465–474. doi:10.1007/s00412-013-0425-x

258. Luco RF, Allo M, Schor IE, Kornblihtt AR, Misteli T. Epigenetics in alternative pre-mRNA splicing. Cell. Elsevier; 2011;144: 16–26. doi:10.1016/j.cell.2010.11.056

259. Ensemble. Ensemble: Cdk8 [Internet]. 2019. Available: http://www.ensembl.org/Mus_musculus/Gene/Summary?db=core;g=ENSMUSG00000029635;r=5:146231230-146302874;t=ENSMUST00000161181

260. Sherwood V, Leigh IM. WNT Signaling in Cutaneous Squamous Cell Carcinoma: A Future Treatment Strategy? J Invest Dermatol. Elsevier; 2016;136: 1760–1767. doi:10.1016/j.jid.2016.05.108

261. Kwon M, Libutti SK. Expert Opinion on Therapeutic Targets Filamin A interacting protein 1-like as a therapeutic target in cancer Filamin A interacting protein 1-like as a therapeutic target in cancer. 2016;8222. doi:10.1517/14728222.2014.957181

262. Jho E, Zhang T, Domon C, Joo C-K, Freund J-N, Costantini F. Wnt/beta-catenin/Tcf signaling induces the transcription of Axin2, a negative regulator of the signaling pathway. Mol Cell Biol. 2002;22: 1172–83. doi:10.1128/mcb.22.4.1172-1183.2002

263. Shtutman M, Zhurinsky J, Simcha I, Albanese C, D'Amico M, Pestell R, et al. The cyclin D1 gene is a target of the beta-catenin... [Proc Natl Acad Sci U S A. 1999] - PubMed result. Proc Natl Acad Sci U S A. 1999;96: 5522–7. Available: http://www.pubmedcentral.nih.gov/articlerender.fcgi?artid=21892&tool=pmcentrez&rendertype=abstract

264. He TC, Sparks AB, Rago C, Hermeking H, Zawel L, da Costa LT, et al. Identification of c-MYC as a target of the APC pathway. Science. 1998;281: 1509–12. doi:10.1126/science.281.5382.1509

265. Shi DQ, Ali I, Tang J, Yang WC. New insights into 5hmC DNA modification: Generation, distribution and function. Frontiers in Genetics. Frontiers Media S.A.; 2017. doi:10.3389/fgene.2017.00100

266. Kalin JH, Wu M, Gomez A V., Song Y, Das J, Hayward D, et al. Targeting the CoREST complex with dual histone deacetylase and demethylase inhibitors. Nat Commun. Nature Publishing Group; 2018;9. doi:10.1038/s41467-017-02242-4